Precision medicine in melanoma

A thesis submitted to the University of Manchester for the degree of Doctor of Philosophy in the Faculty of Biology Medicine and Health.

2018

Rebecca J. Lee

School of Medical Sciences

Table of Contents

Abstract

The treatment of melanoma has fundamentally changed over the past 10 years with the discovery of targeted and immune therapies. Despite this, the majority of patients with late stage melanoma have a median survival of less than 3 years. Resistance and toxicity to therapy remain the key challenges in the era of targeted and immune treatments. In this thesis, I investigate different approaches to overcoming resistance and exploiting vulnerabilities in melanoma biology through the use of patient-derived samples.

I investigate how the brain microenvironment interacts with melanoma cells resulting in resistance to therapy. In a patient with acral melanoma who initially had a complete response to nivolumab an anti-PD-1 therapy, I show that resistance to immune therapy is associated with infiltration of M2-switched macrophages/microglia in the brain microenvironment. Furthermore, factors present in cerebrospinal fluid result in increased phosphatidylinositol 3-kinase/protein kinase B (PI3K/AKT) signalling in brain-derived melanoma cells resulting in resistance to the BRAF inhibitor, dabrafenib.

The novel pan-RAF inhibitor CCT3833 has been shown to be effective in preclinical models of *BRAF* and *NRAS* mutant melanoma. I aimed to investigate if melanoma cells could overcome the inhibitory effects of the drug and explored combination strategies targeting potential mechanisms of emerging resistance. Resistance to CCT3833 was associated with up-regulation of the mitogen-activated protein kinase (MAPK) or PI3K/AKT pathways. Combining CCT3833 with taselisib, a PI3K inhibitor resulted in decreased melanoma growth *in vitro* and *in vivo*. Furthermore, I examined the mechanisms underlying drug addiction, which can develop in targeted therapy resistance. In CCT3833 resistant cells, which had up-regulated the MAPK pathway, ERK and JunB were hyperactivated when drug was withdrawn, resulting

in decreased cell growth *in vitro* and *in vivo*. I showed that this effect could be augmented through the addition of a protein kinase C (PKC) agonist, which increases ERK hyperactivation.

An important strategy in overcoming resistance may be to treat early when melanoma is less complex and tumour burden is reduced. Therefore, I developed a liquid biopsy based on circulating tumour DNA (ctDNA) that identified patients at highest risk of relapse following curative intent surgery. Selecting patients on the basis of detectable ctDNA levels enables intensification of treatment for high-risk patients, whilst those at lower risk may be spared potential toxicity. Finally, I designed clinical trials to test the use of ctDNA as a dynamic approach to monitoring tumour burden in patients with stage IV disease and identifying early relapse in patients with stage IIB/C melanoma following surgery.

Thus, in order to be most effective, precision medicine must anticipate both melanoma cell intrinsic and extrinsic mechanisms of resistance to therapy. CCT3833 is a promising new MAPK inhibitor and combination strategies will optimise the duration of response. The level of ERK activation is finely tuned in melanoma and resistance to targeted therapy results in vulnerability to ERK hyperactivation and decreased growth. Therefore scheduling strategies may further extend the efficacy of targeted therapy. Monitoring with ctDNA enables a more dynamic approach to identification of treatment response, relapse and emerging mechanisms of resistance, allowing early therapeutic decisions to be made. Ultimately, precision medicine approaches in melanoma will enable targeting of patients at highest risk of disease progression whilst sparing others from potential toxicities from treatments that will provide little benefit.

Word Count

Word count = 62587

Declaration

No portion of the work referred to in this thesis has been submitted in support of an application for another degree or qualification of this or any other university or other institute of learning.

Copyright Statement

i. The author of this thesis (including any appendices and/or schedules to this thesis) owns certain copyright or related rights in it (the "Copyright") and she has given The University of Manchester certain rights to use such Copyright, including for administrative purposes.

ii. Copies of this thesis, either in full or in extracts and whether in hard or electronic copy, may be made **only** in accordance with the Copyright, Designs and Patents Act 1988 (as amended) and regulations issued under it or, where appropriate, in accordance with licensing agreements which the University has from time to time. This page must form part of any such copies made.

iii. The ownership of certain Copyright, patents, designs, trademarks and other intellectual property (the "Intellectual Property") and any reproductions of copyright works in the thesis, for example graphs and tables ("Reproductions"), which may be described in this thesis, may not be owned by the author and may be owned by third parties. Such Intellectual Property and Reproductions cannot and must not be made available for use without the prior written permission of the owner(s) of the relevant Intellectual Property and/or Reproductions.

iv. Further information on the conditions under which disclosure, publication and commercialisation of this thesis, the Copyright and any Intellectual Property and/or Reproductions described in it may take place is available in the University IP Policy (see http://documents.manchester.ac.uk/DocuInfo.aspx?DocID=24420), in any relevant Thesis restriction declarations deposited in the University Library, The University Library's regulations (see http://www.library.manchester.ac.uk/about/regulations/) and in The University's policy on Presentation of Theses

Acknowledgements

Firstly, I would like to thank my two supervisors Richard Marais and Paul Lorigan for giving me the opportunity to conduct this research. I have learnt so much from both of you and you have given me an amazing foundation of knowledge on which to build my future research.

I would also like to thank everyone in the molecular oncology group for all their patience when I was learning how to be a scientist. I have learnt so much from everyone and had a lot of fun in doing so. Jackie in particular has helped me so much with setting up the trials and dealing with the administration. Also Clare for all her hard work as the best lab manager and having the amazing ability to find anything you ask for.

Special thanks must go to the fantastic people that I have been lucky to meet in the lab. Clare, Franzi, Kate and Marina -I do not know how I would have kept going without you. I would also like to thank Katie, Garima and Josh for their teaching and moral support; I am so glad I have met such awesome people. Thanks also to Josh who has kept me on track in my thesis writing and to Josh, Garima, Franzi and Marina for reading and editing it.

I would also like to thank the core facilities including histology, molecular biology, flow cytometry, and the animal unit for all their help with my projects. The CRUK Manchester Institute has been a fantastic place to work and I have always enjoyed the discussions with other groups. It has been great working with you. Without the biobank and especially Pippa, I would not have been able to do so much of my research, so thank you for all your work.

In addition, I would like to thank my collaborators, particularly Caroline Springer and the drug discovery unit (especially Filipa) for helping with the work with CCT3833 and Caroline Dive and the CEP group (especially Nigel, Mahmood, Dominic, Ged, Elaine and Jonathon) for the onigoing work setting up trials with ctDNA. I would also like to thank Mark

Middleton, James Larkin, Paul Nathan, Gordon Jayson and Richard Jackson for all their help with the trial designs.

Thanks to my funders CRUK and the Wellcome Trust as without their generosity I would not have been able to do so much work.

I would also like to thank my examiners for spending their time reading this thesis – I look forward to hearing your comments.

Notably, thanks to all the patients who have generously donated their samples to my research. I have learnt so much from your gift.

Finally and most importantly, I would like to thank my family for always being there for me and building me up whenever times have been tough.

Abbreviations and glossary

AE	Adverse Event
AIC	Akaikes Information Criterion
AJCC	American Joint Committee on Cancer
AKT	Protein kinase B
ALC	Absolute lymphocyte count
ATM	Ataxia-telangiectasia mutated
B2M	ß2-Microglobulin
BAP1	BRCA1-associated protein 1
BBB	Blood brain barrier
BP	Base pair
BRAFi	BRAF inhibitor
BTS	Baseline tumour size
CAcTUS	CirculAting Tumour DNA gUided therapy Switch
Cas9	CRISPR-associated protein 9
CDK	Cyclin dependent kinases
CDX	Circulating tumour cell derived xenograft
cfDNA	Cell free DNA
CI	Confidence interval
CLND	Completion lymph node dissection
COX-2	Cyclo-oxygenase-2
CR	Complete response
CRISPR	Clustered regularly interspaced short palindromic repeats
CRP	C reactive protein
CSF	Cerebrospinal fluid
CT	Computerised tomography
CTC	Circulating tumour cells
ctDNA	Circulating tumour DNA
CTLA-4	Cytotoxic T-lymphocyte antigen-4
CXCL	Chemokine (C-X-C motif) ligand
DAG	Diacylglycerol
DNA	Deoxyribonucleic acid
ddPCR	Droplet digital polymerase-chain reaction
D+T	Dabrafenib +Trametinib
DETECTION	circulating tumour DNA guidEd Therapy for stage IIB/C mElanoma after surgiCal resection
DFI	Disease-free interval
DMFI	Distant metastasis-free interval
DTIC	Dacarbazine
DUSP	Dual-specificity phosphatase
E+B	Encorafenib + Binimetinib
EGFR	Epidermal growth factor receptor
EMT	Epithelial to mesenchymal transition
FACS	Fluorescence-activated cell sorting
FDA	Food and drug administration
FDR	False discovery rate

FGFR	Fibroblast growth factor receptor
^{18}FDG	18-fluorodeoxyglucose positron emission tomography
GCP	Good Clinical Practice
G-CSF	Granulocyte-colony stimulating factor
HDACi	Histone deacetylase inhibitor
HR	Hazard ratio
IC_{50}	Half maximal inhibitory concentration
IFN□	Interferon gamma
IGFR	Insulin growth factor receptor
IL	Interleukin
iNOS	inducible nitric oxide synthase
ITT	Intention to treat
JAK1/2	Janus kinase 1 or 2
JNK	c-Jun N-terminal kinase
LDH	Lactate dehydrogenase
MAPK	Mitogen-activated protein kinase
MAPKK	Mitogen-activated protein kinase kinase
MAPKKK	Mitogen-activated protein kinase kinase kinase
MAPKi	MAPK inhibitor
MDS	Multi-dimensional scale
MEKi	MEK inhibitor
MHC	Major histocompatibility complex
MITF	Microphthalmia-associated transcription factor
MM	Metastatic melanoma
MMP	Matrix metalloproteinase
MRD	Minimal residual disease
mRNA	Messenger ribonucleic acid
N+I	Nivolumab + Ipilimumab
NCSC	Neural crest stem-cell like
NED	No evidence of disease
NGS	Next generation sequencing
NSCLC	Non small-cell lung cancer
nsSNV	Non-synonymous single nucleotide variant
ORR	Overall response rate
OS	Overall survival
PB1	Phox/Bem 1
PAK	p21-activated kinase
PARP	Poly (ADP-ribose) polymerase
pCR	Pathological complete response
PCR	Polymerase-chain reaction
PD	Progressive disease
PD-1	Programmed death-1
PD-L1	Programmed death ligand-1
PDGF	Platelet derived growth factor
PDX	Patient-derived xenograft
PFS	Progression free survival
PGE_2	Prostaglandin-E_2
PI3K	Phosphatidylinositol 3-kinase
PIP2	Phosphatidylinositol-4,5-biphosphate

PIP3	Phosphatidylinositol-3,4,5-triphosphate
PKC	Protein kinase C
PLC	Phospholipase C
PLK	Polo-like kinase
PMA	Phorbol 12-myristate 13-acetate
PPI	Patient and public involvement
PR	Partial response
PS	Performance status
PSA	Prostate specific antigen
PSDS	Prognostic separation D statistics
PTEN	Phosphatase and tensin homolog
RB	Retinoblastoma
RCT	Randomised Controlled Trial
RECIST	Response evaluation criteria in solid tumours
RFS	Relapse-free survival
RNA	Ribonucleic acid
RPPA	Reverse phase protein array
RTK	Receptor tyrosine kinase
SAPK	Stress activated protein kinase
SD	Stable disease
SE	Standard error
SEER	Surveillance, Epidemiology, and End Results
SHP2	Src homology phosphatase 2
SOS	Sons of sevenless
SOT	Sotrastaurin
SPRY	Sprouty
SRB	Sulforhodamine B
STAT	Signal transducer and activator of transcription
STK	Serine-threonine kinase
TAB1	Transforming growth factor-ß (TGFß)-activated protein kinase 1-binding protein
TCR	T cell receptor
TGFß	Transforming growth factor-ß
TIL	Tumour infiltrating lymphocyte
TNF-α	Tumour necrosis factor alpha
TNM	Tumour node metastasis
TP53	Tumour protein 53
T_{reg}	Regulatory T cell
TTP	Time to progression
ULN	Upper limit of normal
V+C	Vemurafenib plus cobimetinib
VAF	Variant allele frequency
VCAM-1	Vascular cell adhesion molecule-1
VEGF	Vascular endothelial growth factor
WES	Whole exome sequencing
WNT	Wingless-integration-1

Chapter 1. Introduction

1.1. Melanoma incidence, staging and prognosis

Melanoma has been increasing in incidence over the last two decades due to a number of environmental and social factors as well as increased surveillance (1). In 2014, the incidence of melanoma in the United States was 76,100 (2). It is the 4th most common cancer in the United Kingdom with 13,348 new cases diagnosed in 2011 (Fig. 1.1) (3). Although it is a common cancer, mortality is lower than that of other tumour types, due to the fact that the majority of patients present with early stage disease, which is easily resected (3). However, with increasing incidence, mortality has also been increasing, albeit at a slower rate, likely due to earlier detection and improved treatments. In 2012, there were 2,148 deaths from malignant melanoma in the UK (3). Increasing mortality is particularly concerning in the >75 age group, with 17 per 100,000 deaths in 2012 compared to 4 per 100,000 in 1971 (3).

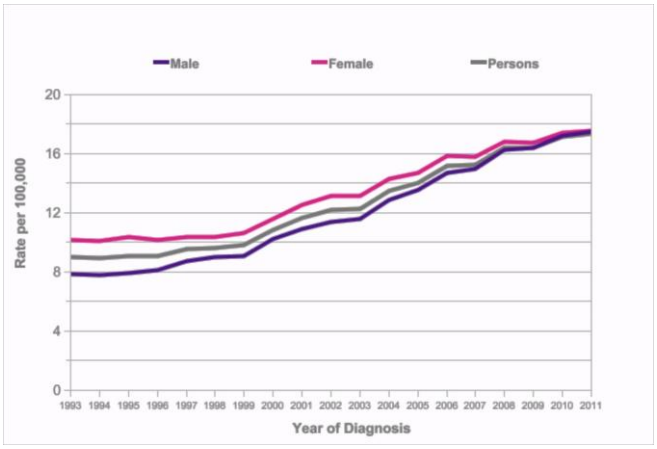

Figure 1.1 Malignant Melanoma, European age-standardised incidence rates per 100,000 population. By sex, UK, 1993-2011. Adapted from skin cancer statistics, Cancer Research UK (3)

Melanoma is staged using the American Joint Committee on Cancer (AJCC) staging classification (4). This is based on primary tumour thickness, ulceration, regional and distant metastatic spread (4). In patients with stage IV melanoma, elevated lactate dehydrogenase (LDH) and brain metastases have been shown to be independent poor prognostic factors (4,5).

In the era of effective targeted and immunological treatments, prognosis for metastatic melanoma (MM) has dramatically changed. Prior to 2011, standard treatment options for

patients with MM were limited to chemotherapy, which in the UK was typically dacarbazine (DTIC) with a response rate of 5% to 12% and median overall survival (OS) of 5.6 to 9.1 months (6). With the advent of treatments targeting the mitogen-activated protein kinase (MAPK) pathway and immune checkpoint inhibitors, patients can typically expect to survive up to 2-3 years with a small proportion achieving durable remissions (7–11).

1.2 Melanoma classification

Melanoma occurs due to genetic changes in melanocytes, which result in uncontrolled proliferation and invasion (1,12). Melanoma is a heterogeneous group of melanocyte derived skin cancers, which have distinct genetic drivers, histopathological features and clinical courses (13). Cutaneous melanoma is the commonest type representing 90% of melanomas (13). It is further classified into superficial spreading, nodular, lentigo maligna and a rarer subtype seen on acral surfaces (palmar-plantars, subungal) called acral lentiginous melanoma, which represents 4% of cutaneous melanoma (13,14) (14). Acral melanoma has a poorer prognosis than common cutaneous melanoma with 5-year and 10-year melanoma-specific survival rates of 80.3% and 67.5%, respectively, compared to cutaneous melanoma survival rates of 91.3% and 87.5%, (P<0.001) in a Surveillance, Epidemiology, and End Results (SEER) database review of registries from 1986 to 2005 (15). In addition, approximately 10% of melanomas are uveal and mucosal melanoma, which are associated with specific mutational drivers (16,17). Mucosal melanoma accounts for approximately 1.2% of melanomas, tending to arise in the head/neck, genitourinary and anorectal areas (17). Uveal melanoma is derived from melanocytes in the choroid plexus, ciliary body, and iris of the eye and has a tendency to metastasise to the liver (16).

1.3 MAPK pathways in melanoma

There are 3 MAPK cascades, the classical MAPK or extracellular signal-regulated kinase (ERK), stress-activated protein kinase (SAPK/JNK [c-Jun N-terminal kinase]) and p38 kinase pathway (18). Each pathway has 3 major components; a serine/threonine protein kinase (MAPKKK), which phosphorylates and activates a dual-specificity protein kinase (MAPKK), which in turn phosphorylates and activates another serine/threonine protein kinase (MAPK) (19). These signal transduction pathways respond to multiple external signals and connect the plasma membrane with cytoplasmic and nuclear events (20). In response to stimuli they regulate cell proliferation, differentiation, development, inflammatory response and apoptosis (18).

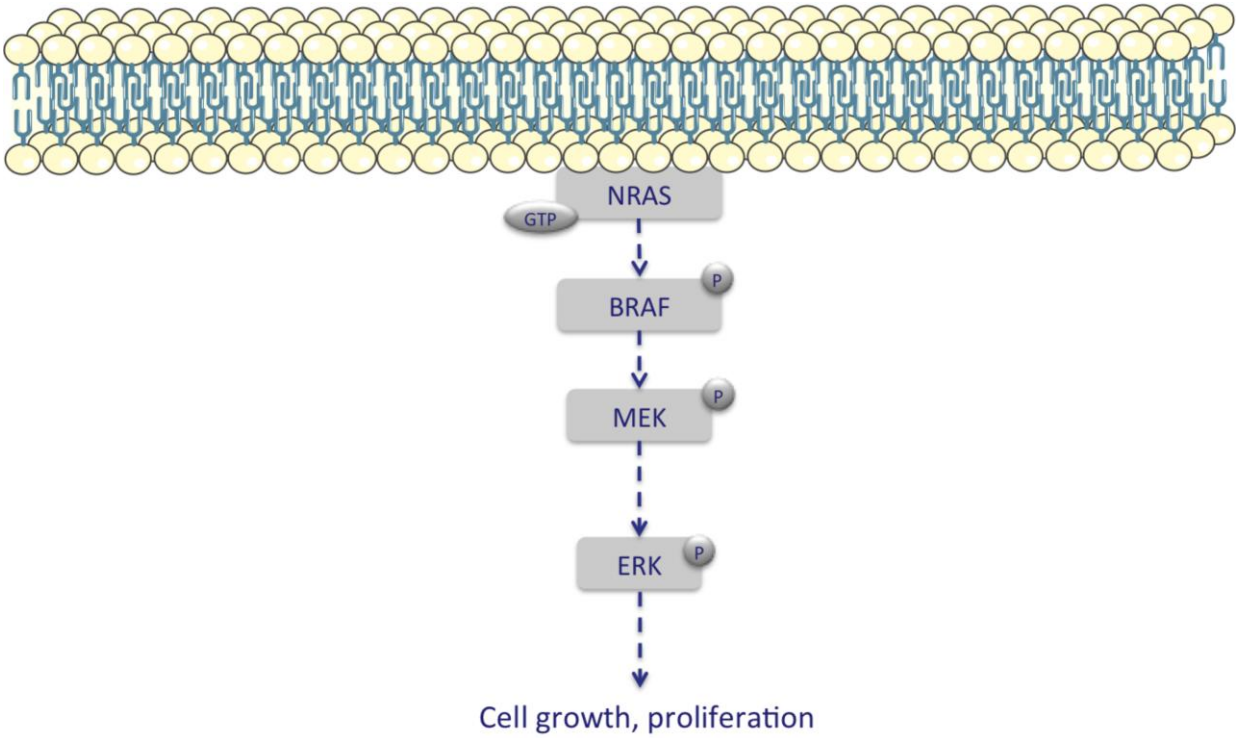

Fig. 1.2 Classical MAPK pathway. Main components of classical MAPK pathway that are important in melanoma

The major components of the classical MAPK pathway are RAS (Rat sarcoma), RAF (MAPKKK), MEK (MAPKK), and ERK (MAPK, Fig. 1.2) (19). RAS was originally identified

through the discovery of retroviruses carrying oncogenes (originally called v-*src*), which induced sarcomas in newborn rodents (21,22). RAS is a small GTPase (guanosine triphosphate), which is activated through a complex of the exchange factor son of sevenless (SOS) and the adapter protein GRB2 being recruited to receptor-tyrosine kinases (23). Activated RAS then interacts with the serine/threonine kinase RAF (24–26). RAF then phosphorylates MEK at serine/threonine residues (27). Finally, MEK must phosphorylate both tyrosine and threonine in order for ERK activation to occur (28). In contrast to the narrow substrate specificity of RAF and MEK, ERK catalyses the phosphorylation of multiple cytoplasmic and nuclear substrates (29,30). One of the major functions of ERK is to regulate the cell cycle in response to extra-cellular signals (31). In addition, ERK activates over 150 substrates including transcription factors, protein kinases and phosphatases, cytoskeletal and scaffold proteins, receptors, signalling molecules, and apoptosis-related proteins (30,32,33).

The complexity of the MAPK pathway is increased due to the number of different isoforms at each level. For example there are 3 RAF isoforms – ARAF, BRAF and CRAF (also known as RAF1) (20). They have different mechanisms of activation and different levels of activity, with BRAF associated with the greatest level of activation (34–36). In addition, the duration of signalling results in different cell responses (19). Sustained activation of ERK leads to its translocation to the nucleus, resulting in phosphorylation of transcription factors and differentiation of cells, whereas transient activation results in a more proliferative phenotype (19).

The second MAPK cascade is the JNK/SAPK pathway, which is activated in response to stress or cytokines such as tumour necrosis factor alpha (TNF-α) and interleukin-1 (IL-1), and growth factors (37–39). JNK is activated by phosphorylation on threonine and tyrosine by MKK4 (also known as SEK1) and MKK7 (40–43). In turn, MKK4 and MKK7 are activated by a number of different members of the MEKK group (MEKK1-4), the mixed-lineage protein

kinase group (MLK1, MLK2, MLK3, DLK, and LZK), the apoptosis signal-regulated kinase group (ASK1 and ASK2), TAK1, and TPL2 (39,44–48). One of the major roles for JNK is the regulation of the activator protein-1 transcription factor (AP-1) as well as JunB, JunD, ELK1, Sap-1 and activating transcription factor-2 (ATF2) (49,50). JNK is required for AP-1 activation in response to stress or cytokines (37,38), however other types of stimuli may active AP-1 independent of JNK (51). AP-1 is a regulator of cell proliferation, differentiation and apoptosis (52). It consists of a number of proteins belonging to the Jun (c-Jun, JunB, JunD), Fos (c-Fos, FosB, Fra-1 and Fra-2), Maf (c-Maf, MafB, MafA, MafG/F/K and Nrl) and ATF (ATF2, LRF1/ATF3, B-ATF, JDP1, JDP2) sub-families (52). C-Jun and Fos are associated with cyclin D-1 induction and cell proliferation (53,54). On the other hand, JunB can antagonise the effect of c-Jun and negatively regulate proliferation as well as inducing transcription of the *CDKN2A* gene, which inhibits retinoblastoma (Rb) phosphorylation by cyclin dependent kinases (CDKs), thereby preventing G1 to S phase transition (55,56). Finally AP-1 can promote apoptosis through transcription of the gene encoding Fas-ligand and through modulation of the tumour suppressor TP53 (56).

The third MAPK cascade was first defined in a screen for drugs inhibiting TNF-α–mediated inflammatory responses (57). It is activated by cellular stress including UVR, heat shock, high osmotic stress, lipopolysaccharide, protein synthesis inhibitors, proinflammatory cytokines (such as IL-1 and TNF-*α*) and certain mitogens (58). There are 4 isoforms of p38: p38α (SAPK1), p38β (SAPK2), p38γ (ERK6, SAPK3), and p38δ (SAPK4) (59–61). Activation of p38 occurs through phosphorylation by MKK3 and MKK6 (58). In addition, p38 is activated in a MAPKK independent way through auto-phosphorylation following interaction with TAB1 (transforming growth factor-β (TGFβ)-activated protein kinase 1-binding protein) (62). The p38 pathway regulates many transcription factors such as ATF1, ATF2, ATF6, Sap1, ELK1, MEF2C, NFAT and TP53 (58,63–66). This results in production of cytokines (e.g. IL-1β, TNF-

α and IL-6), induction of enzymes such as cyclooxygenase 2 (COX-2), expression of inducible nitric oxide synthase (iNOS), which regulates oxidation, and changes to proteins associated with interaction with the extra-cellular matrix such as vascular cell adhesion molecule-1 (VCAM-1) (67–70).

1.4 Driver mutations in melanoma

Activation of the MAPK pathway is crucial to the inititation of melanoma (19). Approximately 35- 45% of patients diagnosed with melanoma harbour a mutation in *BRAF*, which results in increased kinase activity and downstream phosphorylation of MEK and ERK (71,72). Since the initial recognition that mutations in *BRAF* were important drivers of melanoma, further studies have shown a more complex picture. Approximately 20% of melanomas have a mutation in *NRAS,* which is associated with a poorer prognosis in patients with stage IV disease (73). Whole exome sequencing (WES) of 135 melanomas compared to matched germline revealed a number of mutations, which can also drive melanoma (74). These included mutations in phosphatase and tensin homolog *(PTEN),* tumour protein 53 *(TP53), CDKN2A, MAP2K1, PPP6C, RAC1, SNX31, TACC1,* and (serine-threonine kinase) *STK19* (74). Furthermore, in *NRAS* wild type (wt)/*BRAF* wt melanoma, neurofibromatosis type 1 (*NF1)* mutations were seen in 25% of tumours in this series (74).

Acral melanomas are more commonly driven by *KIT* mutations, have a higher rate of genomic amplifications than cutaneous melanoma (75) and a lower non-synonymous single nucleotide variant (nsSNV) burden, which is likely due to the lesser role played by ultra-violet radiation (UVR) (76). However the mutational signatures of most acral and cutaneous melanoma have been shown to be similar, with C>T transitions predominating (77). Mucosal melanoma has also been associated with mutations in *KIT.*

In uveal melanoma, mutually exclusive mutations have been found in *GNA11* and *GNAQ*, which drive progression (78,79). Furthermore, loss of chromosome 3 is associated with high metastatic risk and *BAP1* (BRCA1-associated protein 1) mutations are associated with metastatic disease (80). Our group has also shown that there are also mutations in *SF3B1*, which result in alternative splicing and generally a better prognosis compared to those with monosomy 3 (81).

1.5 The regulation of the MAPK pathway

In order for cells to respond appropriately to external stimuli, the MAPK pathway must be carefully regulated. A number of negative feedback loops therefore exist to control MAPK activity (82). ERK can phosphorylate growth factor receptors such as fibroblast growth factor receptor (FGFR), which down-regulates their signalling, thereby switching off potential initiating signals of the MAPK pathway (82,83).

In addition, dual-specificity phosphatases (DUSPs) play an important role in inactivating MAPKs through de-phosphorylation of threonine and tyrosine residues. There are 3 main groups depending on their location in the cell. The first group is located in the nucleus and includes DUSP1/MKP-1, DUSP2, DUSP4, and DUSP5, which de-phosphorylate ERK, p38, and JNK (DUSP5 specifically phosphorylates ERK) (82). Another group contains the p38/JNK-specific phosphatases DUSP8, DUSP10, and DUSP16 (82). The final group, which includes DUSP6, DUSP7, and DUSP9 are found in the cytoplasm and specifically phosphorylate ERK (82). Furthermore, DUSPs can tether ERK to the nucleus or the cytoplasm, thereby preventing its reactivation (84,85).

Another group of regulatory proteins are the sprouty family (SPRY), which form part of a negative feedback loop following ERK activation (82). Activation of ERK induces *SPRY* transcription, which then inhibits ERK signalling at a number of different levels in the MAPK

pathway (86). These include binding to RAF and disruption of receptor tyrosine kinase (RTK) signalling (87–89).

1.6 Protein kinase C activates the MAPK pathway

One group of positive regulators of the MAPK pathway are the protein kinase C (PKC) family. The PKC family are a large group of kinases split into 3 subgroups that have different structures and functions. The conventional PKC (cPKC) isoforms PKCα, PKCβ and PKCγ are activated by diacylglycerol (DAG) and calcium ion (Ca^{2+}) dependent phospholipid binding to their C2 domains (90,91). The novel PKC (nPKC) isoforms PKCδ, PKCε, PKCη and PKCθ are DAG sensitive but Ca^{2+} insensitive. The atypical PKC (aPKC) isoforms PKCζ and PKCι/λ have altered C1 domains and are not DAG sensitive, therefore regulation occurs through allosteric activation by an interaction of their Phox/Bem 1 (PB1) domain with the partitioning defective 6 (PAR6)–CDC42 complex (90,92).

The PKC family activates the MAPK pathway through RAS and the formation of RAS-GTP–RAF-1 complexes, which is independent of RTK activation (93). In addition to activating the MAPK pathway, the PKC family has an important role in cell migration due to their regulation of cytoskeletal dynamics (94,95) and cell polarity through formation of a complex with the polarity proteins PAR6 and PAR3 in the apex of the cell (92,96). In addition, PKC promotes c-Met trafficking along microtubules, enabling it to activate transcription factor signal transducer and activator of transcription 3 (STAT3) (97). Finally, PKCθ regulates differentiation of cluster of differentiation-4 ($CD4^+$) T cells into different T helper subsets (98). It controls the stability of the immunological synapse, which affects the strength of signalling pathways thus determining whether anergy ensues in response to weak signalling or in response to strong signalling, a T cell differentiation and effector function response (98).

1.7 PI3K-AKT pathway in melanoma

Alternative pathways such as the PI3K (phosphatidylinositol 3-kinase)-AKT (protein kinase B) pathway have been shown to be important in melanoma (99). Initial studies showed that PI3K activity regulated cellular responses to growth factors such as platelet-derived growth factor (PDGF) (100,101). Following on from this, a study of chicken cells infected with an avian retrovirus encoding an activated PI3K catalytic subunit showed that PI3K genes had oncogenic transforming potential (102). There are 3 classes of PI3K enzymes with the class I enzymes being the most extensively studied in cancer. There are four class I catalytic isoforms (p110α, β, γ, and δ encoded by *PIK3CA*, *PIK3CB*, *PIK3CG*, and *PIK3CD*) that catalyse the phosphorylation of phosphatidylinositol-4,5-biphosphate (PIP2) to generate phosphatidylinositol-3,4,5-triphosphate (PIP3) (103). The p110γ and p110δ isoforms are particularly important for immune cells (104–106). *PIK3CA* is the most commonly mutated gene of the four isoforms in cancer (107).

In melanoma, activation of the PI3K pathway occurs through a number of mechanisms. Deletions in *PTEN* or loss of PTEN expression have been shown to occur in 20-40% of melanoma (74). PTEN is a phosphatase that dephosphorylates the PI3K substrate PIP3 and as such is an important tumour suppressor (108,109). Its loss results in accumulation of activation of PIP3, which causes AKT hyper-phosphorylation and enhanced cell proliferation and survival (110). In addition, the PI3K/AKT pathway is activated by over-expression of RTKs such as PDGFR, epidermal growth factor receptor (EGFR) and growth factor receptor insulin growth factor receptor (IGFR) (100,103).

The identification of the PI3K pathway as an important driver of cancer growth and proliferation has resulted in many drug development programmes targeting PI3K isoforms. However, these have generally been impaired by toxicities such as hyperglycaemia and diarrhoea (111). More selective inhibitors such as the beta-isoform sparing PI3K inhibitor

taselisib appear to have better toxicity profiles (112). Efficacy has been largely disappointing with many drug programmes being discontinued (111). One of the ways in which efficacy may be improved is through suppression of insulin feedback mechanisms, which results in re-activation of the PI3K/AKT pathway through IGFR (113). Both ketogenic diets and drugs such as metformin were shown to improve the efficacy of the PI3K inhibitors BKM120 and BYL-719 (113). Thus, inhibition of insulin feedback mechanisms may augment the efficacy of PI3K/AKT inhibitors.

1.8 Targeted therapy in melanoma

Due to the reliance of around 50% of *BRAF* mutant melanomas on the MAPK pathway for their continued survival and proliferation, its discovery has resulted in the development of a number of treatments targeting elements crucial to its signalling (8,114,115) (Fig. 1.3). The Food and Drug Administration (FDA) has approved the BRAF and MEK inhibitior (BRAFi/MEKi) combinations vemurafenib/cobimetinib (V+C), dabrafenib/trametinib (D+T) and encorafenib/binimetinib (E+B) for use in patients with metastatic *BRAF* V600E/K mutated melanoma on the basis of phase III trial data (114–119) (Fig. 1.3). Combination V+C was shown to have improved efficacy versus single agent vemurafenib in a randomised trial of 495 patients, overall response rate (ORR) was 68% for combination treatment vs. 45% for vemurafenib alone (P<0.001) (119). Progression-free survival (PFS) was 9.9 vs. 6.2 months in the combination vs. single agent groups respectively. Interim analyses of overall survival (OS) demonstrated 9 month survival rates of 81% for combination therapy versus 73% for vemurafenib and placebo (119). Similar efficacy with a different side effect profile was seen for combination D+T vs. dabrafenib alone in a Phase III trial ORR was 67% in the D+T group vs. 51% in the dabrafenib/placebo group in 423 randomised patients (9). After 301 events, median PFS was 11 months (95% Confidence Interval (CI) 8.0–13.9) in the D+T arm vs. 8.8 months

(95% CI 5.9–9.3) in the dabrafenib only group (Hazard ratio (HR) 0.67, 95% CI 0.53–0.84; *P*= 0.0004) (120). Recently, the COLUMBUS study reported that encorafenib, a second generation BRAFi with a longer dissociation half-life than dabrafenib or vemurafenib, was more effective as a monotherapy than vemurafenib, with a median PFS of 9.6 months (95% CI 7.5–14.8)

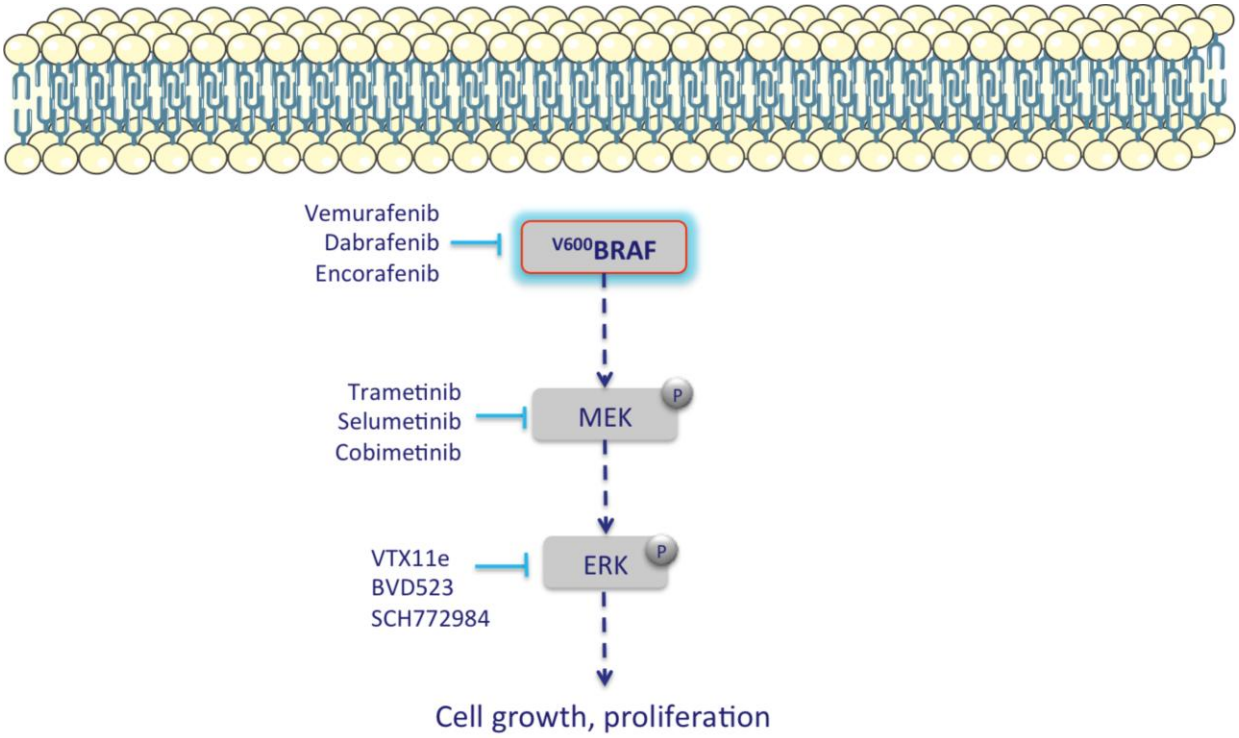

Fig. 1.3 Drugs targeting the MAPK pathway in melanoma.

versus 7.3 months (95% CI 5.6–8.2) and in combination with a MEKi inhibitor PFS was 14.9 months (95% CI 11.0–18.5) (118). This demonstrates that additional clinical benefit from targeted therapy can be obtained through optimising targeted therapy drug pharmacology and combining with multiple inhibitors.

1.9 Predictors of response to targeted therapy

A *BRAF* mutation is the most obvious biomarker of response to BRAF/MEK inhibitors (BRAFi/MEKi), however the duration of response can vary significantly. Multivariate analysis in a study examining predictors of response to vemurafenib in 300 patients identified Eastern

Cooperative Oncology Group (ECOG) performance status (PS) ≥1, immune therapy pretreatment, elevated serum LDH, age >55 years, and chemotherapy pre-treatment as independent predictors of PFS (121). The largest pooled analysis of 3 trials examining response to D+T, which included 617 patients, revealed that patients with a normal LDH and those with less than 3 sites of disease had the longest PFS (122). Additional predictors of response include day 15 18-fluorodeoxyglucose positron emission tomography (^{18}FDG PET) metabolic response (123) and high body mass index (124).

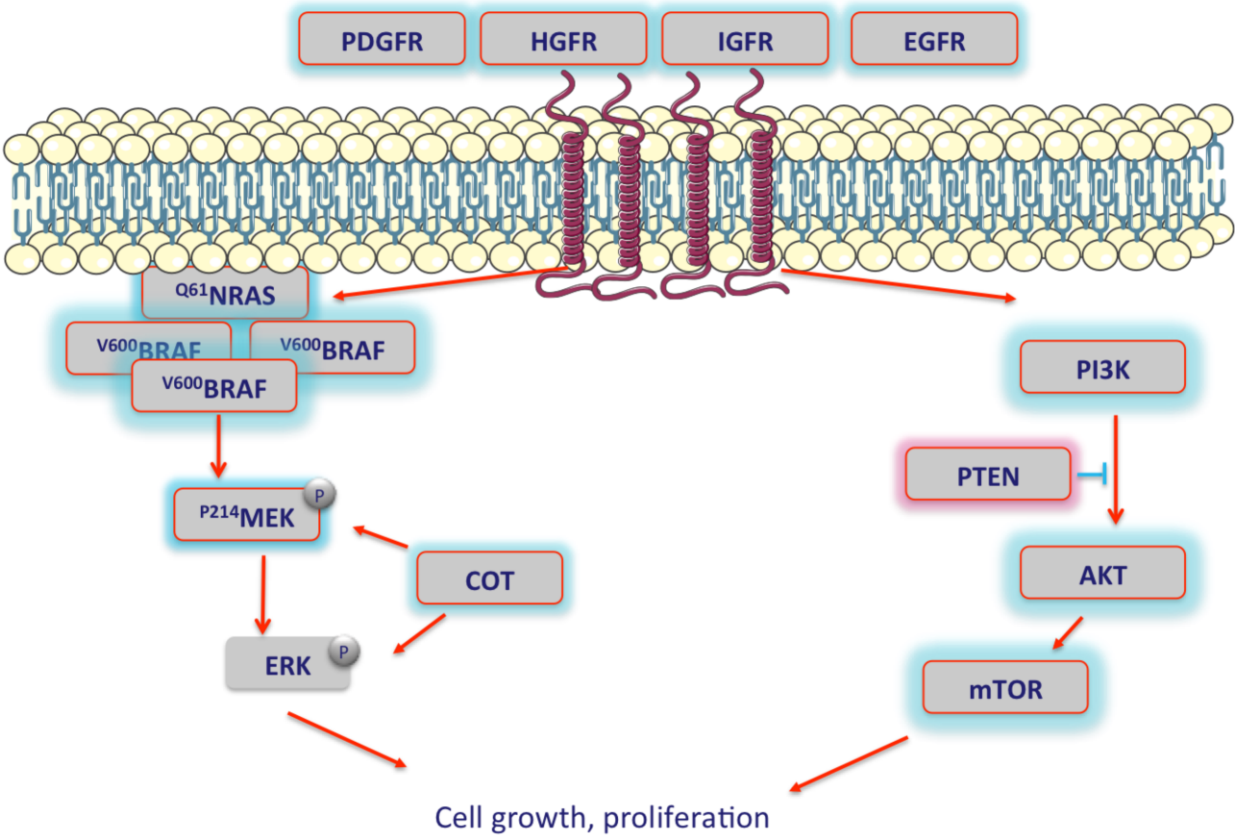

Fig. 1.4 Mechanisms of resistance to targeted therapy in melanoma. In resistance to targeted therapy, melanoma cells can up-regulate expression of tyrosine kinase receptors such as PDGFR, IGFR, EGFR and HGFR (hepatocyte growth factor receptor). Other described mechanisms include mutations in NRAS and MAP2K1, *BRAF* amplification, over expression of COT, activation of the PI3K/AKT pathway and loss of PTEN.

1.10 Resistance to targeted therapy

Resistance to targeted therapy commonly emerges through a myriad of different mechanisms (Fig. 1.4). Studies have shown resistance to BRAFi/MEKi is mediated through dimerisation of aberrantly spliced *BRAF*, amplification of mutant *BRAF*, acquisition of mutations in *RAS* or *MAP2K1*, expression of MAP3K8/COT, up-regulation of the EGFR-SRC family kinase-STAT3 signalling pathway, up-regulation of p21-activated kinase (PAK) signalling and PI3K–PTEN–AKT pathway up-regulating mutations (125–130). Whether it is important to identify emerging resistance at an early stage remains unclear. One line of thinking would be that it is necessary in order to switch to alternative treatments prior to disease outpacing available therapies. However, strategies of treating beyond progression have enabled patients to derive extended benefit from treatment (131,132).

1.11 Tools to understand treatment response and resistance in melanoma

In order to gain insight into likelihood of response to therapy, preclinical models are needed that recapitulate a patient's tumour as accurately as possible. Cell line models have limitations as they have adapted to growth outside of a normal tumour microenvironment and therefore can diverge considerably from the original tumour (133). Therefore, a number of tools have been created to aid drug development.

1.11.1 Patient derived xenografts

Patient derived xenografts (PDX) are created through implanting tumour fragments from patients directly into immunodeficient mice, fish or developing chicks (134). It is generally felt that they are superior to models derived from cell lines as they resemble the original tumour better in terms of histological features, gene expression and copy number variation (134–136). Furthermore their response to treatment has been shown to reflect the patient's clinical course

(135,136). PDXs have also been successfully used to guide therapeutic decisions resulting in disease control (135,137).

1.11.2 Circulating tumour cell derived xenografts (CDX)

Circulating tumour cells (CTCs) are cells found in the circulation that have detached from either a primary tumour or distant metastasis (138). They were first described in 1869 by Thomas Ashworth who noted cells present in the circulation were similar to tumours in a patient with metastatic disease (139). Only a very small proportion of CTCs are thought to survive in the circulation and are capable of forming metastases (140). It has been shown that if cultured tumour cell lines are injected into the circulation of mouse models, 0.1% of these will survive for 24 hours and <0.01% of these will be able to form metastases (141).

Cancer stem cells or tumour initiating cells have similar properties to normal tissue stem cells in that they are capable of self-renewal and multipotency (142). Since Fidler's ground breaking hypothesis that only a small population of cells are capable of surviving in the circulation and forming metastases, associations of these cells with cancer stem cell features have been established (141,143,144). Subpopulations of CTCs with stem cell phenotypes have been identified (144,145). In addition, wingless-integration-1 (WNT) signalling pathways that regulate self renewal have been shown to be enriched in pancreatic CTCs (142,146).

The ability of CTCs to initiate tumours has been shown in mouse xenograft models (CDX). CTCs from patients with metastatic breast cancer have been injected into the femurs of immunocompromised mice, which developed bone, liver and lung metastases (147). A CTC count of >1000 was required in order for successful implantation and only 4/110 patients had successful engraftments (147). Metastases in the CDX had the same receptor status (ER, PR and HER2) as the human tumours (147). CDXs derived from patients with metastatic small cell lung cancer have been shown to have a similar pathological and immunohistochemical

phenotype to corresponding tumour biopsies from the patients from which they are derived (148). Furthermore the take rate compared to the breast cancer model is much higher with an engraftment rate of 47% compared to 5%. In addition, CDXs from 2 patients had a similar genotype to CTCs from the same patients isolated using CellSearch/DEPArray followed by whole genome sequencing and copy number aberration analysis (148). When treated with cisplatin/etoposide, the CDX tumours mirrored the responses of their corresponding patients (148).

1.12 Phenotypic switch in melanoma

One of the fundamental characteristics of melanoma is its ability to transition between different transcriptional and phenotypic programmes – termed phenotypic switch (149,150). One of the key regulators of the phenotypic switch is microphthalmia-associated transcription factor (MITF) (150,151). MITF controls the differentiation of pleuripotent neural crest stem cells into melanoblasts (152). During development, when melanoblasts reach the epidermis they differentiate into pigmented melanocytes (153). On the other hand, those that arrive at the hair follicle become either MITF-positive depending on down-regulation of the transcription factor SOX10 (an activator of MITF) and their expression of TGFβ, which down-regulates MITF expression (154–156). In contrast, both WNT signalling and p38 activity can up-regulate MITF expression and promote melanoma stem cell activation and differentiation (157–159).

At any one time, melanoma cells may exist in at least 3 different states; invasive, proliferative and differentiated (153). Recently a further neural crest stem-cell like (NCSC) phenotype has been proposed, which is associated with minimal residual disease (MRD) in the setting of tolerance to BRAFi/MEKi (160). Differentiated cells are non-proliferative, express MITF, are non-invasive and pigmented (150). The proliferative state is associated with expression of MITF, however also expression of genes associated with proliferation and

survival such as CDK2 and BCL2 (149,161,162). The invasive state is associated with low levels of MITF, depigmentation and increased ability to metastasise (149,150). Finally the NCSC phenotype also has low expression of MITF, but is associated with high expression of NCSC markers, including NGFR, AQP1, GFRA2 and SOX10 (160).

The phenotypic switch has been shown to be important in targeted therapy drug resistance. Primary resistance to an ERK inhibitor (ERKi) has been associated with high levels of MITF. However in acquired resistance, MITF can be increased or decreased (163). Loss of MITF occurs at the messenger RNA (mRNA) level and is associated with a phenotypic switch from a proliferative to the invasive EMT phenotype (163). Furthermore, loss of MITF is associated with increased expression of RTK such as AXL, EGFR, and PDGFRβ (163).

1.13 Drug holiday approaches in targeted therapy

When cancer cells become resistant to drugs targeting the MAPK pathway, an intriguing phenomenon called drug addiction can develop (164–166). Cells resistant to BRAFi/MEKi become addicted to those very drugs (164–166). The phenomenon was first described by Das Thakur *et al* in the context of vemurafenib resistance (167). They noticed a loss of fitness when drug was removed from drug resistant cells of PDXs (167). Following from this it was also shown that cells resistant to D+T also lost fitness upon drug withdrawal (168).

The mechanism by which this occurs was recently described in two papers (165,166). The first used a clustered regularly interspaced short palindromic repeats (CRISPR) and CRISPR-associated protein 9 (Cas9) screen on drug resistant, addicted cells to identify genes that if disrupted would result in increased survival of drug addicted cells when drug was withdrawn. They found that targeting ERK2, JunB and MEK1 resulted in survival of drug addicted cells upon drug withdrawal (165). This was then confirmed *in vivo* through silencing of *ERK2* and *JUNB* in cells, injecting them into mice and showing that the tumours continued to

grow when drug was withdrawn, whereas the control tumours regressed. In addition, they showed that there was ERK rebound upon withdrawal, which resulted in the drug addiction phenotype. This activated transcription factors such as JunB, resulting in transcriptional reprogramming and a phenotypic switch. As the transcription factor MITF is associated with phenotypic switching, they investigated whether its targets were down-regulated upon drug withdrawal (165). The gene targets were down-regulated and AXL, which is inversely correlated with MITF expression was increased in these cell lines. Finally, they showed that the phenotypic switch was associated with up-regulation of fibronectin and down-regulation of e-cadherin which are associated with EMT and increased invasion (165). Accordingly, cells that were drug addicted, were highly migratory upon drug withdrawal (165).

These data were confirmed by another group who showed that ERK hyperactivation following drug withdrawal resulted in either apoptosis or slow-cycling of drug addicted cells (166). They showed that ERK hyperactivation resulted in DNA damage and PAR cytoplasmic localisation (166). By treating cells with an ataxia-telangiectasia mutated (ATM) or poly (ADP-ribose) polymerase (PARP) inhibitor, they showed that this synergised with the DNA damage response upon drug withdrawal in drug addicted cells, causing even the slow-cycling predominant cells to die (166).

1.14 Checkpoint blockade in melanoma

In order to prevent auto-immunity, mechanisms of immune tolerance have developed, which maintain immune responses within a physiological range (169). Immunological tolerance can either be central or peripheral. Central tolerance is mediated by thymic selection of high-affinity self-reactive clones (170). Peripheral tolerance occurs through a number of mechanisms including regulatory T cells (T_{reg}), T-cell anergy, cell-extrinsic tolerogenic signals, and peripheral clonal deletion (169,171–173). Cancer cells have taken advantage of these

mechanisms in order to escape the immune system. One of the major mechanisms cancer cells use to avoid T cell mediated death is by up-regulation of immune checkpoints (Fig. 1.5). There are a huge number of different checkpoint molecules expressed by cancer cells (169,174), so I will focus on cytotoxic T-lymphocyte antigen-4 (CTLA-4) and programmed death-1 (PD-1), as their inhibitors are the furthest in clinical development.

CTLA-4 enables tumour cells to escape immune recognition through inhibiting T cell activation and reducing T cell function or proliferation (175,176). CTLA-4 is expressed on the surface of $CD4^+$, $CD8^+$ and T_{reg} cells (171,177). CTLA-4 is immediately up-regulated following engagement with the T cell receptor (TCR), with its expression peaking 2 to 3 days after activation (175,178). It competes with the co-stimulatory molecule CD28 for binding to B7-1 and B7-2, which are expressed on the surfaces of antigen presenting cells (179,180). Once bound, an inhibitory signal is produced that blocks the T cell response (181). It was shown that blocking this negative regulation caused tumour rejection (176).

Ipilimumab, a CTLA-4 inhibitor, was the first treatment to show a survival benefit in patients with MM (11,182). A phase III study of ipilimumab with or without glycoprotein 100 peptide vaccine versus placebo in 676 patients reported a median OS of 10.1 months for ipilimumab versus 6.4 months for placebo; HR for death 0.68 (P<0.001) (11). ORR in the ipilimumab alone group was 10.9%, with 28.9% achieving disease control (complete response (CR), partial response (PR) or stable disease (SD)) (11). Interestingly of the patients who

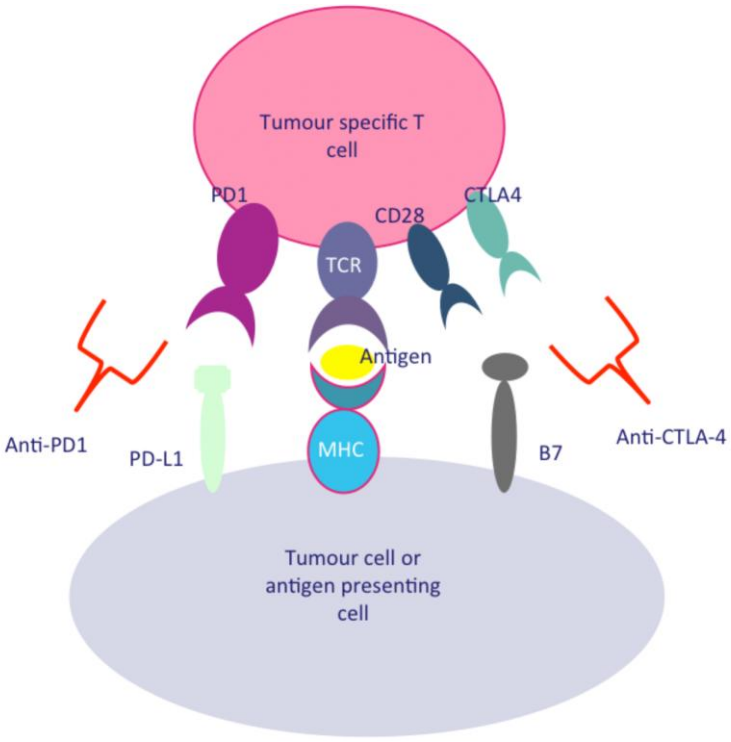

Fig. 1.5 Immune checkpoints. Tumour cells cause T cells to become anergic through PD-1/PD-L1 or CTLA-4/B7 checkpoints.

responded, 60% maintained an objective response for at least 2 years, raising the possibility of durable remissions in a disease that previously had a dismal outlook (11).

Subsequently, programmed death receptor 1 (PD-1) and programmed death receptor ligand 1 (PD-L1) antibodies were developed, which inhibit the PD-1 and PD-L1 immune checkpoints. They have a different mechanism of action compared to ipilimumab (183,184). PD-1 is expressed on the surface of T cells, B cells and monocytes and binds to PD-L1 and PD-L2, which are expressed on the surface of antigen presenting cells as well as normal cells and tumour (185–187). Upon engagement with PD-L1 and PD-L2, PD-1 transmits a negative co-stimulatory signal through the tyrosine phosphatase src homology phosphatase 2 (Shp2), which was originally thought to block T cell activation (188). However other mechanisms may be affecting this as it has recently been shown that mice with Shp-2-deficient T cells do not have a significant improvement in controlling tumours and do not have improved responses to anti-PD-1 treatment (189). The main mechanism of action of anti-PD-1 therapies is to reinvigorate exhausted T cells so they can mount an immune response to tumour (190,191). It appears that PD-1 antibodies are most effective in tumours that have already elicited a T cell response, which has become exhausted, however this is not always the case as responses can also be achieved in PD-L1 negative tumours (192).

The identification of the PD-L1/PD-1 axis as important for T cell responses to cancer cells led to two therapies gaining FDA approval: pembrolizumab and nivolumab. The Phase III Checkmate 066 trial randomised 418 treatment naïve, *BRAF* wild-type patients to receive either nivolumab (3mg/kg) or DTIC (193). It showed an ORR of 40.0% (95% CI, 33.3 to 47.0) in the nivolumab group versus 13.9% (95% CI, 9.5 to 19.4) in the DTIC group (193). Median PFS was 5.1 months in the nivolumab group versus 2.2 months in the DTIC group (HR 0.43; 95% CI, 0.34 to 0.56; P<0.001) (193). The 1 year OS rate was 72.9% (95% CI, 65.5 to 78.9) in the nivolumab group, as compared with 42.1% (95% CI, 33.0 to 50.9) in the DTIC group (HR 0.42;

99.79% CI, 0.25 to 0.73; P<0.001) (193). Similar results were obtained in Phase III trials of pembrolizumab with a response rate of 32.9% vs. 11.9% for ipilimumab and 1 year survival rate of 68.4% for pembrolizumab vs. 58.2% for ipilimumab (HR 0.69; 95% CI, 0.52 to 0.90) (194).

Following on from this, the Checkmate 067 study randomised 945 previously untreated patients to combination nivolumab and ipilimumab (N+I) vs. ipilimumab alone or nivolumab alone (195). The ORR was 43.7% (95% CI, 38.1-49.3) in the nivolumab group, 57.6% (95% CI, 52.0-63.2) in the N+I group, and 19.0% (95% CI, 14.9-23.8) in the ipilimumab group with time to objective response approx. 2.8 months for all groups (195). Median PFS was 11.5 months (95% CI, 8.9-16.7) with N+I, compared to 2.9 months (95% CI, 2.8 to 3.4) with ipilimumab (HR for death or disease progression, 0.42; 99.5% CI, 0.31 to 0.57; P<0.001), and 6.9 months (95% CI, 4.3 to 9.5) with nivolumab (HR compared to ipilimumab, 0.57; 99.5% CI, 0.43-0.76; P<0.001) (195).

Gains in efficacy have come at the expense of toxicity, with 10-15% of patients treated with ipilimumab experiencing grade 3/4 adverse events (AE) the majority of which are immune related, most commonly affecting the gastrointestinal tract and skin (11). There were 14 treatment related deaths in the first phase III trial reported, which improved in later trials due to greater clinician experience in managing toxicity and implementation of stringent protocols (11,182). Anti-PD-1/anti-PD-L1 antibodies have a more favourable, slightly different toxicity profile with more endocrine and respiratory AEs, however grade 3/4 events were still seen in 9% of patients treated with nivolumab in a phase III trial (196). Furthermore, Phase III results of combined N+I were associated with grade 3/4 toxicity in 55% of patients, which although generally reversible (apart from endocrine associated toxicity), impacts greatly on quality of life. It is therefore imperative that biomarkers are identified, which can predict response to checkpoint inhibitors so that patients are not given ineffective yet toxic treatments.

1.15 Predicting response to checkpoint blockade

In order to stratify patients better, a number of attempts have been made to identify biomarkers, which predict response to immune therapy. These can be broadly categorised into circulating, tumour-associated and microenvironment-associated biomarkers.

1.15.1 Circulating biomarkers

A number of potential biomarkers have been proposed which can predict response to immune checkpoint blockade. An absolute lymphocyte count (ALC) >1000μL at start of treatment and an increase in ALC following 2 treatments has been shown to predict response to ipilimumab (197,198). A study examining predictors of response in 95 patients showed decreased levels of LDH, C-reactive protein (CRP), and circulating T_{reg} and increased ALC between baseline and week 12 were significantly associated with survival (199). Another study showed that response to pembrolizumab was associated with an imbalance between T cell reinvigoration and tumour burden. They found that higher pre-treatment Ki67 levels in PD-1^+ $CD8^+$ T cells were an indicator of poor prognosis and correlated with higher tumour burden. In addition, at the peak T cell response 6 weeks following treatment the $Ki67^+$ $CD8^+$ T cells to tumour burden was associated with better clinical outcomes.

1.15.2 Tumour-associated biomarkers

There has been a huge interest in understanding how PD-L1 expressed by tumour cells is associated with response to anti-PD-1 and combination therapy. PD-1 is expressed on T cells and binds to the ligand PD-L1 on tumour cells in order for an inhibitory signal to occur. Initial results from a phase I study investigating the anti-PD-1 therapy nivolumab, 25/42 patients had biopsies positive for PD-L1 expression by immunohistochemical analysis and of these 36% achieved a response, whereas no responses were seen in those patients negative for PD-L1

(200). PD-L1 expression was therefore proposed to be a predictive biomarker. However, further investigation has shown a more complex picture.

Phase III trials have shown that lack of PD-L1 expression does not rule out response to treatment with anti-PD-1 therapy in melanoma, however tumours expressing PD-L1 are more likely to respond (195,196). Moreover, PD-L1 expression appears to be a dynamic process, which can be affected by drugs (such as ipilimumab) and changes in the microenvironment (201). Finally, further work is required to fully optimise and standardise the antibodies used in the immunohistochemical analyses as there is much variation in practice.

An important tumour-associated biomarker has been derived from neoepitope analysis of tumours. Neoepitopes are antigens which have arisen in the tumour due to a mutation (202–204). Figure 1.6 shows how neoantigens are predicted using WES and predictive algorithms based on prior research defining interactions between peptides and major histocompatibility class I (MHC) receptors. Snyder *et al* were able to show that mutations in genes resulting in neoantigen formation (validated by the method shown in Fig. 1.6) could predict whether a patient responded to ipilimumab (202). Furthermore Rizvi *et al* have shown that response to anti-PD-1 therapy correlates with tumours that possess a molecular smoking signature, higher tumour mutational, higher neoantigen burden and DNA repair pathway mutations in non-small cell lung cancer (205). Since these studies were published, further work has revealed a more complex picture. McGranahan *et al* showed that the type of neoantigen is important to response to checkpoint inhibitors (206). Patients with higher numbers of clonal neoantigens compared to subclonal neoantigens were more likely to respond to both CTLA-4 and PD-1 inhibitors (206). These data have recently been further validated in a large study of 249 tumours from 6 different cancers treated with different checkpoint inhibitors (207). Patients with a large proportion of subclonal mutations (>50%), were significantly more likely to have progressive disease ($P = 0.0014$), which was a much better predictor than tumour mutational burden (207). Studies

with greater power and standardised pipelines will be required to gain an in depth understanding of the contribution and validity of these potential biomarkers.

One of the potential uses for neoantigens is personalised cancer vaccines, which use the individual neoantigen repertoire to develop vaccines inducing T cell responses against the tumour (208–210). One of the potential benefits of this approach is that the antigens are not shared by normal cells and therefore on-target, off-tumour toxicities are likely to be less.

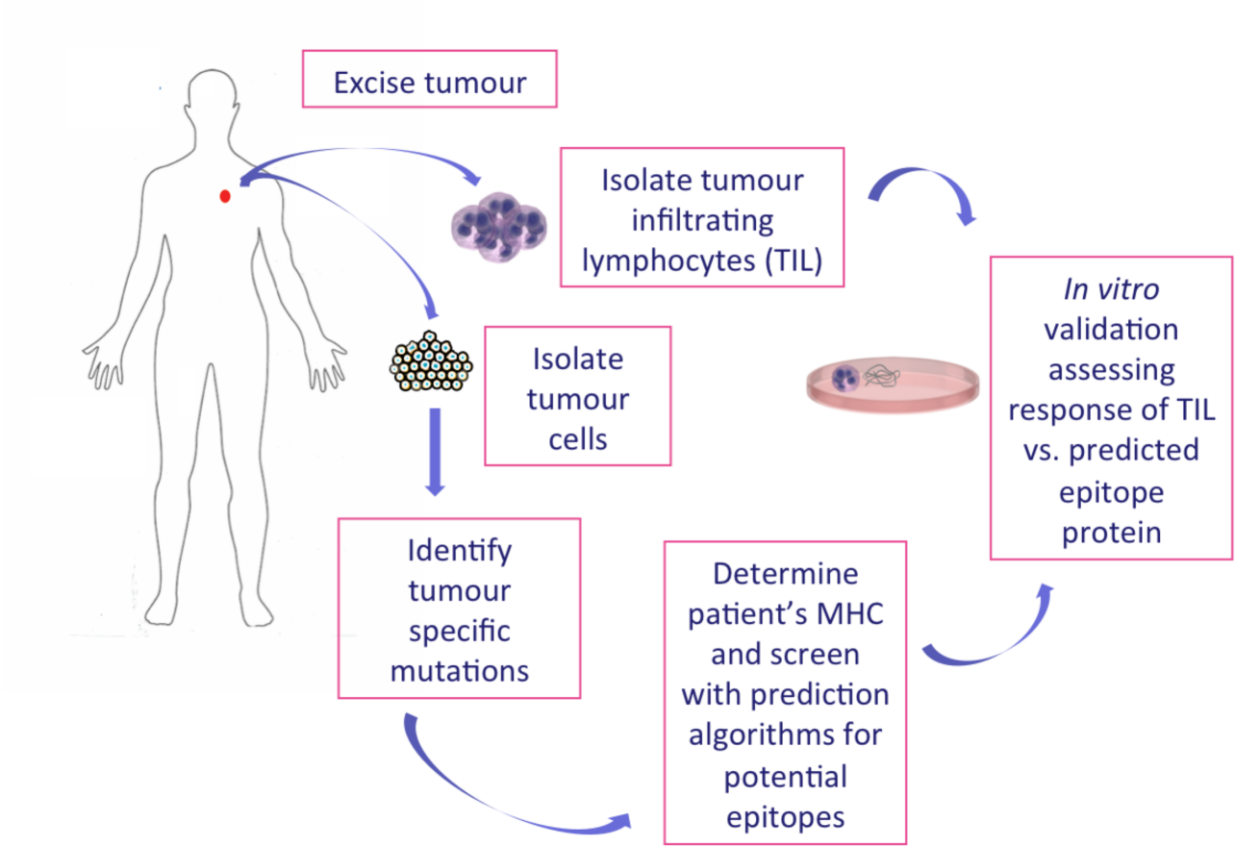

Fig. 1.6 Method to identifiy neoantigens. Tumours are excised, WES is performed and non-synonymous mutations are identified that are screened for their potential as epitopes *in silico*. In order to validate them, the response of T cells to the predicted peptide is evaluated *in vitro*.

1.15.3 Microenvironment associated biomarkers

An elegant study by Tumeh *et al* revealed through quantitative immunohistochemistry and multiplex immunofluorescence that increased numbers of pre-existing $CD8^+$ T cells located

at the tumour invasive margin could predict response to immune therapy. Furthermore in serially sampled tumours, proliferation of intratumoral $CD8^+$ T cells during treatment directly correlated with radiographic reduction in tumour size (211). T cell infiltration into tumours has been shown to increase in response to treatment with anti-CTLA-4 and PD-L1 therapy (212–214). However increased T cell infiltrates could not be correlated with response to the CTLA-4 inhibitor tremelimumab, suggesting that other factors possibly in combination with T cell invasion are required for clinical benefit (212). The involvement of the tumour microenvironment in response to immune therapy is likely to be very complex and the interplay of other immune components such as macrophages, natural killer cells and dendritic cells requires further investigation.

Despite all these studies, currently there is no observation on its own or in combination with other predictors that has been shown to be sufficient to direct clinical decisions in melanoma. At present, it is unlikely that patients with melanoma will be excluded from immune therapy as a treatment option based on a biomarker.

1.15.4 Resistance to checkpoint blockade and immune therapy

In addition to examining biomarkers of response to checkpoint inhibitors, a number of groups have investigated mechanisms of resistance. One of the ways in which melanoma can become resistant to immune checkpoint inhibitors is through loss of response to interferon-γ (IFNγ) signalling and decreased antigen presentation (215). A study examining paired biopsies of melanoma from 4 patients that had initial tumour regression followed by progression revealed that acquired resistance was associated with mutations in Janus kinase 1 or 2 (JAK1/JAK2), which resulted in decreased response to IFNγ (215). In addition, they found a mutation in beta-2-microglobulin (B2M) in another patient that conferred loss of expression of MHC class I (215).

One of the other reported mechanisms of resistance is loss of PTEN, which results in activation of the PI3K/AKT pathway, reduced autophagy in response to T cell stimulation, and decreased tumour infiltrating lymphocytes (216). In addition, up-regulation of the WNT/β-catenin pathway leads to decreased recruitment of dendritic cells due to reduced expression of the chemokine CCL4 (214). Decreased antigen presenting capability then leads to decreased T cell infiltration and an immune "cold" tumour (214). Furthermore, epigenetic modulation may lead to changes in the expression of immune related genes, which can result in resistance to immune therapy (217). These can be modified through treatment with a histone deacetylase inhibitor (HDACi), which have been shown to increase tumour antigen expression, resulting in improved response of tumours to adoptive T cell therapy *in vivo* (218).

Production of immune-mediators by the tumour or cells within the microenvironment such as fibroblasts can modulate the microenvironment, resulting in immune escape and decreased response to checkpoint inhibitors. COX expression and production of prostaglandin E_2 (PGE_2) can result in a tumour promoting microenvironment (219). Both COX2 and PGE_2 have been implicated in key aspects of malignant progression such as proliferation, survival, invasion, angiogenesis and immunosuppression (220). Abrogation of the ability of cancer cells to produce PGE_2 impairs their potential for sustained growth in immunocompetent but not immunodeficient mice, underscoring an essential role for tumour cell-derived PGE_2 in immune escape (219). COX deficiency in cancer cells was associated with a marked shift in the inflammatory signature at the tumour site characterised by lower expression of cancer-promoting factors (e.g. IL-6, Granulocyte-colony stimulating factor (G-CSF) or chemokine (C-X-C motif) ligand 1 [CXCL1]) and concomitant increase in several mediators typically associated with anti-tumour immunity including T-bet, CXCL10 and perforin-1 (219). Inhibition of COX1 and COX2 by aspirin synergised with anti-PD-1 therapy resulted in enhanced tumour responses *in vivo*.

Another cytokine, which results in an immune suppressive microenvironment is TGFβ. Recently, two publications revealed the contribution of TGFβ to immune exclusion and decreased response to checkpoint inhibitors (213,221). Mariathasan *et al* found that lack of response to PD-1 inhibitors was associated with a TGFβ signature in fibroblasts with exclusion of T cells (213). The addition of a TGFβ inhibitor to anti-PD-L1 therapy resulted in TGFβ mediated changes in stroma, increased T cell penetration and resulted in tumour regression (213). Tauriello *et al* also showed that T cell exclusion was associated with increased production of TGFβ in the stroma of micro-satellite stable colorectal cancers (221). They showed that treatment with a TGFβ inhibitor resulted in decreased metastatic potential of mouse colorectal tumour organoids (221). Furthermore, the combination of TGFβ inhibition and anti-PD-L1 therapy resulted in improved regression of liver metastases (221).

Resistance to immune therapy may also occur through infiltration by tumour promoting cells. Increased infiltration of tumours by macrophages has been associated with decreased response to immune checkpoint blockade (104,105,222). Two groups have also shown that selective inhibition of PI3Kγ, which is highly expressed in myeloid cells, results in a switch from M2 alternatively activated macrophages associated with tumour promotion, to M1 macrophages, which are associated with a more immune responsive environment (104,105). Accordingly, a PI3Kγ inhibitor synergised with anti-PD-1 therapy to increase T cell infiltration and tumour regression (104,105).

T_{reg} cells also contribute to immune escape and tumour resistance to immune therapy (217,223). High numbers of T_{reg} cells compared to T effector cells within the tumour has been associated with decreased response to checkpoint inhibitors (224,225). Depletion of T_{reg} cells using an anti-CD25 antibody with enhanced binding to activating inhibitory Fc_{γ} receptor ($Fc_{\gamma}R$) IIb resulted in increased infiltration by T effector cells (223). Combining the antibody with anti-PD-1 therapy resulted in complete regression of tumours (223).

1.16 Adjuvant therapies in melanoma

The first study to show the benefit of adjuvant therapy (treatment following curative intent surgery) was the EORTC 18071 study which randomised 951 patients with completely resected stage III melanoma (excluding lymph node metastasis ≤1 mm) to ipilimumab versus (vs.) placebo. It demonstrated improved relapse-free survival (RFS) in patients receiving ipilimumab compared to placebo with a HR of 0.75 (0.64–0.90 P= 0.0013) (226). Toxicity in this setting was concerning as 52% of patients discontinued treatment due to adverse events with 38.6% discontinuing within 12 weeks and there were 5 (1.1%) treatment related deaths (226).

Following from that study, Checkmate 238 compared nivolumab to ipilimumab in stage IIIB/C or resected stage IV melanoma. The 12-month rate of recurrence-free survival was 70.5% (95% CI, 66.1-74.5) in the nivolumab group (n=452) and 60.8% (95% CI, 56.0-65.2) in the ipilimumab group (n= 453, HR 0.65; P<0.001) (227). Nivolumab was better tolerated with grade 3/4 AE reported in 14.4% of the patients in the nivolumab group and in 45.9% of those in the ipilimumab group (227). The results of Checkmate 915, which compares the combination of N+I (1mg/kg which is lower than the dose used in the stage IV setting) vs. nivolumab, are awaited. Toxicity will be particularly important to assess for this combination, given the high rate of adverse events seen historically, albeit with higher doses of ipilimumab.

Targeted therapy has also shown efficacy in the adjuvant setting. The COMBI-AD trial randomised 870 patients to receive placebo or D+T for one year following curative intent surgery (228). At a median follow-up of 2.8 years, the estimated 3-year rate of RFS was 58% in the combination-therapy group and 39% in the placebo group (HR 0.47; 95% CI, 0.39 to 0.58; P<0.001). The 3-year OS rate was 86% in the combination-therapy group and 77% in the placebo group (HR 0.57; 95% CI 0.42-0.79; P=0.0006). Intriguingly, the Kaplan Meier rapidly

declines after 12 months suggesting that patients at high risk of relapse might benefit from longer duration of treatment, however this would need to be tested in future clinical trials.

No safety data on late effects have been presented, however given the incidence of endocrinopathies associated with immune therapy, it is likely these would impact on future quality of life. Similar toxicities were seen in the D+T group to those previously reported in the stage IV setting, however the rates of treatment discontinuation were higher with 26% discontinuing study drug due to AEs whereas this was 11% in the COMBI-D trial, suggesting that patients may have a lower threshold to discontinue treatment in the adjuvant setting. Therefore, it is imperative to identify sub-populations that are at higher risk of disease progression and would derive greater benefit from treatments that can have considerable toxicity.

1.17 Melanoma brain metastases

Brain metastases occur in up to 75% of patients with stage IV melanoma over the course of their disease, contributing to 20–50% of melanoma-related deaths (229). In newly diagnosed stage IV patients, brain metastases are present in approximately 20% of cases. Furthermore, they are a common site of treatment failure with early progression seen when compared to extra-cranial sites on BRAFi (230).

Hyperactivation of the PI3K/AKT pathway has been observed using reverse phase protein array (RPPA) comparing melanoma brain metastases with lesions in extra-cranial sites (231). Recent studies suggest a role for the brain microenvironment in driving PI3K/AKT activation (230,232). *In vitro* assays of both *BRAF* and *NRAS* mutated melanoma cells cultured in the presence of cerebrospinal fluid (CSF) or astrocyte conditioned media showed decreased cell viability and growth in the presence of PI3K inhibitors (230,232). Furthermore, *in vivo* models of *BRAF* and *NRAS* human melanoma cells injected into mouse brains had significantly

reduced growth when treated with buparlisib, a pan-PI3K inhibitor (232). This data has resulted in the initiation of a clinical trial (NCT02452294) evaluating buparlisib in patients with melanoma brain metastases.

Myeloid cells are of particular importance in the brain microenvironment as microglia have been shown to stimulate tumour promoting inflammation (233). There are two types of myeloid cells in the brain; resident microglia that have migrated at an early stage from erythromyeloid progenitors in the yolk sac and macrophages that have developed in the bone marrow and migrated to the brain (234,235). The populations are hard to differentiate as they have similar markers, although macrophages are associated with higher CD45 expression (236). Microglia have been shown to increase melanoma proliferation, matrix metalloproteinase-2 (MMP-2) activity enabling matrix formation, cell migration and brain endothelial penetration (237).

Despite the challenges of the brain microenvironment, recent studies have shown that patients with brain metastases can obtain benefit from targeted and immune therapies. In an open-label phase II trial, D+T has been shown to have an intra-cranial response rate of 58% (95% CI 46-69) in patients with *BRAF* mutant, asymptomatic brain metastases, with good performance status and having had no previous local brain therapy (238). Crucially, patients with symptomatic brain metastases also achieved an intracranial response (59%; 95% CI 33-82) (238).

Treatment with immune therapy has also shown a benefit for patients with asymptomatic brain metastases. The ABC (Anti-PD-1 Brain Collaboration) Phase II trial resulted in a practice change in the use of immune therapy in patients with brain metastases from melanoma (239). Sixteen of 35 patients (46%) treated with combined N+I (cohort A) and 5/25 (20%) patients treated with nivolumab monotherapy (cohort B) achieved an intracranial response (239). Only 1/16 (6%) of patients with neurological symptoms, progression after

previous local brain treatment, or leptomeningeal melanoma (cohort C) achieved an intracranial response. PFS was not reached in cohort A (95% CI 2.9–not reached), and was 2.5 months (95% CI 1.7–2.8) in cohort B (239). The benefit for N+I was confirmed in the open-label, Phase II, Checkmate 204 trial of 94 patients (240). Of note, patients with leptomeningeal disease, metastases larger than 3 cm in diameter, and those receiving steroids were excluded from the study (240). With a median follow-up of 14 months, the rate of intracranial clinical benefit was 57% (95% CI 47-68); the rate of CR was 26%, PR was 30%, and SD for at least 6 months was 2% (240). The rate of extra-cranial clinical benefit was 56% (95% CI 46-67). The rate of intracranial PFS at 6-months was 64.2% and 9-months was 59.5% (240). Taken together, these data suggest that for asymptomatic brain metastases, combination N+I can be effective, whereas D+T is likely to be a better option for patients with symptomatic brain lesions.

1.18 Circulating tumour DNA

Traditional biomarkers in melanoma include tumour related indices such as mitoses, ulceration, Breslow and circulating biomarkers such as LDH (241). Mandel and Métais first identified circulating nucleic acids in the blood stream in 1948, however it was not until 1994 that their potential utility as biomarkers for cancer detection and monitoring was realised (242). At that time, Sorenson *et al* showed the presence of mutated *KRAS* circulating tumour DNA (ctDNA) sequences in the blood of patients with pancreatic cancer whose tumours also possessed mutated *KRAS* (243). Many studies since then have examined the role of ctDNA as a "liquid biopsy" which can predict disease progression, monitor treatment response and reflect tumour resistance.

Cell-free DNA (CfDNA) is DNA that freely circulates in the bloodstream and is made up of fragments are on an average 140 to 170 base pairs (bp) long (242). CfDNA is found in the blood stream of healthy subjects at an average concentration of 30ng/ml (range 0-100ng/ml)

and in patients with cancer an average of 180ng/ml (range 0-1000ng/ml) (242). CtDNA originates from cancer cells and contributes to the total cfDNA in the blood. It can therefore increase the concentration of cfDNA when cancer is present. The concentration of cfDNA has been shown to reflect disease burden and has been shown to decrease after complete surgical resection for colorectal cancer with an estimated half-life of 114 minutes (244–246). It is thought that nucleic acids are cleared from the circulation by the liver and kidneys as well as through degradation (242). The mechanisms behind the release of cfDNA are not completely understood, however it is thought it is produced by cell necrosis, apoptosis and secretion from macrophages that have phagocytosed cells (242,247). In addition CTCs can also release cfDNA into the blood (242). Levels of cfDNA have been shown to increase 24 hours following chemotherapy in breast cancer patients and is thought to be due to cell death as a result of treatment (248).

There are a number of challenges in the analysis of ctDNA including the variability of mutated loci, allele frequency, stochastic noise and fragmented template (249,250). A number of studies have been published examining specific mutations in ctDNA, which have been observed through polymerase-chain reaction (PCR), digital PCR and digital ligation assays (145,251). These techniques require predetermined identification of targets through analysis of tumour biopsies or examining known specific common mutations for a tumour type. More recently genome wide profiling has been achieved through massive parallel shotgun sequencing (252,253). However these methods are expensive, require better quality DNA, extensive data analysis and are vulnerable to incorrect interpretation of background noise (250). Intermediate approaches have been described which enable coverage of the majority of known mutations known for a particular cancer, but do not require whole genome profiling (249,254). In this way less DNA is required, sensitivity is increased and costs are reduced (254).

There currently is no standardised approach to analysing ctDNA and until this occurs its use is likely to be limited to very specific indications and clinical trials/research. However, it is foreseeable that in the not too distant future a standard "liquid biopsy" will be taken in the clinic, which can be used to inform as to tumour burden, mutation status and the development of resistance. A number of studies have already described these possibilities and are detailed below.

1.19 Clinical applications of cfDNA

1.19.1 Monitoring disease burden, recurrence of disease and response to treatment

Through following known mutations associated with a particular cancer it is possible to follow the tumour dynamics and demonstrate disease progression. Diehl *et al* examined cfDNA in patients with colorectal cancer using BEAMing (beads, emulsion, amplification and magnetics) and showed that following surgical resection those patients who had undetectable cfDNA at first follow up visit did not have recurrence of their disease (245). All but one of 16/20 patients who had detectable cfDNA following resection recurred (245).

CtDNA has been shown to reflect disease status and tumour burden whilst on treatment for a variety of cancers. When compared to CT imaging from patients with metastatic breast cancer on treatment, ctDNA levels correlated with treatment response (255). Increase in cfDNA by on average a factor of 505 (range, 2 to 4457) from nadir also correlated with progression as determined by RECIST criteria on CT in 17/19 (89%) patients (255). CtDNA levels increased on average 5 months (range 2-9) before PD was seen on imaging (255). In 108 patients with colorectal cancer treated with cetuximab and irinotecan, disease control rate was 77% in patients with low ctDNA (<25% quartile) compared with 30% in patients with high levels (>75% quartile) which was statistically significant (P= 0.009) (256).

In melanoma, studies examining *BRAF* mutation levels in cfDNA as a measure of tumour burden have had conflicting results. Schadendorf *et al* used BEAMing to assess the association of ctDNA p.V600E *BRAF* or p.V600K *BRAF* fraction with tumour burden at baseline (as the sum of target lesion diameters) and found no correlation (257). When compared to the tumour *BRAF* mutation status, ctDNA was concordant with p.V600E *BRAF* and p.V600K *BRAF* in 77% and 96% respectively (257). In contrast, Momtaz *et al* using droplet digital PCR (ddPCR) showed that in 11 *BRAF* mutated patients the ratio of p.V600E *BRAF/BRAF* wt cfDNA was correlated with tumour burden (also measured as the sum of target lesion diameters) (244). When compared to imaging, ctDNA levels generally reflected radiological disease status although in 1 patient ctDNA levels increased despite decrease in target lesions, however they had progression in non-target bone lesions (244).

Detecting mutations in ctDNA in order to predict response to targeted treatments has been shown to be an alternative to biopsy in a number of studies (258–261). Detection of the EGFR was compared in tumour biopsies versus ctDNA in patients with NSCLC treated in the IPASS trial (260). No false positives were detected in cfDNA however the false negative detection was 56.9% (260). A recent study compared metastatic biopsies of 27 patients to ctDNA using a multiplexed next-generation sequencing panel and found that 28 out of 29 mutations identified in metastatic biopsies (97%) were also detected in matched ctDNA (262). Detection methods require further validation prior to clinical use but are a potential alternative if no tumour sample is available.

Lipson *et al* examined whether ctDNA levels corresponded to tumour burden in the context of patients undergoing treatment with immune checkpoint inhibitors and correlated with response to treatment (263). They employed two methods of cfDNA analysis – BEAMing and next generation sequencing/PCR to examine the number of mutant alleles. In 4 patients they were able to show that mutations in the tumour were reflected in the cfDNA and changes in the

ctDNA mutational burden reflected the clinical course of the patients (263). In one patient who initially clinically progressed but then responded to treatment, the cfDNA showed evidence of treatment response weeks prior to clinical regression (263). This was a retrospective study in a very small number of patients however it is a promising direction for future research.

BRAF mutant allele quantification has been used to monitor response to chemotherapy. Fifty patients with stage IV melanoma undergoing chemotherapy were assessed using quantitative real time PCR for circulating mutant p.V600E *BRAF* allele at baseline and within 4 weeks following treatment (264). The presence of circulating p.V600E *BRAF* at baseline did not significantly correlate with treatment response. However of the 20 patients who had detectable circulating p.V600E *BRAF* mutations prior to treatment, p.V600E *BRAF* was detected following treatment in only 1/10 patients who responded compared to 7/10 patients in the non-responder group ($P = 0.02$) (264). Although detecting a p.V600E *BRAF* mutation may not be useful in predicting response, its detection can be used to monitor treatment response (264). This study did not examine the relationship between quantities of mutant alleles at baseline and response to treatment.

The Spanish Melanoma group prospective study (GEM1304) is examining cfDNA levels in patients undergoing treatment with BRAFi (265). They use a quantitative 5'-nuclease PCR based assay with a clinical sensitivity of 58% and specificity of 100% to detect V600E versus wild type alleles (265). Preliminary results showed that in 4 responding patients *BRAF* mutation was not present until disease progression and in 2 patients with primary refractory disease p.V600E *BRAF* persisted despite therapy (265).

1.19.2 Prognostic biomarker

Traditionally criteria such as TNM (Tumour, node, metastasis) or AJCC staging, clinical characteristics and biochemistry/haematology have been used to assess a patient's prognosis. However a number of studies have investigated the role of ctDNA in prognostication.

A number of studies have shown correlation between staging and levels of specific mutations in ctDNA in resectable breast, ovarian, pancreatic and colorectal cancer, and oral squamous-cell carcinoma (250). Other studies have not been able to demonstrate an association, however these have often been criticised for the limited number of patients involved (250). In a small study of 41 patients with melanoma, levels of ctDNA p.V600E *BRAF* allele determined by quantitative PCR were related to AJCC stage with mean levels of 44ng/ml for stage I–II patients vs. 104.3ng/ml for stage III patients and 96.5 vs. 115.9ng/ml in plasma from stage III vs. IV patients (266). Larger studies are required to confirm these results.

Genetic mutations conferring prognostic significance have been studied in cfDNA. One example of this is the MYC-related oncogene (MYCN) in neuroblastoma. *MYCN* amplification has been shown to be a poor prognostic factor in neuroblastoma and is used to stratify treatment (267). A study of 267 patients using real time quantitative PCR showed *MYCN* DNA sequences had a sensitivity of 75%-85% depending on if stage III or IV and a high specificity (100%) when compared to tumour DNA (268). In difficult to biopsy locations such as the brain, less invasive methods of stratifying patients using ctDNA are advantageous.

1.19.3 Identification of development of and mechanisms of resistance

A promising role for ctDNA in the clinic is a tool to monitor patients for emerging resistance to treatment. In their seminal study, Murtaza *et al* demonstrated the proof of principle that ctDNA extracted from the plasma of patients over a course of treatment could be used to detect new mutations conferring resistance to therapy (269). They performed WES on patients

previously identified using TamSeq to have a high allele fraction, enabling increased sensitivity at a coverage depth of 31-160x reads (269). In 2 patients they were able to show concordance in copy number aberrations between paired tumour and plasma samples. In 6 patients, they observed the development of a number of mutations associated with resistance to therapy including an activating mutation in *PIK3CA* following treatment with paclitaxel in a patient with breast cancer and a p.T790M *EGFR* mutation on disease progression in a patient with lung cancer on gefitinib (269).

Moreover, as ctDNA from different metastatic sites intermingles in the bloodstream its analysis can give an insight into tumour heterogeneity (253,269). Using massively parallel sequencing of plasma cfDNA it has been shown that ctDNA in a patient with synchronous breast and ovarian cancers is a composite of both tumours in terms of copy number and genetic aberrations (253). Thus, there is the potential to track emerging clones, particularly ones resistant to a certain treatment. One example from the molecular oncology laboratory is a patient with mucosal melanoma which had a heterogeneous response to therapy and using ctDNA it was possible to identify two subclones; one with a *KIT* mutation that responded to imatinib and a second *KIT*-wt subclone that did not respond to imatinib (see Fig. 1.7) (270). However, both subclones responded to carboplatin/paclitaxel (270). This study revealed the power of ctDNA to understand causes of heterogeneous treatment responses without the need

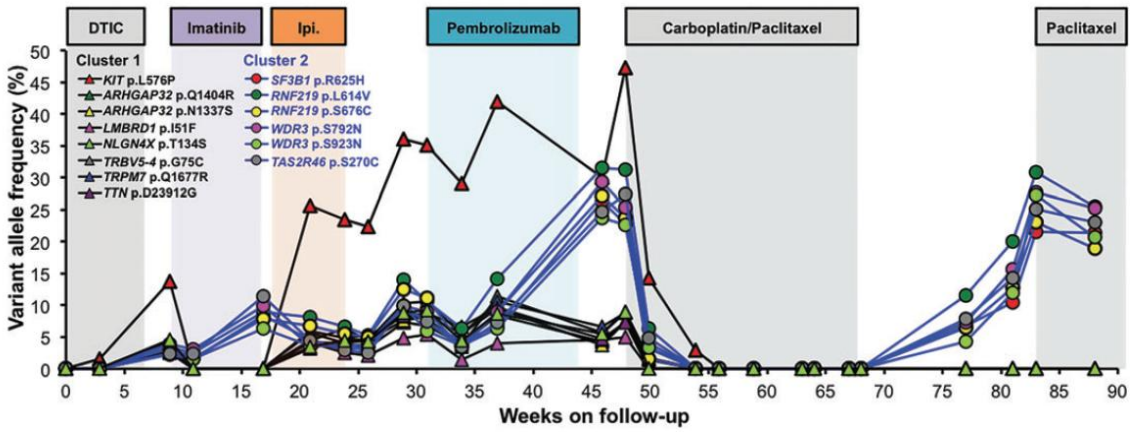

Fig. 1.7 Clonal responses to treatment is seen in ctDNA. VAFs of 14 mutations which can be grouped into 2 clusters, associated with 2 clones that responded differently to targeted and immune therapy. Both clones responded to treatment with carboplatin/paclitaxel (270).

multiple tumour biopsies (270). Therefore, it is possible to identify emerging resistant subclones in patients undergoing treatment for cancer, which could be a useful tool for the clinic.

1.20 Aims of Thesis

The overall focus of this thesis is to develop precision medicine strategies to treating melanoma. The following chapters outline a number of challenges, which must be overcome in order to improve outcomes for patients with melanoma. Furthermore, I investigate different approaches to overcoming resistance and exploiting vulnerabilities in melanoma biology. Finally, I propose ways in which these findings could be translated back to the clinic in order to realise precision approaches to melanoma therapy.

The following aims addressed in this thesis are:

- To understand mechanisms of resistance to therapy through use of patient-derived samples.
- To explore combination strategies targeting potential mechanisms of emerging resistance to a novel pan-RAF inhibitor CCT3833.
- To investigate whether resistance to CCT3833 results in the drug addiction phenotype and if so to gain further insight into the mechanisms of drug addiction.
- To investigate whether ctDNA can be used to predict whether patients are at high risk of relapse following curative intent surgery.
- To develop clinical trials investigating ways in which ctDNA can be used to aid clinical decision-making.

Chapter 2. Methods

2.1. Ethical considerations for collection of patient samples

Patient samples were collected with written full-informed patient consent under Manchester Cancer Research Centre (MCRC) Biobank ethics application #07/H1003/161+5 and approval for the work under MCRC Biobank Access Committee application 13_RIMA_01. Healthy volunteers were consented as part of study protocol ethics/12324 given favourable ethical opinion by the University of Manchester Senate Ethics Committee. For the retrospective ctDNA study (chapter 5), samples were collected as part of the AVAST-M trial (ISRCTN 81261306), which compared bevacizumab vs. placebo in 1,343 patients with resected high risk stage II/III melanoma (271).

2.2. Buffers and solutions

2.2.1 Immunoblotting

- **Cell lysis buffer** 10x (#9803 Cell Signalling Technologies (CST) Leiden, Netherlands) diluted to 1x in ddH20 with 1% protease inhibitor (#87786 ThermoFisher Altrincham UK) and 1% phosphatase Inhibitor (#78420 Thermofisher, Altrincham UK) added.
- **Bradford assay** Pierce™ Coomassie Plus (Bradford) Assay Kit (#23236 Thermofisher, Altrincham UK).
- **Molecular weight marker** Full-range rainbow molecular marker (#RPN800E GE Healthcare, Chalfont, UK)

2.2.2 Crystal Violet (0.5%)

- 500 mg Crystal Violet (#C3886 Sigma Aldrich, Gillingham UK)
- 25 ml Methanol

- 75 ml Water

2.2.3 Sulforhodamine B (SRB) solution

- 5g SRB (#3520-42-1 Sigma Aldrich, Gillingham UK) in 1250 mL 1% acetic acid

2.2.4 Reverse Phase Protein Array (RPPA) solution

- **Lysis Buffer**: 1% Triton x100, 50mM HEPES, pH 7.4, 150mM NaCl, 1.5mM $MgCl_2$, 1mM EGTA, 100mM NaF, 10mM Na pyrophosphate, 1mM Na_3VO_4, 10% glycerol, containing freshly added protease and phosphatase inhibitors (#05056489001 and #04906837001 respectively, Roche, Burgess Hill UK)
- **4x SDS Sample Buffer**: 40% Glycerol, 8% SDS, 0.25M Tris-HCL, pH 6.8. Before use, β-2-mercaptoethanol at 1/10 of the volume was added

2.2.5 PamGene

- **Lysis buffer** M-PER Mammalian Protein Extraction Reagent (#78501 Thermofisher, Altrincham UK)
- **Protease inhibitors** (#87786 Thermofisher, Altrincham UK)
- **Phosphatase Inhibitor** (#78420 Thermofisher, Altrincham UK)

2.2.6 Circulating tumour derived xenograft (CDX) solution

10ml HITES Media

- 10ml RPMI, phenol red free (#11835030 Thermofisher, Altrincham UK)
- 5µl 10 mg/ml insulin, (#I9278 Sigma Aldrich, Gillingham UK)

- 10µl 10 mg/ml transferrin, (#T8158 Sigma Aldrich, Gillingham UK) made in Hank's balanced salt solution (HBSS; #14185052 Thermofisher, Altrincham UK)
- 10µl 10 µM β-estradiol, (#E2758 Sigma Aldrich, Gillingham UK) made in 95% ethanol (EtOH)
- 10µl 30 µM Na Selenite (#S5261 Sigma Aldrich, Gillingham UK) made in HBSS
- 10µl 10 µM hydrocortisone (#H0888 Sigma Aldrich, Gillingham UK) made in 95% EtOH

80ml 90% HBSS/10% HITES

- 8ml 10x stock HBSS (#14185052 Thermofisher, Altrincham UK)
- 8ml HITES media
- 64ml ddH_2O

2.2.7 Media

- Roswell Park Memorial Institute medium (RPMI) 1640 Medium (#11875093 Thermofisher, Altrincham UK)
- Dulbecco's Modified Eagle Medium (DMEM), high glucose, pyruvate (#41966029, Thermofisher, Altrincham UK)
- Media was supplemented with 10% Fetal bovine serum (FBS; Thermofisher, Altrincham UK) and 100 units/mL penicillin and 100 µg/mL streptomycin (Thermofisher, Altrincham, UK)

2.2.8 Cell lines

Table 2.1 Cell lines and culture conditions

Cell line	Source	Catalogue number	Culture media
A375	ATCC	CRL-1619™	DMEM
A375-MA2 (A375M)	ATCC	CRL-3223™	DMEM
D04	Institute of cancer research	-	RPMI
COLO829	ATCC	CRL-1974™	RPMI
WM266.4	ATCC	CRL-1676™	DMEM
SKMEL28	ATCC	HTB-72™	DMEM
RM2	Patient	-	RPMI
RM11 PDX	Patient (PDX)	-	RPMI
RM26 (Subcutaneous)	Patient	-	RPMI
RM26 (Brain)	Patient	-	RPMI
RM33	Patient	-	RPMI
RM44	Patient	-	RPMI
RM62T3	Patient	-	RPMI
RM57 CDX	Patient (CDX)	-	RPMI
RM156 CDX	Patient (CDX)	-	RPMI
RM49 PDX	Patient (PDX)	-	RPMI
RM59	Patient	-	RPMI
RM72	Patient	-	RPMI
RM81	Patient	-	RPMI
RM103	Patient	-	RPMI
RM209	Patient	-	RPMI

2.2.9 Bacterial strains

- *Escherichia coli (E.coli)* strain JM109 cells (#L2005 Promega, Southampton UK)

2.2.10 Plasmids

- gRNA cloning plasmid (Addgene #41824 (272))
- pST1374-NLS-flag-linker-Cas9 (Addgene #44758 (273))

2.2.11 Inhibitors

All inhibitors were solubilised in dimethyl sulfoxide (DMSO).

Table 2.2 Inhibitors and main targets

Reagent	Supplier	Catalogue number	Type
Dabrafenib Mesylate (GSK2118436B)	ChemieTek[1]	CT-DABR	BRAF inhibitor
PLX4720	3WayPharm Inc	SWP-03022	BRAF inhibitor
CCT3833	Prof. Caroline Springer	-	Pan Raf inhibitor
Taselisib	Sellekchem[3]	S7103	PI3Kinase inhibitor
BEZ235	Sellekchem[3]	S1009	PI3Kinase/mTOR inhibitor
SCH772984	Sellekchem[3]	S7101	ERK 1/2 inhibitor
JNK-IN-8	Sellekchem[3]	S4901	JNK 1/2/3 inhibitor
SB203580	Sellekchem[3]	S1076	p38 inhibitor
Phorbol 12-myristate 13-acetate (PMA)	Sigma-Aldrich[4]	P8139	PKC agonist
Bryostatin-1	Sigma-Aldrich[4]	83314-01-6	PKC agonist

1 = Indianapolis, USA, 2= Shanghai, China 3 = Ely UK, 4= Gillingham UK

2.2.12 Drug screen

- Kinase Inhibitor Library L1200-SEL-250µl/well (SelleckChem, Ely UK)

2.2.13 Antibodies

2.2.13.1 Primary antibodies

Table 2.3 Primary antibodies

Primary antibody	Host	Manufacturer	Catalogue number	Dilution factor
MEK1/2 (L38C12)	Mouse	CST[1]	4694	1:1000
Phospho-MEK1/2 (Ser217/221)	Rabbit	CST[1]	9154	1:1000
p44/42 MAPK (Erk1/2) (137F5)	Rabbit	CST[1]	4695	1:1000
Phospho-ERK1/2 (MAPK-YT)	Mouse	Santa Cruz[2]	SC-154	1:10,000
AKT1 (2H10)	Mouse	CST[1]	2967	1:1000
Phospho-AKT (S473)	Rabbit	CST[1]	4060	1:1000
Phospho-AKT (T308, 244F9)	Rabbit	CST[1]	4056	1:1000
SAPK/JNK Antibody	Rabbit	CST[1]	9252	1:1000
Phospho-SAPK/JNK (81E11)	Rabbit	CST[1]	4668	1:1000
p38 MAPK (D13E1) XP	Rabbit	CST[1]	8690	1:1000
Phospho-p38 MAPK (28B10)	Mouse	CST[1]	9216	1:1000
JunB (C37F9)	Rabbit	CST[1]	3753	1:1000
Alpha Tubulin (B-5-1-2)	Mouse	Abcam[3]	ab11304	1:10,000
anti-MHC class I + HLA A + HLA B antibody	Rabbit	Abcam[3]	EPR1394Y	1:100

1= Leiden, Netherlands, 2= Heidelburg, Germany, 3= Cambridge, UK

2.2.13.1 Secondary antibodies

- Mouse, Rabbit (#926-68072, 926-32213 respectively Licor, Cambridge UK)

2.2.14 Transfection reagents

- Lipofectamine 3000 (#L3000001 Thermofisher, Altrincham UK)

2.2.15 Extraction kits

- AllPrep DNA/RNA Mini Kit (#80204 Qiagen, Manchester UK)
- DNeasy Blood & Tissue Kit (#69504 Qiagen, Manchester UK)
- RNeasy Mini Kit (#74104 Qiagen, Manchester UK)
- QIAamp Circulating Nucleic Acid Kit (#55114 Qiagen, Manchester UK)

2.2.16 Primers

Table 2.4 Primer sequences used for pyrosequencing of tumour-derived DNA

Primer Name	Primer Sequence
BRAF_Cdn600F	AGGTGATTTTGGTCTAGCTACA
BRAF_Cdn600R	AAAATGGATCCAGACAACTGTTC
BRAF_Cdn600Seq	TGATTTTGGTCTAGCTACA
NRAS_Cdn12F	GTAGATGTGGCTCGCCAATTAAC
NRAS_Cdn12R	GGGAAAAGCGCACTGACA
NRAS_Cdn12Seq	GTGGTGGTTGGAGCA
NRAS_Cdn13F	GAAAACAAGTGGTTATAGATGGT
NRAS_Cdn13R	TGAGGACAGGCGAAGGCTTC
NRAS_Cdn13Seq	ATACTGGATACAGCTGGA

Table 2.5 Primers and probes used for droplet digital PCR

Digital Primers and Probes	Company	Assay ID	Comments
***BRAF* V600E**	Biorad[1]	dHsaMDV2010027	
***BRAF* V600K**	Biorad[1]	dHsaMDV2010035	
***BRAF* V600R**	Biorad[1]	dHsaMDV2010037	
***NRAS* Q61R**	Biorad[1]	dHsaMDV2010071	
***NRAS* Q61L**	Biorad[1]	dHsaMDV2010069	
***NRAS* Q61K**	Biorad[1]	dHsaMDV2010067	
***NRAS* G12D**	Biorad[1]	dHsaMDV2010095	
***NRAS* G13D**	Biorad[1]	dHsaMDV2510526	
***NRAS* G12N**	Biorad[1]	dHsaMDS122360124	
***TERT* c.-124 C>T**	Integrated DNA technologies (IDT)[2]		**Forward primer sequence:** ACACTGACGACATGGTTCTACAGCAGCGCTGCCTGAAACTCG **Reverse primer sequence:** TACGGTAGCAGAGACTTGGTCTCGTCCTGCCCCTTCACCTTC **Probe**: AGCCCCTTCCGGGCCCTCCCA (FAM)
***TERT* c.-146 C>T**	IDT[2]		**Forward primer sequence:** ACACTGACGACATGGTTCTACAGCAGCGCTGCCTGAAACTCG **Reverse primer sequence:** TACGGTAGCAGAGACTTGGTCTCGTCCTGCCCCTTCACCTTC **Probe**: ACCCGGAAGGGGTCGGGACG (FAM)

1= Watford, UK, 2= Leuven, Belgium

Table 2.6 Oligonucleotides and donor templates used for CRISPR

Gene	sgRNA 1 Fw	sgRNA 1 Rv	sgRNA 2 Fw	sgRNA 2 Rv
ARAF	TTTCTTGGCTTTATATATCT TGTGGAAAGGACGAAACACC G**TTCCTACATGAGGGGCTC A**	GACTAGCCTTATTTTA ACTTGCTATTTCTAGC TCTAAAAC**TGAGCCC CTCATGTAGGAA**C	TTTCTTGGCTTTATATATCTTGTG GAAAGGACGAAACACCG**CACCGT GAGCCCCTCATGT**	GACTAGCCTTATTTTAACTTG CTATTTCTAGCTCTAAAAC**AC ATGAGGGGCTCACGGTG**C
	Donor template (mutation in bold, PAM site mutation in italics)	GGGTGAGAGGCATGGCTATTAGGAGTCCCTGTAGTGGTCCTTGACCCTGGCGGACATCTT **G**CTACATGAGGGGCTCA*T*GGTGAAGATCGGTGACTTTGGCTTGGCCACAGTGAAGACTCG		
MAP2K1	TTTCTTGGCTTTATATAT CTTGTGGAAAGGACGAA ACACCG**CAGCAGCGAA AGCGCCTTG**	GACTAGCCTTATTTTA ACTTGCTATTTCTAGC TCTAAAAC**CAAGGCG CTTTCGCTGCTG**C	TTTCTTGGCTTTATATATCTTG TGGAAAGGACGAAACACCG**C TGGGTAAGAAAGGCCTCA**	GACTAGCCTTATTTTAACT TGCTATTTCTAGCTCTAAA AC**TGAGGCCTTTCTTACC CAG**C
	Donor template (mutation in bold, PAM site mutation in italics)	CTGGAGGAGCTAGAGCTTGATGAGCAGCAGCGAAAGCGCCTTGA*A*GCCTTTCTTACCCAG **G**AGCAGAAGGTGGGAGAACTGAAGGATGACGACTTTGAGAAGATCAGTGAGCTGGGGG CT		
PIK3R4	TTTCTTGGCTTTATATAT CTTGTGGAAAGGACGAA ACACCG**TGGAGTAATAC GATCCAAA**	GACTAGCCTTATTTTA ACTTGCTATTTCTAGC TCTAAAAC**TTTGGAT CGTATTACTCCA**C	TTTCTTGGCTTTATATATCTTG TGGAAAGGACGAAACACCG**A GCAATGACTCTGTTCCTA**	GACTAGCCTTATTTTAACT TGCTATTTCTAGCTCTAAA AC**TAGGAACAGAGTCAT TGCT**C
	Donor template (mutation in bold, PAM site mutation in italics)	TCCAAACTAGCTGCTTTGGAACTGATTCTTCATTTGGCTCCAAGATTAAGTGTTGAAATC**T** TTTTGGATCGTATTACTCCATATCTTTTGCATTTCAGCAATGACTCTGTTCCTAGG*A*TG		

Purchased from Sigma Aldrich, Gillingham UK

- Primers against plasmid SP6 and T7 promoter sequences

- T7: 5' TAATACGACTCACTCTAGGG 3' and

- SP6: 5' ATTTAGGTGACACTATAG 3'

2.2.17 Animals

- CD-1® Nude Mouse Crl:CD1-Foxn1^{nu} (Charles River, Harlow, UK)
- NOD SCID gamma (NSG) JAX^{TM} NOD.Cg-Prkdc^{scid} Il2rg0^{tm1WjI}/SzJ (Charles River, Harlow, UK)

2.3 Experimental procedures

2.3.1 Cell culture

Cells were cultured under standard conditions (5% CO2 at 37°C) and were passaged every 3-4 days depending on growth. Briefly, media (supplemented as 2.2.12) was aspirated, the cells were washed with phosphate-buffered saline (PBS) and trypsinised at 37°C until the cells detached then they were split according to cell growth into new flasks. They were routinely monitored for mycoplasma contamination by polymerase chain reaction (PCR) performed by the molecular biology core facilities (MBCF).

2.3.2 Establishment of patient derived cell lines

A piece of tumour from a patient biopsy/surgical sample (cut into approx. $0.5cm^3$) was finely chopped with a scalpel in a 6 well plate (#3516 Corning, St David's Park UK) then 3ml of media added. 10µl of collagenase type I was added (#17100-017 Thermofisher, Altrincham UK) and the cells incubated at 37°C overnight. The following day the supernatant was aspirated and replaced with 3ml fresh media.

2.3.3 Cryopreservation of cell lines

Cells were trypsinised and centrifuged at 250g, the media aspirated then the cells were washed with PBS, centrifuged again at 250g to pellet them, then approximately 1 million cells were re-suspended in 1ml freezing media (FBS with 10% DMSO) per cryovial (#V7509 Nunc, Thermofisher, Altrincham UK). Cells were gradually frozen in a Mr Frosty™ (#5100-0001 Thermofisher, Altrincham UK) freezing container and stored at -80°C for at least 24 hours before being transferred to a liquid nitrogen tank for long term storage.

2.3.4 Recovery of cryopreserved cell lines

Cells were quickly thawed in a water bath at 37°C then pipetted into a 15ml falcon tube, 3ml of PBS added to the cell suspension and then it was centrifuged at 250g. Then media was added and it was transferred to a T-25 flask.

2.3.5 Determination of cell number

Following trypsinisation of cells and re-suspension in media containing FBS for neutralisation of trypsin activity, 10µl of the media/cells was pipetted 1:1 with Trypan blue (#15250061 Thermofisher, Altrincham UK) into a cell counter slide and then viable cell number per ml estimated using an automated TC20 cell counter (Biorad, Watford, UK).

2.3.6 Short term growth inhibition assays with CellTiter-Glo®

Cells were seeded into 96-well plates (2,000-3,000 cells per well depending on cell growth; (#136101 Nunc™ F96 MicroWell™ white polystyrene plate Thermofisher, Altrincham UK). Twenty-four hours later, serial dilutions of drug were added (starting concentration dependent on efficacy of drug). The cells were incubated for a further 72 hr, then the media removed and viability measured by adding 100µl of CellTiter-Glo® (CTG) Luminescent Cell Viability Assay (Promega, Southampton UK) diluted 1:4 in PBS according to manufacturer's instructions. Relative survival in the presence of drugs was normalised to the untreated DMSO controls.

2.3.7 Isobologram analysis

The half maximal inhibitory concentration (IC_{50}) of each cell line to taselisib and CCT3833 was determined using short-term growth assays as section 2.3.6. The assays were

repeated with a starting concentration of each drug and the combination of the two drugs at IC_{50} x8 then over a 1:2 serial dilution. The combination index (CI) was calculated according to the Chou Talalay method, which denotes the effects of drugs as antagonistic, additive or synergistic according to the kinetics of dose-effect (274,275).

2.3.8 24-hour growth inhibition assay in the presence of cerebrospinal fluid (CSF)

Cells were cultured overnight under serum-free conditions in RPMI or 50% rat CSF (Charles River, Harlow, UK) and then treated with DMSO, dabrafenib (1μM), BEZ235 (5μM), or dabrafenib (1μM) plus BEZ235 (5μM) for 24hrs, at which point viability was measured by CellTiter-Glo® assays (Promega, Southampton UK). Relative survival was normalised to DMSO controls in either media or in the presence of CSF.

2.3.9 SRB Assay

Cells were seeded (2000-5000 cells per well according to cell growth) in a 96 well plate (#353072 Falcon, Thermofisher, Altrincham UK) and cultured in DMSO or inhibitors (different inhibitors depending on the experiment) for 96 hours. The media was removed, 100μl cold 10% trichloroaceitic acid (TCA Sigma Aldrich, Dorset UK) added and the plate incubated at 4°C for 1 hour. The plates were washed 4 times under slow running water then dried overnight. 50μl SRB solution (see section 2.2.3) was added to each well and the plate was incubated at room temperature for 30 minutes. The plates were rinsed with 1% acetic acid 3 times to remove the unbound dye and dried overnight at room temperature. Finally 100μl of 10mM Tris base pH 10.5 was added to dissolve the dye and then the absorbance measured at 490, 510, 530, nm using a SpectraMax M5 plate reader (Molecular Devices, California USA) (276).

2.3.10 Clonogenic assay

Cells were seeded (2000-10,000 cells per well according to cell growth) in a 6 well plate (#3516 Corning, St David's Park UK) and cultured in DMSO or inhibitors (CCT3833, PMA or SCH772984) at the concentration shown. Cells were cultured for 10-15 days depending on the assay and media was replaced every 3-4 days with the same concentration of drug maintained. The media aspirated and the cells fixed with 4% paraformaldehyde in PBS (Electron Microscopy Sciences, Hatfield USA) for ten minutes before aspirating and washing with PBS. The cells were stained by adding crystal violet solution and rocking the plates gently for 3-4 hours. The crystal violet was finally aspirated and the excess washed off under slow running water before drying overnight.

2.3.11 Immunoblotting

Briefly, after aspirating media, cells were washed with ice cold PBS, then cell lysis buffer was added (volume dependent on size of plate/well). The cells were scraped and pipetted up and down into a 1.5 ml microcentrifuge tube and incubated for 30 minutes on ice. Then the sample was centrifuged for 30 minutes at 4°C at 20,000g. The supernatant was pipetted into a new 1.5ml microcentrifuge tube at 4°C and frozen at -80°C.

In order to load equal amounts of protein on to the sodium dodecyl sulphate polyacrylamide (SDS) gel, a Bradford assay was performed to determine the protein concentration. A standard curve was generated using bovine serum albumin (0-10µg) and the concentration determined as per manufacturer's instructions using Bradford Pierce™ Coomassie Plus Assay Kit 23236 (Thermofisher, Altrincham UK). The absorbance at 660nm was determined using a SpectraMax M5 plate reader (Molecular Devices, California USA).

NuPAGE™ LDS Sample Buffer (4x) (Thermofisher, Altrincham UK) with 1:100 beta-2-mercaptoethanol was added to 20µg protein lysate to denature the protein (1:4 buffer:sample). The samples were vortexed, incubated at 100°C for ten minutes then loaded on to the SDS gel (4-12% gradient Nupage™ Bis-Tris protein gels, Thermofisher, Altrincham UK or Trupage™ gels Sigma Aldrich, Dorset UK were used). A rainbow marker RPN800E (GE Healthcare, Chalfont, UK) was used to determine the approximate size of the protein. Either NuPAGE™ MOPS SDS Running Buffer (20x) or TruPAGE™ Tris-MOPS SDS Express Running Buffer (20X) were used as a running buffer diluted to 1x using ddH20. The protein lysates were separated at 130V for 60-90 minutes.

The proteins were then transferred on to a Polyvinylidene difluoride (PVDF) pre-cut membrane (Biorad Watford, UK) using an electrophoretic transfer cell (Biorad Watford, UK) at 25V for 30 minutes according to manufacturer's instructions. The membrane was then reactivated using methanol and washed in PBS once then further washed in 0.1% Tween/PBS (PBST) washing buffer 4 times. The membrane was then blocked for 1 hour with Odessey® blocking buffer (Licor, Cambridge UK).

Primary antibodies for the protein of interest were diluted according to manufacturers instructions (see table 2.3) in 1:1 PBST and blocking buffer, and incubated overnight with the membrane at 4°C. The membranes were then washed four times in PBST and a fluorescent-labelled secondary antibody (Invitrogen; Li-COR Biosciences) added (1:10,000 in 1:1 PBST and blocking buffer) in order to visualise the primary antibody and incubated for 1 hour. The membranes were then washed 4 times with PBST and analysed using an Odyssey Infrared Scanner (Li-COR Biosciences).

2.3.12 Reverse Phase Protein Array (RPPA)

500,000 cells were seeded in a 6 well plate and cultured overnight under serum-free conditions in RPMI or 50% rat cerebrospinal fluid (CSF). Media was aspirated from plates and wash twice with PBS on ice before RPPA lysis buffer was added to the cells (150µl for each well). The plates were incubated on ice for 20 minutes with shaking every 5 minutes. The cells were scraped off the plates and lysates collected into micro-centrifuge tubes then centrifuged at 20,000g for 10 minutes at 4°C and the supernatant collected.

The cellular protein concentration was determined by Bradford assay (see section 2.3.11) and the protein concentration was adjusted to 1mg/ml with lysis buffer. RPPA was performed by Kenneth Macleod (Edinburgh cancer discovery unit) as previously described (277).

2.3.13 PamGene analysis

PamGene ('s-Hertogenbosch Netherlands) has developed a method of analysing kinase activity through measuring the phosphorylation of 140 Ser/Thr containing peptides on a membrane. The kinases in the sample actively phosphorylate substrates on the PamChip®, in the presence of adenosine triphosphate (ATP). An antibody mix is used to detect the phosphorylated Ser/Thr, and a second fluorescein isothiocyanate (FITC)-conjugated antibody is used in a “detection mix” to quantify the phosphorylation signal (PamGene, 's-Hertogenbosch Netherlands).

Cells were cultured in CCT3833 (1µM A375/Colo829 cell lines and 2µM D04 cell line) or “drug off” (media only) for 24 hours (Fig. 4.6A-C) and for Fig. 4.6D A375/R (3833) cells were cultured in DMSO or SCH772984 for 24 hours. Media from cells was aspirated and washed twice with ice-cold PBS, before lysis buffer was added and incubated on ice for 15

minutes. The lysate was centrifuged for 15 minutes at 16,000g at 4°C then the supernatant collected and transferred to new micro-centrifuge tubes then stored at -80°C.

The protein concentration was quantified using Bradford assay (see section 2.3.11). The samples were analysed in triplicate on the PamGene station (PamGene, 's-Hertogenbosch Netherlands) as per manufacturer's instructions. Briefly, 1x protein kinase (PK) wash buffer and 1X PBS/0.01% Tween were prepared then a syringe filled with the 1x PK wash buffer and placed into the machine. Then, 1-3 Serine/Threonine Kinase PamChip® arrays (PamGene, 's-Hertogenbosch Netherlands) were placed into the machine and 30 µl of 2% BSA applied to each array. The machine then blocked the membrane and when prompted, another syringe with 1x PBS/0.01% Tween was filled and used to replace the syringe containing PK wash buffer.

The antibody master mix was prepared according to Table 2.7 and 40µl was applied to each array. The machine then pumped the mix over the membrane. When prompted, 30µl detection mix (Table 2.8) was applied to each array. The machine then completed the remaining run.

Finally the Bionavigator software developed by PamGene ('s-Hertogenbosch Netherlands) was used to analyse the data. This software quantifies the fluorescence from images taken by the PamGene station in order to assess which peptides have been phosphorylated by peptides in the sample. The software then uses published data sets such as UniProt (278), to interpret which kinases are active depending on the peptides that have been phosphorylated. The normalised kinase statistic represents the relative change in activity of each kinase between the samples. The specificity score is how likely it is that the same kinase statistic could be observed with a random set of peptides from the array; the higher the score the more specific it is to that kinase.

Table 2.7 Antibody master mix

Solution	Volume (µl)
Water	To a final volume of 40
10x PK buffer	4
100x BSA solution	0.4
STK antibody mix	0.46
Sample (lysate)	Max 10
4 mM ATP solution	4
Total Volume	40

Table 2.8 Detection mix

Solution	Volume (µl)
Water	26.6
10x Ab buffer	3
100x BSA solution	0.4
STK antibody FITC-labelled	0.4
Total Volume	30

2.3.14 Flow cytometry analysis for cell death

$5x10^5$ cells were seeded and cultured overnight in RPMI or 50% CSF, treated with DMSO or Dabrafenib (1µM) for 24hrs, then fixed with ice cold methanol. Cell death was assessed through blocking with 0.5% bovine serum albumin for 1 hour before incubating with 0.3% cleaved PARP conjugated with Alexa Fluor 647 (#6987, CST Leiden, Netherlands) in 0.5% bovine serum albumin for 1 hour and acquiring stained cells on a LSR II flow cytometer

(BD Biosciences, Wokingham UK). Data of duplicate experiments were analysed using FlowJo software version 10.0.8.

2.3.15 DNA quantification

DNA concentrations were calculated using 1µl of sample DNA on a Nanodrop 1000 spectrophotometer (ThermoFisher Altrincham, UK), according to the manufacturers guidelines.

2.3.16 Polymerase Chain Reaction (PCR)

PCR was performed with Phusion® using a 25µl reaction as per manufacturer's instructions. Briefly, a reaction mixture of 5µl 5x Phusion® (ThermoFisher, Altrincham UK), 0.5µl 10mM deoxyribonucleotide triphosphates (dNTPs; U1511 Promega, Southampton UK), 1.25µl 10µM forward and reverse primers 100µM concentration, variable amount of template DNA (dependent on application. 1-10ng plasmid, 50-250ng genomic DNA), 0.25µl Phusion® DNA polymerase and nuclease-free water to make up to 25µl. A PCR reaction was performed using the following cycling conditions: 98°C for 30 seconds; 25-35 cycles of 98°C for 10sec and 45-72°C (dependent on primer annealing temperature) for 10-30 seconds; followed by 72°C for 10min and a final hold at 4°C.

2.3.17 Sanger sequencing

Primers were designed using Primer3Plus (279) and checked for any unintended targets using Primer-BLAST (280). A PCR was performed (see section 2.3.16) and 15ng of DNA submitted with 1.5µl of forward or reverse primers and nuclease-free water to a total volume of 20µl to the MBCF who performed Sanger sequencing. Briefly, PCR amplification was performed on a Veriti thermal cycler (Applied Biosystems, Thermofisher, Altrincham UK). The

reaction mixture of 10µl final volume contained 6µl of template, 0.5µl BigDye™ Terminator v3.1 and 1.75µl of 5x Sequencing Buffer (#4337455 Applied Biosystems, Thermofisher, Altrincham UK), and 1.75 µl of PCR grade H2O. PCR conditions were as follows: amplification for 25 cycles of 10s at 96°C, 5s at 50°C, and 2 min at 60°C, and hold at 4°C. To clean up the PCR products, 10µl AxyPrep Mag PCR clean up Kit (#AX403, Appleton woods, Birmingham UK) was added along with 42µl of 80% EtOH. The plate was placed onto a SPRIPlate (#A32782 Thermofisher, Altrincham UK) for 3 minutes before washing three times with 100 µl of 80% Ethanol and then left to dry for 10mins. PCR product was then resuspended with 75 µl of PCR grade H2O for analysis on the 16-capillary ABI 3130xl Genetic Analyzer (#4359571 Applied Biosystems, Thermofisher, Altrincham UK). POP-7™ (#4352759 Applied Biosystems) was utilized on a 36 cm capillary array (#4404683 Applied Biosystems, Thermofisher, Altrincham UK) with 1x Running buffer (#4335613 Applied Biosystems, Thermofisher, Altrincham UK). Samples were injected electrokinetically for 18s at 1.2 kV. The bases were separated at 8.5kV at a run temperature of 60°C. SnapGene® version 4.2.4 or ChromasPro version 2.6.5 were used to visualise the results.

2.3.18 CRISPR Cas-9

Multiple guide RNAs for CRISPR Cas-9 were designed using Chopchop (http://chopchop.cbu.uib.no/) (281) to introduce double stranded breaks within 100 base pairs (bps) of the mutation of interest. The intended target site sequences were used to generate two 60bp oligonucleotide sequences where the 3' 20bp of each oligonucleotide are the reverse complement of the sequences designed by chopchop and 5' end of each are homologous to sequences in the gRNA cloning plasmid (Addgene #41824 (272)). Oligonucleotide sequences are in Section 2.2.16 Table 2.6.

Briefly the 60bp oligonucleotides were annealed and extended by diluting to a concentration of 25µM, then a Q5 polymerase reaction was set up as per the manufacturer's instructions (New England Biolabs (NEB), Hitchin UK) without the inclusion of additional template DNA. Cycling conditions were:

1. 94°C for 5 mins
2. 94°C for 30 seconds
3. 50°C for 30 seconds
4. 72°C for 30 seconds,

Steps 2-4 were repeated for 2-3 cycles then 72°C for 5 mins. This generated a 100bp DNA fragment, which could be utilised for Gibson assembly.

An empty gRNA expression vector (see section 2.2.10) was linearised using Aflll restriction enzyme (#R0520 NEB, Hitchin UK), and then combined with the annealed and extended oligonucleotides using Gibson assembly mastermix (#E2611, NEB, Hitchin UK) as per manufacturers instructions and incubated at 50°C for 1 hour. Two µl of the Gibson assembly reaction product was then transformed into competent *Escherichia coli* (*E.coli*) strain JM109 cells generated and transformed using the Mix and Go E coli transformation kit (Zymo, Frieburg, Germany) following the manufacturer's protocols.

The transformed *E coli* were plated on to lysogeny broth (LB)/kanamycin (50µg/mL) agar plates. These were incubated overnight at 37°C, then individual colonies were picked and grown in LB broth supplemented with 50 µg/mL kanamycin in a shaking incubator overnight. Plasmid DNA was purified using a QIAprep Spin miniprep kit (Qiagen, Manchester UK). Sanger sequencing was performed to confirm the plasmid sequence was correct using primers designed against the SP6 and T7 promoter sequences. Plasmids with the correct insert were then amplified in *E coli* overnight and purified using Nucleobond Xtra Midi plasmid purification kit (Macherey-Nagel, Duren, Germany).

Single stranded donor templates were designed where 60bp either side of the guide RNA double stranded break cut sites were homologous to the sequence of the gene of interest with the sequence modified to include the mutation of interest in order to insert the mutation following homologous recombination (sequences are in Section 2.2.16 Table 2.6). In addition a synonymous mutation was introduced into the protospacer adjacent motif (PAM) sequence of the donor template to prevent further Cas-9 mediated cleavage of the inserted donor template.

Generated gRNA plasmids (0.5µg) were then transfected into A375 cells with 0.5µg pST1374-NLS-flag-linker-Cas9 (Addgene 44758 (273)) and 2µl of the appropriate donor template (10µM) using lipofectamine 3000. The cells were incubated overnight and the media replaced the next day with CCT3833 0.5µM. The concentration was increased to 1µM within a week of transfection.

2.3.19 Animal procedures

All procedures involving animals were performed in accordance with National Home Office regulations under the Animals (Scientific Procedures) Act 1986 and within guidelines set out by the Cancer Research UK Manchester Institute's Animal Welfare and Ethical Review Body (AWERB), and carried out under license PPL PE3DF1A5B (formerly PPL 70/7701).

2.3.20 Establishment of patient-derived xenografts (PDX)

The PDX cohort was established by Dr Romina Girotti, Dr Elena Galvani, Dr Gabriela Gremel, Mr Matthew Smith or myself. Patient tumour samples (~80mm^3) were implanted subcutaneously into the flank of 6-8 week old, female NSG mice under anaesthetic. Tumours were measured twice weekly until they reached limit then the tumour was excised and cryopreserved (see Section 2.3.22).

2.3.21 Establishment of CDX

Ten ml of HITES media and 80ml HBSS with 10% HITES media were prepared at room temperature. Blood was taken from patients (processed within 4 hours of taking). Then 50µl/ml of blood of RosetteSep™ circulating tumour cell (CTC) Enrichment Cocktail Containing anti-CD56 (Stem cell technologies, Cambridge, UK) was added to the blood and incubated for 20 minutes on a roller. 10 ml 90% HBSS/10% HITES was added to the blood sample and then mixed gently by inversion. Blood/HBSS mix was gently layered on top of 3ml Ficoll-Plaque Plus (GE healthcare, Little Chalfont, UK) in four 10ml falcon tubes. The tubes were centrifuged at 1200g for 20min at RT with the acceleration set to 15 and deceleration to 0. The interphase was collected with a fine end pasteur pipette to collect the CTCs and diluted with 30ml 90% HBSS/10% HITES, inverted and centrifuged at 250g for 5 minutes. The supernatant was discarded and the pellet was re-suspended in 20µl of ice-cold HITES before adding 100µl of Matrigel® Growth Factor Reduced (GFR) Basement Membrane Matrix, LDEV-free (Corning, Flintshire UK). The CTC embedded in matrigel were subcutaneously into 2 NSG mice (100µl per mouse). Mice were monitored for tumour growth weekly and on tumour appearance were measured twice a week until tumour limit, then passaged or cryopreserved.

2.3.22 Cryopreservation of PDX/CDX

The tumours were excised and cut into pieces of approx. 0.5cm^3 and 1ml freezing media (FBS with 10% DMSO) was added cryopreservation. They were gradually frozen in a Mr Frosty™ freezing container and stored at -80°C.

2.3.23 Generation of cell lines from PDX/CDX

Pieces of tumour were cut into approx. 0.5cm^3 and cell lines generated as per section 2.3.2. PDX/CDX derived cell lines were all cultured in RPMI.

2.3.24 Implantation of PDX/CDX tumour pieces

Tumour pieces approx. 0.5cm^3 were either implanted following thawing from frozen or passaged from another mouse. An incision was made approx. 0.5cm in the right flank of an anaesthetised NSG mouse, a blunt dissection performed in order to create a small pocket subcutaneously and the tumour piece placed into it. The wound was clipped in order to optimise healing. Mice were monitored for tumour growth and signs of weight loss twice weekly.

2.3.25 Animal dosing experiments

Chapter 2. NSG mice were dosed by daily orogastric gavage with dabrafenib 25mg/kg or vehicle (5% DMSO in water). For the subcutaneous lesion, 14 animals were randomised when tumours reached between 50-120mm^3 into dabrafenib or vehicle cohort for 40 days. For the brain lesion, 20 animals were randomised on a rolling recruitment basis when tumours reached 50-120mm^3 into groups receiving dabrafenib or vehicle for 38 days.

Chapter 3. CCT3833 and taselisib combination experiment. One million A375M cells were injected subcutaneously into CD1 nude mice and when tumours reached 50-120mm^3 mice were randomised into groups (n=6 per group) receiving daily orogastric gavage of vehicle (5% DMSO in water), taselisib (10mg/kg), CCT3833 (40mg/kg) or taselisib (10mg/kg) plus CCT3833 (40mg/kg).

Drug addiction in vivo experiment. 1x10^6 A375/R (3833) cells (A375 cells made resistant to CCT3833) were injected subcutaneously into CD1 nude mice dosed with CCT3833 (40mg/kg) from day 0. When tumours reached 600mm^3, mice were randomised into two

cohorts, one that continued CCT3833 and one that was switched to vehicle (5% DMSO in water).

2.3.26 Histology and immunohistochemistry (IHC)

The histology department (Mr Garry Ashton and Mrs Caron Behan) formalin-fixed and stained tumours with hematoxylin and eosin (H&E) and anti-MHC class I + HLA A + HLA B antibody [EPR1394Y] (Abcam). Representative images of IHC slides were taken by Dr Amaya Viros.

2.3.27 Multiplexing and Definiens Quantification

The histology department (Mr Garry Ashton) stained 5 μm sections from each formalin-fixed, paraffin-embedded (FFPE) block with anti-CD4 (0.3μg/ml, MABF750 Merck, Watford UK), anti-CD8 (2μg/ml, M7103 Merck, Watford UK), anti-CD-163 (5μg/ml, NCL-CD163 Leica, Milton Keynes UK) and HMB45 (2μg/ml, ab732 Abcam Cambridge UK). The IHC was performed on a Ventana Discovery Ultra platform (Roche, Burgess Hill UK). Following de-paraffinisation and blocking of endogenous peroxidase, the antibodies were applied sequentially in the order listed. Following heat induced epitope retrieval using cell conditioning 2 (32mins @ 95^{o}) omnimap anti mouse horse radish peroxidase (HRP; 760-4310, Roche, Burgess Hill UK) or omnimap anti rabbit HRP (760-4311, Roche, Burgess Hill UK) were used to detect the primary antibodies. Following labelling, a Perkin Elmer Opal plex kit was used (NEL791001KT, Perkin Elmer, Waltham, MA). CD4 was labelled with fluorophore Cy5.5, CD8 with FITC, and HMB45 (Cy3). A heat step of 8 minute (using CC2 @ 95^{o}) was applied after each label.

Mr Kang Zeng visualised multiplexed tissue (bright-field and fluorescence) at x400 total magnification and acquired x20 image fields. Vectra 2.0 and Nuance 2.0 software packages

(Perkin Elmer, Waltham, MA) were used for automated image acquisition and development of the spectral library, respectively.

Vectra multispectral image files were converted into multilayer TIFF format using inForm (PerkinElmer, Waltham, MA) and created a customised spectral library. These were then converted to single layer TIFF files using Imagej (Fuji, NIH, US). Tumour and stroma identification and marker quantification was performed by using Definiens Developer XD (Definiens AG, Munich, Germany) and Definiens tissue studio (Definiens AG, Munich, Germany).

2.3.28 Plasma extraction

Retrospective ctDNA study. Blood was collected in ethylenediaminetetraacetic acid (EDTA) tubes as part of the AVAST-M study protocol, kept on ice and processed for plasma within 30 minutes of collection at 2000g for 10 minutes at 4°C, then stored at -80°C until analysis.

Prospective ctDNA study. Blood was collected in EDTA tubes and centrifuged for 10 minutes at 2000g. The plasma phase was transferred to a 15ml falcon tube and centrifuged it for 10 minutes at 2000g. The plasma was then pipetted into cryovials (1ml per vial) and frozen at -80°C.

2.3.29 RNA/DNA extraction

2.3.29.1 Tumour

The histology department micro-dissected the tumour in attempts to ensure tumour purity and extracted RNA/DNA using the AllPrep DNA/RNA Micro Kit (Qiagen) according to manufacturer's instructions.

2.3.29.2 Cells

RNA from cell pellets was extracted using an RNeasy Mini Kit (Qiagen, Manchester UK) and DNA using DNeasy Blood & Tissue Kit (Qiagen, Manchester UK) according to manufacturer's instructions.

2.3.29.3 Plasma

CfDNA was isolated from up to 2ml of plasma (retrospective study) or 4ml (prospective study) using QIAamp Circulating Nucleic Acid kits according to the manufacturer's instructions (Qiagen, Manchester UK) with the following alterations: Carrier RNA (R5636-1ml, Sigma-Aldrich, Gillingham UK) was added at a concentration of 0.6 µl of 10µg/µl stock per 1 ml ACL. For the retrospective study, an elution volume of 30µl was used and for the prospective study 50µl was used.

2.3.30 Whole exome sequencing (WES)

The molecular biology core facility performed all the WES in this thesis. DNA (1µg) was sheared in a Covaris S2 ultrasonicator (Covaris Inc) to an average size of 150-200bp. Multiplexed libraries were prepared using the SureSelectXT Target Enrichment System for Illumina Paired-End Sequencing Library kit and the SureSelect Exome, (V4 for chapter 2 and

V6 for chapter 3) Capture Library (Agilent, Cheadle UK). Library quality was checked using the Agilent Bioanalyzer. Libraries were quantified by quantitative polymerase chain reaction (qPCR) using the KAPA Library Quantification Kit for Illumina (Kapa Biosystems, Massachusetts USA). Pooled libraries were clustered at 14pM on a cBot and 2x100bp sequencing was carried out using the High Throughput mode of a HiSeq 2500 analyser using TruSeq SBS Kit v3 chemistry (Illumina, Cambridge UK).

2.3.31 RNA sequencing (RNA Seq)

The molecular biology core facility performed all the RNA Sequencing in this thesis.

Libraries:

Indexed PolyA libraries were prepared using 200ng of total RNA and 14 cycles of amplification with the Agilent SureSelect Strand Specific RNA Library Prep Kit for Illumina Sequencing (Agilent, Cheadle UK)

Quantifying and sequencing libraries- HiSeq (chapter 2):

Libraries were quantified by qPCR using a Kapa Library Quantification Kit for Illumina sequencing platforms (Kapa Biosystems, Massachusetts USA). Pooled libraries were clustered at 15pM on the cBot and 2 x100bp sequencing was carried out using the High Throughput mode of a HiSeq 2500 using TruSeq SBS Kit v3 chemistry (Illumina, Cambridge UK)

Quantifying and sequencing libraries- NextSeq (chapter 3):

Libraries were quantified by qPCR using a Kapa Library Quantification Kit for Illumina sequencing platforms (Kapa Biosystems Inc., Cat No: KK4835). 2pM pooled libraries were loaded onto the NextSeq 500 and 2x76bp sequencing was carried out using a NextSeq 500/550 High Output v2 kit (Illumina Inc.). Pooled libraries were clustered at 15pM on the cBot and

2x100bp sequencing was carried out using the High Throughput mode of a HiSeq 2500 using TruSeq SBS Kit v3 chemistry (Illumina, Cambridge UK).

2.3.32 Determining mutational status in primary/lymph node dissection

In order to test for mutations in ctDNA, the mutational status of patient's tumours from formalin fixed, paraffin embedded tissue (FFPE) was established. For the AVAST-M samples this was determined using pyro-sequencing of FFPE tissue from the resected primary lesion or involved lymph node, or both where available by the Oxford Experimental Cancer Medicine Centre, University of Oxford. Discordant results were repeated in triplicate to provide a consensus result.

For the prospective cohort, analysis of patient's tumour mutational status was performed by the Manchester Centre for Genomic Medicine, Manchester UK which is an accredited medical laboratory operating to ISO15189. FFPE specimens were fixed as either 5µM thick unstained slide mounted sections or unmounted rolled sections. Where possible, slide mounted sections were macrodissected using H&E guide slide marked by a reviewing pathologist. Macrodissected FFPE material or 2 x 5uM rolled sections were then de-paraffinised in xylene followed by an ethanol wash. DNA was then extracted from the de-paraffinsed material using the Roche cobas® DNA Sample Preparation Kit (Roche, Burgess Hill UK) following the manufacturer's instructions. DNA was recovered and re-suspended in 100µL of cobas® elution buffer (Roche, Burgess Hill UK).

Somatic mutations from the prospective cohort were identified through pyrosequencing or ddPCR analysis of DNA extracted from FFPE samples. PCR amplification and pyrosequencing was carried out in triplicate in all samples. In brief, PCR amplification was undertaken of a fragment of *BRAF* exon 15/*NRAS* exon 12/*NRAS* exon 13 using unmodified forward and a 5' biotinylated reverse primer and a sequencing primer was used for

pyrosequencing along with a custom dispensation order which can detect and discriminate between recurrent activating variants (see Section 2.2.16 Table 2.4 for primers). All pyrosequencing analyses were independently blind checked. Any discrepant results were repeated and at least two concordant replicates were required for a reportable result.

The *TERT* promoter mutation status was determined from FFPE samples using the ddPCR method as below. Briefly, 1ng of DNA from FFPE samples was run in one reaction carried out in duplicate. Positive and negative controls were included in each run using DNA from A375 (C250T mutation) and HepG2 (C228T mutation) cell lines.

2.3.33 Droplet Digital PCR (ddPCR)

Chapter 3 analyses: Each negative control or cell line sample was run over three replicate wells. 10ng input DNA was added per well to 11µl ddPCR Supermix for probes (no UTP) (Bio-Rad, Watford UK) and 0.55µl of custom designed probe (Lifetech, Warrington UK) for PI3K L25S made up to a total volume of 22µl with water. The PCR reaction was run using the following cycling conditions: 95°C for 10min; 40cycles of 94°C for 30sec and 55°C for 1min; followed by 98°C for 10min (all at a ramp rate of 2°C/sec), and a final hold at 4°C (ramp rate 1°C/sec).

Chapter 5 analyses*:* For the retrospective ctDNA study, cfDNA was extracted from 30 healthy volunteer plasmas for assay validation and included as a negative control sample in each ddPCR assay. Assay specificity was tested in 60 reactions using healthy volunteer cfDNA and were all found to be negative.

Each well (22µl total) contained 8.8 µl of cfDNA sample, ddPCR Supermix for probes (no UTP) (Bio-Rad Watford UK), wt and mutant probes (See Section 2.2.16 Table 2.5) according to the manufacturer's instructions. Droplets were generated using a QX200 Automated Droplet Generator (Bio-Rad, Watford UK) and a PCR reaction was run using the

following cycling conditions: 95°C for 10min; 40 cycles of 94°C for 30sec and 55°C for 1min; followed by 98°C for 10min (all at a ramp rate of 2°C/sec), and a final hold at 4°C (ramp rate 1°C/sec). Droplets were read using a QX200 Droplet Reader (Bio-Rad, Watford UK) and the data analysed using QuantaSoft version 1.4.0.99 software (Bio-Rad, Watford UK). All the runs included negative controls of cfDNA extracted from 2ml of healthy volunteer plasma and positive control DNA extracted from cell lines or patient tumours with known mutational status (*BRAF* p.V600E from A375 [ATCC]; *NRAS* p.Q61K and *NRAS* p.Q61L from patient-tumours). Positive control samples were assayed in a single well using 2.2µl of input DNA (1ng/µl), ddPCR Supermix for probes (no UTP), appropriate wt and mutant probes and water. A sample was called positive if ≥1 mutant droplet was present.

For the prospective study, protocol established by the Dawson laboratory was followed in order for the methods to be consistent across the two cohorts. The method varied from the above in that 10µl of cfDNA sample was used in two replicate wells (total reaction volume was 25µl). Furthermore, in order for the sample to be called positive, both replicates were required to have ≥1 mutant droplet.

2.3.34 Bioinformatics analysis

Dr. Garima Khandelwhal, performed all bioinformatics analyses with the exception of the neoantigen analysis, which was performed by Dr. Amit Mandal and the CIBERSORT analysis, which was performed by Dr. Yamil Mahmoud. I discussed all analyses with the bioinformaticians regarding types of analyses required to address my questions and interpreted the results.

2.3.34.1 WES

Dr. Garima Khandelwhal aligned the WES data to Human GRCh37 with bwa-mem (version 0.7.7) (282). Deduplication, realignment and recalibration was performed on the aligned data as suggested in the GATK framework (283). Somatic mutation calling was then done using Mutect (version 1.1.7) (284).

2.3.34.2 Neoantigen determination

Dr. Amit Mandal scanned non-synonymous mutations and identified candidate nonamer peptides using the WES data. The HLA type of the patient was determined by Central Manchester University Hospital (Laboratory reference no 03-GB-009.991) to be HLA A 02:01. Candidate sequences were input into NetCTLpan1.1 previously validated by other groups (285).

2.3.34.3 RNA-Sequencing

For chapter 3, the RNA-Sequencing data was aligned to Human GRCh37 assembly by Mapsplice (version 2.1.6) (286) and further analyses performed in R (version 3.1.0). Gene counts were extracted using featureCounts (version 1.16.1) (287) for Ensembl 73 annotation (version 1.16.1), which were then converted into Read Per Kilobase Million (RPKM). The RPKM values are used for all expression level quantification of the genes. Genes over-expressed in the brain lesion (log2 fold change (FC) ≥2) as compared to the baseline lesion were used to perform over representation analysis using the gProfileR package (version 0.5.3) (288). The over representation analysis of biological processes was displayed as a network using Cytoscape™ (289).

For chapter 4, the same pipeline was used. For Fig. 4.3A a multi-dimensional scaling (MDS) plot including genes with ≥1 count per million in at least 4 samples was generated

comparing CCT3833 resistant cell lines to its parental cell lines. For Fig. 4.2I unsupervised hierarchical clustering was performed on genes expressed at a log2FC≥2 of CCT3833 resistant cell lines compared to parental. In Fig 4.4E an MDS plot was generated comparing the expression of genes with ≥1 count per million in at least 3 samples at time 0 (drug on – cultured in CCT3833 1μM) in A375/R (3833) cells compared to 30 minutes, 24 hours and 5 days drug off (CCT3833 withdrawn and cells cultured in media; 3 replicates per timepoint). For Fig. 4.4F unsupervised hierarchical clustering was performed on genes expressed in A375/R (3833) cells with a log2FC≥1 at time 0 (drug on), 30 minutes, 24 hours and 5 days drug off. For Fig 4.4G, MITF and invasion signatures were taken from Rambow *et al* (160) and a mean (+/-standard deviation of the triplicates) RPKM expression of the signature was determined at each timepoint. Fig 4.4H gene set enrichment analysis (GSEA) was performed using the method described in Kong *et al* (165). Briefly, MITF target gene lists were obtained from http://www.jurmo.ch/work_mitf.php and analyses were performed using GSEA software (290) and the output re-plotted using replotGSEA function (https://github.com/PeeperLab/Rtoolbox) (165). For Fig. 4.4I-K, GSEA was performed using hallmark gene signatures and GSEA software from the Broad Institute (290,291).

2.3.34.4 CIBERSORT analysis

The leukocyte signature matrix LM22 (547 genes) that differentiate 22 types of tumour-infiltrating immune cells was used for the analysis. Normalised gene expression data from RNA-Sequencing analysis of each sample (subcutaneous and brain lesions) were processed with the CIBERSORT web tool (http://cibersort.stanford.edu/) using default parameters at 100 permutations.

2.3.35 Modelling of ARAF mutation

All modeling was performed by Dr. Alfonso Zabon. The homology between ARAF and BRAF is 68% identity and 80% similarity between the sequences and therefore as the crystal structure of the ARAF protein has not been solved, the effect of the mutation was modeled using the BRAF structure. Homology models of ARAF and subsequent studies were carried out using the Schrodinger's Maestro Suite Version 11.1.012. Co-crystal structures of BRAF were chosen as templates in the active and inactive conformations. The PDB structures 5CT7 (inactive conformation) and 3D4Q (active conformation) were first prepared using the protein preparation wizard in the Schrodinger's Maestro Suite; bond orders were assigned to the ligand in the crystal structure and Hydrogen atoms were added to the protein-ligand complex consistent with physiologic pH (7.0). The multiple sequence viewer (MSV) tool was then used to align the three sequences, and finally the models were generated using the protein modeling and refinement package prime of Maestro including the ligands in the model generation steps. The mutants were derived from the models with the Residue and Loop Mutation tool. For the docking of compound CCT3833 in the active site, grids were defined by centering them around the ligand in the crystal structure using a 10 A box size setting in the Glide program. All docking calculations were performed using the ''extra precision'' (XP) mode of Glide.

2.3.36 Statistical analysis

2.3.36.1 Sample size calculation for the retrospective ctDNA study

The sample size calculation was performed by Mr. David Ryder. 150 patients were determined to provide 80% power to detect a hazard ratio (HR) of at least 3.5 between patients with undetectable and detectable ctDNA for disease-free interval (DFI) with a 5% significance level, assuming marker prevalence of 10% and an event rate of 40%.

2.3.36.2 Statistical analysis of retrospective ctDNA study

The baseline ctDNA result (undetectable/detectable) was compared against patient and tumour characteristics (age, gender, AJCC stage, nodal classification, primary melanoma Breslow and ulceration), as well as Eastern Cooperative Oncology Group performance status (PS) collected at the time of trial entry using Wilcoxon rank sum test for continuous factors and a chi-square test or Fisher's exact test with small number for categorical factors. A stepwise logistic regression model was used to identify the independent factors for predicting detectable ctDNA, with a P-value of 0.05 for inclusion and exclusion.

DFI, distant metastasis-free interval (DMFI) and OS were calculated from the date of randomisation to the trial until date of first recurrence, date of distant metastases or date of death, respectively. The Kaplan-Meier method was used to construct survival curves for differences between DFI, DMFI and OS in patients with detectable ctDNA levels versus undetectable levels and compared using a Cox proportional hazards model to obtain HRs and 95% CIs. Baseline ctDNA (detectable or undetectable) and other factors associated with prognosis (Breslow, ulceration, stage, nodal classification and ECOG performance status) were analysed using univariate and multivariate Cox proportional hazards regression models for DFI, DMFI and OS.

Internal validation of ctDNA performed using bootstrapping with 1000 samples and the performance of the ctDNA model assessed using prognostic separation D statistics (PSDS) (292). The performance of modelling the current AJCC prognostic variables (Breslow, ulceration, stage and N classification) compared to this model including ctDNA (i.e. adjusted for ctDNA) were assessed by determining discriminative and predictive ability through obtaining the PSDS, Nagelkerke R^2 and assessing model calibration (292–294). All analyses were performed using the SAS statistical package (version 9.4).

2.3.37 T tests

Unpaired, two tailed T tests were performed using GraphPad Prism software version 7.0

Chapter 3. Tumour microenvironment-driven resistance to immune and targeted therapies in acral melanoma

Despite the impressive advances in stage IV melanoma treatment, most patients still progress and die from the disease. Brain metastases in particular remain a persistent clinical challenge (238,295,296). In a comparison of patients treated with first line targeted therapy with (n=24) or without (n=44) brain metastases, median OS was 14 (95% CI 5.4–22.6) vs. 17 (95% CI 12.1–21.9) months respectively (296). Patients treated with first line immune therapy with (n=10) or without (n=42) brain metastases, median OS was 7 (95% CI 0–17.9) vs. 35 (95% CI 25.5–44.5) months respectively (296). The inferior prognosis of patients with central nervous system (CNS) metastases has been acknowledged in the new AJCC version 8 guidelines with the creation of an M1d category specifically for them (4). Stage IV survival data from their international database are pending (4).

Acral melanoma is a rare melanoma subtype (see Introduction Section 1.1) and therefore the majority of clinical trials involve only a small number of patients with acral melanoma with the majority of patients having common cutaneous melanoma (297). Interrogation of the response of acral melanoma to immune and targeted therapies is an important aim.

In order to better understand the biology of melanoma in the clinic, the Molecular Oncology Group (Cancer Research UK (CRUK) Manchester Institute) has developed a number of patient-derived tools to study melanoma, which included tumour tissue, patient derived xenografts (PDX, Fig. 3.1) and patient-derived cell lines (136). I identified a patient with metastatic acral melanoma, who responded to both immune and targeted therapies, but as often seen with common cutaneous melanoma, resistance developed to both modalities. Through longitudinal sampling of isolated lesions progressing on treatment with on-going response

elsewhere, I was able to gain insight into the heterogeneity of the tumour microenvironment resulting in resistance to standard melanoma treatments.

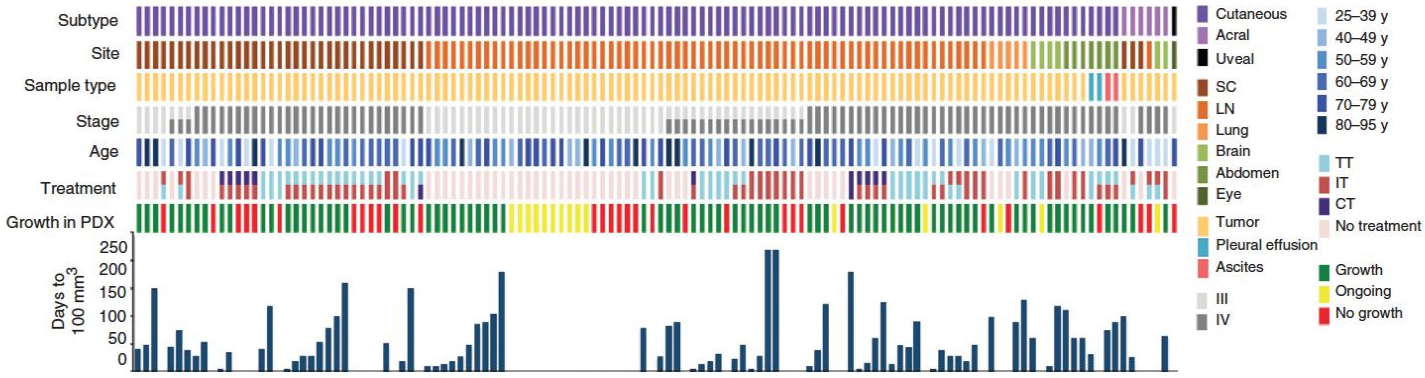

Fig. 3.1 Patient derived xenograft collection. Samples from 126 patients with stage III and IV cutaneous, acral and uveal melanoma were collected and implanted into nod scid gamma mice.

3.1 Patient Case History

A patient in their early 40s presented with acral melanoma on the sole of the right foot (Fig. 3.2). The tumour was resected, but recurred at the original scar site two years later and was again removed. A year later, the patient developed widespread disease, with a subcutaneous lesion in the right thigh, and several metastases in the hilar lymph nodes, liver and lungs (Fig. 3.2). To alleviate clinical symptoms, the subcutaneous thigh metastasis was resected, providing a pre-treatment baseline sample. The other lesions were inoperable, so the anti-PD-1 agent nivolumab (3mg/kg every 2 weeks) was administered and the patient achieved an excellent partial response, with disappearance of all of the tumours in hilum, liver and lung. These tumours did not return, but an isolated lesion in a mediastinal lymph node slowly progressed and 7 months after starting nivolumab was confirmed to be avid (high metabolic activity suggesting active cancer) on PET scan. This immune refractory lesion was resected, and imaging confirmed the patient was disease free and continued to respond to nivolumab.

Unfortunately, despite the excellent on-going response, after 12 months the patient developed grade 3 diarrhoea, necessitating nivolumab withdrawal. Within a month, the patient presented with neurological symptoms and an MRI scan revealed a new solitary metastasis in the brain that was resected (Fig. 3.2).

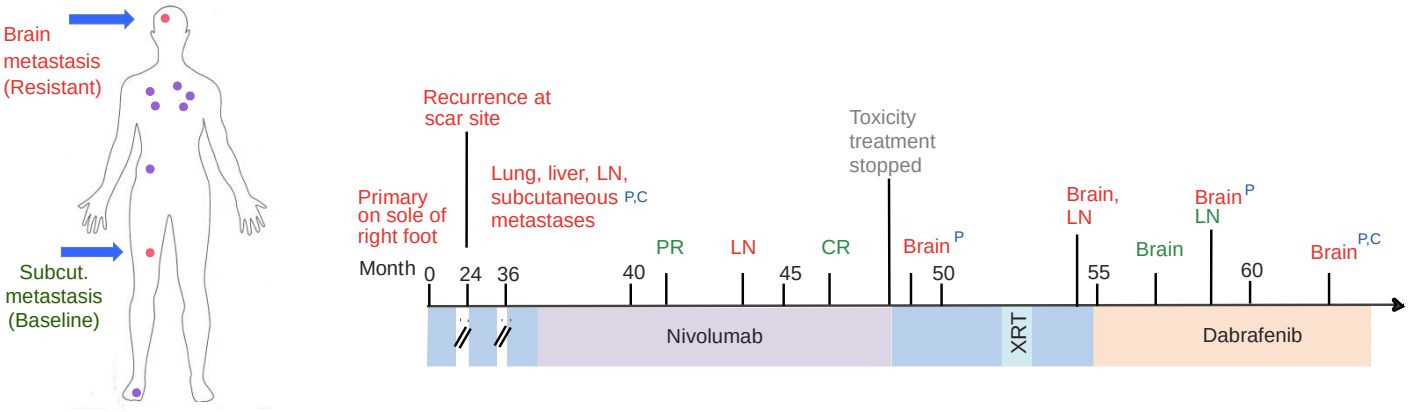

Fig. 3.2 Timeline of patient's clinical history. Green font=response, Red font=progressive disease, Grey font=toxicity, CR=complete response, PR=partial response, P=PDX, C=cell line, XRT=whole brain radiotherapy, red lesions are areas sampled, purple lesions are sites of disease. Subcut. = subcutaneous metastasis.

Following resection of the brain lesion, the patient received whole brain radiation, but progressed within 3 months with regrowth of the brain tumour, and the appearance of a new para-oesophageal lymph node tumour (Fig. 3.2). As the patient's tumour harboured a p.V600E *BRAF* mutation, dabrafenib was administered and the patient achieved resolution of the lymph node lesion and a partial response in the brain. Intriguingly, despite an on-going extra-cranial response to dabrafenib, after 3 months the brain lesion progressed and was resected (Fig. 3.2). The patient continued on dabrafenib, but the brain metastasis progressed after a further 4 months and was once again resected. The patient remained stable on dabrafenib until

progression 2 months later, when tumour infiltrating lymphocyte (TIL) therapy was administered, but the patient passed away shortly after.

Longitudinal sampling of this patient's tumours provided a rare opportunity to investigate the mechanisms of resistance of acral melanoma to both immune and targeted

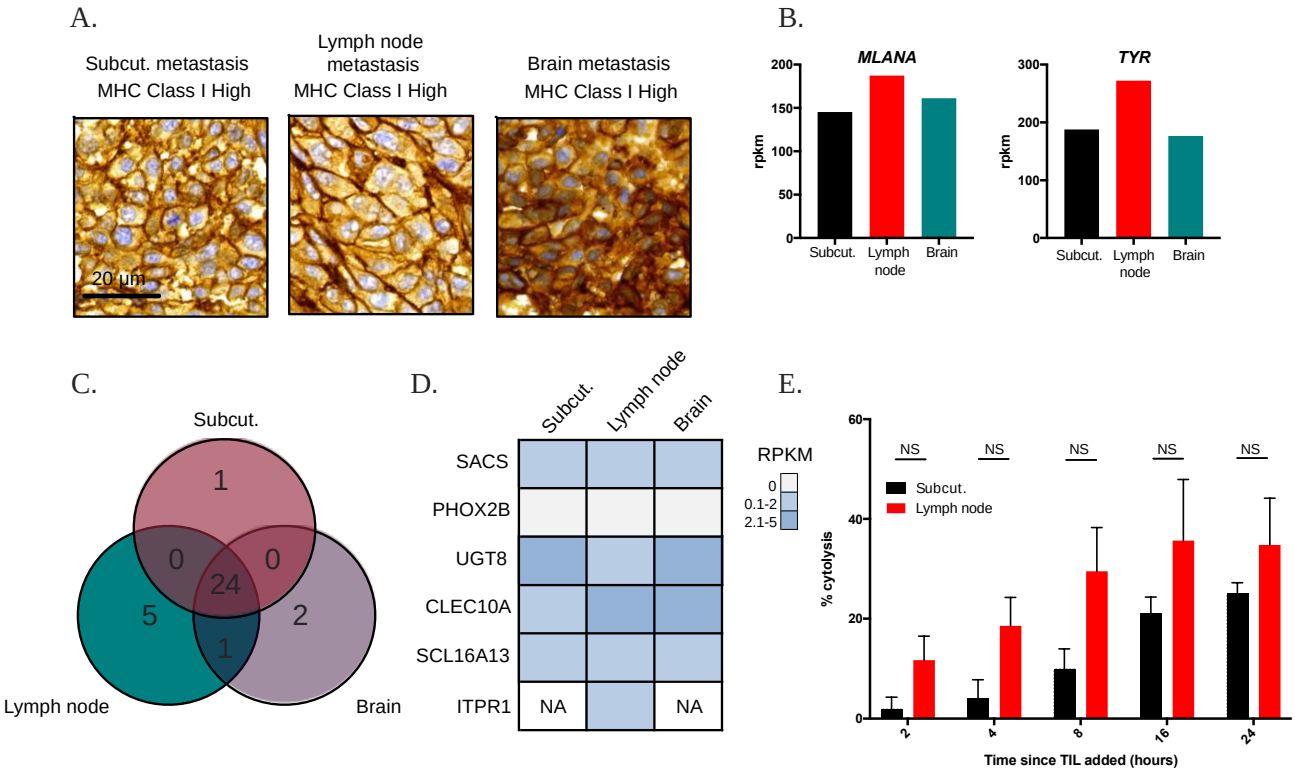

Fig 3.3 T cells are able to recognise and kill tumour cells from the nivolumab resistant lesions

A. MHC class I expression is conserved in the immune-escape lesions compared to baseline lesion. Immunohistochemistry showing MHC class I expression in the 2 lesions. Scale bar, 20µM.

B. Genes associated with melanoma antigens are expressed in both baseline and immune-escape lesions. RNA-Seq data showing gene expression in the 2 lesions.

C. Venn diagram of distribution of non-synonymous mutations identified by WES across the two lesions.

D. Neoantigens present in the baseline and immune-escape brain lesion. Mutations identified through WES were analysed using NetCTL and predicted neoantigens with a high affinity for MHC class I binding (score <1) are depicted. In shaded blue, the gene expression (reads per kilobase per million; RPKM) of the mutated genes present in the baseline and immune-escape lesion.

E. Tumour infiltrating lymphocytes (TIL) can kill nivolumab resistant tumour cells. At 8 hours post addition of TIL at an effector:target ratio of 5:1, the % cytolysis is compared in the nivolumab resistant and baseline lesion.

therapy during the course of her disease (Fig. 3.2). The thigh resection provided a baseline pre-treatment tumour and the lymph node an immune refractory lesion from a patient, who presented an otherwise complete response to nivolumab. The first brain resection provided a tumour that had escaped immune control following complete response to checkpoint blockade and the second brain resection a lesion that had progressed on targeted therapy with on-going extra-cranial response.

3.2 Neoepitope expression, IFNγ signalling and antigen processing are conserved in the lymph node and brain lesions that had escaped immune surveillance

One of the ways cancer can escape immune system surveillance is through defective antigen presentation or through loss of antigens (298–300). However, immunohistochemistry (staining performed by Garry Ashton and pathology by Dr Amaya Viros) revealed that MHC class I proteins remained highly expressed in both the immune refractory lymph node metastasis and immune-escape brain tumour (Fig. 3.3 A) and melanoma associated antigen gene expression was also unaltered (Fig. 3.3 B). Thus, the immune escape in this patient's lesions did not appear to be mediated by changes in antigen presentation or loss of melanoma associated antigens.

Neoantigens are proteins expressed by cancer cells arising due to tumour-specific mutations, which can be recognised by T cells resulting in an immune response (301). Loss of tumour associated neoantigens has also been correlated with resistance to immune therapy (302). I therefore investigated whether there were any changes in the number of mutations resulting in neoantigens or changes in their expression in the resistant lesions compared to the baseline tumour. Consistent with previous studies in acral melanoma (76), WES (all bioinformatics in this chapter performed by Dr Garima Khandelwhal) revealed a very low

mutation burden, with 25 nsSNVs in the baseline tumour, 30 in the lymph node and 27 in the brain metastasis (Fig. 3.3 C; Appendix 1). Twenty-four of these nsSNVs were shared mutations, revealing low genomic heterogeneity (Fig. 3.3 D) and only six mutations (*SACS, PHOX2B, UGT8, CLEC10A, SCL16A13, ITPR1*) were predicted to generate high affinity MHC class I epitopes for cytotoxic T lymphocytes (CTL) (Appendix 2; www.cbs.dtu.dk/services/NetCTL/; Snyder et al., 2014; Verdegaal et al., 2016). RNA-Sequencing revealed that expression of these genes did not decrease in the brain lesion and only the *UGT8* neoantigen decreased in the resistant lymph node lesion, but its expression fell by only ~2 fold (Fig. 3.3 C), insufficient to modulate immune therapy responses (303) (Fig. 3.3 C). In addition, the *ITPR1* neoantigen appeared rather than disappeared in the resistant lymph node tumour. Moreover, all 6 candidate neoantigens were expressed at low levels in baseline and immune escape tumours (<5 RPKM; Fig. 3.3 D, Appendix 2). Thus, immune escape was unlikely to have been mediated by loss of neoantigen expression.

In order to functionally validate the sequencing data, I performed a T cell cytolysis assay through plating tumour cells from the baseline subcutaneous lesion and the refractory lymph node and adding tumour TILs, which had been extracted from the lymph node and expanded in the presence of interleukin 2 (IL2). I then analysed the electrical impedance over time using a real-time analysis xCelligence platform as a measure of tumour cell killing. When in contact with tumour cells from both baseline and resistant lesions, the TILs were able to cause tumour cell death at every time point (Fig. 3.3E). There was no significant difference between cytolysis of tumour cells from the baseline or resistant lesion (Fig. 3.3 E).

Finally, I did not observe mutations in *JAK2* or related genes, which drive immune therapy resistance through IFNγ signalling or mutations resulting in loss of *PTEN*, which has been shown to result in immune suppression (215,304,305). These data are consistent with nivolumab resistance being driven by changes in tumour-immune cell interactions within the

tumour microenvironment, rather than T cells being unable to identify and kill tumour cells due to the loss of neoepitope expression, altered antigen presentation, or the acquisition of mutations that alter signalling.

3.3 Nivolumab resistance is associated with a distinct gene signature and immune infiltrate

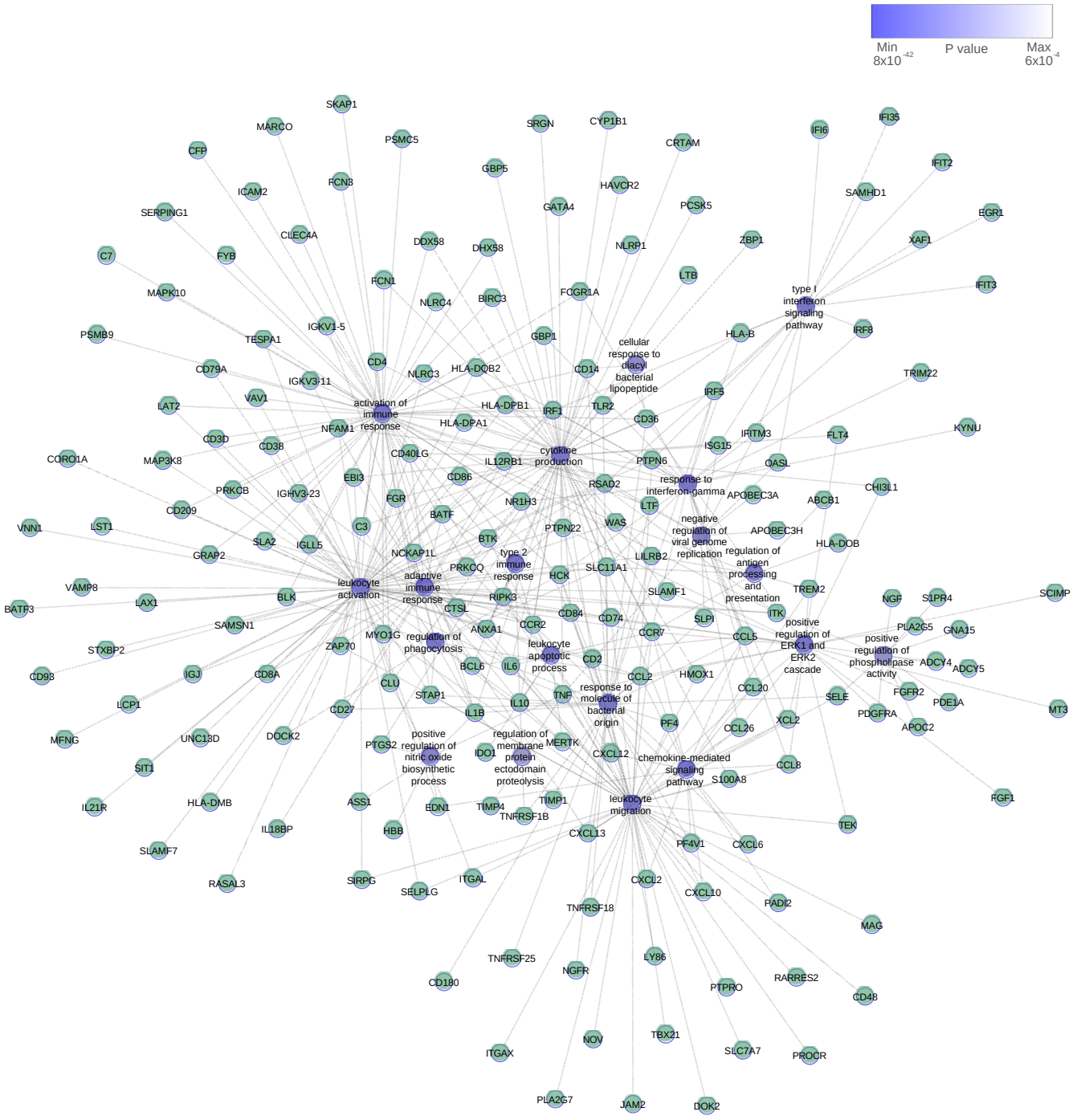

Fig. 3.4 Genes associated with an inflammatory profile are up regulated in the resistant lesion. Over representation analysis of Gene Ontology:biological processes reveals genes up regulated in immune response and inflammation in RNA-Seq data from baseline compared to resistant lesion. Results were visualised in a network structure using Cytoscape (Shannon et al., 2003). Green nodes=gene, purple nodes=pathway; colour shade represents *P* value of pathway - the darker the purple, the more significant the *P* value.

One of the major challenges I encountered in further analysis of the resistant lesions compared to baseline was differentiating tumour and tumour immune cell infiltrate from the surrounding stroma. This was a particular issue with the lymph node metastasis due to the high immune cell content within lymph nodes and therefore I focussed on the brain metastasis in further analyses.

To investigate the underlying mechanisms of immune escape, I examined gene expression in micro-dissected tumour samples (to improve tumour purity) from the subcutaneous and brain lesions. I used biological processes and Kyoto Encyclopaedia of Genes and Genomes (KEGG) pathway analyses of unsupervised RNA-Sequencing expression data to reveal differences between the baseline and immune-escape brain metastasis. This showed that biological processes such as cytokine-secretion, type 2 immune response and chemokine-mediated signalling were significantly up regulated in the resistant lesion (Fig. 3.4, Fig. 3.5 A, Appendix 3). Previously described gene signatures associated with loss of PTEN were not apparent in my data (Appendix 4) (304,305) nor was there evidence of increased activation of WNT/β-catenin and down-regulation of chemokines associated with increased WNT/β-catenin expression and resistance to anti-PD-1 therapy (Appendix 5 and 6) (214). Although there was an increase in expression of genes associated with many inflammatory factors, there was particularly high expression in the brain metastasis of *CXCL1* and interleukin 10 (*IL10)* which are involved in tumour progression, immune tolerance and infiltration of immune-suppressive cells (Fig. 3.5 A) (306–308).

Fig. 3.5

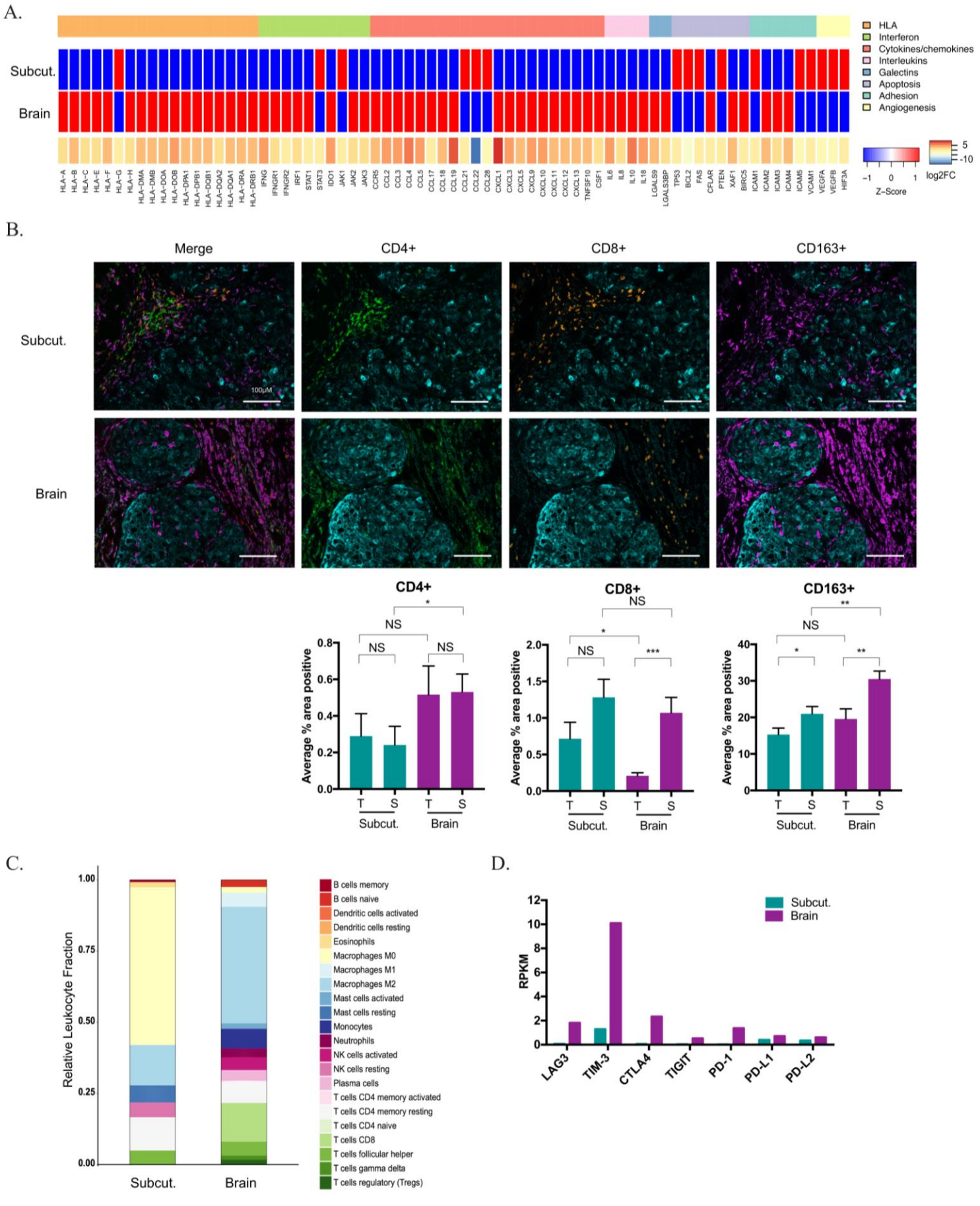
A.
Subcut.
Brain
HLA
Interferon
Cytokines/chemokines
Interleukins
Galectins
Apoptosis
Adhesion
Angiogenesis
Z-Score
log2FC
B.
Merge
CD4+
CD8+
CD163+
Subcut.
Brain
100μM
Average % area positive
NS
Subcut.
Brain
C.
Relative Leukocyte Fraction
B cells memory
B cells naive
Dendritic cells activated
Dendritic cells resting
Eosinophils
Macrophages M0
Macrophages M1
Macrophages M2
Mast cells activated
Mast cells resting
Monocytes
Neutrophils
NK cells activated
NK cells resting
Plasma cells
T cells CD4 memory activated
T cells CD4 memory resting
T cells CD4 naive
T cells CD8
T cells follicular helper
T cells gamma delta
T cells regulatory (Tregs)
D.
RPKM
Subcut.
Brain
LAG3
TIM-3
CTLA4
TIGIT
PD-1
PD-L1
PD-L2

Fig. 3.5 Immune escape in the brain is associated with a distinct microenvironment

A. RNA-Seq reveals the upregulation of immune related genes. Supervised analysis of selected genes associated with tumour-immune interaction of the baseline and immune escape brain lesion. Blue=down regulated, red= up-regulated. Log2 Fold change of the brain lesion compared to the subcutaneous lesion is depicted in blue/red gradient.

B. Immune escape is associated with heterogeneous immune cell infiltration using immunohistochemistry. Example photomicrograph images depicting heterogeneous composition of immune cell infiltrates within tumour and stroma. Left panel is overlay of the four different markers: green=$CD4^{+}$, orange=$CD8^{+}$, purple=CD163+, cyan=HMB45. Quantification (mean and standard deviation) for multiple panels of immune cell infiltrate in each lesion using Definiens is below each representative panel. NS= not significant, **P*<0.05, ***P*<0.01, ****P*<0.001.

C. Immune-escape is associated with heterogeneous immune cell infiltration using CIBERSORT. Bar chart summarizing immune cell subset proportion of 22 types of adaptive and innate immune cells quantified by CIBERSORT for the 3 lesions. CIBERSORT p-values for each sample: Subcut. *P*= 0.027; Brain *P*= 0.003.

D. Immune-escape is associated with heterogeneous immune modulator mRNA expression. Gene expression of immune modulators quantified in the 2 lesions based on RNA-Seq analysis.

Thus, compared to the baseline, the immune escape tumour presented a distinct gene signature, so I examined immune cell infiltrates in these lesions by multiplex immunohistochemistry and Definiens® to quantify cells (Fig. 3.5 B, multiplex staining performed by Garry Ashton). This revealed a trend towards higher $CD4^+$ and $CD163^+$ infiltrate in the brain metastasis in both tumour and stroma areas compared to the subcutaneous lesion (Fig. 3.5 B). Critically, $CD8^+$ infiltrate was significantly decreased in the brain lesion tumour area compared to both its surrounding stroma and also compared to the tumour area of the subcutaneous lesion (Fig. 3.5 B).

In addition, I performed CIBERSORT (Cell type Identification By Estimating Relative Subsets Of known RNA Transcripts; bioinformatics performed by Dr Yamil Mahmoud; (Newman et al., 2015)) to further examine the immune cell infiltrate. This revealed that the sub-cutaneous lesion had a high presence of memory T cells while the brain lesion presented a high proportion of M2 and T_{reg} cells, which are immune suppressive and have been linked to the lack of response to anti-PD-1 therapy (Fig. 3.5 C) (310,311). Finally, the brain metastasis also presented mRNA up-regulation of immune modulators such as *TIM3 (CD366)* and *LAG3 (CD223)*, which are associated with T cell exhaustion (312) and thereby tumour escape from the immune system (Fig. 3.5 D). Thus, the immune-escape brain lesion was associated with a general increase in inflammation and negative immune mediators with infiltrate of cells associated with immune suppression and decreased infiltrate of effector T cells compared to the pre-treatment subcutaneous lesion.

3.4 Resistance to targeted therapy in the brain

The patient commenced the BRAFi dabrafenib following further progression in the brain and a para-oesophageal lymph node. Initially the patient had a partial response to treatment in the brain, however, despite an on-going extra-cranial response, after 3 months the brain lesion progressed and was resected (Fig. 3.6A). As part of the precision medicine programme in our laboratory, Dr Romina Girotti, Dr Gabriela Gremel and Dr Elena Galvani had generated PDX and cell lines from the patient's baseline subcutaneous lesion and the pre-

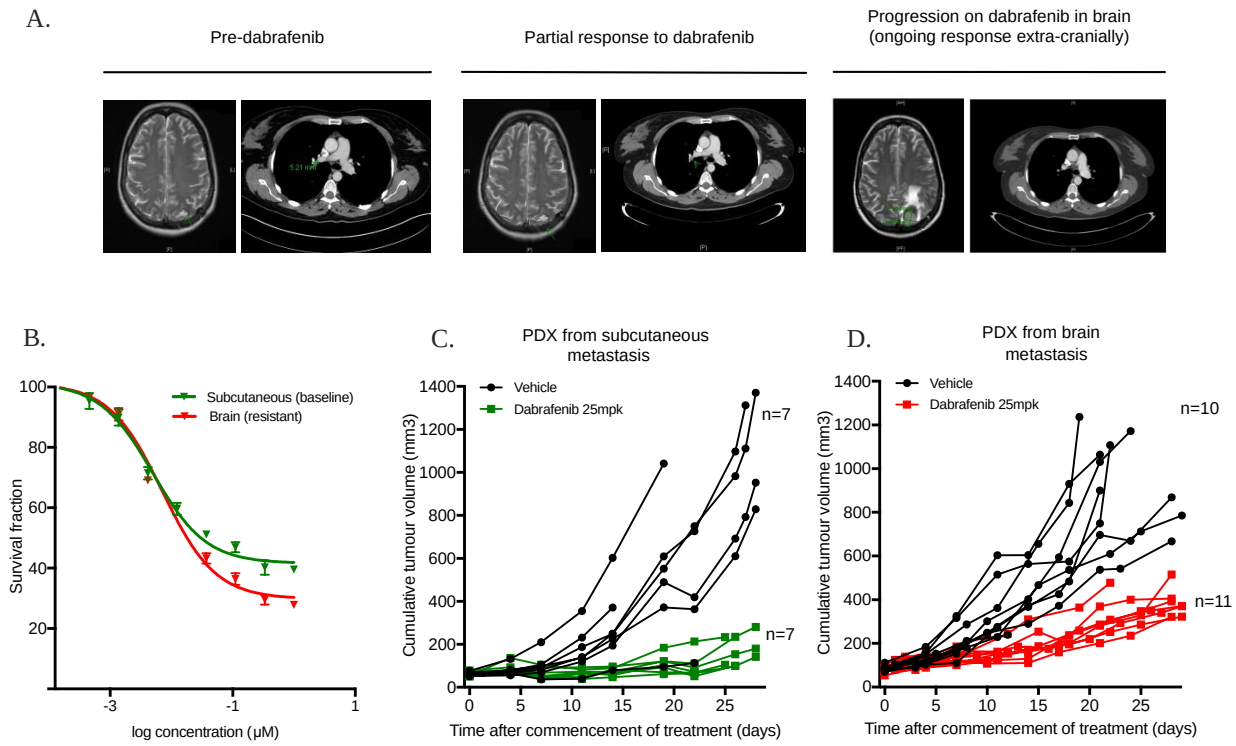

Fig. 3.6 Brain lesions retain sensitivity to dabrafenib outside the brain microenvironment.

A. Computerised tomography (CT) images of patient's brain lesion and para-oesophageal lesion in response to dabrafenib. Left CT images show pre-dabrafenib, middle images show partial response to dabrafenib and right images show disease progression in the brain and on-going response in extra-cranial sites on dabrafenib.

B. Cells derived from the dabrafenib resistant brain lesion remain sensitive to dabrafenib *in vitro*. Short-term growth inhibition assays (72 hours) of cells from the subcutaneous metastasis (GI_{50} 0.005μM) and a brain metastasis (GI_{50} 0.007μM) grown in the presence of dabrafenib (0.15nM-1μM).

C-D. PDX derived from the subcutaneous and brain lesions are both sensitive to dabrafenib when grown outside of the brain microenvironment *in vivo*. Mice were treated with dabrafenib (25 mg/kg/day) or vehicle by oral gavage. Drug treatments commenced immediately after tumours reached 80-100 mm^3 and show individual tumour volumes (n = 7-11 per group). ***P*<0.01, *****P*<0.0001.

dabrafenib brain lesion. Furthermore, I derived a cell line from the progressing brain lesion. I therefore used these patient-derived samples to determine how dabrafenib resistance in the brain was mediated.

Notably, cell lines derived from both the subcutaneous (baseline) and the brain lesion (dabrafenib resistant) displayed similar sensitivity to dabrafenib *in vitro* (Fig. 3.6 B). Similarly, when I grew PDXs from the two sites (weights and measures and some oral gavage performed by Mr Matthew Smith, I designed the experiments, implanted the tumour pieces and performed some of the oral gavage), they were equally sensitive to dabrafenib when grown in the flank of immuno-compromised mice (Fig. 3.6 C, D). Consistent with these results, WES of a cell line derived from the progressing brain metastasis did not reveal any mutations that could explain resistance to dabrafenib (a L25S *PIK3CA* mutation outside of the binding domain was associated with strand bias and was not confirmed by ddPCR; Appendix 7 and 8).

In line with other clinical responses (238,313), the initial response of the brain lesion to dabrafenib suggested that the drug did cross the blood brain barrier (BBB), and my data suggested that resistance was not mediated by cell-intrinsic events, so I examined if resistance was mediated by factors in the brain microenvironment. Seifert *et al* had shown that extrinsic factors present in CSF resulted in human and mouse cell lines becoming resistant to dabrafenib through CSF induced PI3K/AKT signalling (230).

I therefore recapitulated the brain microenvironment by culturing the cells from the patient's dabrafenib resistant brain metastasis in the presence of CSF. Cells were grown in serum-free medium for 24 hours in the presence or absence of dabrafenib, with or without CSF. Dabrafenib inhibited cell growth, and induced apoptosis in cells derived from the resistant tumour, but in the presence of CSF overcame both the growth inhibition and induction of apoptosis mediated by dabrafenib (Fig. 3.7 A, B).

Intriguingly, despite rescuing proliferation and survival, CSF did not reactivate ERK signalling in the cells from the resistant lesion (Fig. 3.7 C), so I performed RPPA (in collaboration with Dr Kenneth Macleod, Edinburgh) to identify which pathways were activated. I performed the RPPA in cell lines derived from both the brain and subcutaneous metastasis to test whether any changes in the presence of CSF were similar in both, suggesting a cell extrinsic cause. CSF did not reactivate MEK/ERK signalling (Fig. 3.7 D, 3E), and downstream S6 phosphorylation (314) was not re-activated (Fig. 3.7 F, G). However, the RPPA analysis revealed that CSF significantly increased phosphorylation of PDGFR, whereas phosphorylation of other receptor tyrosine kinases was not increased (Fig. 3.7 H, Appendix 9). Consistent with this, CSF also increased AKT phosphorylation (Fig. 3.7 I, J), suggesting that CSF mediated resistance through the PDGFR-PI3K-AKT signalling pathway rather than alternative pathways investigated in the RPPA screen. This effect was seen in cell lines from both the brain and subcutaneous metastases, supporting an extrinsic cause for PDGFR/PI3K/AKT activation rather than an intrinsic cause such as a newly acquired mutation in the brain lesion cells. In addition, immunoblot analyses showed an increase in AKT phosphorylation in the presence of CSF with and without dabrafenib, however I was not able to confirm the PDGFR activation with immunoblot (Fig. 3.7 K). Accordingly, the PI3K/mTOR inhibitor BEZ235 inhibited growth in the brain lesion cells in the presence of CSF, whereas dabrafenib had no significant effect (Fig. 3.7 L, I optimised the assay, however the final experiment in this figure was performed by Dr. Alessio Cannistraci). The PDGFR inhibitor crenolanib also exerted some effect but only at concentrations where it was likely that off target effects were contributing to the response (data not shown).

Fig 3.7

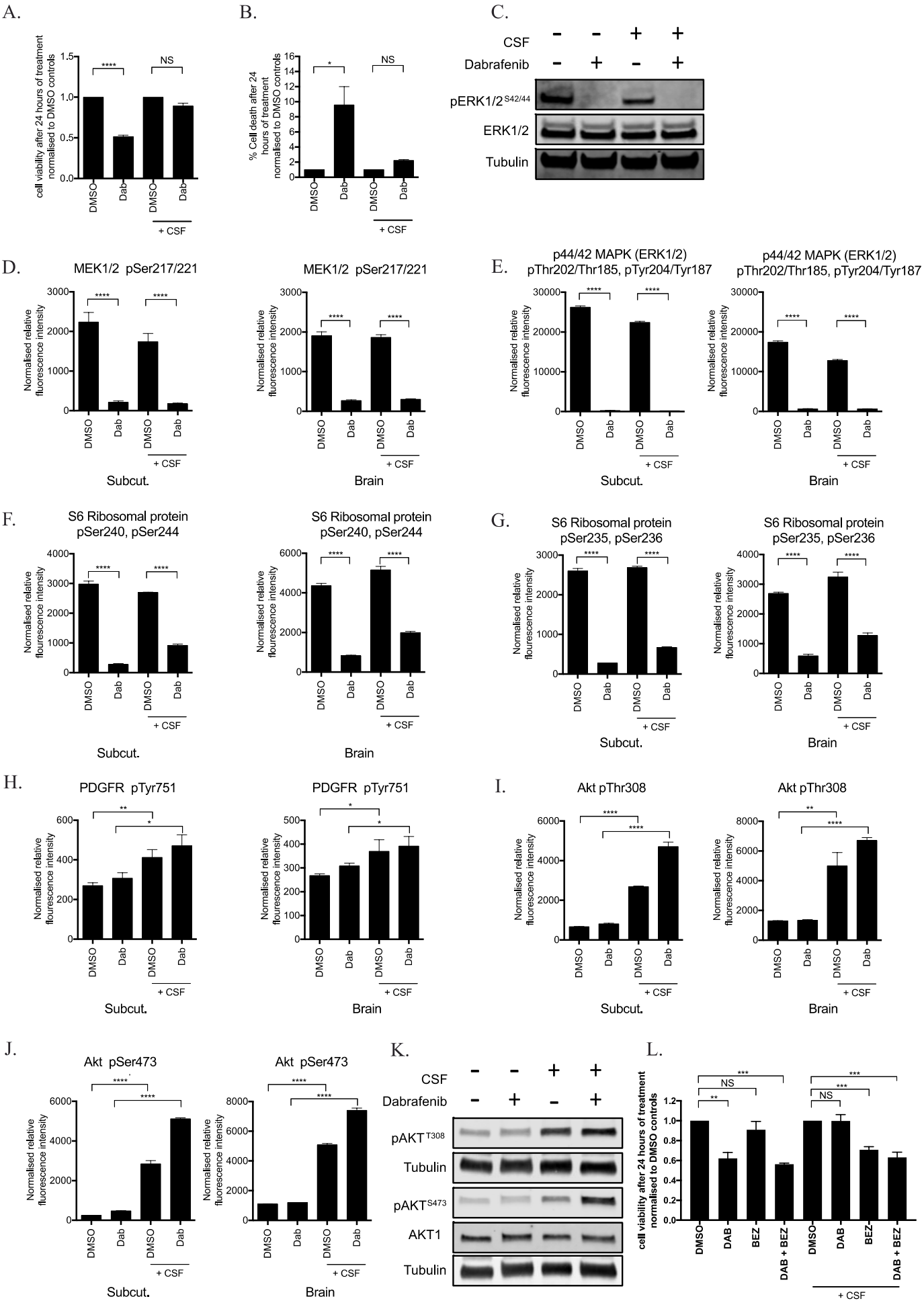
A.
cell viability after 24 hours of treatment normalised to DMSO controls
****
NS
DMSO
Dab
+ CSF
B.
% Cell death after 24 hours of treatment normalised to DMSO controls
*
NS
C.
CSF
Dabrafenib
pERK1/2 S42/44
ERK1/2
Tubulin
D.
MEK1/2 pSer217/221
Normalised relative fluorescence intensity
Subcut.
Brain
E.
p44/42 MAPK (ERK1/2) pThr202/Thr185, pTyr204/Tyr187
F.
S6 Ribosomal protein pSer240, pSer244
G.
S6 Ribosomal protein pSer235, pSer236
H.
PDGFR pTyr751
I.
Akt pThr308
J.
Akt pSer473
K.
pAKT T308
pAKT S473
AKT1
L.
DMSO
DAB
BEZ
DAB + BEZ

Fig 3.7 Cerebrospinal fluid (CSF) mediates resistance to dabrafenib through the PDGFRβ/PI3K/Akt pathway.

A. CSF overcomes dabrafenib-induced inhibition of cell growth. Short-term growth assays showing cell (derived from the brain metastasis) growth after 24 hours following treatment with DMSO or dabrafenib (Dab; 1μM) in RPMI or 50% RPMI/50% CSF using CellTiter-Glo ****P<0.0001, NS= not significant.

B. CSF overcomes cell death induced by dabrafenib. Cells were cultured overnight under serum free conditions in RPMI or 50% CSF and then treated with DMSO or dabrafenib (1μM) for 24hrs before assessing cell death using cleaved PARP staining measured by flow cytometry. *P<0.05, NS= not significant.

C. CSF does not rescue MEK/ERK signalling in dabrafenib-treated cells. Cells derived from the brain metastasis were plated and incubated overnight in RPMI or 50% RPMI/50% CSF under serum-free conditions before treatment of DMSO or dabrafenib 1μM for 4 hours. Immunoblot analysis shows phosphoERK $Thr^{202/185}$ $Tyr^{204/187}$ and ERK 1/2. Tubulin was used as a loading control.

D-J. CSF rescues cell growth through the PDGFR/PI3K/AKT pathway. Cells from the brain and subcutaneous (subcut.) metastasis were treated with DMSO or dabrafenib, cultured with or without CSF. Cell lysates were obtained and fluorescence-based nitrocellulose RPPA was performed for phospho-MEK1/2 (D), phospho-ERK (E), phospho-S6 (F, G), phospho-PDGFRβ (H), phospho-AKT (I,J). *P<0.05, **P<0.01, ****P<0.0001.

K. Immunoblot reveals increased phosphorylation of AKT. Cells derived from the brain metastasis were incubated overnight in RPMI or 50% CSF under serum-free conditions before treatment of DMSO or dabrafenib 1μM for 4 hours. Immunoblot analysis shows phospho AKT^{T308}, phospho AKT^{S473} and total AKT1. Tubulin was used as a loading control.

L. PI3K/MTOR inhibitor reduces cell growth in the presence of CSF. Graph showing cell growth measured by CellTiter Glo 24 hours after treatment with DMSO, Dabrafenib (Dab 1μM), BEZ235 (Bez 5μM) or Dabrafenib (Dab 1μM) plus BEZ235 (Bez 5μM) in RPMI or 50% CSF. **P<0.01,***P<0.001, NS = not significant.

3.5 Chapter discussion

This patient's case highlights a number of challenges that need to be overcome to improve the treatment of brain metastases in melanoma. Recent studies have shown that although response to targeted and immune therapies can be obtained in melanoma brain metastases, duration of response is shorter than for patients with extra-cranial disease alone and patients with symptomatic brain metastases have particularly poor outcomes (238,239,315). Understanding of mechanisms of resistance is therefore crucial.

3.5.1 Tumour mutational burden and response

A number of studies have reported that immune therapy responses are associated with high mutation and neoantigen burden (202,205,206). Typical for acral melanoma (76), the tumours presented here had low mutation and neoantigen burden. Nevertheless, the patient responded to nivolumab for 12 months and treatment was only discontinued due to toxicity. My data therefore show that clinical benefit can be achieved by immune therapy in tumours that present low mutation and neoantigen burden. This is in line with clinical studies showing that acral melanoma responses to immune therapy are similar to those of cutaneous melanoma (297).

I observed very little clonal inter-tumoural heterogeneity in the lesions, which may have contributed to the patient's response (206). Low intra-tumoural heterogeneity combined with high neoantigen burden has been associated with response to CTLA-4 inhibitors (ipilimumab and tremelimumab) (206). Furthermore, increased clonal vs. subclonal mutational load was associated with response to nivolumab (316). Whilst I did not analyse the tumours for intra-tumoural heterogeneity, the lack of inter-tumoural heterogeneity suggests that there was very little mutational diversity across time and space in this patient's tumours, which might increase the likelihood of response.

One of the major questions regarding this patient's case was why the patient responded to immune therapy. My cytolysis assay suggested that TIL were able to recognise and kill tumour cells. Although small in number, neoantigens were still identified in the tumour, however I did not validate them by functional TIL assays examining interferon response to the peptides generated from my *in silico* prediction. It is possible that one of the neoantigens was recognised by the T cells or that other tumour antigens such as PMEL or tyrosinase elicited an immune response. A potential method of identifying a broader repertoire of antigens would be to use DNA-barcoded libraries of MHC-I multimers to screen for T cell reactivity (317). This strategy enables rapid detection of antigens without requirement for large quantities of sample (317).

3.5.2 Immune therapy resistance was not due to intrinsic changes in IFNγ signalling or antigen presentation

The patient initially mounted an impressive anti-tumour response on nivolumab with shrinkage of all lesions apart from the lymph node. The isolated progression in the brain also suggested a specific change in cells within the brain metastasis that enabled them to escape immune control. I did not find significant changes in MHC class I expression and did not discover mutations that would impair PTEN, IFNγ or similar signalling pathways, which can drive resistance to immune therapies (215,216,303,305). Although these mechanisms have been reported in the literature, it is unclear as to how frequently they are the cause of resistance as they are mainly small case series. As I did not see these mechanisms present in my analyses, it suggests that alternative mechanisms were driving resistance.

3.5.3 Brain microenvironment and resistance to immune therapy

Notably, the brain lesion presented a gene and immune infiltrate signature associated with a significantly different microenvironment to the subcutaneous (baseline) lesion. Immunohistochemistry suggested high numbers of $CD163^+$ cells both in the tumour and the stroma of the brain metastasis. These are most likely to have been macrophages or microglia, which are a type of macrophage which resides in the central nervous system (318). There are no definitive markers to distinguish between microglia and macrophages however, microglia tend to be $CD45^+$ low and macrophages $CD45^+$ high, therefore if tissue availability had permitted, these stainings would have enabled their differentiation (318). The CIBERSORT data based on RNA-Sequencing indicated that the $CD163^+$ cells were M2 switched macrophages/microglia. Microglia/macrophages have a number of different roles in the tumour microenvironment and this is dependent on their state (318,319). Traditionally microglia/macrophages have been classified into two main types, classically activated or M1 and alternatively activated or M2, although it is likely that further research will identify more subtypes (319). M2 macrophages/microglia are associated with a pro-tumourigenic phenotype producing pro-tumourigenic factors such as IL6 and TGFβ and prostaglandins (318,319). They can also produce MMPs, which degrade the extracellular matrix enabling tumour cell migration and invasion (318,319). In addition, they can stimulate angiogenesis through production of vascular endothelial growth factor (VEGF) (319). Two papers have shown that through controlling the molecular switch from M1 to M2 macrophages using PI3Kγ inhibitors, there was a delay in tumour growth *in vivo* in a number of different tumour types including the B16 immunocompetent model of melanoma (104,105). Thus, the literature on the role of M2 macrophages in tumour progression suggests they may have contributed to immune escape in this patient, however it is not possible to show a directly causative relationship using my data.

In addition to the high numbers of tumour associated M2 macrophages/microglia seen in the immune escape brain lesion, I saw strongly increased expression of genes associated with immunosuppression and an immune suppressive infiltrate. *CXCL1* and *IL10,* had the highest fold change in gene expression in the brain compared to the subcutaneous metastasis (306–308). Melanocytes which overexpress CXCL1 have been shown to be capable of forming tumours in mice (320,321). Furthermore, a study examining gene expression signatures using microarray of nevi, primary melanomas, and melanoma metastases showed that an increasing level of *CXCL1* was associated with melanoma primaries compared to naevi (322). IL10 reduces T-lymphocyte proliferation, type 1 (Th1) cytokine production, antigen presentation, and lymphokine-activated killer cell cytotoxicity, reduces production of tumour necrosis factor-α (TNF-α), interleukin 1 (IL1) and interleukin 12 (IL12), which are immune stimulatory factors and decreases IFNγ production by macrophages and Th1 lymphocytes (323–325). Increased gene expression of *IL10* is also associated with tumour progression; a study performing real time PCR on FFPE melanoma tissue showed that primary and metastatic melanomas had significantly higher expression of *IL10* than melanoma *in situ* (326). Another study overexpressed *IL10* in the B16 melanoma cell line, which normally does not produce high levels of IL10. When grown in immunocompetent mice, the IL10 transfected cells showed higher growth and proliferation rates and although there was no difference in $CD8^+$ cells, numbers of $CD4^+$ cells increased (although they did not further characterise the cells to see if they were regulatory T cells) (325). Furthermore, they observed increased angiogenesis determined by endothelial marker Von Willebrand factor and automated morphometry in the tumours from IL10 transfected cells (325).

Intriguingly, chemokine ligand 4 and 19 (*CCL4, CCL19)* transcripts also showed high expression but have been associated with increased T cell infiltration (327). It may be that

although there was increased expression of these cytokines, their effect was overwhelmed by other immunosuppressive cytokines.

Finally, transcripts associated with increased T cell exhaustion and resistance to immune checkpoint blockade inhibitor such as *TIM3* and *LAG3* were increased in the brain metastasis compared to the subcutaneous lesion (312). Unfortunately, the lack of tissue prevented me from confirming the expression of these using IHC.

Critically, the brain metastasis was associated with significantly decreased $CD8^+$ effector T-cell infiltration in the multiplex immunohistochemistry compared to the surrounding stroma, which was not seen in the baseline subcutaneous lesion (Fig 3.5 B). The CIBERSORT data however showed that the relative frequencies of $CD8^+$ T cells were higher in the brain lesion compared to the subcutaneous lesion (Fig 3.5 C). There are a number of potential reasons for this; firstly the RNA-Sequencing is performed on a small area of the micro-dissected tumour, whilst the IHC was examining across a slice of the whole tumour and therefore may better represent the immune cell infiltration. Alternatively there may have been stromal contamination of the brain metastasis through insufficient micro-dissection of the tumour. That appears less likely as even if more of the T cells in the brain stroma had been included, the IHC showed these were not significantly higher in number than the T cells in the subcutaneous tumour. Finally, the CIBERSORT analysis is based on relative abundance of one cell type compared to other cell types whereas the immunohistochemistry Definiens® analysis quantifies absolute numbers. Therefore, if other cells were less abundant in the CIBERSORT data this would increase the relative T cell count (309).

Although limited, my data suggests that immune escape did not appear to be driven by loss of the intrinsic ability of T cells to recognise and kill the tumour cells, but by the acquisition of a distinct microenvironment.

3.5.4 Brain microenvironment and resistance to targeted therapy

Despite surgery and radiotherapy, the brain lesion progressed necessitating treatment with dabrafenib. Initially, the patient mounted an excellent response including shrinkage of the brain lesion. This in accordance with the BREAK-MB trial which showed that 20/65 patients (30.8%, 19.9- 43.4) post prior local therapy achieved an intracranial response to dabrafenib, supporting the findings in this patient that the drug is able to cross the BBB (313).

However, despite a continued extra-cranial response, the brain lesion relapsed rapidly. I did not find new mutations to explain resistance, and cells from the dabrafenib-resistant brain lesion remained sensitive to dabrafenib *in vitro*, as did the PDXs in immuno-compromised mice. In accordance with a recent study (230), I found that CSF overcame the anti-proliferative and pro-apoptotic effects of dabrafenib on cells from the cranial lesion. Notably, the rescue of cell growth by CSF was not accompanied by MEK-ERK pathway reactivation, but by hyper-activation of the PDGFR/PI3K/AKT pathway. The same effect was seen in cells from the subcutaneous metastasis suggesting an extrinsic rather than intrinsic cause for the dabrafenib resistance. Unfortunately, due to the limited tissue, I was unable to confirm increased phosphorylation of AKT in the brain lesion by immunohistochemistry. However, BEZ235, a dual PI3K/mTOR inhibitor, blocked the growth of cells both as a single agent and in combination with dabrafenib in the presence of CSF, whereas dabrafenib alone had no significant effect on growth. In the absence of CSF, dabrafenib inhibited the growth of the cells whereas BEZ235 had no significant effect.

Thus, my data adds to a body of evidence showing that the PI3K/AKT pathway plays an important role in the progression and potential resistance to therapy of brain metastases. One of the first studies to suggest a role for the PI3K/AKT pathway in melanoma brain metastases was a study characterising 16 pairs of matched melanoma brain and extra-cranial metastases (231). No differing patterns of mutations, copy number variations or gene

expression signatures were seen in the brain metastases compared to extra-cranial tumours (231). However, RPPA revealed activation of the PI3K/AKT pathway in brain metastases compared to extra-cranial disease (231). Following from this, Seifert *et al* showed that the brain was a common site of relapse in patients treated with BRAFi for melanoma and that there was reduced sensitivity to dabrafenib of mouse derived and human melanoma cells grown in the presence of CSF (230). The addition of a PI3K/AKT inhibitor to dabrafenib resulted in decreased melanoma cell number after 24 hours of treatment (230). Furthermore, Niessner *et al* showed that cells grown in the presence of astrocyte conditioned medium increased phospho-AKT levels and had increased sensitivity to the PI3K inhibitor buparlisib compared to cells grown in the presence of media for 72 hours (232). *In vivo* models of orthotopically injected cells into the right striatum of 8 week-old mice, which were then treated from day 20 post-inoculation with either buparlisib or vehicle, showed an improved survival of mice treated with drug (232). Thus, the PI3K/AKT pathway appears to have an important role in growth of melanoma brain metastases.

3.5.5 Study Limitations

The main limitation of this study was that it included only one patient and therefore it is unclear whether my findings would be relevant to other patients. In addition, some analyses of the RNA-Sequencing were limited by the number of samples. In order to address this challenge, it would have been better to perform RNA-Sequencing on at least 3 replicates from the same lesion or perform single cell analysis (with the caveat of intra-tumoural heterogeneity) however I did not have sufficient tissue available. This was also a recurrent issue when it came to validate the data seen in RNA-Sequencing for the immune therapy progression and testing of phosphorylation of AKT in the pre and post dabrafenib treatment

lesions. This study highlights the importance of planning and prioritising IHC analyses during the course of a study especially in limited patient samples.

Ideally, a number of patients with tissue from brain metastases which had progressed on immune therapy would be compared to their baseline tumours, however it is rare that patients have resection of brain metastases in melanoma and a brain biopsy for research purposes is ethically impossible to justify due to the risk of such a procedure. It would be difficult to model this in mice as the ideal experiment would be to inject cells into the flank that are known to metastasise to the brain (such as B16, clone G3.12 (328)), biopsy the flank tumour and then treat with anti-PD-1 comparing progressing brain lesions to the baseline biopsy. Alternatively, it would be possible to examine changes seen in progressing brain metastases on anti-PD-1 therapy compared to no treatment in immunocompetent mice by injecting cells directly into the brain and comparing anti-IgG (control) treated group with an anti-PD-1 treatment group (329). Further analyses could be performed through injection into the flank modelling extra-cranial disease and then, when that had established, to perform a further cell injection into the brain. The flank tumour would then be sufficiently large to perform a biopsy prior to starting anti-PD-1 therapy.

3.6 Chapter Summary

I show in this chapter that progression on immune and targeted therapy was mediated by interactions between the tumour and brain microenvironment. In the case of immune therapy, immune escape was associated with a heterogeneous immune infiltrates and gene expression profile compared to the baseline lesion, whereas CSF factors contributed to resistance to targeted therapy through the PDGFR/PI3K/AKT pathway. The brain is a common site of treatment failure in many cancers and continues to be a challenge in the era of immune and targeted therapy in melanoma. However, patients with brain metastases are often excluded from clinical trials and their optimal management remains uncertain. This chapter provides insight into the importance of the microenvironment in mediating resistance and I show that improved knowledge of the underlying mechanisms can provide hypothesis-driven salvage treatment strategies. Thus, both the mutational characteristics and the site-specific microenvironment characteristics of individual melanoma lesions need to be considered to optimise precision medicine strategies for melanoma patients.

Chapter 4. Sequencing combination PI3K/Pan-RAF inhibitors and a PKC agonist overcomes resistance in *BRAF* and *NRAS* mutant melanoma

Targeted therapy remains an important option in melanoma management. Long term follow up of patients treated with combination dabrafenib and trametinib have shown that those with favourable prognostic features such as normal baseline LDH and less than 3 disease sites can have durable responses, with approximately 25% of patients progression free at 5 years (330).

At present, standard of care, targeted therapy is limited to patients with *BRAF* mutant melanoma whilst patients with *NRAS* mutant melanoma are typically treated with immune therapy or other agents within a clinical trial. A Phase II trial is examining whether trametinib in combination with anti-PD-1 therapy (NCT02910700) will improve response rates and survival for patients with *NRAS* mutant melanoma, however results are awaited. The identification of drug targets for RAS has been the focus of intense research for decades, however have largely been ineffective. Whilst research is on-going to develop drugs targeting RAS, alternative approaches such as downstream targeting are required.

There is a clear clinical need to develop agents that target both NRAS and BRAF in melanoma. Furthermore, despite improvements in PFS, acquired resistance remains a huge challenge with a myriad of mechanisms reported in the literature (see Section 1.7) (127,163,310,331–334). In addition, scheduling of these treatments may be important to prevent onset of resistance (see Section 1.10 (167)) currently being assessed in the INTERIM trial (NCT03352947), which is testing drug holiday approaches with the aim of extending treatment and reducing toxicity. Finally, emerging data suggests that when resistance to drugs develops, cells can become dependent on them for survival (164–166,168). The mechanism

for this is thought to be due to ERK2 hyperactivation, which occurs when drug is withdrawn in drug resistant cells, (165).

In collaboration with Prof. Caroline Springer's group, our laboratory has developed a pan-RAF inhibitor CCT3833 that is currently being tested in a Phase I clinical trial (NCT02437227). CCT3833 has a similar structure to published drugs in the drug series, which have shown inhibition of BRAF, CRAF and SRC as well as some effect on p38 and LCK kinases, depending on the compound (335). As the drugs inhibit both CRAF and BRAF, they are able to overcome paradoxical activation of CRAF and phosphorylation of MEK/ERK, which can occur in *RAS* mutant cells if BRAFi are given (71). The drugs showed *in vitro* and *in vivo* efficacy in both *BRAF* and *NRAS* mutant melanoma and had improved response compared to PLX4720 (an analogue of vemurafenib) (335).

I therefore decided to perform a study with the following aims:

1. To establish whether resistance to CCT3833 occurs *in vitro*
2. If resistance is acquired, to identify underlying mechanisms of resistance to CCT3833, which might be used to interrogate upfront combination therapy strategies
3. To investigate whether resistance to CCT3833 results in a drug addiction phenotype and if so to gain further insight into the mechanisms of drug addiction

To do this, I used a combination of human cell lines that were available from ATCC and patient-derived cell lines (derived from patients attending The Christie NHS Foundation Trust) in order to understand mechanisms of resistance and drug addiction, then validated my findings *in vivo*, however due to time constraints, some of this work is on-going.

4.1 Resistance to CCT3833 results in activation of the MAPK or PI3K/AKT pathways

I treated *BRAF* mutant (A375/COLO829) or *NRAS* mutant (D04/ RM59 [a patient derived cell line see Appendix 10 clinical characteristics]) cell lines with increasing concentrations of CCT3833. After approximately 4-9 months depending on the cell line, the cell lines were able to grow in either 1μM (A375/COLO829) or 2μM (D04/RM59) CCT3833 and shifts in the half maximal inhibitory concentration (IC_{50}) were observed (Fig. 4.1 A-D, Table 4.1 IC_{50} vs. resistant cell lines). Intriguingly, the parental RM59 cell line were less sensitive to CCT3833 both in short term assays (Fig. 4.1 D) and clonogenic assays (Fig. 4.1 E) than other cell lines, suggesting a degree of intrinsic resistance to drug, although it became resistant to higher concentrations when cultured in the presence of CCT3833.

Table 4.1. IC50 parental vs. CCT3833 resistant cell lines

Cell line	Parental IC50 μM (standard deviation)	Mean* CCT3833 resistant IC50 μM (standard deviation)
A375	0.12 (0.06)	1.58 (0.18)
Colo829	0.14 (0.07)	1.73 (0.38)
D04	1.19 (0.41)	2.26 (1.58)
RM59	1.61 (0.15)	4.58 (0.14)

*Of 3 technical replicates and at least 2 separate experiments

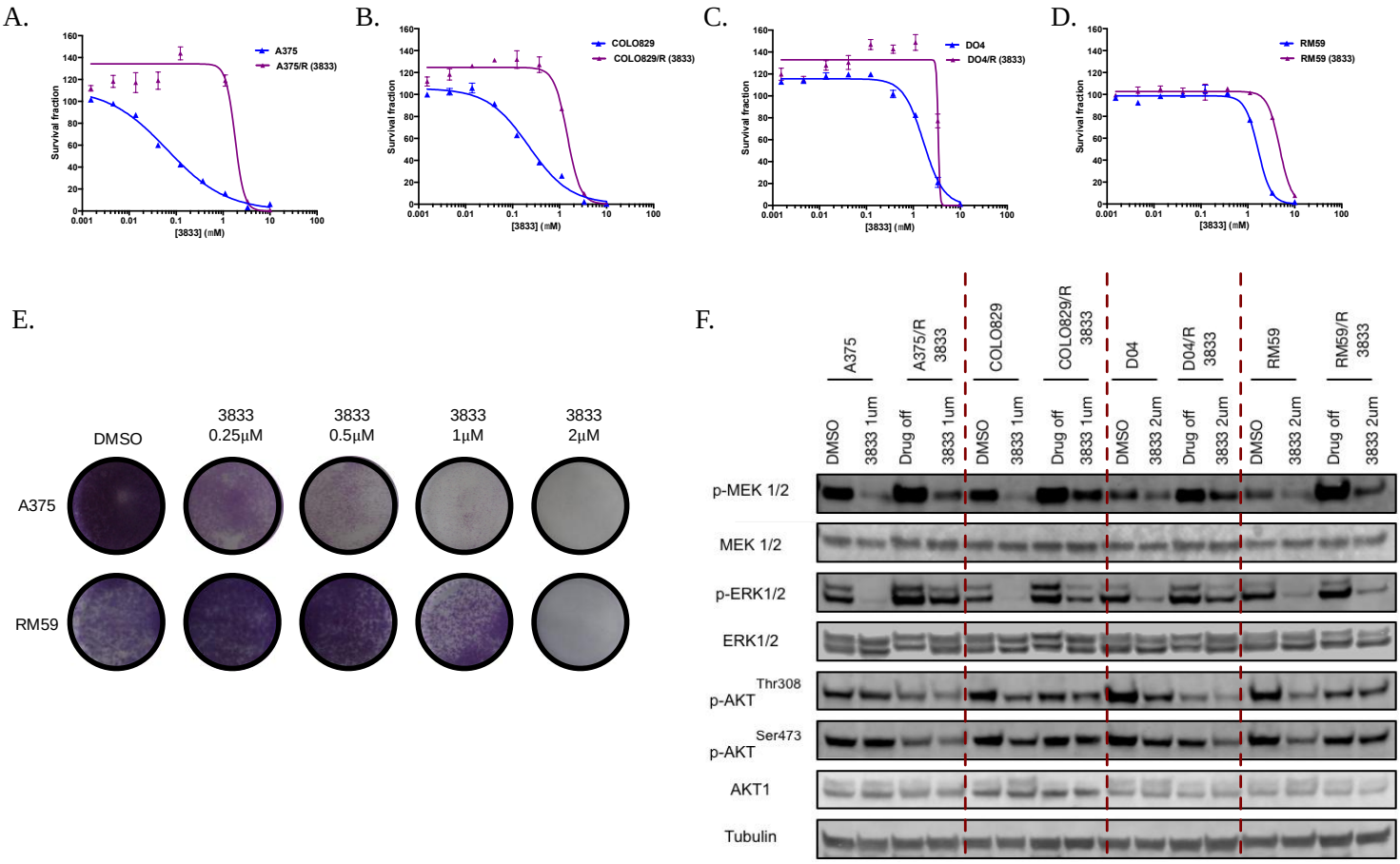

Fig. 4.1. Resistance to CCT3833 results in re-activation of the MAPK pathway or activation of the PI3K/AKT pathway

A-D. *BRAF* and *NRAS* mutant cell lines resistant to CCT3833 (3833). Cells were grown in increasing concentrations of CCT3833 then short-term growth inhibition assays (72 hours) performed of parental and CCT3833 resistant cells grown in the presence of CCT3833 (1.5nM-10μM). A. A375 (*BRAF* V600E mutant) B. COLO829 (*BRAF* V600E mutant) C. D04 (*NRAS* Q61L mutant) D. RM59 (*NRAS* Q61R mutant).

E. Long term clonogenic assays of parental A375 and RM59 cells show different sensitivity to CCT3833. A375 and RM59 cells cultured in CCT3833 0.25-2μM for 10 days (example from 1 experiment shown, assay performed in duplicate and in 2 separate experiments).

F. Mechanisms of resistance result in either MAP kinase (MAPK) pathway reactivation or PI3K/AKT pathway reactivation. Phospho-MEK, phospho-ERK or phospho-AKT in parental and CCT3833 resistant cell lines (A375, Colo829, D04, RM59) cultured in DMSO or CCT3833 for 4 hours (representative immunoblot from at least 2 separate experiments).

Previous research has shown that resistance to BRAFi/MEKi reactivates the RAS/RAF/ERK (MAPK) or PI3K pathways (331,333,336). Thus, I performed immunoblot of phospho-MEK and phospho-ERK, which revealed that resistance to CCT3833 (cell line/R (3833)) resulted in reactivation of the MAPK pathway in 3 cell lines (A375/R [3833], Colo829/R [3833] and D04/R [3833]), with an increase in phospho-MEK in the presence of CCT3833 in the RM59/R (3833) cell line, however phospho-ERK remained inhibited (Fig. 4.1 F). In addition, immunoblot revealed increased phosphorylation of AKT^{Thr308} and AKT^{S473} in the RM59/R (3833) cell line, whereas it was similar to the parental cells or decreased in the presence of CCT3833 in the other cell lines (Fig. 4.1 F).

4.2 Genetic and transcriptional alterations are associated with resistance to the pan-RAF inhibitor CCT3833

To identify mechanisms of resistance to CCT3833, which could cause activation of the MAPK and PI3K pathways, I performed WES of the CCT3833 resistant cells and compared them to the parental cells (Appendix 11-14 acquired mutations of cell lines). Bioinformatics have been performed by Dr. Garima Khandelwhal in this chapter, and I discussed all analyses with her and interpreted the results. WES revealed a p.K57E *MAP2K1* mutation in A375/R (3833) (Fig. 4.2 A) and a p.F436L *ARAF* mutation in Colo829/R (3833) (Fig. 4.2 B). I did not observe any acquired mutations in D04/R (3833) or RM59/R (3833) that could explain the increase in ERK phosphorylation in the D04/R (3833) cell line, or the activation of the PI3K/AKT pathway in the RM59/R (3833) cell line (Appendix 13 and 14). However, when I compared the parental and resistant RM59 cell lines to the patient's germline DNA, I identified a p.L414F *PIK3R4* mutation in the cell line, which may have resulted in the initial decreased sensitivity to CCT3833 (Fig 4.2 C).

Fig. 4.2.

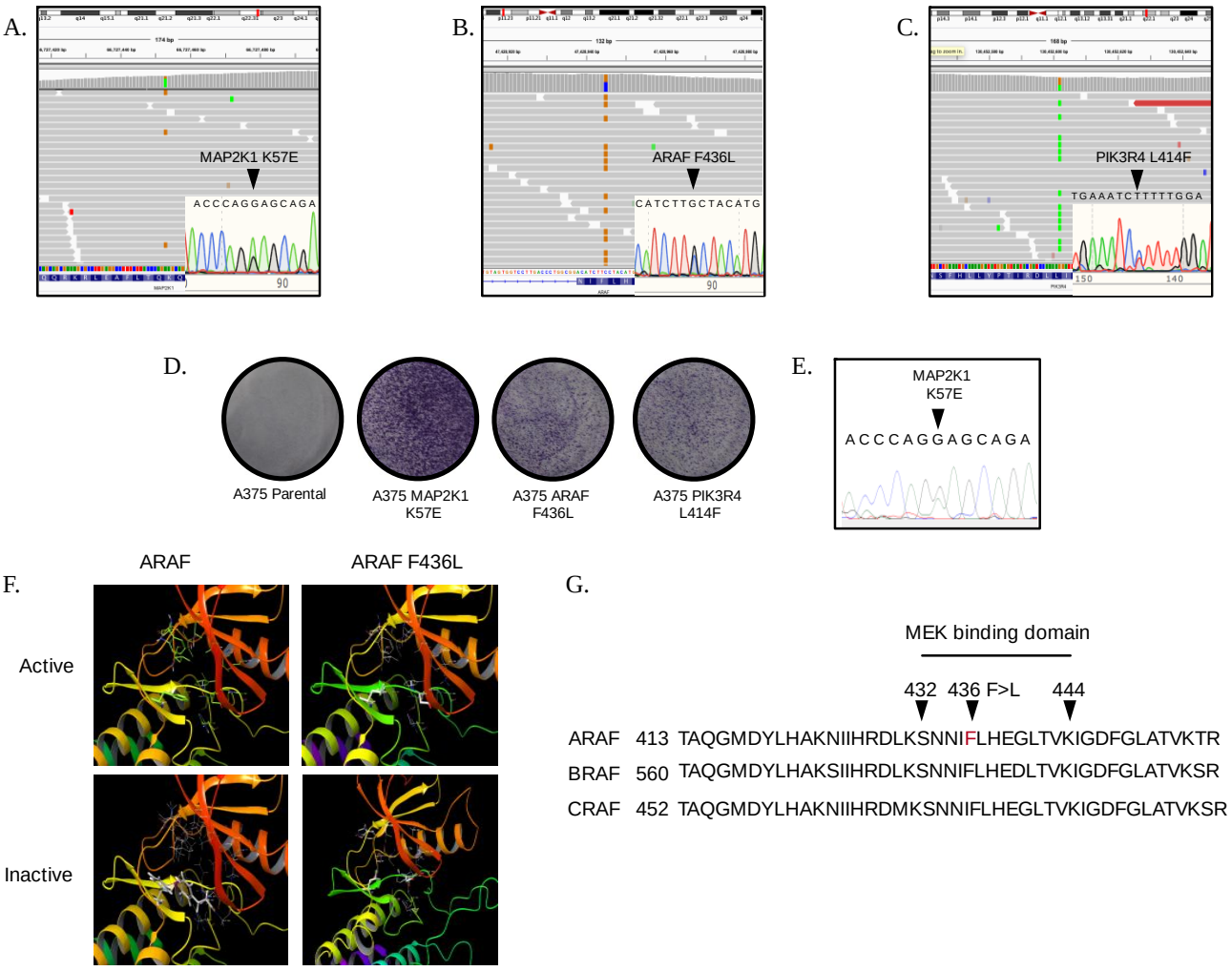

Fig. 4.2. Genetic and transcriptional alterations are associated with resistance to the pan-RAF inhibitor CCT3833

A-C. Mutations in cell lines associated with resistance to CCT3833. Integrative genome viewer display of acquired mutations occurring in resistant cell line but not present in parental cells validated with Sanger sequencing in **A.** A375/R (3833) = p.K57E *MAP2K1* **B.** COLO829/R (3833) = p.F436L *ARAF* **C.** Mutation in p.L414F *PIK3R4* occurring in parental RM59 and RM59/R (3833) cells.

D. Mutations inserted into A375 cells using CRISPR cas9 targeted genome editing result in increased growth of cells in the presence of CCT3833. Indicated mutations were inserted into parental A375 using CRISPR cas9 targeted genome editing. 100,000 cells were plated and grown in the presence of CCT3833 1μM (A375) for 7 days, fixed and stained.

E. Confirmation of the presence of a p.K57E *MAP2K1* mutation in A375 cells. Sanger sequencing was performed to confirm the presence of the p.K57E *MAP2K1* mutation in A375 cells.

F. p.F436L *ARAF* mutation is present in the active site pocket of the kinase domain. The ARAF kinase was modelled based on the structure of BRAF (80% homology) with the F436L amino acid change shown in the active and inactive conformations.

G. *ARAF* F436L mutation is present in the MEK binding domain of the active site. Schematic representation of ARAF, BRAF and CRAF adapted from Baljuls *et al* (337) showing the homology of the MEK binding domain and the mutation resulting in an amino acid change F>L at position 436.

To validate whether these mutations contributed to resistance to CCT3833, I utilised CRISPR/Cas9 technology and homology directed repair to insert mutations p.K57E *MAP2K1*, p.F436L *ARAF* and p.L414F *PIK3R4* into parental A375 cells. The cells were selected through culturing in CCT3833 from day 1 following transfection (day 0) at a concentration of initially 0.5μM increasing to 1μM CCT3833 within 2 weeks. I confirmed their resistance to drug using long-term clonogenic assays culturing cells in CCT3833 1μM over seven days (Fig. 4.2 D). I was able to confirm the p.K57E *MAP2K1* mutation in the A375 using Sanger sequencing (Fig. 4.2 E), however was not able to confirm the p.F436L *ARAF* and p.L414F *PIK3R4* mutations as there appeared to be parentals still remaining in the population, therefore this will be repeated. Single cell isolation could also be performed to better isolate clones with the mutation present.

As *MAP2K1* mutations have previously been reported in resistance to BRAFi/MEKi (168,331) and PI3K/PTEN/AKT mutations as resistance mechanisms to BRAFi (128,331,333), I focussed on understanding how the p.F436L *ARAF* mutation contributed to CCT3833 resistance as it has not previously been described. The crystal structure of ARAF has not been solved. However as the mutation was in a highly conserved region with greater than 80% homology to BRAF and CRAF, attempts were made to model the structure of ARAF utilising homology base modelling on the resolved crystal structure of BRAF to gain provisional insight into how the mutation could confer resistance to CCT3833 (modelling performed by Dr. Alfonso Zambon). This revealed that although the mutation was present in the kinase domain, it was not predicted to result in a large change in the geometry of the active site in both active and inactive conformations and therefore was not likely to impede kinase activity (Fig. 4.2 F). In addition, modelling did not suggest that binding of drug to the kinase domain was affected. However, literature review (34) revealed that the mutation was present in the MEK binding domain in ARAF, BRAF and CRAF kinases and therefore could be affecting interaction with MEK (Fig. 4.2 G).

Fig. 4.3.

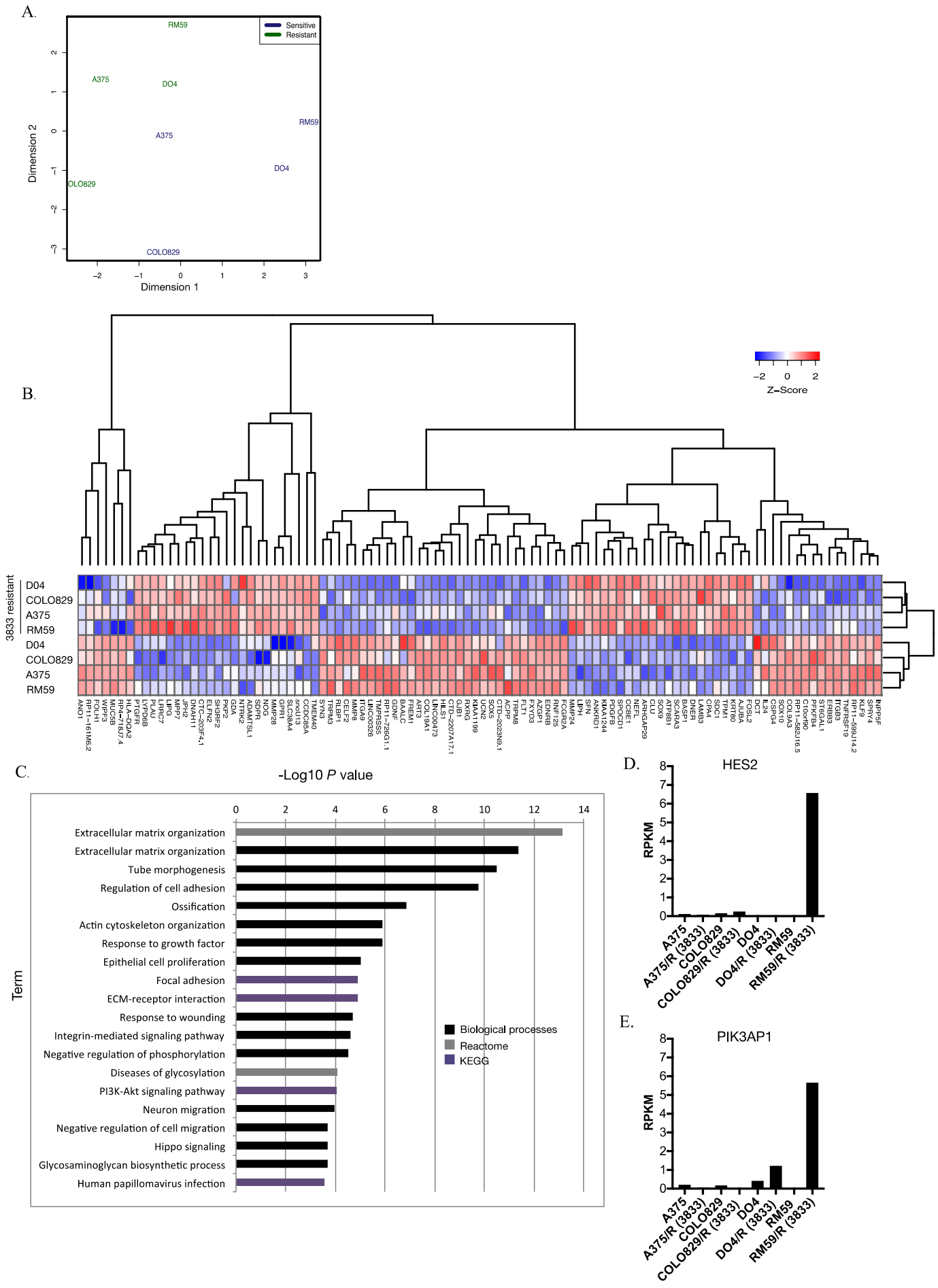
A.
Sensitive
Resistant
RM59
A375
DO4
RM59
A375
DO4
COLO829
COLO829
Dimension 1
Dimension 2
B.
Z-Score
3833 resistant
D04
COLO829
A375
RM59
D04
COLO829
A375
RM59
C.
-Log10 P value
Extracellular matrix organization
Extracellular matrix organization
Tube morphogenesis
Regulation of cell adhesion
Ossification
Actin cytoskeleton organization
Response to growth factor
Epithelial cell proliferation
Focal adhesion
ECM-receptor interaction
Response to wounding
Integrin-mediated signaling pathway
Negative regulation of phosphorylation
Diseases of glycosylation
PI3K-Akt signaling pathway
Neuron migration
Negative regulation of cell migration
Hippo signaling
Glycosaminoglycan biosynthetic process
Human papillomavirus infection
Term
Biological processes
Reactome
KEGG
D.
HES2
RPKM
A375
A375/R (3833)
COLO829
COLO829/R (3833)
DO4
DO4/R (3833)
RM59
RM59/R (3833)
E.
PIK3AP1
RPKM
A375
A375/R (3833)
COLO829
COLO829/R (3833)
DO4
DO4/R (3833)
RM59
RM59/R (3833)

A. Multi-dimensional scaling (MDS) plot of RNA-Sequencing of CCT3833 resistant vs. parental cell lines. RNA-Sequencing was performed on A375, Colo829, D04 and RM59 parental (cultured in media) and CCT3833 resistant (cultured in CCT3833 1μM A375/COLO829 or 2μM D04/RM59) cells. The gene expression of resistant vs. parental cells was plotted using MDS.

B. RNA-Sequencing reveals transcriptional differences in *BRAF* and *NRAS* mutant parental vs. CCT3833 resistant cells. Unselected hierarchical clustering of RNA-Sequencing data reveals changes in gene expression of parental vs. CCT3833 resistant A375/Colo829/D04/RM59 cells.

C. Gene set enrichment analysis of CCT3833 resistant cells compared to parental cells. Genes with a ≥1 log2 fold change in CCT3833 resistant A375/Colo829/D04/RM59 cells compared to parental cells were analysed for enrichment of biological processes, reactome and KEGG pathways.

D-E. RM59/R (3833) cells are associated with high expression levels of genes associated with PI3K/AKT up-regulation. RNA Sequencing of parental vs. CCT3833 resistant cells (A375/Colo829/D04/RM59). Genes associated with activation of the PI3K/AKT pathway are shown D. *HES2* E. *PIK3AP1*.

Previous studies have shown that resistance to inhibitors of the MAPK pathway results in transcriptional changes due to altered expression of MITF (see Chapter 1) (163). To investigate whether similar phenotypic changes occurred in cells when resistant to CCT3833, I performed RNA-Sequencing on the four CCT3833 resistant and parental cell lines and compared their gene expression. A multidimensional scaling (MDS) plot of genes with ≥1 count per million in at least 4 samples, showed a shift in the first and second dimension when cells were resistant to higher concentrations of CCT3833, corresponding to a similar change in gene expression profiles in both the *BRAF* and *NRAS* mutant cell lines (Fig. 4.3 A). Unsupervised hierarchical clustering revealed similar variations in gene expression in both *BRAF* and *NRAS* mutant CCT3833 resistant cell lines (Fig. 4.3 B). Of note, genes previously associated with resistance to BRAFi such as *PDGFβ* and *SOX9* were up-regulated in the *BRAF* and *NRAS* resistant cell lines compared to parental (Fig. 4.3 B). Gene set enrichment analysis after filtering for genes with a log2 fold change ≥1 revealed an up-regulation of genes associated with remodelling of the extracellular matrix, focal adhesion and the PI3K/AKT pathway (Fig 4.3 C). This suggests

that both *BRAF* and *NRAS* mutant cells undergo similar phenotypic changes when they become resistant to CCT3833. Furthermore, the RM59 cells, which were less sensitive to CCT3833, still underwent changes associated with culturing in and resistance to CCT3833 resulting in a phenotypic shift from parental to RM59/R (3833) cells.

To explore whether there were any transcriptional changes, which could explain the increase in phospho-ERK in the D04/R (3833) cell line and the increased phospho-AKT in the RM59/R (3833) cell line, I examined the top 20 differentially expressed genes in each cell line (Appendix 15). Intriguingly, the D04/R (3833) cell line had up-regulated many long non-coding RNAs in comparison to parental cells. Conversely, the RM59/R (3833) cell line had significantly up-regulated two genes associated with activation of the PI3K/AKT pathway *HES2* and *PIK3AP1* (Fig. 4.3 D and Fig. 4.3 E). The gene expression changes could have contributed to the increase in phospho-AKT seen in RM59/R (3833) cells on the immunoblot (Fig 4.1 F).

Taken together, these data suggest that resistance to CCT3833 results in a similar transcriptional phenotype both in *BRAF* and *NRAS* mutant cells, as well as reactivation of the MAPK pathway or up-regulation of the PI3K/AKT pathway.

4.3 *CCT3833 resistant NRAS* and *BRAF* mutant cells exhibit decreased sensitivity to MAPKi and increased sensitivity to PI3K or cell cycle inhibitors

To identify potential drugs or drug targets that cells would be sensitive to in resistance to CCT3833 I worked with Mr Denys Holovanchuk a PhD student in the group, to perform a kinase inhibitor drug screen. He had optimised a method of screening cells against a kinase inhibitor library (Selleck; L1200) to identify drugs that inhibited cell viability. We therefore designed an experiment to compare the sensitivity of parental vs. CCT3833 resistant cells to the compound library. He plated cells (the CCT3833 resistant cells in 0.25μM CCT3833 to prevent any loss of fitness, see section 4.5). The next day he treated them for 72 hours with a kinase library at a concentration of 0.1μM. Cell viability was analysed using CellTiter-Glo of cells with the kinase inhibitors present compared to DMSO controls (termed "death fraction" Fig. 4.4 A and B). The death fraction of CCT3833 resistant cells was then plotted against the death fraction of parental cells cultured in the presence of each respective kinase inhibitor. Kinase inhibitors were categorised into groups of targets e.g. cell cycle. Both the A375/R (3833) and D04/R (3833) cells showed decreased sensitivity compared to their parental cells to drugs targeting the MAPK pathway (Fig. 4.4 A and B). In contrast, the death fraction of A375/R (3833) and D04/R (3833) cells was increased compared to parental cells when treated with inhibitors targeting PI3K, mTOR, polo-like kinase (PLK) or CDKs (Fig 4.4 A and B).

Fig. 4.4.

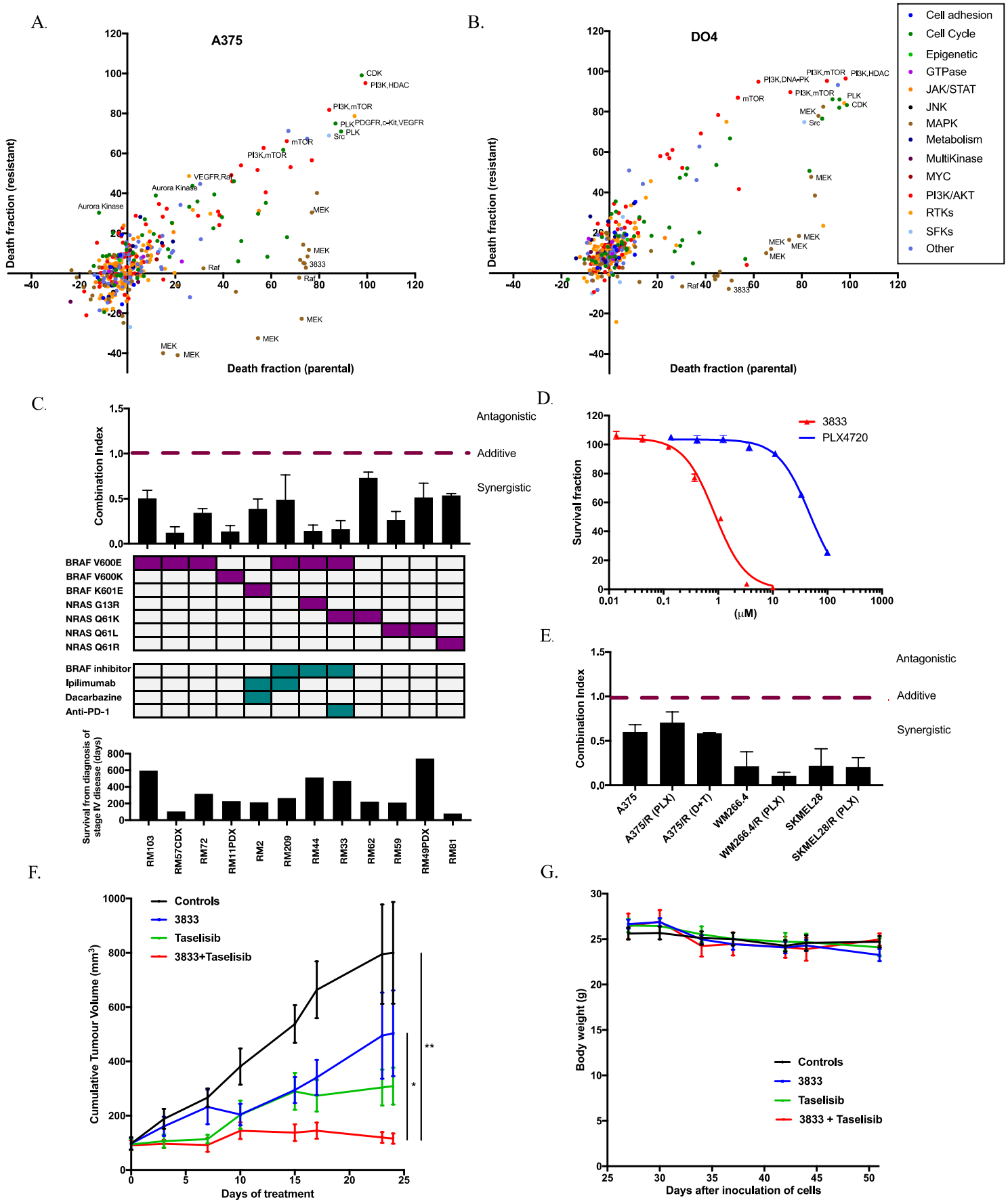
A.
A375
Death fraction (resistant)
Death fraction (parental)
CDK
PI3K,HDAC
PI3K,mTOR
PLK
PDGFR,c-Kit,VEGFR
Src
mTOR
PI3K,mTOR
VEGFR,Raf
Aurora Kinase
Aurora Kinase
MEK
MEK
3833
Raf
Raf
MEK
MEK
MEK
B.
DO4
Death fraction (resistant)
Death fraction (parental)
PI3K,DNA-PK
PI3K,mTOR
PI3K,HDAC
mTOR
PI3K,mTOR
PLK
CDK
MEK
Src
MEK
MEK
MEK
MEK
Raf
3833
Cell adhesion
Cell Cycle
Epigenetic
GTPase
JAK/STAT
JNK
MAPK
Metabolism
MultiKinase
MYC
PI3K/AKT
RTKs
SFKs
Other
C.
Combination Index
Antagonistic
Additive
Synergistic
BRAF V600E
BRAF V600K
BRAF K601E
NRAS G13R
NRAS Q61K
NRAS Q61L
NRAS Q61R
BRAF inhibitor
Ipilimumab
Dacarbazine
Anti-PD-1
Survival from diagnosis of stage IV disease (days)
RM103
RM57CDX
RM72
RM11PDX
RM2
RM209
RM44
RM33
RM62
RM59
RM49PDX
RM81
D.
Survival fraction
3833
PLX4720
(μM)
E.
Combination Index
Antagonistic
Additive
Synergistic
A375
A375/R (PLX)
A375/R (D+T)
WM266.4
WM266.4/R (PLX)
SKMEL28
SKMEL28/R (PLX)
F.
Cumulative Tumour Volume (mm³)
Controls
3833
Taselisib
3833+Taselisib
Days of treatment
**
*
G.
Body weight (g)
Controls
3833
Taselisib
3833 + Taselisib
Days after inoculation of cells

Fig. 4.4. CCT3833 synergises with PI3kinase inhibitors.

A-B. Drug screen reveals both *BRAF* and *NRAS* mutant resistant cells have increased sensitivity to inhibitors of the PI3K/AKT/mTOR pathway and cell cycle. Cells were cultured for 72 hours in the presence of 0.1μM concentration drug library of 360 kinase inhibitors classified according to predominant mechanism of action then viability was measured using CellTiter-Glo. The decrease in viability ("death fraction") of cells in the presence of inhibitor compared to DMSO controls was calculated. Graphs depict the death fraction of parental cells plotted against the death fraction of CCT3833 resistant cells.

C. Taselisib is synergistic with CCT3833 in multiple patient-derived cell lines. Growth inhibition assays were performed (72 hours in drug) of CCT3833, taselisib and CCT3833 plus taselisib on patient-derived cell lines with a variety of different *BRAF/NRAS* mutations, having received a variety of prior treatments and who were associated with diverse outcomes following diagnosis of stage IV disease. Viability was measured using CellTiter-Glo. The combination index (CI) was calculated to analyse whether effects were antagonistic, additive or synergistic.

D. Cell line with p. K601E *BRAF* mutation is resistant to PLX4720 but sensitive to 3833. Short-term growth inhibition assays (72 hours) performed in p. K601E *BRAF* mutant cells grown in the presence of CCT3833 (1.5nM-10μM) or PLX4720 (15nM-100μM)

E. Taselisib is synergistic with CCT3833 in both parental and BRAFi/MEKi resistant cells. Growth inhibition assays were performed (72 hours in drug) of CCT3833, taselisib and CCT3833 plus taselisib on isogenic cells sensitive and resistant to BRAFi or BRAFi/MEKi. The combination index (CI) was calculated to analyse whether effects were antagonistic, additive or synergistic.

F. Taselisib is synergistic with CCT3833 in *BRAF* V600E mutant A375M cells grown *in vivo*. Mice (n=5 per group) were treated with vehicle, CCT3833 (40 mg/kg/day), taselisib (10 mg/kg/day) or CCT3833 (40 mg/kg/day) + taselisib (10 mg/kg/day) by oral gavage. Drug treatments commenced immediately after tumours reached 20-150 mm^3. **P*<0.05, ***P*<0.01.

G. Combined CCT3833 and taselisib is well tolerated by mice. Weight over time of mice treated with vehicle, CCT3833 (40 mg/kg/day), taselisib (10 mg/kg/day) or CCT3833 (40 mg/kg/day) + taselisib (10 mg/kg/day) by oral gavage.

4.4 Combining CCT3833 with a PI3K inhibitor is synergistic in vitro and in vivo

The kinase library screen of CCT3833 resistant vs. parental cells chiefly enriched for PI3K/AKT inhibitors and therefore I decided to target the PI3K/AKT pathway to forestall CCT3833 resistance. Previous studies have suggested that upfront combination therapy is likely to be most effective provided no mutations conferring cross-resistance are present (338). Furthermore, clinical experience of D+T has shown that when the drugs are combined, PFS is significantly longer than either monotherapy (339–341). I therefore tested whether the combination of CCT3833 and a PI3K inhibitor was synergistic. First, I chose two compounds on the basis of their toxicity profiles and stage of development in clinical trials. Alpelisib is an α-selective PI3K inhibitor which inhibits the α-isoform only at nanomolar concentrations (342), whereas taselisib inhibits all isoforms apart from the β isoform (343). Initial experiments in patient-derived cell lines (RM2, RM11, RM33, RM49, RM57, RM59, RM62, RM81, RM103, RM209) showed that taselisib (IC_{50} range 0.9-12.2 μM) had a stronger growth inhibitory effect than alpelisib (IC_{50} range 8.8-40.2μM, Appendix 16). I therefore focussed on taselisib and calculated combination indices using isobolograms to analyse its synergy with CCT3833 in early passage, patient-derived cell lines (Appendix 10 clinical information). Critically, this revealed the two compounds were synergistic with combination indices <1 in all patient-derived cell lines independent of their mutation status (*NRAS*/*BRAF*), therapy received prior to excision of the lesion (targeted/ chemo /immune therapy) or the aggressive course of the melanoma within the patient (defined by survival from diagnosis of stage IV disease to death, Fig. 4.4 C). Of note, RM33 had a p.K601E *BRAF* mutation, and consistent with the literature as a class 2 type BRAF mutation, was resistant to PLX4720 (344), but sensitive to CCT3833 and showed synergy in combination with taselisib (Fig. 4.4 C and D). Furthermore, I calculated combination indices for isogenic

cells made resistant to PLX4720 (by Dr. Franziska Baenke) or A375 cells that I had made resistant to D+T (Fig. 4.4 E). This showed that in these cell lines, CCT3833 and taselisib were synergistic whether cells were BRAFi +/- MEKi sensitive or resistant (Fig. 4.4 E).

Finally, to evaluate whether the combination of taselisib plus CCT3833 was synergistic *in vivo*, I designed an experiment (the experiment was performed by Miss. Filipa Lopes), treating CD-1 nude mice (Crl:CD1-*Foxn1*^{nu}) bearing xenografts of A375M (A375-MA1 ATCC® CRL-3222™, metastatic variant of A375) cells with daily oral gavage of vehicle (5% DMSO), taselisib (10mg/kg), CCT3833 (40mg/kg) or the combination of taselisib (10mg/kg) + CCT3833 (40mg/kg). This confirmed that the combination resulted in reduced growth of tumours compared to monotherapy with taselisib or CCT3833 (Fig. 4.4 F) and crucially the mice tolerated treatment well with no AEs or weight loss (Fig. 4.4 G). I plan to perform a further experiment using D04 cells to test that the combination is also synergistic in *NRAS* mutant cells *in vivo*.

4.5 Only cells activating the MAPK pathway when resistant to CCT3833 are drug addicted

Curiously, when I performed clonogenic assays to confirm that the A375/Colo829/D04/RM59 cells were resistant to CCT3833, I noticed that when they were cultured in DMSO ("drug off") there was a significant loss of fitness (Fig. 4.5A). Growth of the cells was decreased compared to cells with "drug on" or parental cells and they only started to recover after 18 days following drug withdrawal (Fig. 4.5 B).

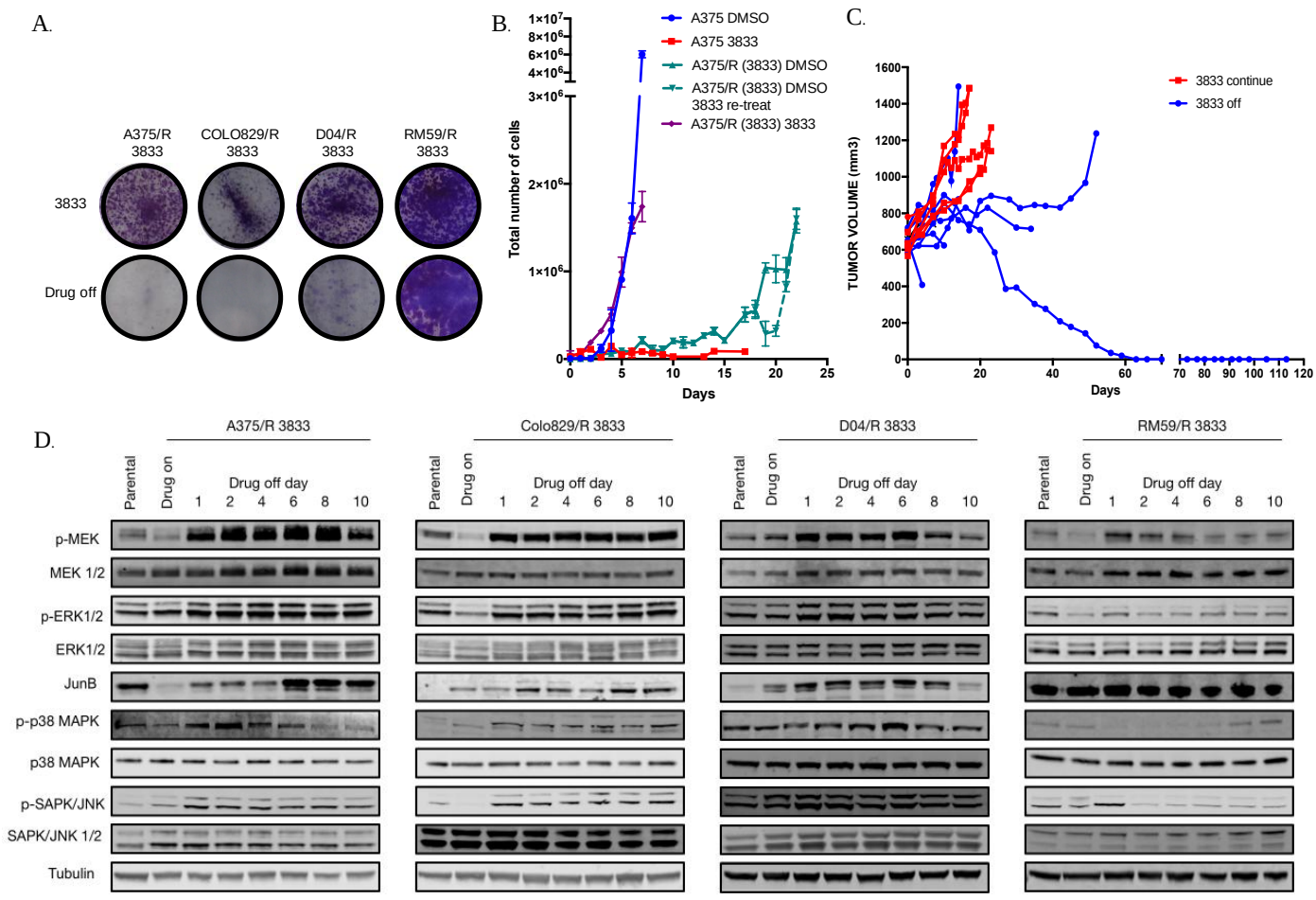

Fig. 4.5. Different mechanisms of resistance to CCT3833 result in variable degrees of drug addiction and hyper-activation of stress pathways.

A. Cells that reactivate the MAPK pathway are drug addicted, however cells activating the PI3K/AKT pathway do not show a drug addiction phenotype. Clonogenic assays of cells cultured for 10 days in 3833 1μM (A375/R 3833, COLO829/R 3833) or 2μM (D04/R 3833, RM59/R 3833) or DMSO ("drug off").

B. Growth of cells is significantly decreased when drug is withdrawn from drug addicted cells. A375 parental cells compared to A375/R (3833) cells cultured in DMSO or CCT3833 1μM and counted daily. In the A375/R (3833) cells drug was added after 18 days and compared to cells cultured in DMSO.

C. Drug addiction phenotype *in vivo* in A375/R 3833 cells. A375/R (3833) xenograft treated with CCT3833 (40mg/kg) from day 0 until tumours were ≥600mm^3 then mice randomised to continue CCT3833 (n=6) or drug off (n=8).

D. Drug addiction phenotype reveals hyper-phosphorylation of ERK, p38 and JNK. Cells were cultured in 3833 1μM (A375/R 3833, COLO829/R 3833) or 2μM (D04/R 3833, RM59/R 3833) or drug was withdrawn and lysates made on days 1, 2, 4, 6, 8, 10. Immunoblot was performed, analysing for phospho-MEK$^{Ser217/221}$, MEK 1/2, phospho-ERK Thr$^{202/185}$ Tyr$^{204/187}$, ERK 1/2, JunB, phospho-p38$^{Thr180/Tyr182}$, total p38, phospho-SAPK/JNK$^{Thr183/Tyr185}$, total SAPK/JNK and tubulin was used as a loading control.

Furthermore, when cells were recultured in CCT3833 following the "drug off" period, they started to grow again within 24 hours (Fig. 4.5 B). I confirmed this effect *in vivo* by treating mice bearing A375/R (3833) xenografts with CCT3833 (40mg/kg) from day 0 until they reached 600mm^3 and then randomising them to continue CCT3833 or switch to "drug off" vehicle (dosing and weight and measures were performed by Mr. Jonathan Greenall, I designed the experiment, performed cell injections, randomisation and data analysis). Apart from one tumour, growth in the vehicle treated group was delayed compared to tumours in CCT3833 treated mice and some tumours decreased in size or became so necrotic that the mouse had to be culled (Fig. 4.5 C). A similar observation termed "drug addiction" had previously been reported in vemurafenib and D+T resistant cells when drug was withdrawn (165–168). Intriguingly, this phenomenon only occurred in cells that had reactivated the MAPK pathway, whilst the RM59/R (3833) cells, which had up-regulated the PI3K/AKT pathway, did not lose fitness (Fig. 4.5 A).

4.6 Drug addiction results in ERK/p38/JNK hyperactivation

Previous work had shown that when drug was withdrawn, ERK was hyperactivated which in turn hyperactivated its downstream transcription factor JunB (165). In addition, another group had shown that levels of phospho-p38 also increased on drug withdrawal (166). I therefore performed immunoblot to assess whether levels of phospho-ERK and phospho-p38 increased in the CCT3833 resistant cell lines upon drug withdrawal. This revealed that the A375/R (3833), Colo829/R (3833) and D04/R (3833) cell lines displayed increased levels of phospho-MEK, phospho-ERK, JunB and phospho-p38 following CCT3833 withdrawal (Fig. 4.4 D). However, only an increase in phospho-MEK was seen in

the RM59/R (3833) cells on days 1 and 2 whereas phospho-ERK, JunB and phospho-p38 did not change (Fig. 4.5 D).

As both the p38 and MAPK pathways are involved in cellular stress response (345), I examined whether levels of phospho-JNK, which is another SAPK, was also increased on drug withdrawal. Again, the A375/R (3833), Colo829/R (3833) and D04/R (3833) cells all increased levels of phospho-SAPK/JNK, whereas the RM59/R (3833) cells decreased rather than increased phospho- SAPK/JNK after day 1 of drug withdrawal (Fig. 4.5 D).

4.7 Early changes in gene expression are seen following removal of CCT3833 in drug addicted cells

Up-regulation of stress kinases results in activation of many transcription factors such as JunB, ATF1 and ATF2 (346–348). Therefore, I investigated how gene expression changed over time following drug withdrawal. I performed RNA Sequencing of A375/R (3833) cells with "drug on" (0 hr) vs. "drug off" for 30 minutes (30 min), 24 hours (24 hr) and 5 days (5 day). An MDS plot of genes with ≥1 count per million in at least 3 samples showed that after only 30 min of "drug off" there were changes seen in gene expression in dimension 2 (Fig. 4.6 A). This was more pronounced at 24 hr with changes seen in dimension 1 and even further changes seen in both dimensions at 5 days (Fig. 4.6 A). Unsupervised hierarchical clustering again showed changes in gene expression occurred as early as 30 min and became more pronounced at 5 days (Fig. 4.6 B). Gene set enrichment analysis of genes filtered by a >1 log2 fold change and an false discovery rate (FDR) of <0.05 between day 5 ("drug off") and time zero ("drug on") revealed an up-regulation of pathways such as response to type I interferon, notch signalling and extracellular matrix

Fig 4.6

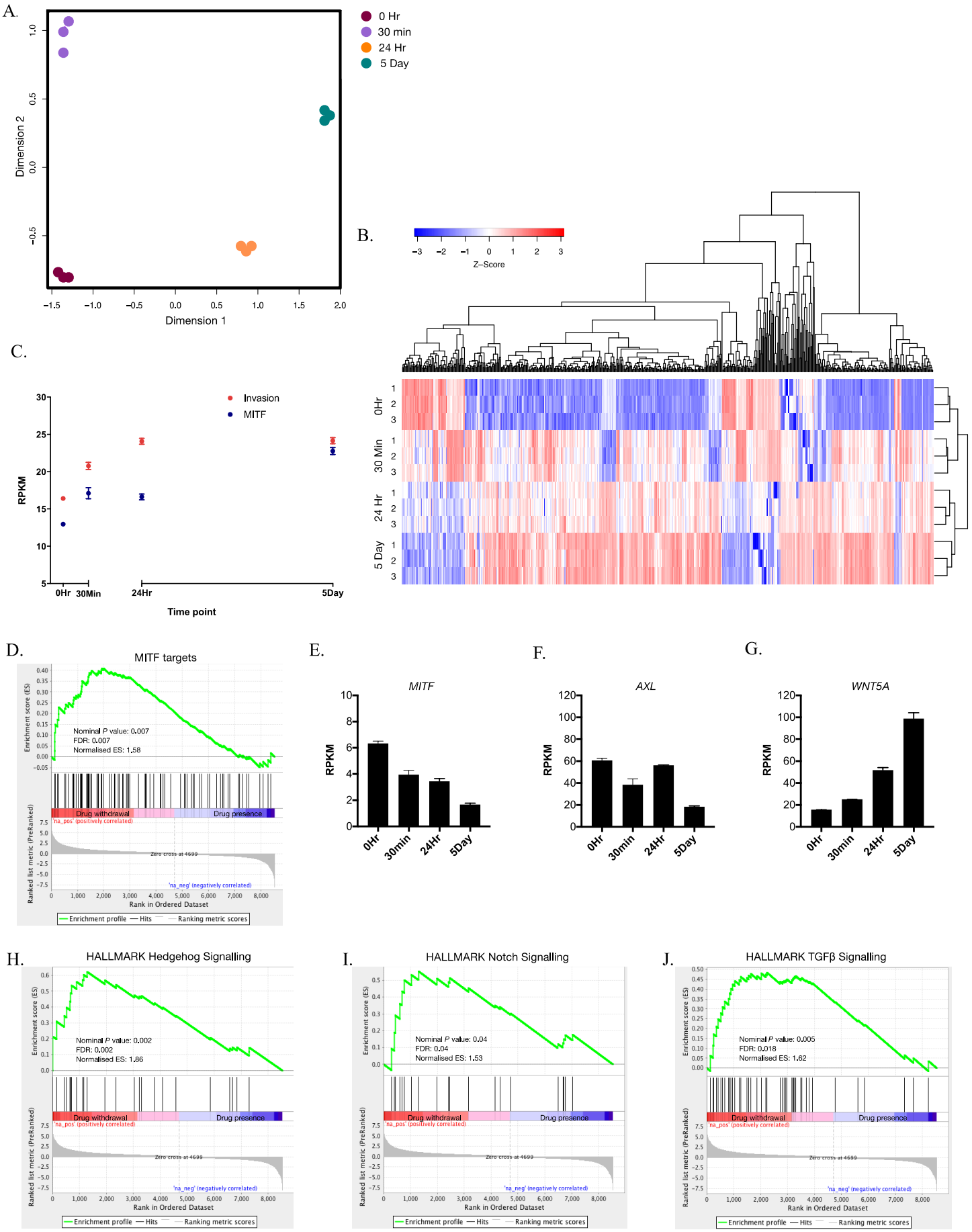
A.
0 Hr
30 min
24 Hr
5 Day
Dimension 2
Dimension 1
B.
Z–Score
0Hr
30 Min
24 Hr
5 Day
C.
Invasion
MITF
RPKM
0Hr
30Min
24Hr
5Day
Time point
D.
MITF targets
Nominal P value: 0.007
FDR: 0.007
Normalised ES: 1.58
Drug withdrawal
Drug presence
Zero cross at 4699
Rank in Ordered Dataset
Enrichment profile
Hits
Ranking metric scores
E.
MITF
F.
AXL
G.
WNT5A
H.
HALLMARK Hedgehog Signalling
Nominal P value: 0.002
FDR: 0.002
Normalised ES: 1.86
I.
HALLMARK Notch Signalling
Nominal P value: 0.04
FDR: 0.04
Normalised ES: 1.53
J.
HALLMARK TGFβ Signalling
Nominal P value: 0.005
FDR: 0.018
Normalised ES: 1.62

Fig. 4.6. Drug withdrawal from drug addicted cells is associated with stem-cell like, invasive transcriptional characteristics

A. Changes in gene expression occur early following CCT3833 withdrawal from drug resistant cells. MDS plot showing gene expression of A375/R (3833) cells cultured in CCT3833 1μM (0 Hr) vs. drug withdrawal at 30 minutes (30 Min), 24 hours (24 Hr) and 5 days (5 Day). Samples performed in triplicate.

B. Changes in gene expression following CCT3833 withdrawal from drug resistant cells. Unsupervised hierarchical clustering of RNA-Sequencing data showing gene expression of A375/R (3833) cells cultured in CCT3833 1μM (0 Hr) vs. drug withdrawal at 30 Min, 24 Hr and 5 Day. Samples performed in triplicate.

C. Invasive and MITF signatures change over time following drug withdrawal in drug resistant cells. Mean (+/- standard deviation of the 3 replicates) gene expression changes of invasive and MITF signatures (Rambow *et al* (160)) based on RNA-Sequencing data of A375/R (3833) cells cultured in CCT3833 1μM (0 Hr) vs. drug withdrawal at 30 Min, 24 Hr and 5 Day. Samples performed in triplicate.

D. Gene set enrichment analysis reveals increased expression of genes associated with MITF in drug addicted cells, 24 hours following drug withdrawal. MITF gene set enrichment analysis of A375/R (3833) cells cultured in CCT3833 1μM vs. 24 hours drug withdrawal. FDR = false discovery rate, ES = enrichment score.

E-G. Expression of MITF, AXL and WNT5A changes following CCT3833 withdrawal in A375/R (3833).

RNA Sequencing data showing gene expression of E. *MITF*, F. *AXL* and G. *WNT5A* in A375/R (3833) cells cultured in CCT3833 1μM (0 Hr) vs. drug withdrawal at 30 Min, 24 Hr and 5 Day. Samples performed in triplicate.

H-J. Gene set enrichment analysis reveals increased expression of genes associated with stem cell-like features 24 hours following drug withdrawal.

Hallmark gene set enrichment analysis of RNA-Sequencing data of A375/R (3833) cells cultured in CCT3833 1μM vs. 24 hours drug withdrawal. I. Hedgehog signalling J. Notch signalling K. TGFβ signalling. FDR = false discovery rate, ES = enrichment score.

organisation (Appendix 17). Furthermore pathways such as DNA replication, cell cycle checkpoints, cell cycle and mitotic pro-metaphase were down-regulated (Appendix 18).

Previous studies have shown that cells undergo EMT and become more invasive when drug is withdrawn from drug-addicted cells. Furthermore, Kong *et al* observed that upon drug withdrawal, MITF decreased resulting in down-regulation of MITF targets (165). Therefore, I examined invasion and MITF gene signatures by taking gene sets from Rambow *et al* (160) and tracking their mean expression over time (Fig. 4.5 C). This revealed that genes associated with invasion increased even at 30 min following drug withdrawal and further increased over time to 5 days (Fig 4.6 C). Unexpectedly, the MITF gene signature increased rather than decreased over time following drug withdrawal in these cells, which is contrary to the Kong *et al* data. I therefore also tested whether MITF targets were enriched following drug withdrawal at 24 hr using the method Kong *et al* had reported in their paper and found that in this cell line MITF targets increased when drug was withdrawn which differed from what they had reported (Fig. 4.6 D) (165). Although *MITF* decreased following drug withdrawal, it did not change significantly from "drug on" to 24 hr "drug off" (average log2FC= -0.88 across replicates) and at 5 days "drug off" it had decreased by an average log2FC of -1.92 (Fig 4.6 E). The receptor tyrosine kinase AXL has been reported to be high when MITF is decreased and therefore I examined its expression in the "drug off" vs. "drug on" RNA-Sequencing. This revealed that *AXL* expression decreased rather than increased, with an average log2FC= -0.1 at 24 hr and log2FC= -1.7 at 5 days following drug withdrawal compared to "drug on" (Fig. 4.6 F). Conversely, the WNT ligand gene *WNT5A*, which is associated with melanoma

invasion and metastasis increased with an average log2FC= 1.7 at 24 hr and log2FC= 2.7 at 5 days following drug withdrawal compared to drug on (Fig. 4.6 G).

As *WNT5A* had increased and notch signalling was increased in the pathway analysis, I examined whether genes associated with a stem cell like phenotype were increased following drug withdrawal. Gene set enrichment analysis of hallmark gene sets revealed that hedgehog (Fig. 4.6 H), notch (Fig. 4.6 I), and TGFβ signalling (Fig. 4.6 J), were significantly enriched in the cells 24hr following drug withdrawal compared to drug on. Genes associated with WNT/β-catenin (*P*= 0.086, FDR= 0.097) and EMT (*P*= 0.01, FDR= 0.068) trended towards being up-regulated upon drug withdrawal at 24 hr, but this was not significant.

Taken together, these data suggest that MITF has played less of a role in the phenotypic changes seen upon withdrawal in this cell line. However the cells exhibit gene expression changes associated with a more stem cell like, invasive phenotype with up-regulation of genes associated with notch, hedgehog and TGFβ signalling. Furthermore, expression of genes associated with growth and proliferation is decreased in "drug off" cells.

4.8 Inhibition of ERK but not p38 or JNK rescues the drug addiction phenotype

Kong and colleagues had shown that drug addiction is exquisitely dependent on ERK2 hyperactivation (165). I therefore examined whether pharmacological inhibition of p38, ERK or JNK was able to rescue cell growth when CCT3833 was withdrawn. Both an SRB assay to measure total protein content of cells as a measure of growth (Fig 4.7 A) and a clonogenic assay (Fig 4.7 B) showed that the addition of an ERK inhibitor (SCH772984) but not a p38 (SB203580) or JNK inhibitor (JNK-IN-

8) rescued the cells from the drug addiction phenotype. Furthermore, removing drug from CCT3833 drug addicted cells and culturing them for 10 days in DMSO significantly changed their morphology compared to CCT3833 controls from a rounded, flat, epithelial-like morphology to a more spindly, elongated, mesenchymal phenotype with thin protrusions (Fig 4.7 C). Only if the cells were cultured in a specific ERK1/2 inhibitor (SCH772984) did the morphology resemble the "drug on" phenotype, whereas cells cultured in a p38 (SB203580) or JNK (JNK-IN-8) inhibitor more closely resembled the "drug off" phenotype (Fig 4.7 C).

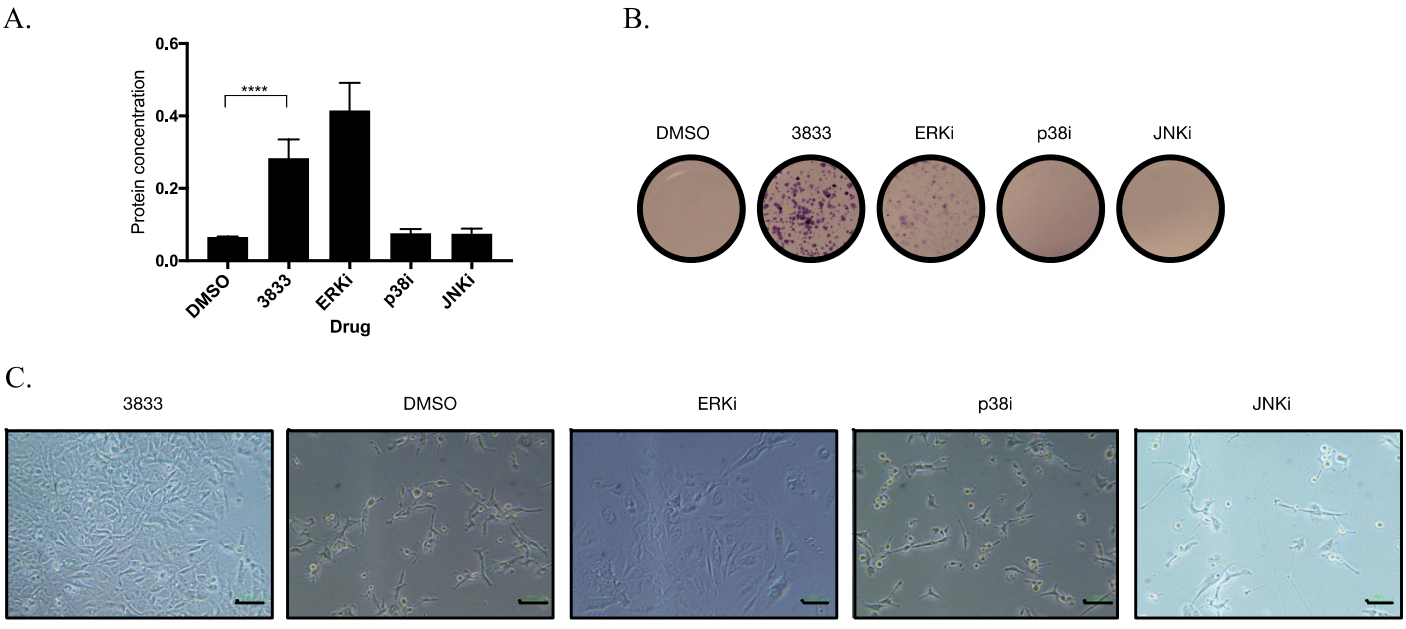

Fig. 4.7. Drug addiction is ERK dependent

A. Inhibition of ERK but not p38 or JNK results in rescue of drug addiction phenotype. A. Short term growth assay (96 hours) measured with SRB assay and **B.** Clonogenic assay of A375/R (3833) cells cultured in 3833 1μM, ERK inhibitor (ERKi) SCH772984 0.1μM, p38 inhibitor (p38i) SB203580 0.1μM, JNK inhibitor JNK-IN-8 0.1μM or DMSO for 10 days. ****P<0.0001

C. Drug addicted cells grown in CCT3833 or an ERK inhibitor have a similar phenotype. Image of A375/R (3833) cells cultured in 3833 1μM, ERK inhibitor (ERKi) SCH772984 0.1μM, p38 inhibitor (p38i) SB203580 0.1μM, JNK inhibitor JNK-IN-8 0.1μM or DMSO for 10 days. Scale 100 pixels.

4.9 PKC family members decrease their kinase activity upon drug withdrawal in drug addicted cells

The MAPK pathway controls a huge number of biological processes and is regulated by a number of feedback mechanisms. To interrogate whether other kinases were affected by drug withdrawal in drug addicted cells, I performed a kinase screen using a serine-threonine kinase (STK) array (PamGene®; I designed the experiments and made the lysates; the A375, Colo829 and D04 experiments were performed by Miss. Marta Gomez-Martinez at the Institute of Cancer Research, London and I performed the ERK inhibitor experiment). I compared the kinase activity of STKs in A375/R (3833) cells on day 1 and day 5 following "drug off" vs. "drug on". Consistent with the immunoblot data (Fig. 4.5 D), this showed that of the top 25 kinases with the highest specificity score (measure of how likely the kinase can be predicted to have changed in activity from the set of phosphorylated peptides) ERK, p38 and JNK had an increased normalised kinase statistic (measure of the relative change in activity of a kinase) in the day 1 "drug off" cells compared to "drug on" (Fig 4.8 A). Notably, a number of members of the PKC family had decreased kinase activity when drug was withdrawn (Fig. 4.8 A). Furthermore, on day 5 activity of the PKC family had reduced even further (Fig. 4.8 B). I confirmed the decrease in PKC family kinase activity at day 1 and day 5 following drug withdrawal in the two other drug addicted cell lines Colo829/R (3833) and D04/R (3833) (Fig. 4.8 C).

The PKC family is associated with activation of the MAPK pathway (93,349). I therefore hypothesised that the decrease in PKC activation could be due to negative feedback arising from ERK hyperactivation. Accordingly, when I withdrew CCT3833

Fig. 4.8.

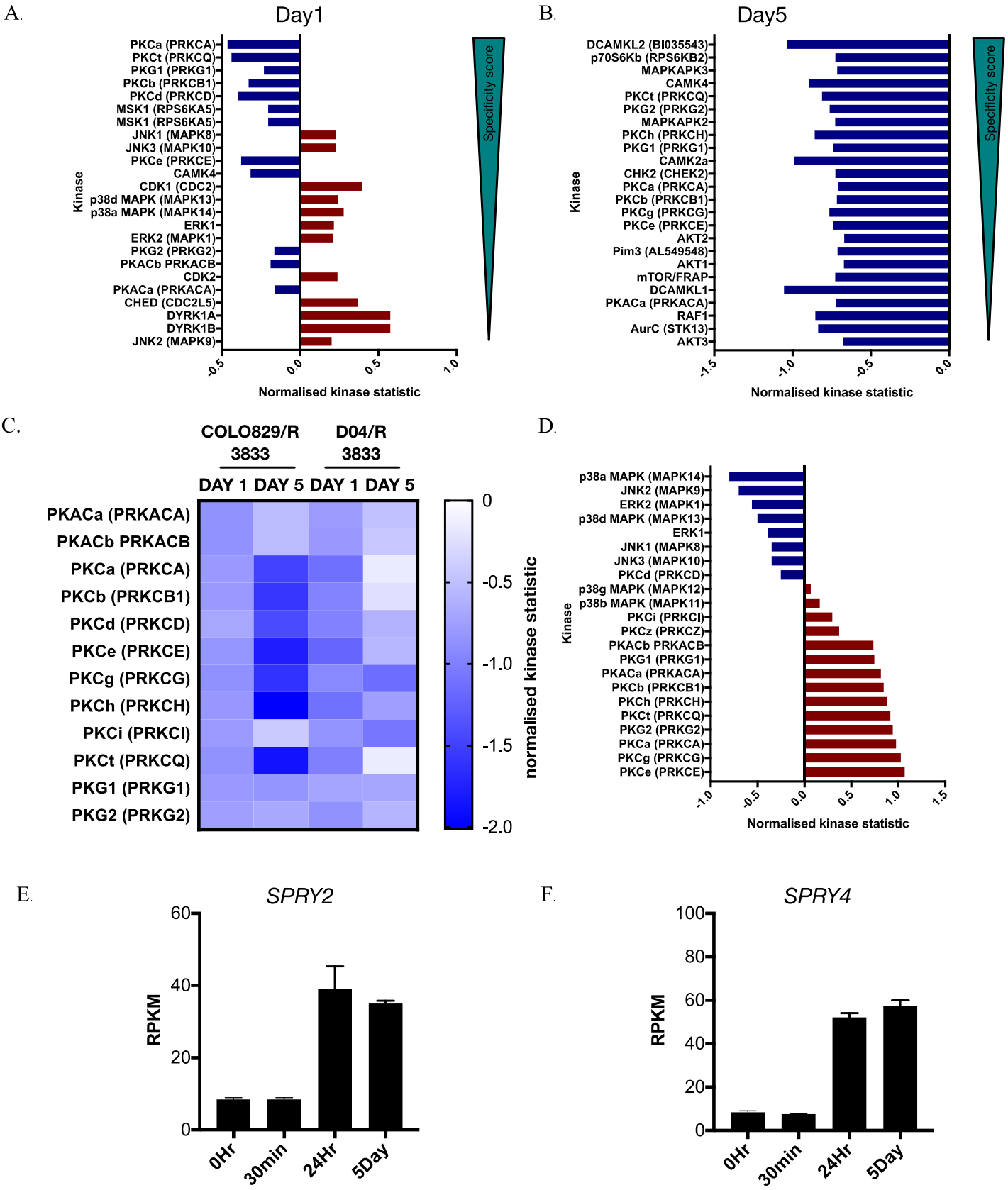
A.
Day1
PKCa (PRKCA)
PKCt (PRKCQ)
PKG1 (PRKG1)
PKCb (PRKCB1)
PKCd (PRKCD)
MSK1 (RPS6KA5)
MSK1 (RPS6KA5)
JNK1 (MAPK8)
JNK3 (MAPK10)
PKCe (PRKCE)
CAMK4
CDK1 (CDC2)
p38d MAPK (MAPK13)
p38a MAPK (MAPK14)
ERK1
ERK2 (MAPK1)
PKG2 (PRKG2)
PKACb PRKACB
CDK2
PKACa (PRKACA)
CHED (CDC2L5)
DYRK1A
DYRK1B
JNK2 (MAPK9)
Kinase
-0.5
0.0
0.5
1.0
Normalised kinase statistic
Specificity score
B.
Day5
DCAMKL2 (BI035543)
p70S6Kb (RPS6KB2)
MAPKAPK3
CAMK4
PKCt (PRKCQ)
PKG2 (PRKG2)
MAPKAPK2
PKCh (PRKCH)
PKG1 (PRKG1)
CAMK2a
CHK2 (CHEK2)
PKCa (PRKCA)
PKCb (PRKCB1)
PKCg (PRKCG)
PKCe (PRKCE)
AKT2
Pim3 (AL549548)
AKT1
mTOR/FRAP
DCAMKL1
PKACa (PRKACA)
RAF1
AurC (STK13)
AKT3
Kinase
-1.5
-1.0
-0.5
0.0
Normalised kinase statistic
Specificity score
C.
COLO829/R
3833
D04/R
3833
DAY 1 DAY 5 DAY 1 DAY 5
PKACa (PRKACA)
PKACb PRKACB
PKCa (PRKCA)
PKCb (PRKCB1)
PKCd (PRKCD)
PKCe (PRKCE)
PKCg (PRKCG)
PKCh (PRKCH)
PKCi (PRKCI)
PKCt (PRKCQ)
PKG1 (PRKG1)
PKG2 (PRKG2)
0
-0.5
-1.0
-1.5
-2.0
normalised kinase statistic
D.
p38a MAPK (MAPK14)
JNK2 (MAPK9)
ERK2 (MAPK1)
p38d MAPK (MAPK13)
ERK1
JNK1 (MAPK8)
JNK3 (MAPK10)
PKCd (PRKCD)
p38g MAPK (MAPK12)
p38b MAPK (MAPK11)
PKCi (PRKCI)
PKCz (PRKCZ)
PKACb PRKACB
PKG1 (PRKG1)
PKACa (PRKACA)
PKCb (PRKCB1)
PKCh (PRKCH)
PKCt (PRKCQ)
PKG2 (PRKG2)
PKCa (PRKCA)
PKCg (PRKCG)
PKCe (PRKCE)
Kinase
-1.0
-0.5
0.0
0.5
1.0
1.5
Normalised kinase statistic
E.
SPRY2
RPKM
60
40
20
0
0Hr
30min
24Hr
5Day
F.
SPRY4
RPKM
100
80
60
40
20
0
0Hr
30min
24Hr
5Day

Fig. 4.8. Drug withdrawal from CCT3833 resistant cells is associated with decreased kinase activity of the PKC family kinases.

A-B. Kinase screen reveals increased activity of stress kinases and decreased activity of PKC family kinases. A kinase screen using Pamgene chips containing fluorescent phospho-specific antibodies detecting activity of kinases was performed at **A.** 24 hours post drug withdrawal (day 1 drug off) vs. time 0 (drug on; CCT3833 1μM) **B.** 5 days post drug withdrawal vs. time 0 (drug on; CCT3833 1μM). The relative change in activity of each kinase is denoted by the normalised kinase statistic and the specificity score represents a measure of how likely the kinase can be predicted to have changed in activity from the set of phosphorylated peptides according to predetermined algorithms.

C. Kinase screen shows decreased activity of PKC family kinases. A kinase screen using Pamgene was performed at 24 hours and 5 days post drug withdrawal (day 1 or day 5 drug off) vs. time 0 (drug on; CCT3833 1μM COLO829/R [3833] or 2μM D04/R [3833]) in COLO829/R (3833) and D04/R (3833) cells.

D. Kinase screen reveals decreased activity of stress kinases and increased activity of PKC family kinases in the presence of an ERK inhibitor vs. DMSO. A375/R 3833 cells were cultured in DMSO or SCH772984 1μM for 24 hours and a kinase screen performed using Pamgene. The relative change in activity of each kinase is denoted by the normalised kinase statistic.

E. Expression of *SPRY2* and *SPRY4* changes following CCT3833 withdrawal in A375/R (3833). RNA Sequencing data showing gene expression of **E.** *SPRY2* and **F.** *SPRY4* in A375/R (3833) cells cultured in CCT3833 1μM (0 Hr) vs. drug withdrawal at 30 Min, 24 Hr and 5 Day. Samples performed in triplicate.

and cultured A375/R (3833) cells with an ERK inhibitor for 24 hr and compared to cells cultured in DMSO only, p38, JNK and ERK kinase activity decreased due to the rescue effect of the ERK inhibitor and the activity of the PKC family was increased (Fig 4.8 D).

The MAPK pathway and PKC family are regulated by a number of inhibitors including DUSPs and the SPRY family (84,88,350). As ERK activation has been shown to increase transcription of *SPRY* genes (86), I examined my RNA-Sequencing data of A375/R (3833) to see if *SPRY* showed increased gene expression when there was ERK hyperactivation due to drug withdrawal. This revealed that *SPRY2* and *SPRY4* gene expression was upregulated at 24 Hr and 5 days following drug withdrawal compared to when CCT3833 was present (Fig. 4.8 E and F).

Next, I tested whether adding a pan-PKC inhibitor Sotrastaurin (SOT) could rescue the effect of drug withdrawal in A375/R (3833) and Colo829/R (3833) cells through reducing activation of the MAPK pathway. However, SRB assays did not show any rescue of cell growth after 96 hr of treatment in A375/R (3833) (Fig. 4.9 A) and Colo829/R (3833) cells (Fig. 4.9 B). In addition, a clonogenic assay treating A375/R (3833) cells for 10 days did not show rescue of cell growth by SOT when CCT3833 was withdrawn (Fig. 4.9 C).

4.10 Addition of a PKC agonist results in loss of fitness in drug resistant cells

Taken together, the results of section 4.9 suggest that although PKC kinase activity decreases when ERK is hyperactivated following CCT3833 withdrawal, inhibiting PKC is not sufficient to rescue the growth of cells. However, as the PKC family activates the MAPK pathway, I hypothesised that the addition of a PKC

agonist could augment the loss of fitness following CCT3833 withdrawal. I therefore cultured A375/R (3833), Colo829/R (3833) and D04/R (3833) and RM59/R (3833) cells in CCT3833, DMSO, Phorbol 12-myristate 13-acetate (PMA, a PKC agonist) 10nM and the combination of PMA 10nM plus CCT3833 (1µM or 2µM depending on the cell line) for 96 hr and performed an SRB assay to quantify total protein. This revealed that whilst PMA did not have much affect in A375/R (3833) cells that already had significantly impaired growth from drug withdrawal alone, when cultured in the presence of CCT3833 in combination with PMA the cells also had reduced fitness (Fig. 4.9 D). Crucially, the RM59/R (3833) cells that did not display a drug addiction phenotype had significantly impaired growth when CCT3833 was withdrawn and they were cultured in PMA (Fig. 4.9 E). To further validate the loss of fitness associated with culturing CCT3833 resistant cells in the presence of PMA and to investigate whether parental cells were also sensitive to PMA, I performed clonogenic assays for 15 days in A375 and A375/R (3833) cells (Fig. 4.9 F). This showed that only the CCT3833 resistant cells were sensitive to PMA and that PMA increased rather than decreased cell viability of parental cells in the presence of PMA (Fig 4.9 F). I also confirmed that PMA impaired long term growth of the other CCT3833 resistant cells including the non-addicted RM59/R (3833) cell line (Fig. 4.9 G; Colo829/R (3833) assay performed by Dr. Alessio Cannistraci). These were consistent with the SRB assays in showing that PMA even at 1nM concentration was sufficient to reduce growth in all CCT3833 resistant cell lines and at a concentration of 10nM growth was completely abrogated when CCT3833 was withdrawn (Fig. 4.9 G). The combination of CCT3833 plus PMA blunted the growth inhibitory effect, however it remained significantly decreased compared to when the resistant cells were grown in CCT3833 alone (Fig. 4.9 G).

Fig 4.9.

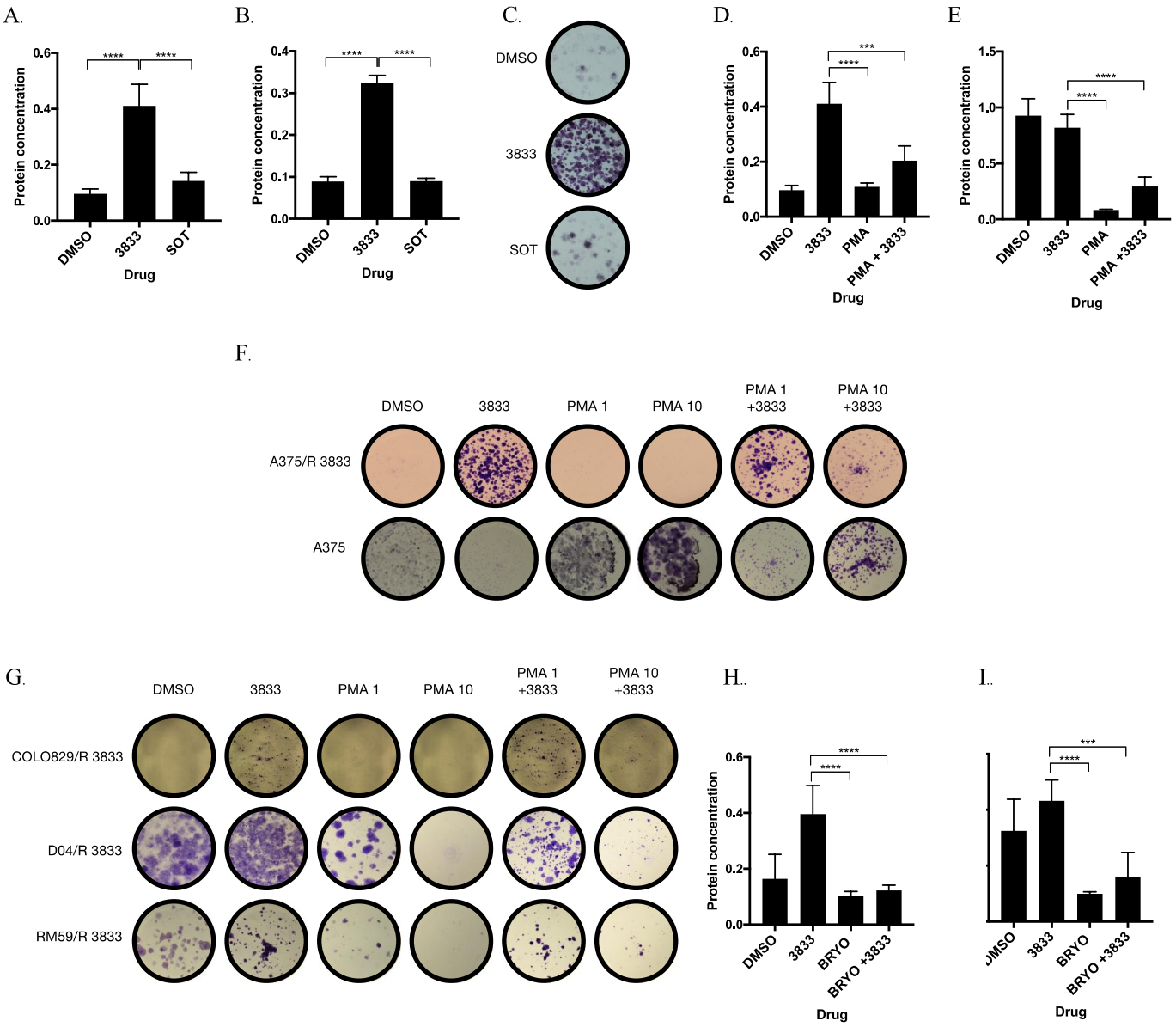
A.
B.
C.
D.
E.
F.
G.
H..
I..
Protein concentration
Drug
DMSO
3833
SOT
PMA
PMA + 3833
PMA +3833
BRYO
BRYO +3833
PMA 1
PMA 10
PMA 1 +3833
PMA 10 +3833
A375/R 3833
A375
COLO829/R 3833
D04/R 3833
RM59/R 3833

Fig. 4.9. PKC agonist results in decreased cell growth in CCT3833 resistant cells.

A-B. A pan-PKC inhibitor Sotrastaurin (SOT) does not rescue drug addicted cells when CCT3833 is withdrawn in short term culture. Short term growth (96 hours) measured with SRB assay of **A.** A375/R (3833) cells **B.** Colo829/R (3833) cells cultured in DMSO, 3833 1μM or SOT 1μM. ****P<0.0001.

C. SOT does not rescue drug addicted cells when CCT3833 is withdrawn in long term culture. Clonogenic assay of A375/R (3833) cells cultured for 15 days in DMSO, CCT3833 1μM, or SOT 1μM.

D-E. Treatment with a PKC agonist in presence or absence of CCT3833 results in decreased cell viability in both drug addicted and non-addicted CCT3833 resistant cells. Short term growth (96 hours) measured with SRB assay of **D.** A375/R (3833) cells and **E.** RM59/R (3833) cells cultured in DMSO, CCT3833 1μM (A375/R) CCT3833 2μM (RM59/R), PMA 10nM and CCT3833 1μM + PMA 10nM. ***P<0.001, ****P<0.0001.

F. Treatment with a PKC agonist in presence or absence of CCT3833 results in decreased cell viability in CCT3833 resistant cells but not parental cells. Clonogenic assay of A375 and A375/R (3833) cells cultured in DMSO, 3833 1μM, PMA 1 or 10nM and 3833 1μM+ PMA 1 or 10nM for 15 days.

G. Treatment with a PKC agonist in presence or absence of CCT3833 results in decreased cell viability in both drug addicted and non-addicted CCT3833 resistant cells in clonogenic assays. Clonogenic assay of CCT3833 resistant cells cultured in DMSO, 3833 1μM (COLO829/R) 3833 2μM (D04/R, RM59/R), PMA 1 or 10nM and 3833 1μM/2μM + PMA 1 or 10nM for 15 days.

H-I. Treatment with Bryostatin-1 in presence or absence of 3833 results in decreased cell viability in both drug addicted and non-addicted CCT3833 resistant cells. Short term growth (96 hours) measured with SRB assay of **H**. A375/R (3833) cells and **I.** RM59/R (3833) cells cultured in DMSO, CCT3833 1μM (A375/R [3833]) CCT3833 2μM (RM59/R [3833]), Bryostatin-1 (BRYO) 10nM (A375/R [3833]), BRYO 100nM (RM59/R [3833]) and CCT3833 1μM/2μM + BRYO 10nM/100nM. ***P<0.001, ****P<0.0001.

Finally, to test that the effect was comparable when the cells were cultured in the presence of other PKC agonists, I repeated the experiment using Bryostatin-1 (BRYO) which is a partial agonist of classical PKC (α, βI, βII, and γ) and novel PKC (δ and ε, ε', η, θ and μ) isoforms (351). Consistent with the PMA data, SRB assays revealed that growth was inhibited when cells were cultured in BRYO 10nM for 96 hr

(A375/R (3833) cells; Fig. 4.9 H) or BRYO 100nM for 96 hr (RM59/R (3833) cells Fig. 4.9 I).

4.11 Augmenting ERK phosphorylation in drug resistant cells results in loss of fitness which is rescued by an ERK inhibitor

To investigate whether the growth inhibitory effect of PMA on CCT3833 resistant cells was due to increased hyperactivation of ERK, I performed immunoblots of the A375/R (3833) cells and compared them to parental A375 at 4 and 24 hr when cultured in the presence of increasing concentrations of PMA and PMA plus CCT3883 (Fig. 4.10 A). In the parental cells there was an increase in phospho-ERK only in cells without CCT3833 present and this resulted in only a slight increase in JunB (Fig. 4.10 A). In contrast, in the A375/R (3833) cells phospho-ERK was increased in all concentrations of PMA and remained increased in the presence of CCT3833, although to a lesser degree (Fig. 4.10 A). Furthermore, JunB was significantly up-regulated particularly at 24 hr, with only lower concentrations of PMA (≤1nM) in combination with CCT3833 not showing an increase (Fig. 4.10 A).

To test whether an ERK inhibitor could rescue the effect of PMA, I cultured A375/R (3833) (Fig. 4.10 B) and RM59/R (3833) (Fig. 4.10 C) cells for 96 hr in DMSO, CCT3833 (1μM A375/R [3833]), 2μM RM59/R [3833]), PMA 10nM or PMA 10nM + SCH772984 0.05μM (ERK inhibitor) and quantified protein content using an SRB assay. Both the A375/R (3833) and RM59/R 3833 cells had significantly increased growth in the presence of PMA plus ERK inhibitor compared to PMA alone (Fig. 4.10 B and C). Clonogenic assays culturing cells for 15 days in CCT3833 (1μM A375/R [3833]), 2μM RM59/R [3833]), PMA 1nM/10nM or PMA 1nM/10nM + SCH772984 0.05μM also showed increased colony formation when the

ERK inhibitor was added to PMA (Fig. 4.10 D). Finally, immunoblot of A375/R (3833) cultured for 24 hr in the presence of PMA 1nM/10nM, PMA 1nM/10nM + CCT3833 1μM, PMA 1nM/10nM + SCH772984 0.05μM or PMA 1nM/10nM + CCT3833 1μM + SCH772984 0.05μM showed that the ERK inhibitor reduced the PMA induced hyperactivation of phospho-ERK and JunB (Fig. 4.10 E).

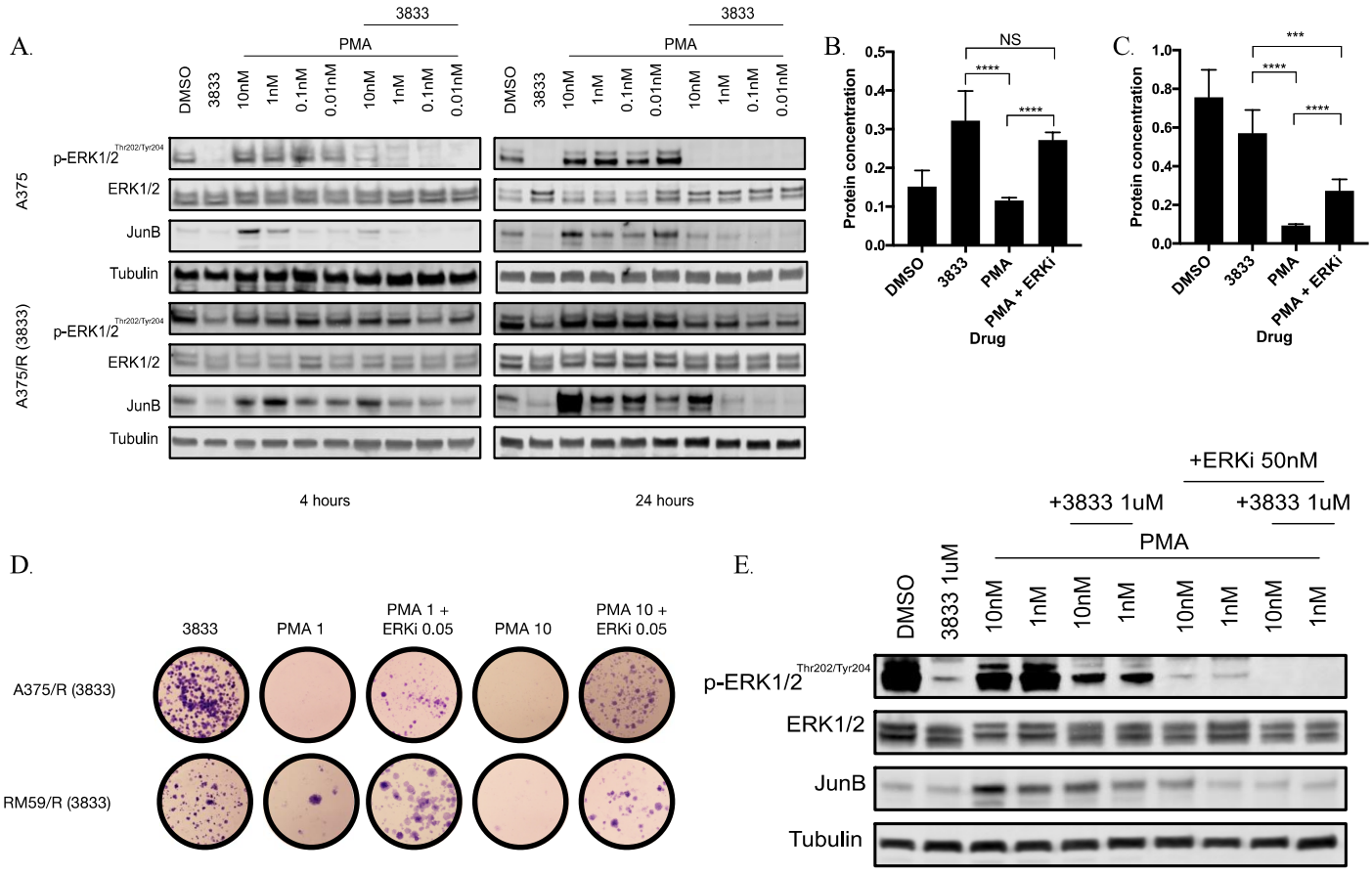

Fig. 4.10. A PKC agonist results in increased ERK hyperactivation in CCT3833 resistant cells and its effect is rescued by ERK inhibition.

A. Immunoblot reveals hyperactivation of ERK and JunB in cells cultured in PMA. A375 and A375/R 3833 cells were cultured in DMSO, 3833 1μM, PMA 0.01nM-10nM or 3833 1μM + PMA 0.01nM-10nM for 4 and 24 hours. Immunoblot was performed, analysing for phospho-ERK $Thr^{202/185}$ $Tyr^{204/187}$**,** ERK 1/2, and JunB. Tubulin was used as a loading control.

B-C. ERK inhibitor increases cell viability in the presence of PMA. Short term growth (96 hours) measured with SRB assay of B. A375/R (3833) cells and C. RM59/R (3833) cells cultured in DMSO, 3833 1μM (A375/R [3833]) 3833 2μM (RM59/R [3833]), PMA 10nM and PMA 10nM +SCH772984 0.05μM.

D. ERK inhibitor increases colony formation in the presence of PMA. Clonogenic assay of A375/R (3833) and RM59/R (3833) cells cultured for 15 days in PMA 1nM, PMA 10nM and SCH772984 0.05μM + PMA 1nM or 10nM.

E. ERK inhibitor decreases phospho-ERK and JunB activity in the presence of PMA. A375/R (3833) were treated with PMA 0.01nM-10nM +/- 3833 1μM and +/- SCH772984 0.05μM for 4 hours and immunoblots performed analysing phospho-ERK $Thr^{202/185}$ $Tyr^{204/187}$**,** ERK 1/2 and JunB.

4.12 Chapter discussion

4.12.1 Resistance to 3833 occurs through up-regulation of the MAPK or PI3K/AKT pathway

Resistance to BRAFi/MEKi has been extensively studied (see Chapter 1), however, little is known about mechanisms of resistance to pan-RAF inhibitors. Other pan-RAF inhibitors such as LXH254 and MLN2480 are currently in early phase studies, however mechanisms of resistance to them have not yet been reported. Through treating cells with increasing concentrations of CCT3833, I was able to identify a number of potential mechanisms of resistance. It took considerably longer (4-9 months vs. 3 months) to make cells resistant to CCT3833 compared to historical data of resistance to PLX4720 made resistant using the same method (127), which suggests that in a pre-clinical context the drug may be a more effective inhibitor. Resistance associated with *MAP2K1* mutations has previously been described in patients treated with BRAFi/MEKi combination therapy (352). Another study suggested that in order to overcome resistance to BRAFi/MEKi, cells had to develop multiple resistance mechanisms such as a *BRAF* amplification plus a *MAP2K1* mutation that synergised to overcome the drugs (168). Furthermore, resistance through alterations of the PI3K/AKT pathway have been reported in the context of BRAFi/MEKi treatment. Baseline mutations in *PIK3CA* and *AKT3* as well as deletions in *PTEN* were associated with short duration of response (<5 months PFS) in patients treated with D+T (352). In addition, in a *BRAF* mutant cell line that had developed an *NRAS* mutation in resistance to a BRAFi, *PTEN* knockdown was associated with increased phospho-AKT and resistance to combination BRAFi/MEKi (168).

Of note, the p. F436L *ARAF* mutation has not been previously described as a mechanism of resistance to BRAFi/MEKi. *ARAF* is very rarely mutated in cancer and its role in RAS/RAF/MEK signalling has not been fully characterised. A previous study has shown that Ser^{432} on ARAF is a phosphorylation site that is particularly important for EGF-mediated ARAF catalytic activity (353). It is therefore possible that the mutation is affecting MEK binding and result in increased kinase activity of ARAF. Future work will be performed to assess how the binding interaction with MEK is affected by the mutation. Furthermore, as dimerisation of BRAF and CRAF has previously been shown to be important in resistance to BRAFi (71,125), silencing experiments of ARAF, BRAF and CRAF will be performed in the *ARAF* mutant Colo829/R (3833) cells to test whether mutant ARAF causes resistance in isolation or requires an interaction (e.g. scaffolding/dimerisation) with BRAF or CRAF to cause resistance (71,344,354). Co-immunoprecipitation assays of ARAF in Colo829 cells with or without the *ARAF* mutation will also be performed to assess whether there is an increased interaction between ARAF, BRAF and/or CRAF in the *ARAF* F436L CCT3833 resistant cells. In addition, it will be important to understand whether the mutation is mediating resistance via a RAS dependent or independent mechanism to determine whether resistance can be affected by upstream signalling (344).

All the mechanisms of resistance were associated with activation of either the MAPK or PI3K/AKT pathways, with up-regulation of downstream phospho-ERK or phospho-AKT observed on immunoblot. Furthermore, gene expression showed a similar phenotypic shift in resistance compared to parental cells independent of *BRAF* or *NRAS* mutation status. Many of these changes are associated with changes in extracellular matrix, cell migration or activation of PI3K pathways. Critically, both *BRAF* and *NRAS* mutant, CCT3833 resistant cells were more sensitive to

PI3K/AKT/mTOR inhibitors than parental cells, suggesting that PI3K/AKT/mTOR inhibition might be a good strategy to target emerging CCT3833 resistant populations. Of note, drugs targeting the MAPK pathway showed decreased inhibition of *BRAF* and *NRAS* mutant cell lines resistant to CCT3833 compared to parental cells, suggesting that cross-resistance occurs to these drugs.

Accordingly, when I treated a heterogeneous panel of patient-derived cell lines including cells resistant to BRAFi, with CCT3833 in combination with the PI3K inhibitor taselisib, the drugs were synergistic. Furthermore, CCT3833 and taselisib had synergistic activity in isogenic cell lines sensitive or resistant to BRAFi/MEKi. This was further confirmed *in vivo* where the combination resulted in decreased growth of *BRAF* mutant xenografts compared to either drug as a monotherapy. Further experiments will be performed to test the combination in *NRAS* mutant xenografts. Other studies have shown that combining short hairpin RNA targeting of both *BRAF* and *PIK3CA* or *MEK 1/2* and *PIK3CA* resulted in reduced growth of IPC298 *NRAS* mutant xenografts (355). A study has previously shown that combining pan-RAF and MEKi *in vitro* was synergistic and overcame resistance to BRAFi (356). Furthermore pan-RAF inhibitors and MEKi have been shown to be synergistic in inhibiting growth of *NRAS* mutant cells (357). However, my data would suggest that targeting the PI3K/AKT pathway in combination with pan-RAF inhibition might be a better strategy as it could prevent cross-resistance. A study showed that aside from resistance via an *NRAS* mutation, BRAFi resistance also resulted in resistance to a MEKi, however cells were sensitive to targeting of the PI3K/AKT pathway through genetic or pharmacological inhibition (358). Thus, cross-resistance is particularly important in the context of BRAFi/MEKi resistant tumours where up-regulation of PI3K/AKT signalling has commonly been associated with resistance to treatment.

Furthermore, as *NRAS* mutant melanoma activates both the MAPK and PI3K pathways, inhibition of both downstream of RAS may be important to obtain a greater response (359).

4.12.2. Drug addiction is dependent on the mechanism of resistance

When some of the cell lines became resistant to CCT3833, I observed that a drug addicted phenotype developed. This has also been previously reported in the context of BRAFi/MEKi and EGFR tyrosine kinase inhibitor resistance (165,166,168). Critically, it only occurred in cells that had developed resistance through a mechanism that significantly affected MAPK signalling, whereas the growth of RM59/R (3833) cells, which had up-regulated PI3K/AKT signalling, were not affected following CCT3833 withdrawal. Future work will validate this data through comparing whether A375 cells with the p.L414F *PIK3R4* or p.K57E *MAP2K1* mutations created using CRISPR/Cas9 show the drug addiction phenotype following drug withdrawal after being cultured in CCT3833.

Previously, Kong and colleagues suggested that the drug addiction phenotype occurred independently of the mechanism of resistance (165). They observed that drug addiction occurred in cells with distinct mechanisms of resistance including a cell line exhibiting a mechanism of resistance that did not result in increased phosphorylation of ERK (although the authors did not report the exact mechanism of resistance observed in these cells) (165). Therefore, they concluded that drug addiction was independent of the cause of resistance to drug (165). Of note, despite on-going phospho-ERK inhibition, the A101D BRAFi/MEKi resistant cell line described in their paper showed increased phosphorylation of MEK and therefore this could have contributed to the drug addiction phenotype maintained in these cells

(165). My data would suggest that the extent of growth inhibition/cell death following drug withdrawal is dependent on the mechanism of resistance. Cells that are less reliant upon up-regulation of the MAP kinase pathway as a mechanism of resistance are less likely to exhibit the drug addiction phenotype. This theory is supported by data from Hong *et al* who showed that through enhancing phospho-ERK levels through engineering p.V600E *BRAF* amplification into BRAFi/MEKi resistant cells, apoptosis was increased and growth was inhibited following drug withdrawal (166). Therefore, enhancement of the MAPK pathway through BRAF/MEK/Pan-RAF resistance is associated with a stronger drug addiction phenotype.

Through upfront targeting of mechanisms of resistance such as PI3K/AKT up-regulation that are less likely to result in drug addiction, it may be possible to drive tumour evolution towards a drug addicted phenotype. Future work on this project will show whether taselisib inhibits growth and survival of *PIK3R4* mutant cells, suggesting that these non-addicted cells can be targeted through upfront combinations of CCT3833 and taselisib. However, to test this hypothesis properly parental cells would need to be cultured in either CCT3833 or CCT3833 + taselisib and resistant colonies tested for the presence of resistance mechanisms up-regulating the PI3K pathway vs. MAPK pathway in addition to whether they displayed a drug addiction phenotype.

4.12.3. Drug withdrawal results in an invasive, stem-cell-like phenotype

Intriguingly, MITF gene targets did not decrease in the drug addicted cells following drug withdrawal. This differs from the Kong *et al* data, which suggested that MITF and its gene targets decreased when drug was withdrawn (165). Previous data has shown that MITF can exist in different states following development of drug

resistance (163). In some cells MITF remains high, however other cells can lose MITF in acquired resistance. Kong *et al* had drug addicted cells with high levels of MITF following acquired resistance, however in my study MITF decreased as they became resistant. Therefore, a further decrease in MITF gene expression upon drug withdrawal in the A375/R (3833) cells was less significant. Further RNA-Sequencing needs to be performed in order to clarify whether this is specific to the A375/R (3833) cells or occurs in the other cell lines. However, this suggests that the phenotypic changes seen in this cell line may not be as reliant on MITF down-regulation as the Kong *et al* paper would suggest.

My RNA-Sequencing data suggests that cells develop an invasive phenotype as early as 30 mins following drug withdrawal in drug-addicted cells. Furthermore, genes associated with a stem cell like phenotype are up-regulated in the drug off cells, with up-regulation of notch, hedgehog and TGFβ signalling. Further work needs to be performed to test whether the gene changes results in increased cell invasion *in vitro* using invasion-assays. However, these data have potential implications for the clinic and drug holiday strategies because cells which do not die when drug is withdrawn my have more invasive features and propensity to metastasise. In addition cells with a stem cell like phenotype are more likely to develop resistance to multiple different therapies (360). Therefore, drug holiday approaches reliant on drug withdrawal alone may increase the likelihood of melanoma spreading. To reduce this potential challenge, drugs targeting stem cell like pathways and transcriptional/epigenetic regulators such as WNT, ALDH and HDAC (360) may be beneficial as part of alternate scheduling strategies, although this needs further pre-clinical testing.

4.12.4. PKC agonism augments the drug addiction phenotype

In addition, a screen revealed that kinase activity of the PKC family was decreased in response to ERK hyperactivation when CCT3833 was withdrawn. The PKC family activate the MAPK pathway through RAS (93). I also showed that if ERK hyperactivation is reduced through inhibition by SCH772984 the kinase activity of PKC family members increases in A375/R (3833) cells in comparison to ERK hyperactivated cells treated with DMSO only (Fig 4.8 D). This suggests that there is negative feedback from ERK resulting in reduction in PKC family activity. One mechanism by which this may occur is via up-regulation of sprouty proteins. Activation of ERK results in increased transcription of sprouty proteins, which have been associated with negative regulation of the MAPK pathway (361,362). In addition sprouty has been shown to inhibit phosphatidylinositol-specific phospholipase C (PLC)-γ activity (363). Activated PLCγ1 hydrolyzes PIP_2 into inositol (1,4,5)-triphosphate (IP_3) and DAG, which recruits PKC isoforms to the plasma membrane resulting in their activation (363). Therefore, PKC activity may be affected by increased transcription of *SPRY*. RNA-Sequencing of A375/R (3833) cells after 5 days "drug off" vs. "drug on" revealed increased expression of *SPRY2* and *SPRY4* at 24Hr and 5 days. Negative regulation of PKC via increased transcription of *SPRY* by hyperphosphorylated ERK could be tested through silencing of *SPRY*2 and *SPRY4* and evaluation of whether PKC activity was still down-regulated when drug was withdrawn in CCT3833 resistant cells. However, as multiple feedback mechanisms may be acting on PKC when ERK is hyperactivated, inhibition of one mechanism may not be sufficient to show an effect.

PKC inhibition did not result in rescue of cell growth following drug withdrawal in CCT3833 resistant cells. However, agonism of PKC using PMA

resulted in augmentation of the drug addiction phenotype. Even the RM59/R (3833) cells, which did not exhibit the drug addicted phenotype, showed reduced growth when CCT3833 was withdrawn and cells were cultured in PMA. Furthermore, although the effect was blunted, PMA also inhibited the growth of CCT3833 resistant cells when CCT3833 was present. Further work is currently being performed to assess whether culturing in PMA results in changes of the cell cycle or apoptosis of CCT3833 resistant cells. My data shows that PMA drives JunB and ERK hyperactivation in CCT3833 resistant cells. Notably, the phosphorylation of ERK and was significantly increased in A375/R (3833) cells compared to parental cells especially if they were cultured in the presence of CCT3833. Furthermore, ERK inhibition rescued the growth of CCT3833 resistant cells cultured in PMA. This suggests that PMA is impairing growth of CCT3833 resistant cells through an ERK dependent mechanism. When drug is withdrawn from CCT3833 resistant cells, the PKC family decreases activity in response to ERK hyperactivation, which decreases their activation of the MAPK pathway, however this is not sufficient to rescue the cells (Fig. 4.11 A). However, when a PKC agonist is added, the PKC family can drive MAPK activity resulting in further increased ERK and JunB hyperactivation, which impacts on cell growth (Fig. 4.11 B).

The growth of *BRAF*/*NRAS* mutant parental cells was decreased through CCT3833 mediated inhibition of ERK activity. However, with the exception of RM59 cells, both *BRAF* and *NRAS* mutant cells resistant to CCT3833 developed mutations in genes affecting kinase activity within the MAPK pathway, which overcame inhibition of drug. This made them vulnerable to drug withdrawal and ERK hyperactivation, whereas the RM59/R (3833) cells which relied on PI3K/AKT signalling had no loss of fitness. However, all the cells showed similar changes in

Fig. 4.11

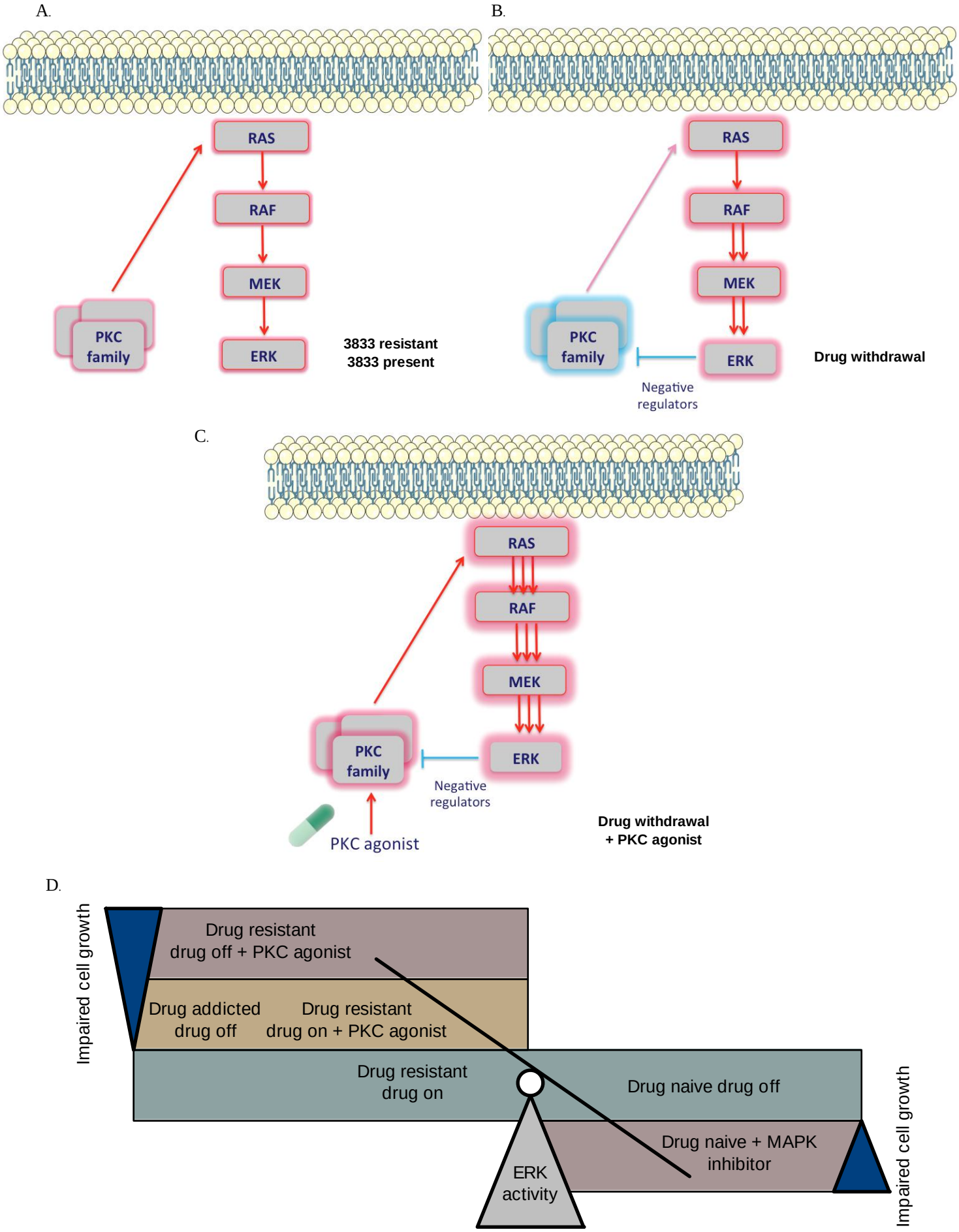
A.
B.
RAS
RAF
MEK
ERK
PKC family
3833 resistant
3833 present
Drug withdrawal
Negative regulators
C.
PKC agonist
Drug withdrawal
+ PKC agonist
D.
Impaired cell growth
Drug resistant
drug off + PKC agonist
Drug addicted
drug off
Drug resistant
drug on + PKC agonist
Drug resistant
drug on
Drug naive drug off
Drug naive + MAPK
inhibitor
ERK
activity
Impaired cell growth

Fig. 4.11 Models of ERK hyperactivation in CCT3833 resistant cells

Signalling affected by drug withdrawal and PKC agonists in CCT3833 resistant cells. A. In CCT3833 resistant cells the MAPK pathway can be reactivated despite drug being present. **B.** In drug addicted cells, withdrawal of drug results in ERK hyperactivation. In response, the kinase activity of PKC family members decreases reducing their positive regulation of the MAPK pathway. **C.** If a PKC agonist is added when drug is withdrawn then this activates the MAPK pathway further, resulting in augmentation of ERK hyperactivation and decreased cell growth.

D. Model of ERK activity. Melanoma cells have an optimum level of ERK activity dependent on whether they are resistant to CCT3833, their mechanism of resistance and whether they are growing in the presence or absence of MAPKi. The drug addiction phenotype is amplified in MAPKi resistant cells if cultured in PKC agonists resulting in decreased cell viability independent of whether a MAPKi is present.

gene expression with decreased expression of negative regulators of the MAPK pathway such as *SPRY4* and *DUSP4* and up-regulation of genes such as *PDGFRβ* that activate MAPK signalling. It is therefore possible that the drug resistant phenotype contributed towards susceptibility to ERK hyperactivation that could be enhanced by a PKC agonist. Thus, culturing all CCT3833 resistant cell lines in PMA resulted in ERK hyperactivation and impaired cell growth. Agonism of the PKC family therefore can augment ERK hyperactivation, shifting the balance of ERK signalling to result in inhibition of growth.

These data imply that the balance of ERK activity is crucial to *BRAF/NRAS* mutant melanoma cell growth and survival and furthermore the balance can change depending on whether the cell is resistant to MAPK pathway inhibitors (Fig. 4.9 F, Fig. 4.10 A, Fig. 4.11 B). When cells are drug naïve, inhibition of ERK activity by a MAPKi results in impaired growth (Fig. 4.11 B). When cells are MAPKi resistant via a mechanism that activates the MAPK pathway, they are most fit in the presence of

drug. However when drug is withdrawn, ERK becomes hyperactivated, resulting in decreased cell growth (Fig. 4.11 B). Agonism of PKC in MAPKi resistant cells results in loss of fitness due to ERK hyperactivation even in the presence of a MAPKi. This is further augmented in MAPKi resistant cells when the MAPKi is withdrawn and a PKC agonist added (Fig. 4.11 B). Therefore, MAPKi drug resistance results in vulnerability of the cells to hyperactivation of ERK through PKC agonism (Fig. 4.11 B).

4.12.5 Limitations of the study

The main limitation of the study so far is this work has mainly been performed *in vitro* and therefore the results need confirming *in vivo*. It is hard to recapitulate in a two-dimensional environment the signalling processes that occur *in vivo* and therefore it will be important to test whether the cells behave in the same way in a more complex microenvironment. Furthermore, I did not have any samples from patients treated with CCT3833 as the number of biopsies was limited in the trial. This is something that could be examined in future work. In addition, the maximum tolerated dose has not yet been reached in the trial and therefore any lack of efficacy could just be due to suboptimal dosing.

Furthermore, the crystal structure of ARAF has not yet been solved, thus, the modelling had to be based on BRAF. Although there is approximately 80% homology between the two kinases and the area surrounding the mutation was completely homologous, the differences between the two models could affect the interpretation of results, therefore this data needs to be treated with caution.

4.12.6. Implications of the data for future work and the clinic

4.12.6.1. Future work

There are a number of areas for future work in this study. Firstly it will be important to establish whether decreased expression of *HAS2* and *PIK3AP1* through genetic ablation results in decreased phospho-AKT activation in RM59/R (3833) cells. In addition, as the CCT3833 resistant D04 cells were associated with many changes in long non-coding RNA expression examining whether these are associated with resistance and reactivation of the MAPK pathway could be a potential area of future work.

Another important experiment will be to compare growth using clonogenic assays of A375 cells with a *PIK3R4* mutation inserted to cells with *MAP2K1* inserted in drug on/off conditions. This will test whether drug addiction is chiefly related to a mechanism of resistance activating the MAPK pathway compared to mechanisms via alternative pathways. I hypothesise that the mutation in *PIK3R4* is less likely to result in loss of fitness when drug is withdrawn compared to the *MAP2K1* mutation.

Future experiments will also test whether the effect of PMA is ERK2 dependent by ablation of ERK2 assessing cell growth and cell death. Previous studies have reported that ERK hyperactivation following drug withdrawal results in cell death and "slow-cycling" (165,166). I hypothesise that PMA will exacerbate that effect, particularly in the RM59/R (3833) cells. In addition, Simpson *et al* (preprint, not peer reviewed) have shown that the effect of BRAFi/MEKi on ERK activity is dependent on their cell cycle phase (364). They showed that *BRAF* mutant melanoma cells given BRAFi/MEKi in G_1-phase have maximal inhibition of ERK whereas cells in S- or G_2-phase must complete mitosis before nadir is reached (364). Positive and negative feedback loops affecting ERK activity were cell cycle dependent (364). Therefore, it

would be interesting to examine what effect timing of drug withdrawal and/or the addition of PMA would have on feedback loops, dynamic ERK signalling and the degree to which ERK hyperactivation resulted in cell cycle arrest/cell death. This could be done through engineering the cells to express an ERK reporter in order to dynamically measure ERK activity (230) and a fluorescently tagged proliferating cell nuclear antigen which would enable levels of ERK to be monitored in different stages of the cell cycle, which could be tracked upon drug withdrawal.

Furthermore, ERK hyperactivation results in striking phenotypic changes in cells. It would be interesting to explore this further using more quantitative approaches by staining for nucleus and cell markers (i.e. DAPI, actin) with software such as Definiens and Columbus. In addition it would be important to examine ERK signalling changes in 3D culture especially as many of the changes in gene expression when cells become resistant to drug are associated with extracellular matrix organisation.

In addition, I have designed an *in vivo* experiment to test whether the effect of PMA is seen in CCT3833 resistant cells growing in mice. Mice bearing A375/R (3833) xenografts will be treated with CCT3833 from day 0 until they reach 600mm^3. At that threshold they will be randomised to either continue CCT3833 (40mg/kg) or switch to vehicle (5% DMSO), PMA (dose to be determined by toxicity experiment), or PMA + CCT3833 (40mg/kg). Monitoring will continue until tumours reach just below licence limit. If my *in vitro* data are supported, I would expect that the PMA treated tumours will delay growth the most, followed by tumours treated with vehicle, then the combination of PMA + CCT3833.

I aim to bring the two strategies together of combination CCT3833/taselisib followed by drug withdrawal and treatment with a PKC agonist in an *in vivo* setting.

Continuous dosing of CCT3833 will be used as a control and compared to scheduling combination CCT3833/taselisib until tumours escape control and grow to 600mm^3 when they will be randomised to continued CCT3833/taselisib or drug withdrawal and treatment with PMA or DMSO. This will test whether using an optimal combination upfront followed by treatment with a PKC agonist rather than drug withdrawal alone can delay tumour growth. I hypothesise that treating with the combination will result in a deeper response, improving control on the combination and making the tumours susceptible to the PKC agonist upon CCT3833/taselisib withdrawal. Such an experiment may be difficult to perform as it relies on the mice tolerating drug treatment for a long time and the therapeutic window is a lot smaller in mice compared to humans to their size. However, the previous experiments will provide data as to the tolerability of treatments and whether the strategies on their own inhibit tumour growth, which will aid the design of this experiment.

In addition, based on previous studies, a PKC agonist may synergise with a DNA damaging agent or a PARP inhibitor to augment cell death (165,166). Kong and colleagues showed that apoptosis due to drug withdrawal was increased when cells were also treated with DTIC through further suppressing MITF and its pro-survival target B-cell lymphoma 2 (BCL-2), and by inducing DNA damage in cancer cells (165). In addition, Hong *et al* showed that impairing DNA damage repair through treatment with a PARP inhibitor following withdrawal augmented the drug addiction phenotype and increased cell death. My RNA-Sequencing data also suggested that DNA damage was associated with drug withdrawal as pathways such as “activation of ATR in response to replication stress” were up-regulated when drug was withdrawn. Thus, the combination of increased ERK hyperphosphorylation through addition of a

PKC agonist with a DNA damaging agent/inhibitor of DNA repair may result in increased efficacy.

Finally, one of the aspects that would be extremely interesting to investigate is how a PKC agonist could synergise with immune therapy following targeted therapy drug withdrawal in resistant cells. PKC family members have a number of different functions in immune cell activation (365). PKCθ has been shown to be essential for TCR activation and signalling (365). Furthermore, PKCß has been shown to control survival of peripheral B cells possibly through NF- κB activation (365). Finally PKCε has been implicated as important for the function of macrophages (365). Therefore treating with a PKC agonist and immune therapy following resistance to BRAF/MEK/pan-RAF inhibition might have a dual role in killing tumour cells through ERK-hyperactivation and augmenting T cell responses, which could synergise with checkpoint blockade. First, it would be important to assess whether this resulted in the right kind of immune response as it could potentially just cause generalised tumour promoting inflammation. In addition, understanding of the effect of augmenting different PKC family members is likely to be critical given their diverse roles in the immune system, which could potentially result in additional toxicities through off-target effects.

4.13 Chapter Summary

Targeted therapy resulted in a paradigm change in how melanoma is treated in the clinic. However, resistance remains a huge challenge with patients typically progressing after 11 months of combination therapy. Using the novel pan-RAF inhibitor CCT3833, I show that resistance can result from genomic and transcriptional changes that result in up-regulation of the MAPK and PI3K/AKT pathways in both

BRAF and *NRAS* mutant melanoma cells. A drug screen of kinase inhibitors revealed that when cells become resistant to CCT3833 they are less sensitive to drugs targeting the MAPK pathway and more sensitive to PI3K/AKT inhibitors than parental cells. Accordingly CCT3833 synergises with taselisib a PI3K inhibitor both *in vitro* and *in vivo*.

Furthermore, I show that cells resistant to CCT3833 via up-regulation of the MAPK but not the PI3K/AKT pathway display a drug addiction phenotype. Withdrawal of drug results in an EMT phenotype with up-regulation of genes associated with an invasive signature and loss of fitness associated with ERK, p38 and JNK hyperactivation. However inhibition of ERK activity alone was sufficient to rescue the cells, whereas no response was seen to JNK or p38 inhibition, which validates previous data showing that BRAFi/MEKi result in drug addiction dependent on ERK2 hyperactivation. Furthermore, I show that ERK hyperactivation can be augmented through culturing cells in a PKC agonist. This results in loss of fitness even in the presence of CCT3833 and also in cells that do not exhibit the drug addiction phenotype through drug withdrawal alone. I show that PKC agonism using PMA results in ERK and JunB hyperactivation and that inhibition of ERK rescues cells from the effect of PMA. Taken together, these data suggest that cells require a balance of ERK activity for optimal growth and survival. Disrupting this balance through inhibiting ERK activity in MAPK inhibitor sensitive cells or withdrawing drug/culturing in a PKC agonist in MAPK inhibitor resistant cells results in growth arrest.

Strategies optimising combinations that target both the MAPK and PI3K pathways may prevent cross-resistance and result in more durable responses to targeted therapy. In addition, cells can be driven towards a drug addicted phenotype, which results in

vulnerability to a PKC agonist. Therefore approaches that combine scheduling of CCT3833/taselisib with drug withdrawal and a PKC agonist when resistance develops, could prolong responses to targeted therapy.

Chapter 5. Circulating tumour DNA predicts survival in patients with resected high-risk stage II/III melanoma

The previous chapters have demonstrated the potential challenges in treating established metastatic disease and overcoming mechanisms of resistance. Despite modern therapies, the majority of patients with stage IV melanoma will only survive approximately 3 years and resistance to therapy remains a problem. One strategy is to treat disease at an early stage, when tumours are smaller and less well established. The rationale for this approach was developed in the context of adjuvant chemotherapy, which has been shown to result in cure for many cancers (366–368). Preclinical data from the 1950s suggest that the smaller the tumour burden, the higher the likelihood of achieving cure with chemotherapy (369). Tumours were treated with 6-mercaptopurine at different times following implantation, with treatment at 24 hours associated with a 57% cure rate whilst none of the larger, more established tumours treated at 15 days were cured (Figure 5.1) (369).

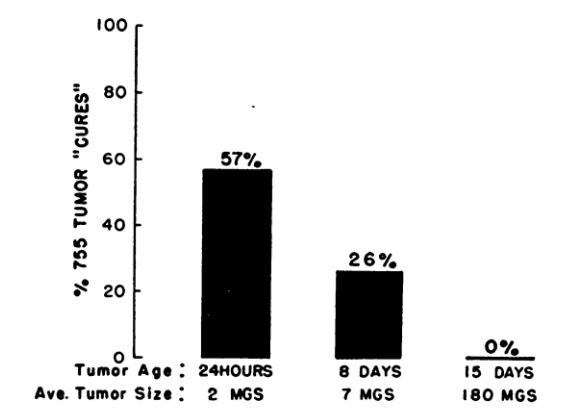

CHART 1.—Decreasing chemotherapeutic (6-MP) "cure" rates with increasing tumor size (or age) (four experiments).

Fig. 5.1 Relationship between tumour size/time from implantation and chance of cure from chemotherapy *in vivo. (369).*

In addition, preclinical data suggest that response to immune therapies may also be increased when tumours are treated at an earlier stage (370,371). A study examining baseline tumour size (BTS) taken as the sum of sum of the longest dimensions of all measurable baseline target lesions and response to pembrolizumab

(anti-PD-1) in 583 patients showed that a BTS below the median was associated with higher ORR (44% vs. 23%; $P<0.001$) and improved OS (HR 0.38; $P<0.001$) (372). It remained an independent prognostic factor in multivariate analyses for OS ($P<0.001$) (372). Furthermore, recent clinical trials (NCT00636168, NCT02388906, NCT02362594, NCT01682083) investigating adjuvant immune or targeted therapy in high risk resected stage 3 melanoma have reported a significant benefit in terms of OS and/or RFS (227,228,373,374). Together, these studies show that treatment of micro-metastatic disease results in improved outcomes for patients.

However all these treatments have associated toxicity, including risk of death. For example, in the EORTC 18071 study of adjuvant ipilimumab vs. placebo in resected stage III/IV no evidence of disease (NED) patients, immune related grade 3 AEs occurred in 36.5% of patients, grade 4 AEs occurred in 5.5%, and there were five treatment related deaths (375). Although adjuvant anti-PD-1 inhibitors will become standard of care due to their higher efficacy and lower toxicity compared to ipilimumab (with results from low dose N+I adjuvant combination therapy awaited), they still are associated with approx. 15% grade 3-4 toxicity (227,373). Furthermore, patients can develop endocrinopathies and other chronic autoimmune complications, which can have a long-term impact on quality of life. Moreover, targeted therapy in the adjuvant setting has been associated with increased numbers of patients discontinuing treatment early suggesting that drugs may be impacting on quality of life. This is in a patient population that is potentially cured by surgery alone, without the need for systemic treatment.

Thus, it is important to develop tools that can accurately identify patients who are at highest risk of progression to stage IV disease. CtDNA is emerging as a useful measure of tumour burden and prognostic marker in stage IV melanoma

(263,376,377). I therefore designed a study to determine whether having detectable ctDNA levels within 12 weeks of surgery carried out with curative intent for high-risk stage II/III disease was associated with worse survival in a subgroup of patients, whose tumours were known to have either a *BRAF* or *NRAS* mutation. I used samples that had been collected as part of the AVAST-M trial, which randomised patients with AJCC (version 7) stage IIB/C and III patients with resected cutaneous melanoma to receive either adjuvant bevacizumab (7.5mg/kg 3 weekly for 1 year) or standard observation (271,378). I then validated these findings prospectively in a small cohort of patients, who underwent surgery at The Christie NHS Foundation Trust and combined this data with a larger prospective cohort obtained and analysed by Prof. Sarah Jane Dawson's laboratory (Melbourne, Australia).

5.1 Patient demographics and detection of baseline ctDNA

To evaluate the potential for ctDNA to identify melanoma patients at high risk of relapse following surgery with curative intent, I analysed ctDNA in the plasma from 161 patients in the AVAST-M trial carrying either a *BRAF* or *NRAS* mutation in their baseline resected tumour (Dr. Gabriela Gremel analysed half of the samples) (379). With statistical input from Mr. David Ryder I calculated that at least 150 samples would provide 80% power to detect a HR of at least 3.5 between patients with undetectable and detectable ctDNA for disease free interval (DFI) with a 5% significance level, assuming a 10% marker prevalence and an event rate of 40% (379).

Patient demographics are presented in Table 5.1. Within the cohort, 132 tumours had a p.V600E *BRAF* mutation and 29 presented with a p.Q61L/K *NRAS* mutation (379). CtDNA was detected in 19 (12%) of the plasma samples (10 from the

treatment arm and 9 from the observation arm). Of the 19 positive plasma samples, 15 had a p.V600E *BRAF* mutation and 4 had a p.Q61L/K *NRAS* mutation (379). The Poisson-corrected ctDNA levels ranged from 1.4 to 1608 copies, with a median of 2.8 (Table 5.2).

With statistical input from Dr. Andrea Marshall for all of the following results, I performed univariate analyses of known prognostic factors to determine whether there was any association with detectable ctDNA. Only PS was identified as significantly associated with detectable ctDNA (P=0.03) (Table 5.1) (379). This was confirmed using a multivariate logistic regression.

There was a significantly increased chance of having positive ctDNA in patients with PS 1 compared to 0 (odds ratio=3.61; 95% CI 1.20-10.82, P=0.02) (379).

Table 5.1. Demographics of patients with detectable or undetectable ctDNA

Characteristic	Total N (%)	Undetectable ctDNA N (%)	Detectable ctDNA N (%)
Age in years			
Median (range)	52 (19-87)	52 (19-79)	59 (22-87)
***P* value**	0.29		
Gender			
Male	77 (48)	70 (49)	7 (37)
Female	84 (52)	72 (51)	12 (63)
***P* value**	0.31		
Breslow of primary tumour			
≤2.0mm	61 (38)	53 (37)	8 (42)
>2-4.0mm	49 (30)	43 (30)	6 (32)
>4.0mm	42 (26)	38 (27)	4 (21)
Unknown	9 (6)	8 (6)	1 (5)
***P* value**	0.96		
Ulceration of primary tumour			
Present	63 (39)	57 (40)	6 (32)
Absent	77 (48)	69 (49)	8 (42)
Unknown	21 (13)	16 (11)	5 (26)
***P* value**	0.19		
Disease stage			
II	36 (22)	33 (23)	3 (16)
IIIA	29 (18)	27 (19)	2 (11)
IIIB	59 (37)	51 (36)	8 (42)
IIIC	37 (23)	31 (22)	6 (32)
***P* value**	0.61		
Nodal classification			
II (No or N/A)	36 (22)	33 (23)	3 (16)
III (N1a and N2a)	41 (26)	36 (25)	5 (26)
III (other N)	84 (52)	73 (52)	11 (58)
***P* value**	0.81		
ECOG performance status			
0	138 (86)	125 (89)	13 (68)
1	22 (14)	16 (11)	6 (32)
***P* value**	0.03		
Mutation status			
BRAF V600E	132 (82)	117 (82)	15 (79)
NRAS Q61K/L	29 (18)	25 (18)	4 (21)
***P* value**	0.75		
Trial arm			
Bevacizumab	81 (50)	71 (50)	10 (53)
Observation	80 (50)	71 (50)	9 (47)
***P* value**	0.83		

Table 5.2. Frequency of ctDNA copy numbers

ctDNA copy number	N (%)
0	142 (88)
1-3	10 (6)
3.1-10	4 (2)
10.1 -50	2 (1)
50.1-1608	3 (2)

5.2 Patient outcomes

At a median of 5 years, 21% (95% CI 7-41%) of patients with detectable ctDNA were alive and recurrence-free compared to 49% (95% CI 40-57%) for those with undetectable ctDNA (379). Of the 4 patients who did not recur, 1 patient had stage II disease, 1 stage IIIA, and 2 patients had stage IIIB disease, 3 were on the treatment arm and 1 on the observation arm (379). The time from surgery was variable (blood taken at 6, 9, 10 and 11 weeks) and importantly was not close to the time of resection compared to the rest of the cohort (median time from the last surgery to the date the bloods were taken was 8.3 weeks; range 2.4-12 weeks). Therefore timing of blood taking did not appear to be related to a false positive result. All 9 patients with >3 mutant copies have recurred (1 had regional lymph nodes metastases; 2 recurred distantly only and 6 had both loco-regional recurrence and distant metastases) (379). For one of the patients with detectable ctDNA within 12 weeks who did not relapse within the follow up period, subsequent analysis was found to be negative for ctDNA at 3, 6, 12, 18, 24, 36, 48 and 60 months. Fifty-two percent (74/142) of patients with undetectable ctDNA have recurred (patterns of the relapses/outcomes are presented in Table 5.3 and 5.4) (379). Twelve (63%) of the 19

patients with detectable ctDNA are known to have died compared to 49 (35%) of the 142 patients without detectable ctDNA (379).

Table 5.3. Outcomes of patients with detectable and undetectable ctDNA

	Undetectable ctDNA		Detectable ctDNA		Total	
	N	**%**	**N**	**%**	**N**	**% of total**
Total first local relapse	37		10		47	
Site of first local relapse[a]						
Local recurrence at primary site	14	38	2	20	16	34
In transit metastases	6	16	0	0	6	13
Regional lymph node metastases	12	32	5	50	17	36
Multiple sites	5	14	3	30	8	17
Subsequent therapy for first local relapse						
Immune therapy	1	3	0	0	1	2
Targeted therapy	3	8	0	0	3	6
Chemotherapy	0	0	1	10	1	2
Radiotherapy	6	16	1	10	7	15
Total first distant relapse	41		7		48	
Site of first distant relapse[a]						
Soft tissue	9	22	2	29	11	23
Liver	1	2	0	0	1	2
Pulmonary	6	15	0	0	6	13
Brain	3	7	1	14	4	8
Bone	1	2	0	0	1	2
Other	2	5	0	0	2	4
Multiple sites	19	47	4	57	23	48
Subsequent therapy for first distant relapse						
Immune therapy	2	5	0		2	4
Targeted therapy	9	22	0		9	19
Chemotherapy	8	20	3		11	23
Radiotherapy	10	24	3		13	27

[a]Patients can have simultaneous local/distant relapse.

Table 5.4. Sites of relapse

	Undetectable ctDNA		Detectable ctDNA		Total	
	N	**%**	**N**	**%**	**N**	**% of total**
Total first local relapse	37		10		47	
Multiple sites of first local relapse	5	14	3	30	8	17
Local recurrence at primary site and Regional lymph node metastases	1		0		1	2
Local recurrence at primary site, in transit metastases and Regional lymph node metastases	2		2		4	9
In transit metastases and regional lymph node metastases	2		1		3	6
Total first distant relapse	41		7		48	
Multiple sites of first distant relapse	19	47	4	57	23	48
Soft tissue and Pulmonary	5	12	0	0	5	12
Soft tissue, liver and Pulmonary	2	5	0	0	2	5
Soft tissue, Pulmonary and brain	1	2	0	0	1	2
Soft tissue, Pulmonary, bone and brain	1	2	0	0	1	2
Soft tissue and bone	1	2	0	0	1	2
Soft tissue and other	1	2	0	0	1	2
Pulmonary and liver	2	5	1	14	3	6
Pulmonary and bone	1	2	0	0	1	2
Pulmonary and brain	0	0	1	14	1	2
Pulmonary, bone and other	0	0	1	14	1	2
Pulmonary and other	2	5	0	0	2	4
Liver and brain	1	2	0	0	1	2
Bone and other	1	2	0	0	1	2
Brain and other	1	2	1	14	2	4

5.3 Prognostic significance of detectable ctDNA

In order to determine the prognostic significance of detecting ctDNA within 12 weeks of surgery, I performed Kaplan-Meier analysis. Median DFI was 0.3 years (95% CI 0.1-1.0) in patients with detectable ctDNA compared to 4.2 years (95% CI 2.5 – limit not reached) in those where ctDNA was not detected (Fig. 5.2.) (379).

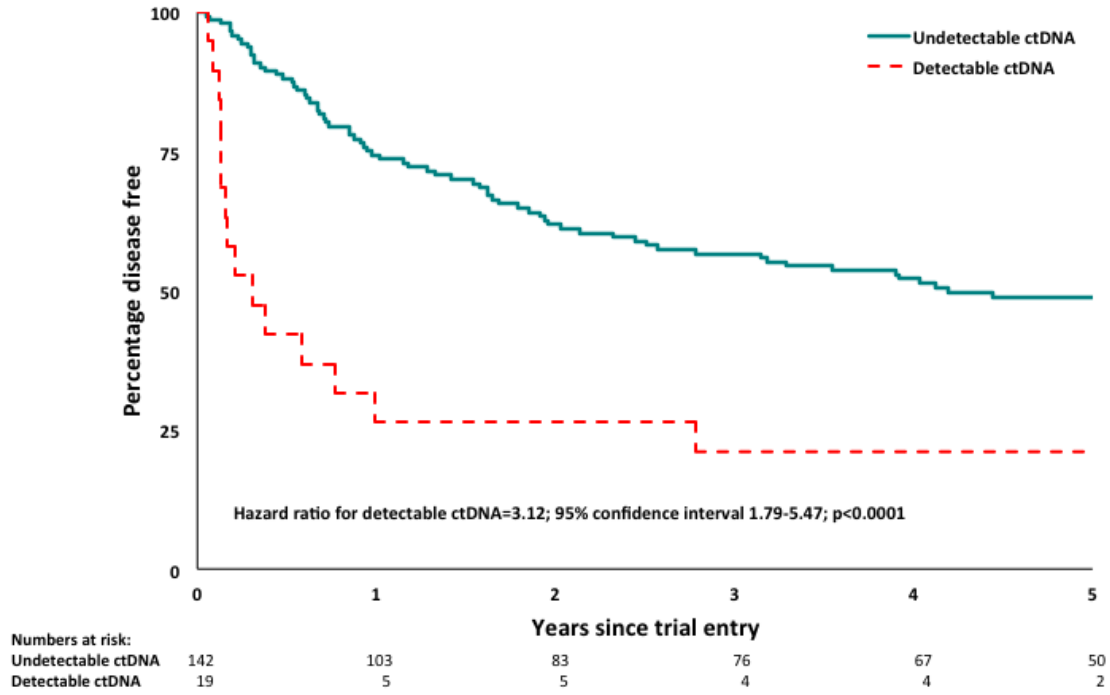

Fig. 5.2. CtDNA predicts DFI for patients with *BRAF/NRAS* mutations. Kaplan-Meier curves for DFI.

Patients with detectable ctDNA had significantly increased risk of recurrence compared to those with undetectable ctDNA (HR for detectable ctDNA 3.12; 95% CI 1.79-5.47; *P*<0.0001; prognostic separation D statistics (PSDS)=0.97; standard error (SE)=0.24; Table 5.5). As there was no independent validation cohort available at the time, I performed bootstrapping to provide internal validation, with ctDNA being a significant predictor of DFI in 92% of the bootstrapped samples (PSDS=0.99,

SE=0.24). At one year, 26% (95% CI 10-47%) of the patients with detectable ctDNA were disease free compared to 74% (95% CI 66-81%) for patients with undetectable ctDNA (Table 5.5). Sensitivity for predicting relapse was 18% and specificity 95%, with a positive predictive value of 79% and negative predictive value of 51%.

The AVAST-M study did not meet its primary endpoint as OS at 5 years was 64% for both the bevacizumab and observation arms (HR 0.98; 95% CI 0.82–1.16, $P = 0.78$) (378). Exploratory subgroup analysis of the observation arm revealed that *BRAF* mutant patients had a trend towards poorer OS compared with *BRAF* wild-type patients ($P = 0.06$). In the AVAST-M study, the only statistically significant result was that 51% of patients were disease-free on bevacizumab versus 45% on the observation arm at 5 years (HR 0.85; 95% CI 0.74-0.99, *P*=0.04) (380). There was no difference in numbers of patients with detectable or undetectable ctDNA in either trial arm within the 161 patients analysed for ctDNA. However, to ensure that treatment/trial arm did not affect the ability of ctDNA to predict DFI, I analysed our cohort in further detail. In my subgroup of 161 patients (total trial population 1343), trial arm had a borderline effect on DFI in univariate analysis (HR 0.68; 95% CI 0.45-1.03, *P*=0.07). There was no significant interaction between trial arm and the ctDNA in predicting DFI (*P*=0.60). After adjusting for trial arm, ctDNA was still a highly significant predictor of DFI (*P*<0.0001). Also after adjusting for PS, disease stage and trial arm, ctDNA remained a significant predictor for DFI (HR 3.31, 95% CI 1.84-5.94, *P*<0.0001). Therefore trial arm appeared to have no affect on the ability of ctDNA to predict relapse in this study.

Table 5.5. Univariate Cox proportional hazards regression analysis for prediction DFI, DMFI and OS, DF = disease free, DMF = distant metastasis free, CI = confidence interval, HR=hazard ratio

Parameter	Disease free interval				Distant metastasis free interval				Overall survival			
	% DF	% DF at 1 year (95% CI)	Univariate analysis *P*	Univariate analysis HR (95% CI)	% DMF	% DMF at 1 year (95% CI)	Univariate analysis *P*	Univariate analysis HR (95% CI)	% alive	% alive at 1 year (95% CI)	Univariate analysis *P*	Univariate analysis HR (95% CI)
ctDNA			<0.0001				<0.0001				0.003	
Undetectable	48	74 (66-81)		1.00	58	84 (77-89)		1.00	65	94 (89-97)		1.00
Detectable	21	26 (10-47)		3.12 (1.79-5.47)	26	37 (17-57)		3.22 (1.80-5.79)	37	72 (46-88)		2.63 (1.40-4.96)
Breslow			0.51				0.67				0.42	
<=2.0mm	48	65 (52-76)		1.00	51	75 (62-84)		1.00	57	90 (79-95)		1.00
>2-4.0mm	49	69 (54-80)		0.94 (0.56-1.58)	59	79 (65-88)		0.79 (0.45-1.40)	67	91 (79-97)		0.76 (0.41-1.42)
>4.0mm	33	69 (53-81)		1.27 (0.77-2.11)	50	81 (65-90)		0.96 (0.55-1.68)	57	95 (82-99)		0.98 (0.54-1.79)
Unknown	56	89 (43-98)		ND	67	89 (43-98)		ND	89	89 (43-98)		ND
Ulceration			0.94				0.93				0.57	
Present	43	71 (58-81)		1.00	54	77 (65-86)		1.00	59	92 (81-96)		1.00
Absent	45	67 (56-77)		0.96 (0.62-1.50)	53	82 (71-89)		0.97 (0.60-1.58)	62	95 (86-98)		0.86 (0.50-1.45)
Unknown	48	67 (43-83)		ND	57	71 (47-86)		ND	71	81 (57-92)		ND
Disease stage			0.03				0.03				0.14	
II	56	86 (69-94)		0.47 (0.25-0.88)	64	91 (76-97)		0.45 (0.23-0.89)	67	97 (81-100)		0.60 (0.28-1.25)
IIIA	59	79 (60-90)		0.42 (0.21-0.84)	69	93 (75-98)		0.37 (0.17-0.80)	79	96 (77-99)		0.37 (0.15-0.94)
IIIB	41	62 (49-73)		0.75 (0.45-1.25)	51	74 (61-84)		0.67 (0.39-1.16)	56	91 (81-96)		0.86 (0.47-1.58)
IIIC	30	54 (37-68)		1.00	38	62 (45-76)		1.00	54	83 (67-92)		1.00
N classification			0.06				0.12				0.38	
II (No or N/A)	56	86 (69-94)		0.56 (0.32-0.99)	64	91 (76-97)		0.58 (0.32-1.08)	67	97 (81-100)		0.69 (0.36-1.33)
III (N1a and N2a)	51	73 (57-84)		0.64 (0.38-1.07)	61	83 (67-91)		0.64 (0.36-1.14)	68	93 (79-98)		0.70 (0.37-1.32)
III (other N)	37	59 (48-69)		1.00	46	71 (60-80)		1.00	57	89 (80-94)		1.00
ECOG performance status			0.02				0.01				0.01	
0	48	73 (65-80)		0.51 (0.30-0.88)	57	83 (76-88)		0.46 (0.26-0.83)	66	96 (91-98)		0.43 (0.23-0.80)
1	27	45 (24-64)		1.00	36	54 (32-72)		1.00	41	68 (44-83)		1.00

Median distant metastasis-free interval (DMFI) was 0.6 years (95% CI 0.2-2.8) with detectable ctDNA, but was not reached with 5 years of follow-up (95% CI 5.0 – limit not reached) for those with undetectable ctDNA (Fig. 5.3). Patients with detectable ctDNA had a significantly increased risk of distant metastatic recurrence compared to those with undetectable ctDNA (Table 5.5, HR 3.22; 95% CI 1.80-5.79; P<0.0001, PSDS=0.99, SE=0.25). I performed bootstrapping to confirm ctDNA as a significant predictor of DMFI in 92% of samples (PSDS=1.03, SE=0.26). At one year, 37% (95% CI 17-57%) of the patients with detectable ctDNA were free of distant metastases compared to 84% (95% CI 77-89%) for patients with undetectable ctDNA (Table 5.2). Sensitivity for predicting distant relapse was 20% and specificity 95% with a positive predictive value of 74% and negative predictive value of 61%.

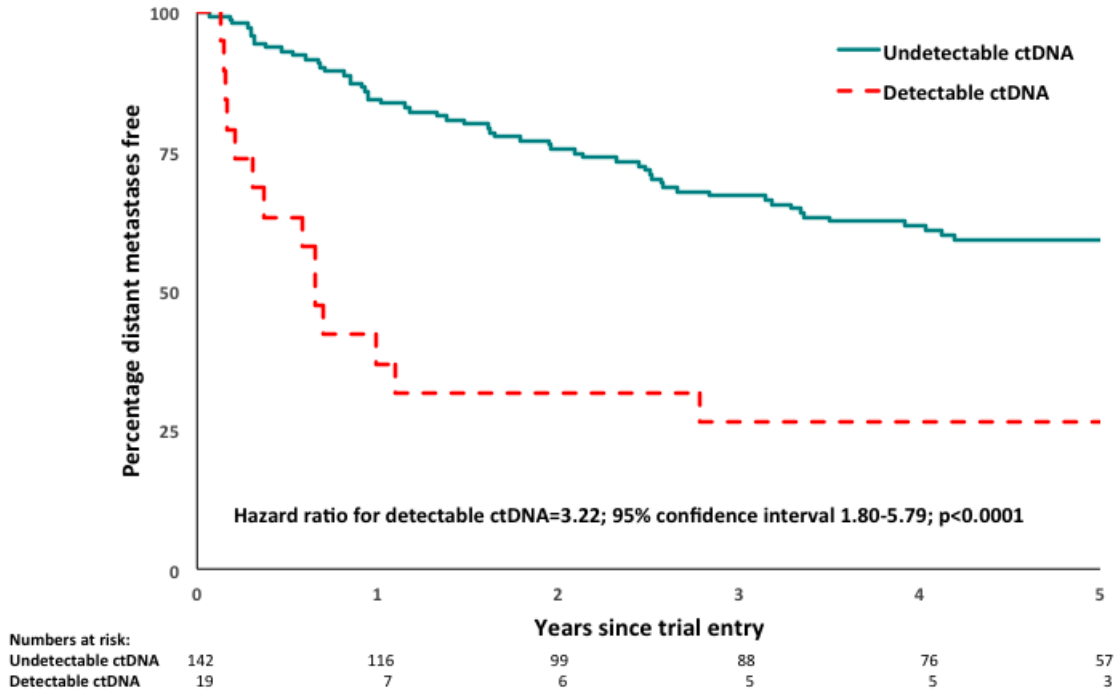

Fig. 5.3. CtDNA predicts DMFI in patients with *BRAF/NRAS* mutant melanoma. Kaplan-Meier curves for DMFI.

OS was significantly worse for the 19 patients that had detectable ctDNA compared to the 142 with undetectable ctDNA (Table 5.2, HR 2.63; 95% CI 1.40-4.96); *P*=0.003, PSDS=0.82, SE=0.27). I performed bootstrapping to confirm ctDNA as a significant predictor of OS in 81% of samples (PSDS=0.83, SE=0.26). Median OS was 2.9 years (95% CI 0.9-limit not reached) with detectable ctDNA compared with median not reached with 5 years follow-up for those with undetectable ctDNA (95% CI 6.0-limit not reached, Fig. 5.4).

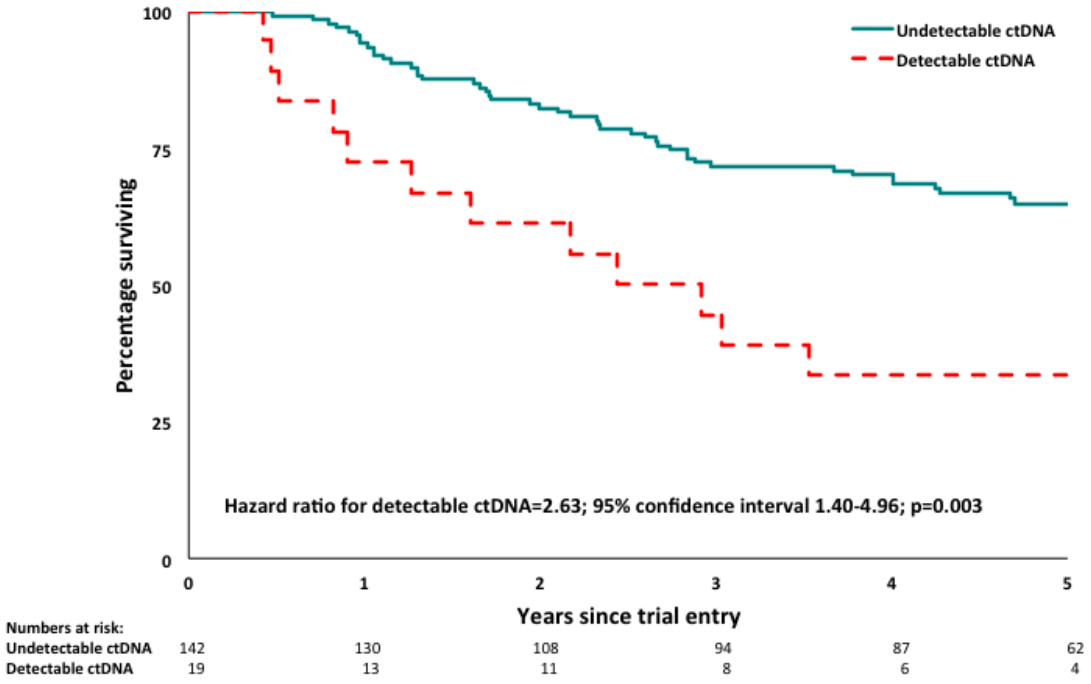

Fig. 5.4. CtDNA predicts OS in patients with *BRAF/NRAS* mutation. Kaplan-Meier curves for OS.

At one year, 72% (95% CI 46-88%) of patients with detectable ctDNA were alive compared to 94% (95% CI 89-97%) for patients with undetectable ctDNA (Table 5.2). At five years, 33% (95% CI 14-55%) of patients with detectable ctDNA were alive compared to 65% (95% CI 56-72%) for those with undetectable ctDNA. Of note, only 12 patients (none in the ctDNA detectable group) received targeted or

immune therapy on relapse due to limited availability of these treatments at the time of the study (Table 5.3).

5.4 Association of prognostic factors and ctDNA on outcome

I performed univariate analyses to assess the impact of both ctDNA and standard prognostic factors associated with decreased time to relapse and survival of patients with melanoma following curative intent surgery. CtDNA (*P*<0.0001) was significantly more predictive of DFI than either PS (*P*=0.02) or disease stage (*P*=0.03) (Table 5.5), and none of the other known prognostic factors (thickness, ulceration, N-classification) were significant. Similarly, ctDNA (*P*=<0.0001) was significantly more predictive of DMFI than PS (*P*=0.01) or disease stage (*P*=0.03) (Table 5.5).

Table 5.6. Multivariate cox proportional hazards regression analysis for prediction of disease free interval (DFI), distant metastasis free interval (DMFI) and overall survival (OS)

Parameter	Disease Free interval		Distant metastasis free interval		Overall survival	
	P	**HR (95% CI)**	***P***	**HR (95% CI)**	***P***	**HR (95% CI)**
ctDNA	<0.0001		<0.0001		0.005	
Undetectable		1.00		1.00		1.00
Detectable		3.26 (1.83-5.83)		3.45 (1.88-6.34)		2.50 (1.32-4.74)
ECOG	0.02		0.01		0.02	
0		0.52 (0.30-0.89)		0.46 (0.25-0.82)		0.47 (0.25-0.87)
1		1.00		1.00		1.00
Disease stage	0.02		0.02			
II		0.46 (0.25-0.87)		0.45 (0.23-0.89)		
IIIa		0.38 (0.19-0.76)		0.34 (0.16-0.74)		
IIIb		0.66 (0.39-1.12)		0.59 (0.34-1.04)		
IIIc		1.00		1.00		

Critically, in a multivariate Cox proportional hazards regression model, ctDNA remained a significant predictor for DFI (HR 3.26, 95% CI 1.83-5.83, $P<0.0001$) and DMFI (HR 3.45, 95% CI 1.88-6.34, $P<0.0001$) after adjustment for PS and disease stage (Table 6). For OS, in univariate analyses ctDNA ($P=0.003$) was significantly more predictive than PS ($P=0.01$), and disease stage was not predictive, nor were other factors associated with AJCC staging (Table 5.5). In multivariate analysis ctDNA remained a significant predictor of OS after adjustment for PS (HR 2.50, 95% CI 1.32-4.74, $P=0.005$, Table 5.6). Finally, to compare the performance of ctDNA in addition to standard prognostic factors, I modelled the prognostic ability of variables associated with AJCC (version 7) staging (stage, N-classification, ulceration, Breslow) and then adjusted for ctDNA (Table 5.7). When adjusted for ctDNA, all indices of discriminative and predictive ability (PSDS, Nagelkerke's R^2, Calibration shrinkage measure (292–294)) showed significantly improved prognostic value for DFI, DMFI and OS (Table 5.7).

Table 5.7. Model performance measures for the staging variables associated with AJCC classification (stage, N-classification, ulceration and Breslow) and the model adjusted for ctDNA. SE= standard error

Model	**AJCC staging variables**			**Adjusted for ctDNA**		
Outcome Measure	**DFI**	**OS**	**DMFI**	**DFI**	**OS**	**DMFI**
Prognostic separation measure D statistic	0.63 (SE=0.17)	0.70 (SE=0.21)	0.53 (SE=0.18)	0.96 (SE=0.20)	0.98 (SE=0.23)	1.01 (SE=0.22)
Predictive ability measure Nagelkerke's R^2	0.093	0.085	0.077	0.17	0.13	0.15
Calibration shrinkage measure	0.43	0.36	0.29	0.65	0.53	0.63

5.5 Prospective validation of detectable ctDNA post surgery

Following the retrospective study I collaborated with Prof. Sarah Jane Dawson's laboratory (Melbourne, Australia) to validate my findings. They had been collecting and analysing plasma both pre- and post-operatively with longitudinal sampling to test for *BRAF/NRAS* and *TERT* promoter mutations in ctDNA. I had also started a prospective collection and therefore could use my cohort as validation for

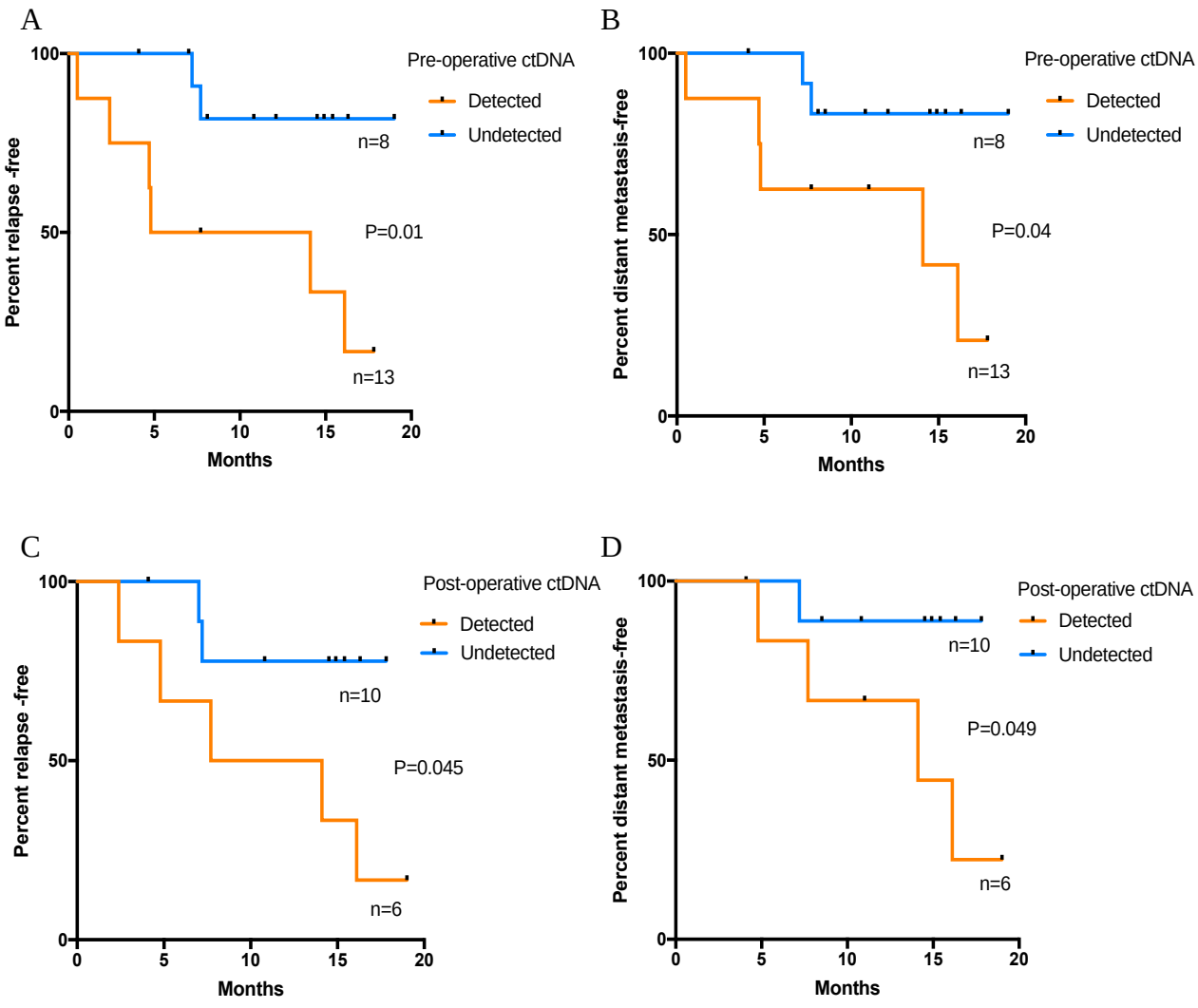

Fig. 5.5 Pre-operative and post-operative detection of ctDNA predicts RFS and DMFS. Kaplan Meier analysis of (A) RFS and (B) DMFS in patients stratified by baseline ctDNA detection. Kaplan Meier analysis of (C) RFS and (D) DMFS in patients stratified by post-operative ctDNA detection.

their data. The technique used was slightly different to my retrospective study in that 10µl was taken from the 50µl elution volume from the cfDNA extraction and used in the ddPCR reaction. This was then repeated in a duplicate reaction and there needed to be ≥1 droplet positive in both replicates for it to be considered a positive result.

In total, I prospectively collected plasma for 29 patients, however only 21 patients had a *BRAF/NRAS* or *TERT* promoter mutation and were used in the analysis; 21 had a baseline pre-operative plasma sample and 16 had a post-operative plasma sample available. Baseline clinical characteristics of patients in the cohort are presented in Appendix 19. For this study I taught a scientific officer Miss. Philippa Middlehurst to extract the cfDNA from the plasma and perform the ddPCR, I performed some of the ddPCR and all of the analysis. Detectable pre-operative ctDNA predicted for RFS (HR 6.8; 95% CI 1.5-29.7; *P*=0.01) and DMFS (HR 4.7; 95% CI 1-22.4; *P*=0.04) (Fig. 5.5 A-B). Furthermore, detectable ctDNA at the post-operative timepoint within 12 weeks of surgery was predictive for RFS (HR 4.9; 95% CI 0.97-21.6; *P*=0.045) and DMFS (HR 6.7; 95% CI 1.09-40.8; *P*=0.049) validating my retrospective findings (Fig. 5.5 C-D).

Finally, we combined the longitudinal sampling of both the Melbourne and Manchester cohorts and examined whether ctDNA was detected in samples that were taken within 6 months of clinical relapse (Fig. 5.6.). Of note, 2 further patients

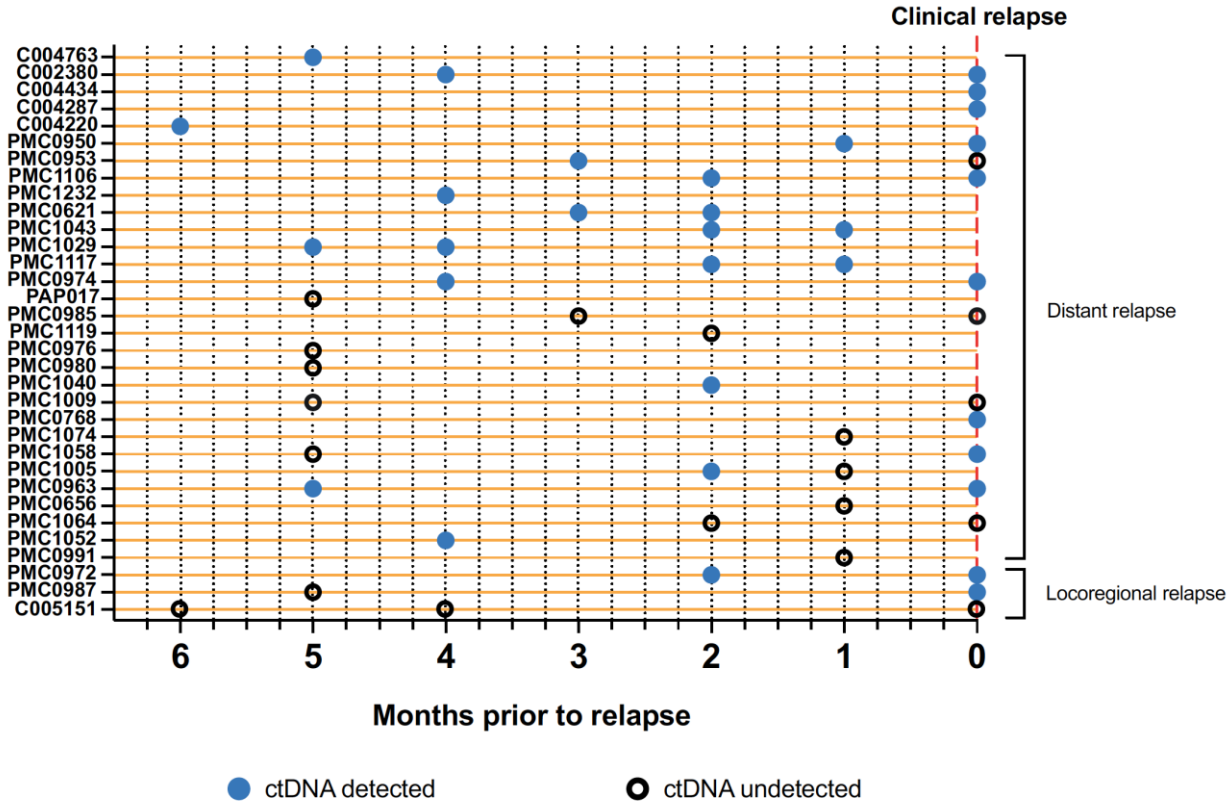

Fig. 5.6 Longitudinal ctDNA analysis and detection of relapse. Post-operative and serial plasma samples collected within 6 months of relapse were included in this analysis (n=33). Clinical relapses were confirmed radiologically, or if equivocal by imaging, were confirmed by biopsy. CtDNA was detected prior to clinical relapse in 17 cases with a further 5 cases detected at the time of clinical relapse. Manchester patients begin with "C", (n=6).

(C004221 and C004340) have ctDNA detected in longitudinal sampling, however have not had clinical confirmation of relapse. Patient C004221 has an equivocal inguinal lymph node on CT scan and is awaiting further PET imaging. Patient C004340 has a lung nodule seen on CT scan but this was not PET avid and is currently being monitored.

CtDNA was detected in 17/33 (52%) patients prior to clinical relapse, with a median lead-time of 3 months. In a further 5 patients, ctDNA was detected at the time of clinical relapse. Thus, ctDNA was able to detect relapse in a total of 22/33 (66%) cases through longitudinal analysis.

5.6 Chapter discussion

In the evolving paradigm of effective adjuvant therapy in melanoma, it is essential to develop biomarkers identifying patients at high risk of relapse. Currently, features of the primary tumour such as ulceration, Breslow and number of mitoses in addition to nodal classification (N-classification) and disease stage are standard measures to predict melanoma progression (5). Furthermore, gene expression profiling has identified subsets that are associated with a poor outcome in stage I-III melanoma, however patient numbers in these studies were small and have yet to be confirmed in larger cohorts (381,382).

5.6.1 CtDNA detects minimal residual disease and patients at high risk of relapse

In this chapter, I showed that detecting ctDNA in plasma taken within 12 weeks of curative intent surgery is highly predictive of relapse in patients with stage II/III melanoma. The majority of patients with detectable ctDNA relapsed within 1 year of surgery suggesting that ctDNA in the plasma reveals occult disease that is not evident on radiological imaging. Notably, I was able to identify patients with melanoma at high risk of both distant metastatic relapse and local recurrence, which is consistent with studies showing that ctDNA can signal micro-metastatic disease after neoadjuvant chemotherapy post-surgical resection in breast cancer, and following surgery for stage II colorectal cancer (383,384).

The concept of MRD and molecular relapse has traditionally been associated with haematological cancers (385–387). Immunofluorescence microscopy was initially used to detect leukemic cells, however with the invention of PCR techniques, laboratories began to use PCR to detect specific immunoglobulin (IG) or TCR gene rearrangements (385). Based on my data and that of others (245,383), I would suggest that ctDNA now enables us to detect MRD and molecular relapse in solid malignancies. Due to the limited numbers of patients in my study, I

could only assess whether a binary outcome of detectable or undetectable ctDNA was associated with prognosis. It would be interesting to investigate whether different levels of ctDNA present are associated with shorter DFS and OS in larger cohorts, especially in the modern era of melanoma treatments.

5.6.2 Comparison with other standard staging indices

My findings were independent of standard staging indices, suggesting that ctDNA could be a useful addition to current prognostic assessments. PS and AJCC stage (AJCC version 7 for the retrospective study and AJCC version 8 for the prospective study) were the only predictors of relapse that were significant in this population. PS is not part of standard AJCC staging and would not typically be thought of as a predictor of survival in the context of early stage disease, however it was also an independent predictor for DFI, DMFI and OS in the overall AVAST-M study population (271). The reasons for this are not known, but even when adjusted for PS and AJCC stage in multivariate analysis, ctDNA was significant in predicting DFI, DMFI and OS. Moreover, in this cohort AJCC variables performed poorly to predict relapse, but when I created a model in which the standard AJCC variables were adjusted for ctDNA (Table 5.7), the performance improved significantly.

5.6.3 Limitations of the study

There are a number of limitations to this study. Although its retrospective nature resulted in sufficient follow up for enough events to have occurred, the samples had been stored for a long period of time, which may have affected the quality of the DNA. In addition, I was limited to only 2ml of plasma for analysis, which is likely to have affected the sensitivity of the assay. In the prospective cohorts, 2 reactions were required to have ≥1 droplet positive to be called as ctDNA detected. This was more stringent than the retrospective study, which may

have reduced false negatives but together with the lower input DNA (1/5 of total sample from 4ml plasma) likely reduced the sensitivity of the assay.

As proof-of-principle, in the retrospective study I focused on the driver mutations *BRAF* and *NRAS,* which account for up to 70% of melanomas, and are well suited to the identification of MRD and molecular relapse because of the low likelihood of clonal diversity with trunk mutations such as these in melanoma. Furthermore, driver mutations usually have the highest VAF, which improves the sensitivity of the test. However, there are cases reported of discordancy in terms of BRAF status between primary and metastatic disease, which could affect the ability to detect ctDNA specific to *BRAF* mutations (388). Reassuringly a recent study of 634 stage I-IV patients showed >90% concordance between tumour and ctDNA for a *BRAF* mutation (389). Intriguingly, for some cases, discrepancy between tissue and ctDNA was associated with either a non-response to BRAFi or a secondary *BRAF*-mutant malignancy (389).

In the prospective cohorts I also included patients with a *TERT* promoter mutation and therefore I was able to determine a trackable mutation in 72% of patients. The Dawson group also performed targeted amplicon sequencing using a 19-gene panel and were able to identify mutations in 80% of patients. However, approximately 20% of patients were still excluded from analysis of ctDNA because a suitable mutation was not identified (19-gene panel) and therefore future studies should focus on performing WES or a larger targeted sequencing panel to identify trackable mutations in all patients.

Finally, the patients evaluated in this study were treated in an era where access to immune and targeted therapies was limited. Based on responses seen in clinical trials, these treatments are likely to have an effect on overall prognosis (8,195). Intriguingly, detection of ctDNA and high levels of ctDNA have consistently been associated with inferior prognosis in stage IV melanoma despite modern treatments (263,376,377). Furthermore, baseline ctDNA

levels in patients treated with both targeted and immune therapy have been shown to correlate with inferior survival and disease burden (377,390). Therefore, I would hypothesise that patients with detectable ctDNA in the adjuvant setting are less likely to respond and have durable responses to these treatments, but further research is required to test this.

5.6.4 Potential methods of improving the test

5.6.4.1 Next generational sequencing (NGS)

Targeted NGS of a panel of commonly mutated genes in melanoma has a number of potential advantages, however it is also associated with disadvantages compared to ddPCR (Table 5.9). For ddPCR, knowledge of the exact point mutations is required for testing, however NGS approaches do not have that requirement. It is possible to screen blood only without need for tissue, although false negative rates would increase, as some patients may not have the mutations present in the panel depending on its size (Table 5.8).

		Droplet digital	**Targeted next generational sequencing**
Sensitivity		0.001%-0.01% (method dependent) (391)	0.01%- 0.5% for custom built panels (391)
Prior knowledge of mutation status required		Yes – exact point mutation required	Preferred *
Multiplexing capability		Limited	Moderate
Bioinformatics requirement		No	Yes
Cost per sample (machine cost not included)		~ £150	~£700
Turn-around time	~3 days	~2 weeks	

Table 5.8. Comparison of ctDNA detection methods for MRD detection.

NGS is a sensitive approach, although in terms of individual point mutations, ddPCR is likely to be more sensitive (391). One of the potential methods of improving the sensitivity of the test is to reduce sampling error through increasing the number of mutations tested (391). The probability of detecting one mutation is decreased in low concentrations due to the increased chance of a mutated piece of DNA not being present in the sample (sampling error) (391). Increasing the number of mutations tested increases the number of independent opportunities for a mutation to be detected, therefore improving sensitivity (391). However, this theory has not been tested experimentally using ddPCR techniques to quantify the potential gains in sensitivity using this approach. NGS methods would enable larger panels of candidate mutations to be tested simultaneously within each patient. In addition, with a larger panel it is more likely that it would be possible to track at least one mutation in every patient tested. The gains beyond a top 10-gene panel of mutated genes in melanoma (identified using the TCGA database) are likely to be small due to the intra-patient heterogeneity of the disease (Table 5.10). Ultimately, for the individual patient the best approach would be to create a bespoke panel following sequencing of their resected tumour. Again the additional benefit of this strategy needs to be assessed.

Number of genes in panel	10	24	110
Percentage of patients estimated to have at least 1 gene mutated	87.5%	91.2%	96.1%

Table 5.10. Estimate of the percentage of patients with at least one gene mutated within the gene panel

* Approximately 87.5% of patients would have at least one mutated gene in a panel of top ten mutated loci in melanoma based on TCGA MuTect calls, increasing false negatives by up to 12.5% if mutation status unknown.

One of the main areas that an NGS approach may be better than ddPCR is in patients that do not have an *NRAS* or *BRAF* mutation present. Mutations in these patients are likely to be at a lower VAF (especially in comparison to *BRAF*) and thus potentially they have increased chances of sampling error.

5.6.4.2 Increasing input DNA

A simple method of improving sensitivity is to increase the amount of input ctDNA through taking larger volumes of plasma and testing one sample over multiple reactions or replicates. This enables a greater proportion of DNA to be screened for mutations at one particular time point. Furthermore, in testing over multiple reactions, a potential mutant DNA molecule would make up a larger proportion of the total DNA in the reaction and therefore is more likely to be detected against background noise (391,392).

5.6.4.3 Longitudinal sampling

Based on the findings of others (383) and the low sensitivity seen in my study, it is unlikely that a single time-point following surgery will identify all patients who are going to relapse even with improvements to the assay (379). One of the ways to further improve the approach is through longitudinal sampling. In breast cancer 80% (12 of 15) of patients had ctDNA detected by serial mutation tracking compared to 50% (6 of 12) of patients with detectable ctDNA in a single post-surgical sample (383). Furthermore ctDNA was detected a median of 7.9 months (range, 0.03 to 13.6 months) before clinical relapse (383). Longitudinal sampling has also identified treatment relapse prior to radiological imaging in stage IV disease providing a rationale for such an approach in melanoma (377).

5.6.4.4 Diversifying test through multi-omics

My work shows that ctDNA is a good liquid biomarker of MRD and molecular relapse. However, there are other blood-based modalities that could be explored, which might further improve a liquid biopsy test if combined with ctDNA.

A recent paper showed the potential value of combining protein and DNA based approaches to early detection of cancers (392). Detecting a mutation in ctDNA had the highest contribution to the test as determined by an importance score evaluated by the decrease in accuracy of the same logistic regression when the ctDNA or protein alone was dropped from the remaining features (392). However, proteins also contributed to the sensitivity of the test, especially in ovarian and liver cancers (392). Additional "omics" modalities may therefore play an additive role in a liquid test of MRD/molecular progression (392).

Methods of cancer/melanoma detection that have been evaluated as single entities include proteomics, metabolomics, methylated DNA, CTC and circulating microRNAs (393). A study evaluated proteomic signatures using matrix-assisted laser desorption/ionisation time-of-flight mass spectrometry and artificial neural networks in the serum of 101 early stage patients with melanoma (394). Using training and test sets they were able to discriminate between patients with stage III disease who went on to progress compared to those who remained disease-free (394). Another group examined differences in metabolites using gas chromatography/triple quadrupole mass spectrometry in the serum of 9 patients with melanoma (stages Tis-IV) compared to healthy volunteers and found that 33 metabolites were significantly different in melanoma (395). The cohort was very small, there was a large variation in stage of disease and there was no validation of their findings, however it does show that potentially there could be differences in metabolites in patients with melanoma compared to a disease-free state.

DNA methylation occurs through the addition of a methyl group to a DNA molecule (396,397). Commonly this is at CpG dinucleotide sites in cancer resulting in CpG islands often

within a promotor region of a gene or in the first exon (396,397). In general it leads to decreased expression of a gene, although hyper-methylation of genes in melanoma has been reported (397). As the methylation sites are specific to cancer these can be potentially used to detect MRD/relapse. Studies to date in melanoma have focussed on methylation in tumour samples as a prognostic biomarker or a predictive biomarker of response to therapy (397). An example of the potential use of DNA methylation as a method of detection of MRD/molecular relapse is in a study of 84 patients with early stage prostate cancer compared to 10 healthy controls (398). Detection of a combination of 3 methylated genes (MCAM, ERα, ERβ) was found to have a sensitivity of 75% and specificity of 70% compared to prostate specific antigen (4ng/ml) with a sensitivity of 77.4% but a specificity of 30% (398).

CTC in melanoma have been examined as a prognostic biomarker in stage IV disease and as a predictive biomarker of early response to immune therapy (399,400). However using current technologies they are unlikely to be a viable option for early stage melanoma detection due to challenges in identifying cells (cut-off in stage IV disease where the numbers of CTC present are likely to be higher was 2 CTC/ 7.5ml blood) (399). There is no universal marker that can be used to identify melanoma unlike epithelial cancers such as prostate or breast for which epithelial cell adhesion molecule (EpCam; CellSearch® is Food and Drug administration (FDA) approved) is used (401). This may change over time as isolation techniques improve.

Circulating micro-RNAs also have the potential to be incorporated into a blood-based melanoma test. Micro-RNA are small (20-22 nt) non-coding RNAs that regulate gene expression (402). They are released by tumours into the bloodstream and therefore can be used to detect the presence of cancer (402). A study examining the sera of 385 patients with stage I-IV melanoma compared to 130 healthy controls showed that a panel of 7 micro-RNA was able to identify melanoma independent of stage if there was ≥4 differentially expressed (over

optimal cut-off point defined for each micro-RNA) micro-RNA present with a sensitivity of 93% and ≥82% specificity (402).

Any combination of these liquid biomarkers could be evaluated as part of a multi-faceted approach to identify MRD/relapse. Using a variety of detection methods could improve sensitivity of the test, however it will be important to be stringent about maintaining specificity as that could decrease if using multiple parameters.

5.6.5 Enabling the test to become "clinic ready"

One of the key aspects of a test being "clinic ready" is its deliverability. The ddPCR platform is a good candidate for this as it does not require much technical skill/bioinformatics support to perform, is mostly automated, has a turnaround time of approximately 3-5 days including quality assurance assessments and is considerably cheaper following the initial outlay of the machine. Furthermore, genomics centres within the UK are already starting to use the technology and therefore it would be possible to roll out the assays to standard GCP laboratories if the evidence was provided in a practice changing clinical trial.

Following my retrospective study, I was able to validate my findings in a small prospective cohort and collaborated with another group who had an additional prospective cohort. I therefore feel that the evidence for use of ctDNA as a biomarker of MRD is strong. The next stage of biomarker development is to test ctDNA in a prospective randomised clinical trial (403), which will be discussed in the following chapter. In addition, there are a number of issues, which will need to be resolved before ctDNA can become part of standard of care.

5.6.5.1 International standardisation of ctDNA

One of the key issues that require international standardisation is the variability of ctDNA testing between both different techniques and different laboratories. This was recently

highlighted as a concern in a paper which compared 2 commercially available targeted sequencing platforms in 40 patients with prostate cancer and analysed the congruence between them (404). They found that in the genes tested in both panels with adequate exome coverage, 16/40 patients had no congruence in mutations called (404). Therefore differences in the platform may result in variability in mutation calls.

My data showed similar findings from two separate laboratories in terms of the ability to validate the principle of ctDNA detection being associated with relapse. However, we did not do a cross comparison of individual samples, which would need to be performed if the test was to be rolled out to multiple laboratories within a clinical trial. In addition, for the prospective study, I used the Melbourne group's method of calling mutations positive, which was different to my original method in that it required at least one droplet positive in 2 duplicate reactions. Using this method some of the patients we would have originally called as having detectable mutations, were instead called as negative. Differences in methods can therefore result in a large difference in whether a patient would be determined to have detectable ctDNA, emphasising the importance for consensus on precise definitions of mutation detection. Furthermore, there were some mutation calls that were more difficult to interpret due to the spread of droplets. These were discussed internally and the test repeated, but machine-learning approaches might improve the quality of mutation calling in this scenario.

5.7 Chapter Summary

In summary, ctDNA is a powerful tool to identify minimal residual disease and molecular relapse. Taken at one timepoint following surgery it can be used to stratify high-risk patients and provide prognostic information to the patient and clinician. Longitudinal sampling can identify early micro-metastatic relapse following surgery and during/post adjuvant therapy, which will need confirming in larger cohorts of patients. Further research is needed to understand whether it is a predictive biomarker of response to adjuvant targeted and immune therapy.

Chapter 6. Translating research back into the clinic

As shown in the previous chapter, ctDNA is a powerful tool to detect the presence of melanoma, its burden and activity. However, the ctDNA field has generally been limited to preclinical research and it has yet to become "clinic ready". Hence, I decided to use it to design trials addressing some of the main questions and challenges in the melanoma clinical field, in order to test whether ctDNA could be used to inform clinical decision-making. For this chapter I had input regarding the study designs from Prof. Lorigan, Prof. Marais, Prof. Middleton, Dr. James Larkin, Dr. Paul Nathan and statistical advice from Mr. David Ryder (CirculAting Tumour DNA gUided therapy Switch; CAcTUS) and Dr. Richard Jackson (circulating tumour DNA guidEd Therapy for stage IIB/C mElanoma after surgiCal resection; DETECTION).

Initially our translational research had focussed on patients in the stage IV setting (Fig 6.1 I identified patients, consented them, extracted plasma and provided clinical data for this study).

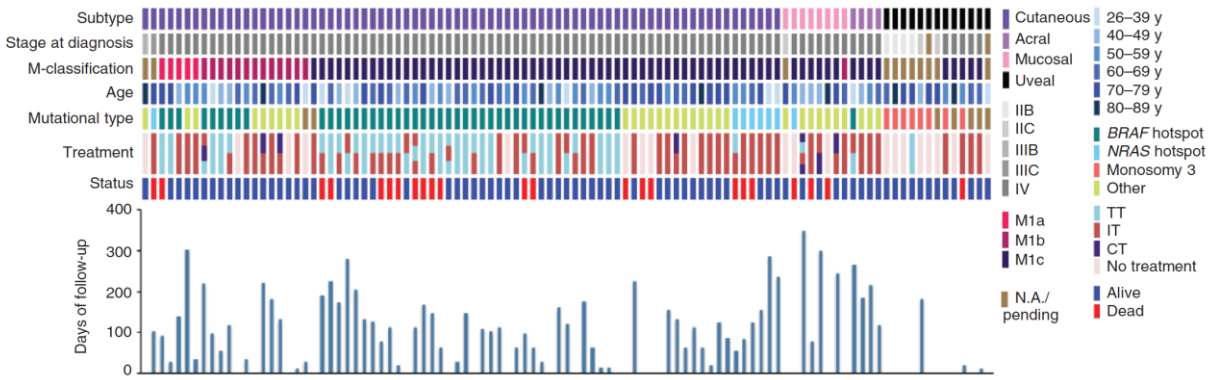

Figure 6.1. Plasma collection of 101 patients with cutaneous, acral, mucosal, and uveal melanoma at different disease stages. Patients with baseline samples prior to treatment and known mutations were then monitored by ctDNA

first ideas were around how ctDNA could be used to improve outcomes for patients with stage IV metastatic melanoma. One of the key results from the ctDNA work in stage IV melanoma was the identification of mutations conferring resistance to BRAFi/MEKi targeted therapy in melanoma such as *NRAS* mutations or mutations in the PI3K family (Fig 6.2). However, second

line treatment targeting these mutations is a challenge and often patients will have already received immune therapy. RAS has been a very difficult target in drug development due to the

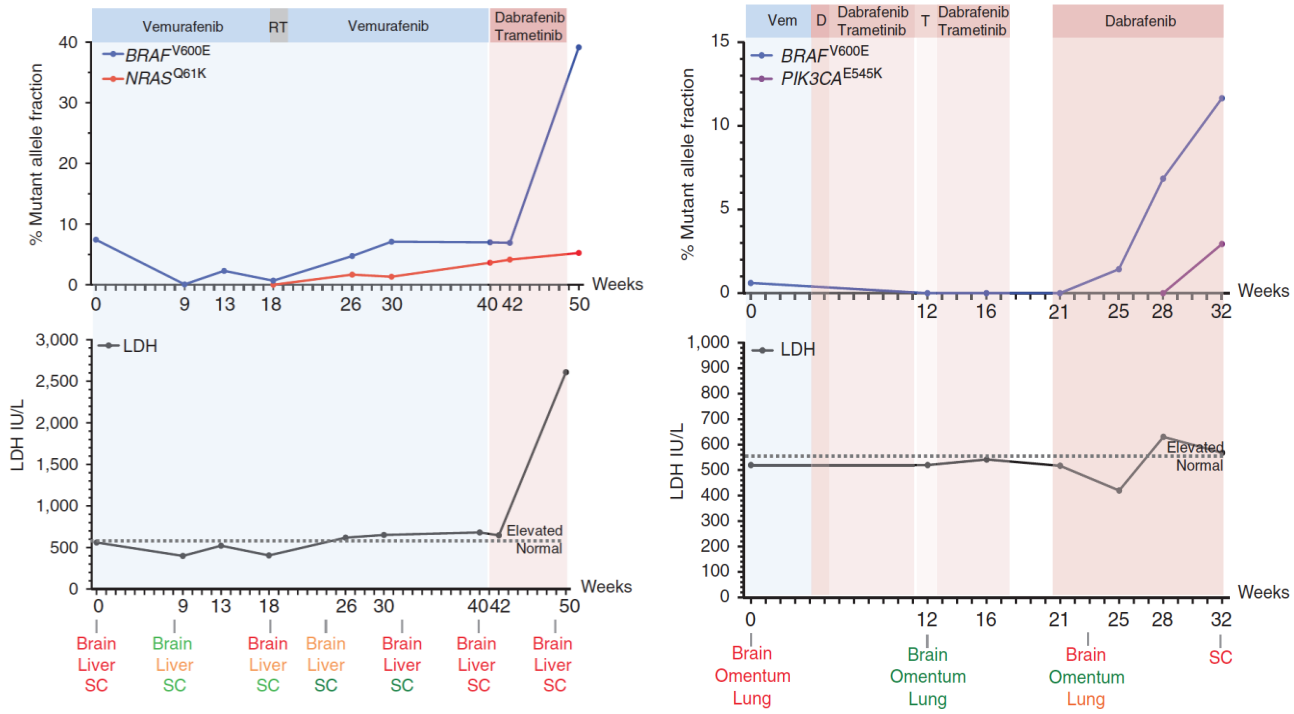

Fig. 6.2. Resistance mutations arising in ctDNA on BRAFi/MEKi targeted therapy. A. Emerging *NRAS* Q61K mutation observed on treatment followed by progression seen on CT scan. **B.** *PIK3CA* mutation seen in ctDNA of a patient receiving dabrafenib therapy, which was a potential cause of resistance to drug.

deep hydrophobic binding pockets which would enable small molecules to bind (405). PI3K inhibitors have also been disappointing to date, although as previously discussed, the SANDPIPER Phase III study of taselisib combined with fulvestrant in hormone receptor positive, *PIK3CA* mutant, locally advanced or metastatic breast cancer showed improved in PFS vs. placebo plus fulvestrant (112). This is encouraging regarding its ability to target the PI3K pathway and elicit a response (112). However, the response was only marginal (median PFS 7.4 vs. 5.4 months for fulvestrant plus taselisib vs. fluvestrant plus placebo), suggesting further work will be needed to understand why targeting the PI3K pathway has not resulted in a larger clinical benefit for patients. In addition, the SWOG S0500 trial has shown that early switching

of therapy in metastatic breast cancer based on persistence of circulating tumour cells has not improved OS (406). One of the contributing factors was a lack of response to second line treatment in this very poor prognostic subgroup. Therefore, this is an important consideration in switches of therapy on early evidence of resistance in stage IV disease, where the next line of treatment may have limited efficacy.

In addition, treatment beyond progression on targeted therapy has been used as a strategy to increase clinical benefit in melanoma (131,132,407). Reports have shown patients obtaining an additional 3-6 months of benefit if targeted therapy continues beyond radiological progression (131,132,407). An emerging *NRAS* mutation could be a concern on single agent BRAFi due to paradoxical activation of the MAPK pathway (71), however as the majority of patients are now treated with combination BRAFi/MEKi targeted therapy, this represents less of an issue. Therefore, switching treatment early based on identification of resistance mutations in ctDNA may not actually provide much additional benefit, particularly if the second line treatment is not likely to provide a deep response.

I therefore decided to focus on one of the major questions in the field, which is how to best optimise scheduling of targeted and immune therapy in melanoma. Hence, the first trial called CAcTUS is a parallel arm, biomarker driven, phase II trial to determine the role of ctDNA in guiding a switch between targeted therapy and immune therapy in patients with advanced cutaneous melanoma. The initial trial is a pilot study only and as such will provide a signal rather than be powered sufficiently to address whether switching treatment to immune therapy in response rather than onset of resistance to targeted therapy improves outcomes for patients with stage IV melanoma.

The second trial design is based on the data presented in chapter 5, which provided proof of principle that it is possible to detect MRD and early disease recurrence in melanoma following curative intent surgery. Although I had more data to show this in stage III melanoma,

adjuvant therapy has only been recently approved and the general consensus in the field was that it was too early to test the assay in the stage III setting. A trial in stage III melanoma would have to reduce rather than add in therapy and therefore it was felt that further evidence would be required to justify this ethically. Therefore, I designed a trial for stage IIB/C patients whose current standard of care is to follow up with clinical/radiological review only. The trial is called DETECTION (circulating tumour DNA guidEd Therapy for stage IIB/C mElanoma after surgiCal resecTION).

6.1 CAcTUS Rationale

The optimal scheduling of targeted and immune therapies in metastatic melanoma is unknown (408–410). Durable responses have been seen with immune therapy and many clinicians have favoured treatment with immune therapy first-line (411). This is mainly due to the association of immune therapy with a subset of patients who are long-term survivors (10). However, subgroup analysis of the Combi-V study has shown that patients with good prognostic factors, i.e. normal LDH, good performance status and single site disease have a 3-year OS of 63% on D+T (339).

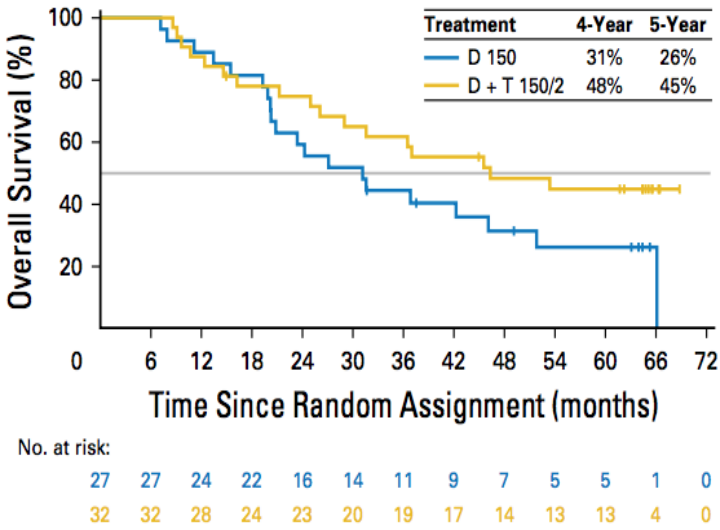

Fig. 6.3. Patients with good prognostic factors have a durable response to BRAFi/MEKi. Kaplan Meier analysis of OS for patients with normal baseline LDH and <3 sites metastasis treated with dabrafenib (D; blue line) vs. dabrafenib plus trametinib (D+T; yellow line) 407.

Therefore, targeted therapy may also be associated with a significant duration of response in selected populations and a plateauing of the Kaplan Meier curve seen with longer follow up (Fig 6.3) (330,339).

Patients with baseline poor prognostic features such as elevated LDH, ECOG PS>0 and visceral disease continue to have inferior outcomes for both treatment modalities (410). It is

clear that further research is required to optimise the scheduling of these treatments in order to improve survival for patients, especially for those with more aggressive disease.

Studies examining combination of targeted and immune therapy are on going (i.e. NCT02967692), however toxicity will potentially be a limiting factor (410). The results of a study examining D+T followed by N+I or N+I followed by D+T in patients with stage III-IV *BRAF* V600 melanoma (i.e. NCT02224781) are awaited. However, this trial switches patients on treatment progression rather than at response to either therapy. An alternative approach is to switch patients when they are responding to targeted therapy as this can result in changes to the tumour and its microenvironment that facilitates immune activation.

6.1.1 Effect of MAPK pathway inhibition on the tumour microenvironment

Pre-clinical data has revealed that BRAFi results in an environment that can enhance immune responses (304,412). Tumours responding to BRAFi have been shown to have increased T cell infiltration, improved T cell recognition of melanoma associated antigens and reduced production of immunosuppressive cytokines (410,412–414). MITF is up-regulated following BRAFi, resulting in increases in the expression of lineage antigens, such as gp100, melan-A, and tyrosinase-related proteins 1 and 2 (410,415). PD-L1 expression has also been shown to increase following 10-14 days of BRAFi therapy, which could enhance the effect of PD-1 inhibitors (211,415).

In addition, a mouse model examining the anti-tumour effect of dabrafenib plus anti-PD-1 with or without trametinib, showed improved responses with the triplet (412,416). Although MEKi have been shown to decrease dendritic cell function and T cell activity (412,417), in the context of treatment with BRAFi they may have an immune enhancing function. This could be due to the prevention of BRAFi induced paradoxical activation of tumour associated macrophages, which impair effector T cell entry into tumours and drive

melanoma cell growth (418). Further investigation as to the mechanisms behind targeted and immune therapy synergy is required.

There is evidence that this immune-promoting picture is lost as the melanoma becomes resistant to targeted therapy. Hugo *et al* analysed tumours from patients who had developed resistance to BRAFi and showed that there were decreased numbers of $CD8^+$ T cells, displaying impaired function and have lost the ability to recognise antigens (310). Tumours that are resistant to MAPK pathway inhibition have decreased expression of MITF and associated suppression of melanocyte-lineage antigen expression (410).

Although further research is required to understand the effects of BRAFi/MEKi on tumour-immune interactions, this initial data suggests that the optimal time for scheduling of immune therapy post targeted therapy is while the tumour remains sensitive to targeted treatment, rather than when the tumour has become resistant. Furthermore, immune therapy has been shown to have better responses in patients with a lower tumour burden and in whom LDH is normal (11,193,195,419). A review by leading experts proposed that high LDH was a key aspect of resistance to immune therapy as it may impair T cell function (420). In mouse models it has been shown that neutralising tumour acidity improves response to immune therapy (421). Lactate dehydrogenase A (LDHA) associated lactate acid production has been shown to impair activation of natural killer cells and T cells (422). Therefore, reducing LDH through targeted therapy before treating with immune therapy could improve responses.

In addition, as discussed in Section 1.10, there is increasing evidence that intermittent schedules or "drug holidays" may delay the onset of resistance to targeted therapy, therefore stopping targeted therapy in response and restarting if there is progression on immune therapy may also prolong response to targeted therapy (165–168). Taken together, these studies suggest that inducing a response with targeted therapy, and then switching to immune therapy when the tumour is still responding could be a promising approach.

6.1.2 Use of circulating tumour DNA to define optimal response

A precise definition of response is required in order to decide upon a switch to immune therapy. A radiological definition of response is currently the standard assessment. However a scan at a fixed time point of 2 or 3 months does not reflect the wide range of response dynamics. The COWBOY trial (NCT02968303) is examining 6 weeks of induction therapy

Patient	Baseline VAF	Lowest VAF achieved on targeted therapy	Maximum VAF decrease (%)	Time to maximal VAF decrease (days)
1	30.5	0	100	13
2	57.6	4.11	92.9	26
3	25.1	1.2	95.2	13
4	58.7	0	100	14
5	5.5	0	100	14
6	13.4	0	100	14
7	14.7	0.3	98	37

Table 6.1 Decrease of VAF of patients on targeted therapy. Prospective longitudinal monitoring of patients on targeted therapy.

with vemurafenib and cobimetinib (BRAFi/MEKi) prior to switching to N+I. However, I felt that more personalised approaches may benefit patients in deciding when to switch treatment. Our data (I obtained samples and isolated plasma, the ddPCR analysis was performed by Dr. Gabriela Gremel), suggested the window of response may be shorter than 6 weeks in some

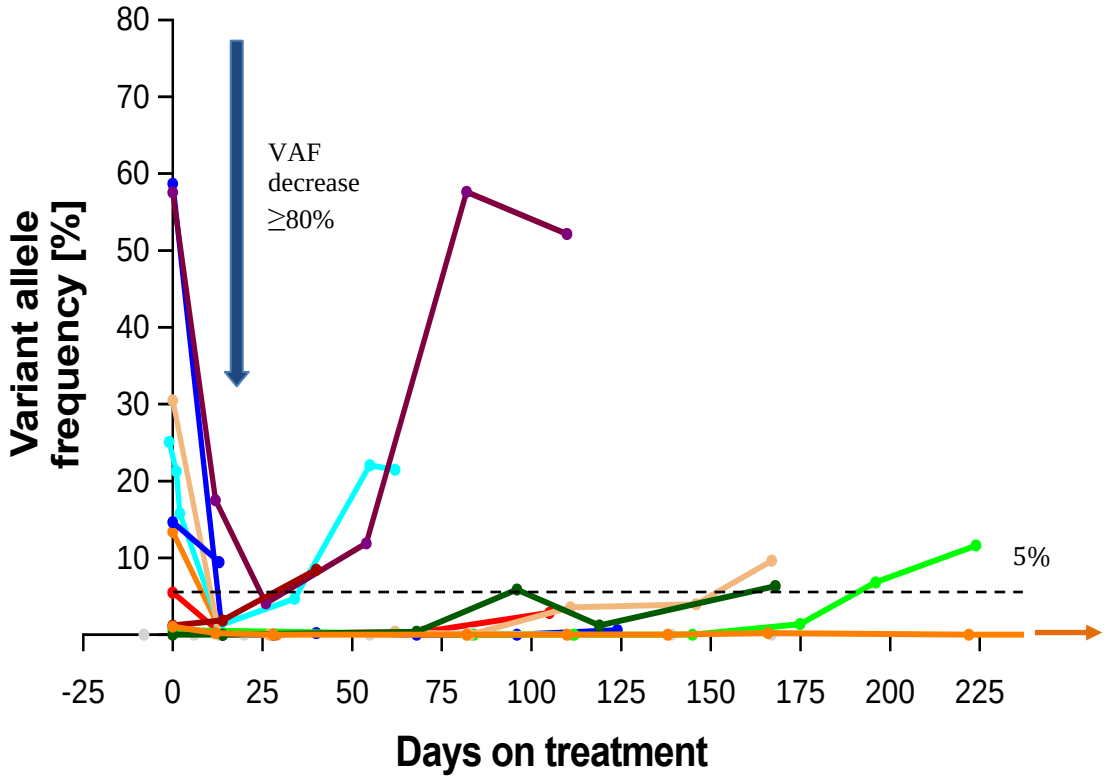

Fig. 6.4 Longitudinal prospective data of mutant *BRAF* VAF ctDNA on first-line dabrafenib. Each coloured line represents an individual patient treated with the BRAFi with the dotted black line showing the 5% exclusion criteria. CtDNA levels rapidly decrease by >80% on targeted therapy and can begin to increase prior to day 90 (3 month standard radiological assessment)

patients with aggressive disease and therefore tailoring treatment to the individual's response is required (Figure 6.4). By following tumour-specific mutations in the blood, we were able to show responses to treatment and detect disease progression at an early stage (423). Other groups have also shown that ctDNA can be used to predict outcome to treatment and follow tumour load over time (264,376). Furthermore, the fraction of mutant ctDNA correlates with LDH; patients with high LDH have higher mutant ctDNA fractions compared to those patients with normal LDH (376). I decided to use ddPCR due to its rapidity, its reproducibility and accuracy based on our data, and its low cost compared to NGS, which will be important for the trial and for general clinical use. Application of ddPCR to quantify *BRAF* mutant ctDNA levels

enables monitoring of tumour burden every 2 weeks to be efficiently performed, in order to achieve an accurate and dynamic view of treatment response.

6.2 CAcTUS Trial overall design and rationale

CAcTUS is a parallel arm, biomarker driven trial of sequential combination D+T therapy followed by the combination of N+I. Patients (n=40) are randomised 1:1 between a standard arm (Arm A) with combination targeted therapy (D+T) followed by combination immune therapy (N+I) upon progression vs. treating with targeted therapy until response as defined by ctDNA levels (Arm B), and switching to immune therapy (See trial schema 6.4.2). If patients progress on immune therapy in Arm B, they will switch back to D+T therapy as resistance will not have developed to the treatment. I decided on the ctDNA delta cut off of ≥80% based on our prospective longitudinal data using ddPCR (see Fig. 6.4. and Table 6.1.), which shows that the majority of patients (including patients with very aggressive disease) treated first-line with a BRAFi alone will achieve at least an 80% reduction in VAF of *BRAF* early (within 1 month) in treatment. This is likely to be enhanced in patients treated with D+T as deeper responses have been achieved compared to BRAFi alone (9).

Although using a different technique, data from Santiago-Walker *et al* suggests that approximately 30% of patients with a *BRAF* V600E mutation will have a VAF of ≥5% at start of treatment and these are likely to have a shorter PFS in response to D+T (390). Therefore I expect a third of patients with *BRAF* mutant melanoma would be eligible for this study using a VAF inclusion criteria cut off of ≥5%. Selecting patients based on this cut off will select patients with poor prognosis, in which this approach may have the greatest benefit due to their high disease burden and where the readout will be quickest. Nonetheless, to determine whether a lower threshold should be used, I will also follow the ctDNA levels in the standard arm to examine the decrease in *BRAF* VAF achieved for patients undergoing treatment with D+T.

Patients will switch treatment within 10 days of ctDNA decrease by 80%. If patients do not achieve an 80% decrease they will remain on targeted therapy and switch on relapse, which is likely to be rapid according to our clinical experience.

In addition to optimising the VAF cut off for optimal response and inclusion criteria, CAcTUS has logistical targets in terms of reporting of ctDNA results in a timely manner to allow treatment decisions to be made. The pilot study will provide the opportunity to establish a stringent pipeline, which will be used for the larger expansion phase. Once the initial study has been conducted and the initial results analysed, I plan to have an expansion phase leading into a Phase III study, which will be randomised with power for PFS and OS, determined by the results of the initial study and utilising the optimised VAF cut off.

6.3. Trial Schema

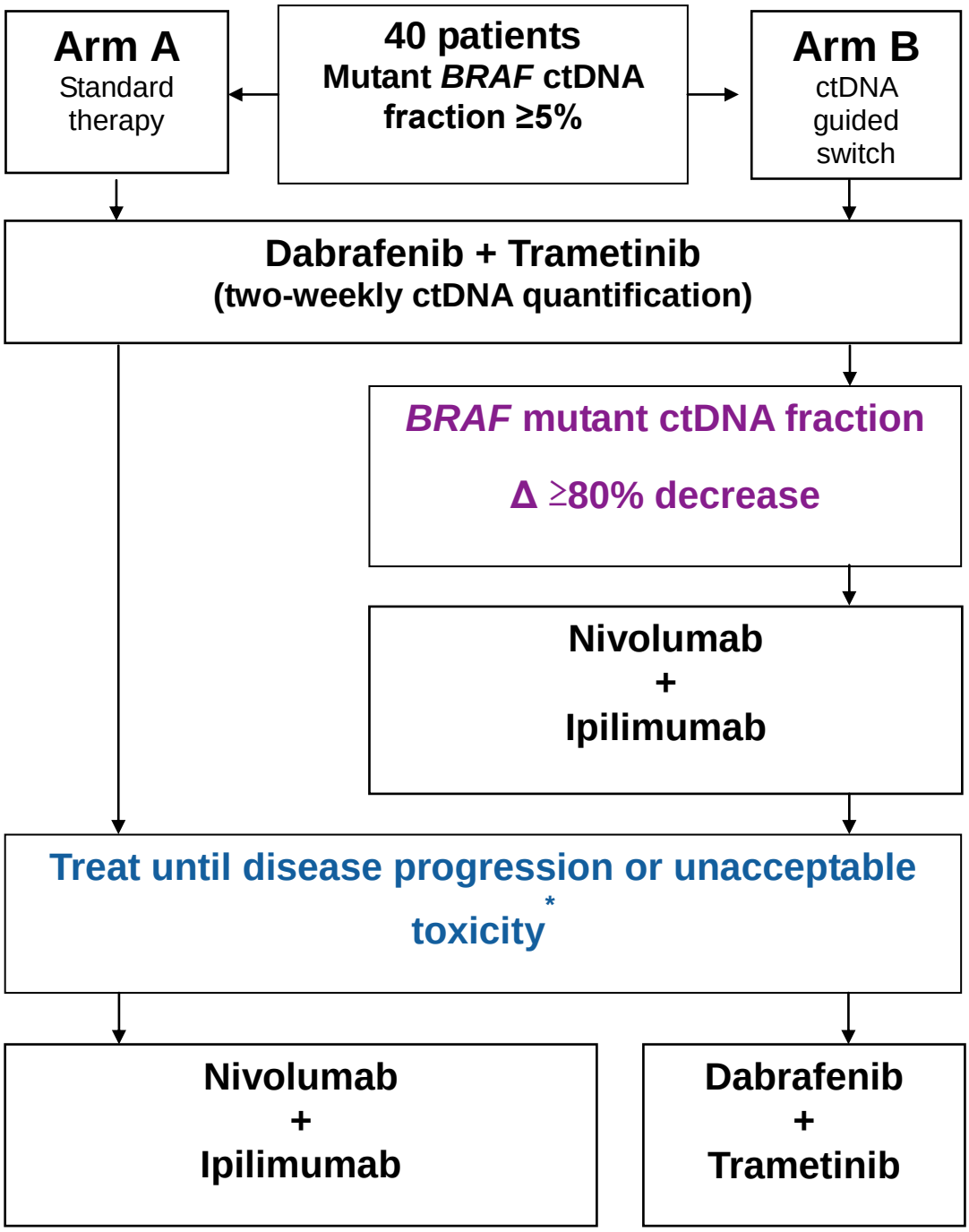

*If toxicity in the immune therapy arm, reassess response and switch to dabrafenib + trametinib only if confirmed disease progression.

Fig. 6.5 CAcTUS trial schema

6.4 CAcTUS Hypothesis

1. Changes in ctDNA levels can be used to accurately inform when to switch from targeted to immune therapy.
2. In *BRAF* mutant melanoma the efficacy of immune therapy is enhanced by response to pre-treatment with MAPK pathway inhibition (D+T).

6.5 CAcTUS Endpoints

6.5.1 Primary endpoint

- PFS at 12 months (54 weeks to allow for permitted window)

6.5.2 Secondary endpoints

- First PFS (PFS curve)
- Second PFS (PFS curve)
- OS (OS curve)
- Best ORR to immune therapy
- Duration of response to immune therapy
- PFS on immune therapy from date of commencement of immune therapy

6.5.3 Exploratory endpoints

- Number of screen failures due to mutant *BRAF* VAF <5%
- Assess whether a decrease in ctDNA levels of mutant *BRAF* by ≥80% on targeted therapy is an appropriate cut off for switching to immune therapy. Success will be demonstrated if ≥90% of the patients achieve ≥80% mutant *BRAF* VAF decrease in both arms
- Time taken for mutant *BRAF* VAF to reach ≥80% decrease on targeted therapy
- Duration of mutant *BRAF* VAF response in both arms to targeted and immune therapy
- To determine level of ctDNA rise that corresponds with ctDNA progression and relapse on treatment and to therefore compare time to ctDNA progression in both study arms
- Increase in VAF during washout period from targeted to immune therapy switch in arm B
- Time between observing rise in mutant *BRAF* VAF and scheduled scan result

- Correlation of ctDNA progression with RECIST progression measured by CT/dual phase MRI scan (TTP of ctDNA versus TTP on RECIST)

6.6 CAcTUS arms and patient flow

6.6.1 Screening

Blood will be taken at the screening visit in order to determine the *BRAF* VAF in plasma ctDNA. Patients with lower disease burden and no clinical need to start D+T straight away will wait for the ctDNA result (5 days + time for the blood to arrive in the laboratory estimated at maximum 8 days). If the *BRAF* ctDNA VAF is ≥5% then the patient will be consented to the study and randomised, however if ctDNA VAF is <5% they will not enter on to the study. In patients where there is rapid disease progression or the patient does not wish to delay start of D+T until the ctDNA result is confirmed, then immediate commencement of D+T is permitted on the day of screening. I allowed this in order to be able to include these patients in the study, as often they would get excluded from clinical trials. The ctDNA result and patient randomisation must occur prior to the next scheduled visit (2 weeks after start of D+T) for the patient to be eligible for the study. If the *BRAF* ctDNA VAF is ≥5% then the patient will be consented to the study and randomised, however if ctDNA VAF is <5% they will not enter onto the study.

6.6.2 Randomisation and treatment arms

Forty patients will be randomised 1:1 to either treatment arm using minimisation with a random element controlling for LDH (<upper limit of normal (ULN) vs. ≥ULN), disease site (<3 sites vs. ≥3 sites), *BRAF* ctDNA VAF (5 to ≤10%, >10 to ≤20%, >20%) and metastasis stage (M1a, M1b, M1c). Patients will be randomised to either Arm A (Standard arm) or Arm B (ctDNA guided switch). Treatment will be as follows:

ARM A Standard arm: Dabrafenib 150mg twice daily with trametinib 2mg once daily. On disease progression or unacceptable toxicity, washout of 7 days for D+T to stop the day before commencement of N+I. Then switch to nivolumab 1 mg/kg administered as an intravenous infusion over 60 minutes every 3 weeks for the first 4 doses in combination with 3 mg/kg ipilimumab administered intravenously over 90 minutes. Then followed by a second phase in which 3 mg/kg nivolumab is administered as an intravenous infusion over 60 minutes every 2 weeks until disease progression or unacceptable toxicity.

ARM B ctDNA guided switch: Dabrafenib 150mg twice daily with trametinib 2mg once daily. Following decrease of mutant *BRAF* VAF by 80% or more, trametinib will be stopped for 7 days with dabrafenib continuing until the day before switching treatment. A CT scan/ dual phase MRI scan will be performed in order to correlate radiological imaging with ctDNA response (additional blood test taken on day of imaging). The patient will then commence nivolumab 1 mg/kg administered as an intravenous infusion over 60 minutes every 3 weeks for the first 4 doses in combination with 3 mg/kg ipilimumab administered intravenously over 90 minutes. Then followed by a second phase in which 3 mg/kg nivolumab is administered as an intravenous infusion over 60 minutes every 2 weeks. If there is disease progression as per RECIST 1.1, then patients will switch back to dabrafenib 150mg twice daily with trametinib 2mg once daily. If patients develop unacceptable toxicity then disease will be re-assessed and if there is disease progression, patients will switch back to D+T.

6.7 CAcTUS Inclusion/Exclusion criteria

See Appendix 20 for inclusion/exclusion criteria.

6.8 CAcTUS Statistical considerations

As this is an initial proof of concept pilot study, I did not power it to detect a specified difference between the trial arms. The aim of this pilot study is to explore whether a decrease in *BRAF* VAF in ctDNA of ≥80% is a promising trigger for a switch from targeted to immune therapy. PFS at one year (first progression) will be derived from the Kaplan Meier estimate. This will help inform sample size calculations to detect a plausible difference in PFS at one year in a future study. PFS will be measured from the date of randomisation into the study until the first date of either death or confirmed progressive disease according to RECIST v1.1.

Furthermore, the Kaplan Meier method will be used to construct survival curves for PFS, PFS on immune therapy and OS in both arms. Cox proportional hazards models adjusting for LDH, disease site, metastasis stage and baseline *BRAF* ctDNA VAF, will be used to obtain HR and 95% CIs – the emphasis being on estimation rather than significance testing. PFS on immune therapy will be measured from the date of commencement of N+I until the first date of either death or confirmed progressive disease following treatment with N+I. From the date of randomization, OS times will be measured until the date of death due to any cause or date last contacted if still alive. Time to their last observation will be used if a patient has not died and the survival time for the patient will be considered censored.

Best ORR of a patient will be defined as the best tumour response that is achieved during immune therapy or within 30 days of any termination of immune therapy due to toxicity that is confirmed according to RECIST v1.1. The difference between treatment arms in the proportion of patients with a CR or PR will be summarised along with the 95% CI. Duration of response will be measured from the time of initial response (CR/PR) until tumour progression and estimated using the Kaplan Meier method.

6.9 DETECTION Rationale

Studies to identify the clinical features that are most likely to predict a benefit for either immune or targeted treatment consistently show low tumour burden and good PS to be among the most powerful indicators (424). As previously discussed I felt that patients with stage II disease were the most appropriate group to target in such a strategy.

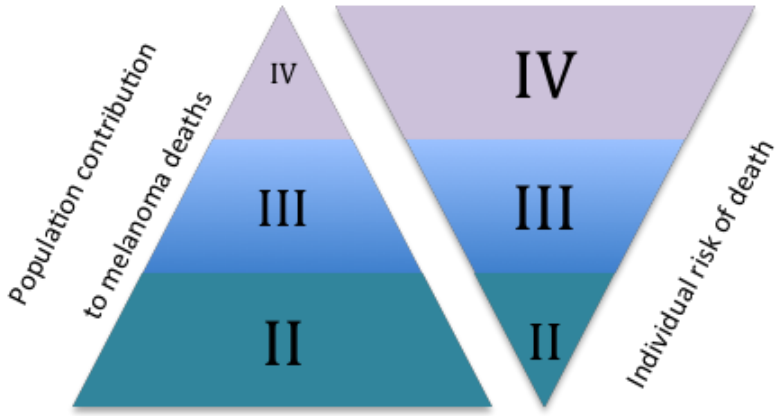

Fig. 6.6 The low risk paradox. The individual risk of death increases with stage, however at a population level the numbers of patients dying from melanoma is highest for those presenting with stage II disease.

6.9.1 Rationale for early treatment of Stage II disease

Recently, four trials (NCT00636168, NCT02388906, NCT02362594, NCT01682083) investigating adjuvant immune or targeted therapy in high-risk resected Stage III melanoma have reported significant benefits in terms of RFS and/or OS. Together, these studies show that treatment of micro-metastatic disease results in improved outcomes for patients with high-risk stage III melanoma.

Presentation	Equivalent stage	Incidence proportion (%)	Mortality proportion (%)
Primary 0.01-1mm thickness	I	68	22.7
Primary 1.01-2.00mm thickness	I and II*	13.6	20.8
Primary 2.01-4.00 thickness	II	8	20.4
Primary >4.00 mm thickness	II	4.7	14.2
Metastasis	III and IV	2.8	15.9
Unknown	-	2.8	6

Table 6.2 Melanoma incidence and survival according to tumour thickness in Queensland 2005-2009 (Whiteman *et al.*) *dependent on ulceration

For Stage II disease, whilst the individual risk of recurrence is low, these patients account for >50% of all those who subsequently develop metastatic disease and die. This is the low risk paradox. The incidence of stage II melanoma is significantly higher than later stages (Fig. 6.6, Table 6.2), which results in a higher overall burden of mortality. Identifying an effective and economical adjuvant treatment in stage II disease is therefore an important and significant challenge. Treating all patients with expensive and potentially toxic treatments is unrealistic. A tool is needed to enable accurate prediction of the important minority of patients who will progress to stage IV disease and may therefore benefit from early therapy, and separate them from the majority of patients cured by surgery alone.

6.9.2 Current standard of care follow up in stage II disease

Current guidelines regarding follow up of stage II disease recognise the heterogeneous prognosis within the group. Patients with stage IIA and IIB are monitored with clinical examination only, every three months during years 1-3, then every six months in years 4-5, and annually thereafter. Patients with stage IIC disease have cross-sectional imaging (CT or PET CT + MRI brain scan every six months years 1-3 and annually thereafter, in addition to clinical follow up. The role of imaging in stage IIB disease is less clear and practice varies internationally (425,426). DETECTION will focus on the higher risk stage IIB and stage IIC patients as stage IIA have extremely low risk of recurrence (5 year survival 93%) (4). One of the main aims of DETECTION is to show that ctDNA testing identifies melanoma relapse earlier than current standard of care follow-up.

6.9.3 Circulating tumour DNA as a biomarker of disease progression and activity

Somatic mutations in ctDNA are extremely specific to cancer because they are based on driver gene mutations expected to be found only in abnormal clonal proliferations of cells (392). A recent study using an approach "CancerSEEK" that tested for mutations in ctDNA and high levels of cancer associated proteins demonstrated the high specificity of ctDNA with only 7/812 healthy individuals scoring positive (392). CtDNA is a biomarker of disease progression in many cancers and increasing VAF amounts are associated with increasing stage or tumour burden (245,255). Furthermore, higher levels of ctDNA are consistently associated with poor prognosis and decreased response to targeted and immune therapy (263,376), suggesting that treatment at lower VAF levels might improve response.

6.9.4 Rationale for early detection of cancer relapse using ctDNA

Detection of ctDNA in plasma after completion of apparently curative treatment, either at a single post-surgical time point or with serial follow up plasma samples, has predicted metastatic relapse with high accuracy in breast, lung and colon cancers (383,427,428). In breast cancer, longitudinal monitoring of ctDNA was able to detect breast cancer relapse with a median of 7.9 months (range 0.03 to 13.6 months) lead-time over clinical relapse in 55 patients receiving neoadjuvant chemotherapy (383). Furthermore, ctDNA identified recurrence a median 167 days (interquartile range 81-279) prior to radiological recurrence following surgery for stage II colorectal cancer in 9 patients (384). This was significantly longer (P=0.04) than the time between serum carcinoembryonic antigen elevation (a serological glycoprotein marker of colorectal cancer) and radiological recurrence (median 61 days; interquartile range 81-279 days) (384). Finally, the $TRACER_X$ lung cancer study showed that in 13 patients the median interval between ctDNA detection and non small cell lung cancer (NSCLC) relapse

confirmed by CT imaging indicated by clinical and chest radiograph follow-up was 70 days (range, 10–346 days) (428).

6.9.5 Rationale for early detection of melanoma relapse using ctDNA

A number of groups including our own (Girotti, Gremel *et al*, I contributed sample collection, plasma extraction and clinical data for the ctDNA part of the study) have shown that ctDNA can be used to track melanoma burden in the setting of stage IV disease (136,270,376,429,430). The data in chapter 5 provided the proof of principle that ctDNA could detect MRD following curative intent surgery for melanoma.

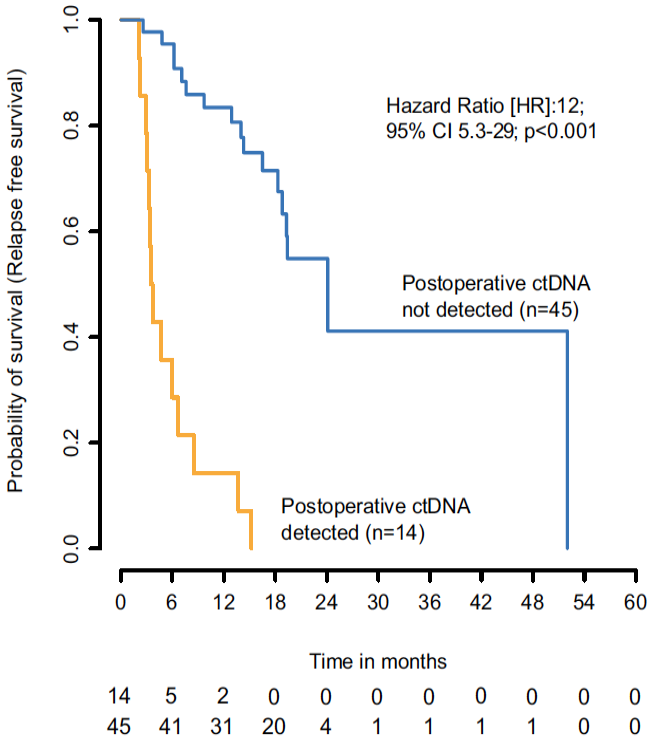

Fig. 6.7 Detection of ctDNA is associated with decreased RFS in Melbourne prospective cohort. Plasma taken within 12 weeks of surgery and patients prospectively monitored for relapse using *BRAF*, *NRAS* or *TERT* promoter mutations.

Following on from this study, I collaborated with the Skin/Melanoma unit and Prof. Sarah Jane Dawson's laboratory at the Peter MacCallum Cancer Centre, Melbourne, Australia to validate my findings in two prospective cohorts (Manchester and Melbourne) and to provide data on longitudinal ctDNA monitoring. Crucially, the analyses performed in two different laboratories are consistent with ctDNA being a sensitive biomarker of melanoma relapse before symptoms appear (Fig. 6.7, chapter 5). Longitudinal monitoring can also identify disease at an early timepoint, one example of which

is a patient with stage IIC melanoma with ctDNA detected both pre- and post-surgical (Fig. 6.7), signifying MRD and the patient relapsed 5 months later (data from Prof. Sarah Jane Dawson's laboratory). Taken together, these data suggest that ctDNA is a measure of micro-metastatic disease activity and is a powerful tool to identify MRD or early "molecular" relapse not detected by imaging.

I therefore designed a study in patients with stage IIB/C melanoma comparing longitudinal monitoring and early treatment upon detection of *BRAF* mutations in ctDNA with clinical/radiological monitoring (current standard of care (425,426)). The assay focuses on driver mutations in the *BRAF* gene that are well characterised in melanoma and has been reproducibly detected at all stages of disease. In addition, a *BRAF* mutation predicts response to BRAFi/MEKi with a disease control rate of 92% seen in the Phase III registration study of E+B in metastatic disease (118).

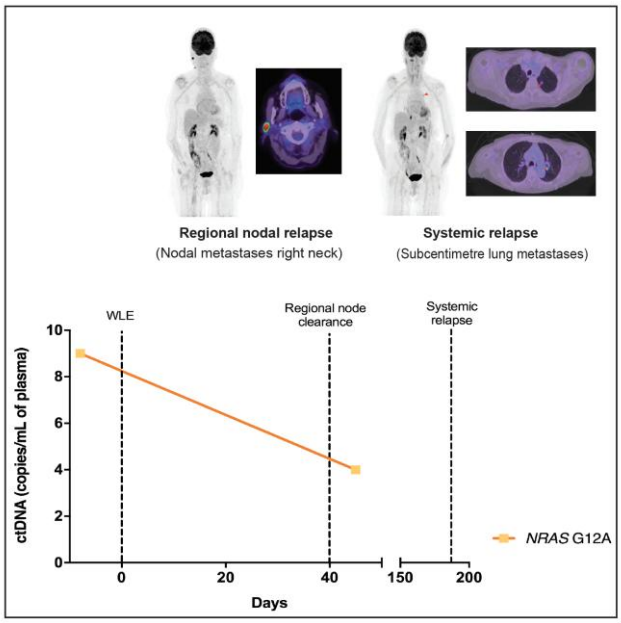

Fig. 6.8 Longitudinal monitoring of stage IIC patient. Patient PMC1052 with stage IIC *NRAS* mutant melanoma with a primary right temple melanoma proceeded to a wide local excision and had a negative sentinel lymph node biopsy. Baseline (pre-surgery) ctDNA was positive and the patient later developed regional nodal relapse as evident on ^{18}FDG-PET. The patient proceeded to regional node clearance and a post-operative ctDNA remained elevated signifying residual disease. This patient later developed systemic relapse 5 months later with small volume bilateral lung metastases as detected on ^{18}FDG-PET scan. The patient was started on immune

6.10 DETECTION overall design and rationale

The design resembles OV05, which was a trial investigating whether early second line treatment of ovarian cancer would improve survival (431). The trial randomised patients to early treatment based on rising cancer antigen 125 (CA125) compared with delayed treatment based on clinical/radiological relapse (431). The study did not show any benefit for early treatment based on rising CA125 (431), however this may have been due to the second line treatment (chemotherapy) having a very similar mechanism of action to the first line treatment and therefore its degree of benefit being marginal. DETECTION is examining early treatment with first line systemic therapy and therefore the context is different, which may increase the likelihood of early treatment improving outcomes.

I designed DETECTION as a Phase III open label, multicentre trial of early vs. delayed treatment of melanoma relapse based on detection of *BRAF* mutant ctDNA, with interim analyses incorporated to enable a stop/go decision and early signal of efficacy. Patients with stage IIB/C melanoma (n=930) will have longitudinal blood sampling to identify the presence of ctDNA. Patients with ctDNA detected will be randomised 1:1 to either Arm A, which is standard of care follow up and treatment on evidence of radiological/clinical progression with patients and the clinical team blinded to the ctDNA result, or Arm B which is unmasking of the patient and team to the ctDNA result and early treatment with BRAFi/MEKi combination therapy (E+B).

6.11 Trial Schema

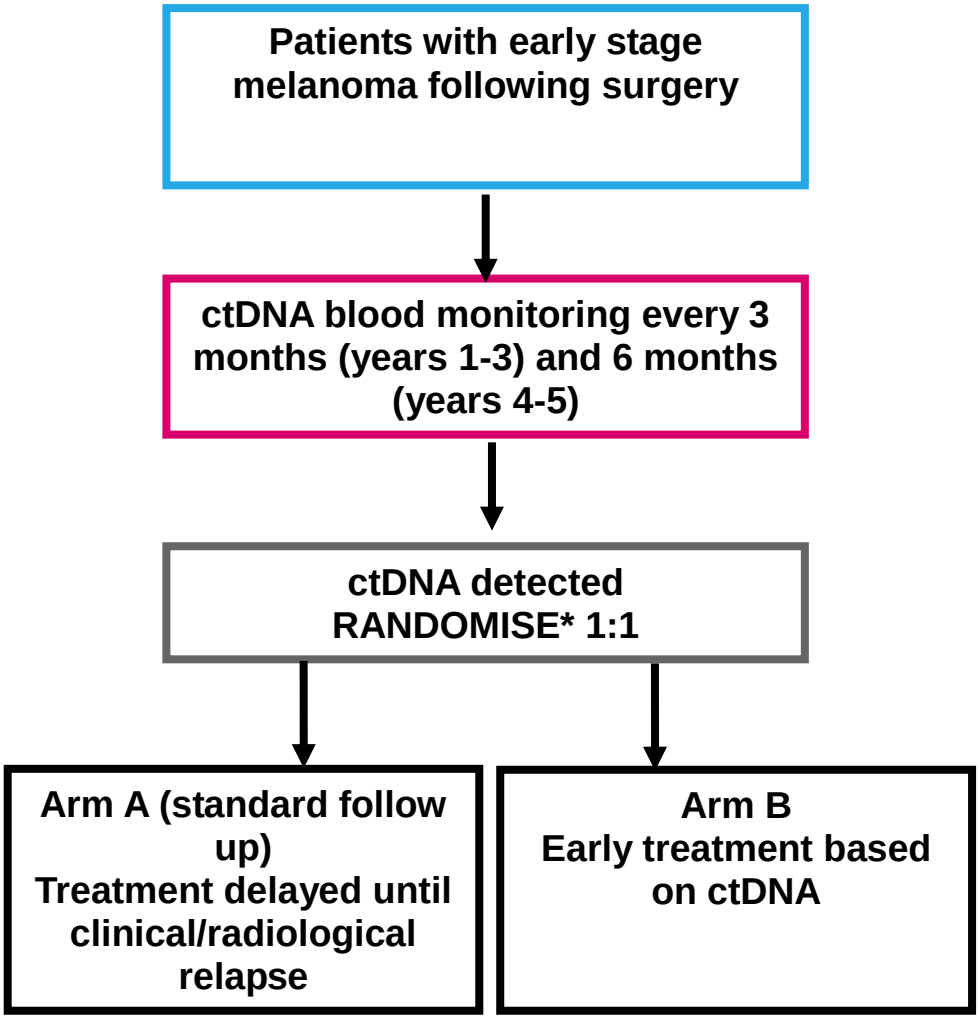

*Randomised centrally, treating clinician and patient blinded to positive result in Arm A and will continue follow up with on-going ctDNA monitoring. Arm B will be unmasked to start early treatment.

Fig. 6.9 DETECTION trial schema

6.12 DETECTION Hypothesis

- CtDNA can be used to detect both MRD following curative intent surgery and early disease relapse (molecular relapse)
- Early treatment of MRD following curative intent surgery/early disease recurrence identified by ctDNA results in improved outcomes for patients with stage IIB/C melanoma

6.13 DETECTION Aims

The primary aims of the study are to assess whether outcomes can be improved in stage IIB/C patients with *BRAF* positive, resected melanoma through:

1. Early identification of MRD following curative intent surgery or identification of micro-metastatic progression by ctDNA (molecular relapse) during longitudinal monitoring.

2. Testing whether ctDNA monitoring can identify MRD/relapse earlier than current standard of care follow up.

3. Early treatment of disease based on detectable ctDNA

6.14 DETECTION analyses and endpoints

Due to the trial targeting a relatively low risk population of patients and the huge change in prognosis of patients with stage IV melanoma, it will take a long time to accrue sufficient OS events. Therefore I have built in analyses to provide an early signal that the hypothesis may be confirmed (Fig. 6.10).

Three primary analyses will be performed:

1. Interim analysis stop/go decision pooled RFS rate (Arm A + Arm B)

2. Interim analysis RFS

3. Final analysis OS

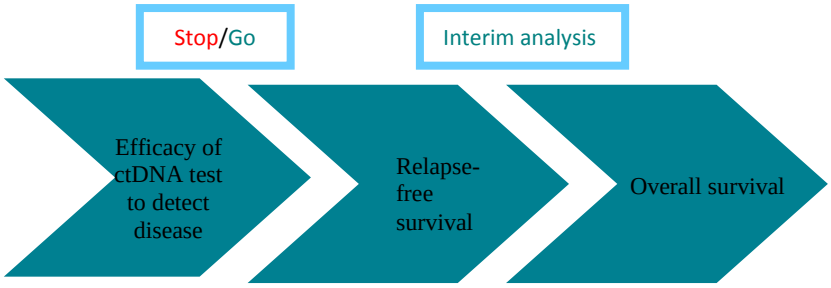

Fig. 6.10 Phase III design with interim stop/go analyses.

In addition, the stop/go decision for the trial to continue or close due to futility tests whether the ctDNA assay is able to detect melanoma relapse significantly earlier than standard of care follow up. If positive, the study will proceed, however if negative the trial will close due to futility. Patients will continue to be accrued during the interim stop/go analysis in order to reduce the trial duration. A second interim analysis will be performed to examine RFS; the time from randomisation to any recurrence (local or regional, or distant) or death from any cause. This has been shown to be a good surrogate of OS in both the adjuvant and metastatic melanoma studies to date. It will provide an earlier signal as to patient benefit through investigating whether relapse can be delayed through early treatment based on ctDNA. The final analysis will definitively test whether early treatment based on detection of ctDNA improves survival for patients with stage IIB/C melanoma. At each stage of analysis, secondary endpoints will also be assessed.

6.14.1 Interim analysis stop/go decision pooled RFS rate (Arm A + Arm B)

A necessary condition of the study is that ctDNA can be detected prior to a patients being diagnosed with clinical disease recurrence, with an estimated lead-time between molecular and clinical relapse of greater than or equal to 3 months. To demonstrate that ctDNA can be detected before clinical evidence of disease, a stop/go decision will be made after the 50th patient has had 3 months follow up following ctDNA detection (performed at around 33 months). An assessment on the 3 months RFS rate shall be made with a median RFS rate ≥3

months required for the study to continue. If a difference in median RFS of <3 months between molecular and clinical relapse is observed, the study will be suspended to recruitment.

6.14.2 Interim analysis Relapse-free survival

An interim analysis to assess RFS will be performed after 100 events of RFS in Arm A (standard follow up and treatment delayed until clinical/radiological progression) compared to Arm B (early treatment based on detectable ctDNA). Through investigating whether relapse can be delayed through early treatment based on ctDNA, it will provide a signal as to patient benefit. RFS has been a good surrogate endpoint of OS in phase III adjuvant and metastatic studies (432).

6.14.3 Final analysis primary endpoint

Overall survival defined as time from randomisation until death from any cause in Arm A (standard follow up and treatment delayed until clinical/radiological progression) compared to Arm B (early treatment based on detectable ctDNA). It is expected that the analysis will be performed at approximately 108 months.

6.14.4 Secondary Endpoints

- Time from randomisation to evidence of disease progression on first therapy (Arm A vs. Arm B)
- RFS, DMFS and OS of patients with undetectable ctDNA (i.e. do not get randomised)
- DMFS Arm A vs. Arm B
- PFS and response rate to first line early vs. late systemic treatment (Arm A vs. Arm B)

    - clinical or radiological assessment (CR or PD both arms and in addition PR in Arm A)
    - molecular assessment (translational endpoint- response and PD criteria will be analysed within trial)
- Outcomes in both Arm A and Arm B (RFS/DMFS/OS) for patients with detectable ctDNA at first blood draw within 12 weeks of curative intent surgery (baseline) vs. subsequent blood draws
- Time to ctDNA detection from entry into trial (baseline blood)
- Time to molecular relapse vs. time to radiological/clinical progression (Arm A only)
- Detectable ctDNA at 12 and 18 months following randomisation Arm A vs. Arm B
- Evaluate the number of patients with disease on PET/CT scan at time of first ctDNA detection
- Evaluate the number of patients with undetectable ctDNA, but clinical/radiological progression
- To assess the overall safety and tolerability of therapy
- Testing of standard operating procedures for assay and roll out to multiple laboratories
- Defining criteria for molecular relapse
- Health economic assessment of treating all patients upfront vs. treatment on molecular relapse vs. treating on clinical/radiological progression
- Patient acceptability of treating based on ctDNA detection of micro-metastatic disease

6.15 Randomisation and treatment arms

Following ctDNA detection, patients will be randomised 1:1 and stratified according to disease stage and whether ctDNA is detected on first blood draw vs. on subsequent blood

draws. My data showed that patients with ctDNA detected within 12 weeks of curative intent surgery are a poor prognostic group. Stratification will therefore enable me to analyse the impact of treatment on their outcomes

6.15.1 Experimental arms

Following consent, patients will have blood taken for ctDNA at baseline within 12 weeks of surgery and at clinic visits every 3 months from consent (+/- 1 week) during years 1-3 (+/- 1 week), followed by every 6 months in years 4-5, and annually thereafter. Samples will be analysed in real time with results validated by quality assurance within 10 days of blood draw. All patients will have bi-annual CT scans (+/- 1 week) in years 1-3 and annually to year 5 unless there is a clinical indication for earlier scan. Both the scanning schedule and blood draw schedule will be adhered to strictly to ensure no lead-time bias in either arm.

Both the ctDNA analysis and randomisation will be performed independently of the recruiting site in order to keep the treating team and patient blinded to the ctDNA result. If ctDNA is detected, patients will be randomised 1:1 to:

Arm A – Delayed treatment until clinical/radiological progression (Current standard of care). The patients will continue follow up as per current UK guidelines (425,426). The patient and treating clinician will not be informed that the randomisation has taken place in order to continue to be blinded to the ctDNA result. By keeping both the treating team and patient blind to the ctDNA test results, the study aims to avoid unnecessary anxiety and earlier than planned imaging. Blood samples for ctDNA analysis will continue to be taken at every clinic visit (every 3 months (years 1-3), then every 6 months (years 4-5) and annually (years 5+)). Follow up will continue until 3 years after the last patient is enrolled on to the study, with scans performed bi-annually CT scans (+/- 1 week) in years 1-3 and annually to year 5. Patients

who develop disease recurrence will be treated as per standard of care current at the time and will switch to 3 monthly scans.

Arm B – Early treatment based on detectable ctDNA. The treating clinician will be informed of the result and the patient brought to clinic to discuss the result, confirm on going consent and have a repeat of ctDNA blood test to confirm presence of ctDNA (see section 6.17). The turnaround of this result from blood draw to clinical team receiving the result will be <7 days, and will have already been validated as a realistic target time in the CAcTUS trial. If detectable ctDNA is not confirmed, a further test will be taken (see section 6.17) and if this remains negative the patient will continue follow up outside of the study, however ctDNA testing for one year will be offered unblinded to provide reassurance. The patient would then commence treatment with encorafenib 450mg once daily + binimetinib 45mg twice daily treated for 2 years or until unacceptable toxicity, disease progression or patient choice. At the 2-year time point if ctDNA is still detected patients will continue on drug. Scans will be performed every 3 months until treatment is discontinued, in line with standard of care treatment of patients on active therapy. Follow up will continue until 3 years after the last patient is enrolled on to the study.

6.16 CtDNA assay

The assays used in the trial will test for the presence of *BRAF* mutations in p.V600E, p.V600R, p.V600D and p.V600K, which are known to arise from driver mutations in melanoma and respond to BRAFi/MEKi (114,341,433). I previously tested these assays in chapter 5.

6.16.1.Sensitivity and specificity of the test

The key factors in determining the clinical sensitivity in terms of detecting relapse are:

1. The assay sensitivity
2. The volume of blood taken
3. The tumour burden/activity in the patient of disease present at that timepoint

6.16.2 Assay sensitivity

According to the manufacturer (Biorad, Watford UK), sensitivity of the test is 0.001% mutant fraction, which is dependent on the number of droplets generated with a copy of DNA present (434). In the AVAST-M study of 161 patients, for 2ml of plasma I generated an average of 3000 droplets with either a wild type or mutant copy present. In the Manchester prospective study due to the amount of input DNA (see chapter 5, which was based on the protocol sent from Prof. Sarah Jane Dawson's laboratory), I generated 2000 droplets with a copy of DNA present. This resulted in a sensitivity of 0.05-0.03%. DETECTION will use 20ml of plasma, which, assuming the number of droplets generated will increase proportionally, the sensitivity improves by a factor of 10 to approx. 0.005% due to the increase in input DNA.

6.16.3 Improvement of test clinical sensitivity with increased plasma volume and prospective analysis

My retrospective research was performed at one time point only, in 2ml of plasma taken within 12 weeks of surgery, which had been stored for a long period, potentially resulting in degradation of DNA over time and this likely contributed to a sensitivity for predicting relapse

of 18%. Despite the criteria for the prospective study being stricter (requiring two reactions vs. one to be positive to call the ctDNA detectable) and the DNA input lower than in the retrospective study, our prospective cohorts showed higher sensitivity at a single time point post surgery (see table 6.3). To improve the sensitivity further I have stipulated that much larger volumes of plasma will be used in the trial, which will increase the likelihood of picking up mutant DNA if present and will not affect specificity. Crucially, I was able to identify relapse prior to CT scan using ctDNA in 71% patients in my post surgery and prospective longitudinal sampling in Manchester and similar clinical/radiological follow up to the trial's follow up protocol. The median time between detectable ctDNA and radiologically identified disease recurrence was 12.1 months.

Cohort	Sensitivity for predicting relapse	Specificity for predicting relapse	Positive predictive value	Negative predictive value
AVAST-M retrospective post surgery single time point n=161 patients	18%	95%	79%	51%
Melbourne prospective post surgery single time point n=59 patients	45%	100%	100%	53%
Manchester prospective post surgery single time point n=21 patients	71%	89%	83%	80%

Table 6.3. Sensitivity, specificity, positive and negative predictive value of detectable ctDNA predicting relapse in plasma samples taken within 12 weeks of surgery.

6.16.4 Specificity

The test is very specific as only mutations present in *BRAF* mutant clonal populations found in melanoma are identified. Although moles can have *BRAF* mutant mutations, unlike cancer they do not have the necrosis and high cell turnover, which contributes to ctDNA production and therefore healthy volunteers with moles have not been shown to have mutant cfDNA. In our retrospective study, specificity at the post-surgical timepoint taken within 12

weeks of surgery was 95%, the Melbourne prospective cohort 100% (Table 6.3) and my prospective Manchester cohort 89% (one patient has detectable ctDNA in all longitudinal samples, with no obvious melanoma progression but an equivocal lymph node on CT scan, which is currently being investigated). In 60 droplet digital reactions of cfDNA isolated from 30 healthy volunteers, I did not observe any mutant droplets.

6.17 Definition of detectable ctDNA MRD/molecular relapse and real-time decision-making

Detectable ctDNA is defined as 1 mutant *BRAF* copy/20ml plasma (equivalent to 40ml of blood/4 tubes) by ddPCR. Patients will be randomised on the basis of this result, however in order to reduce false positives, if ctDNA is detected, a second blood test will be performed

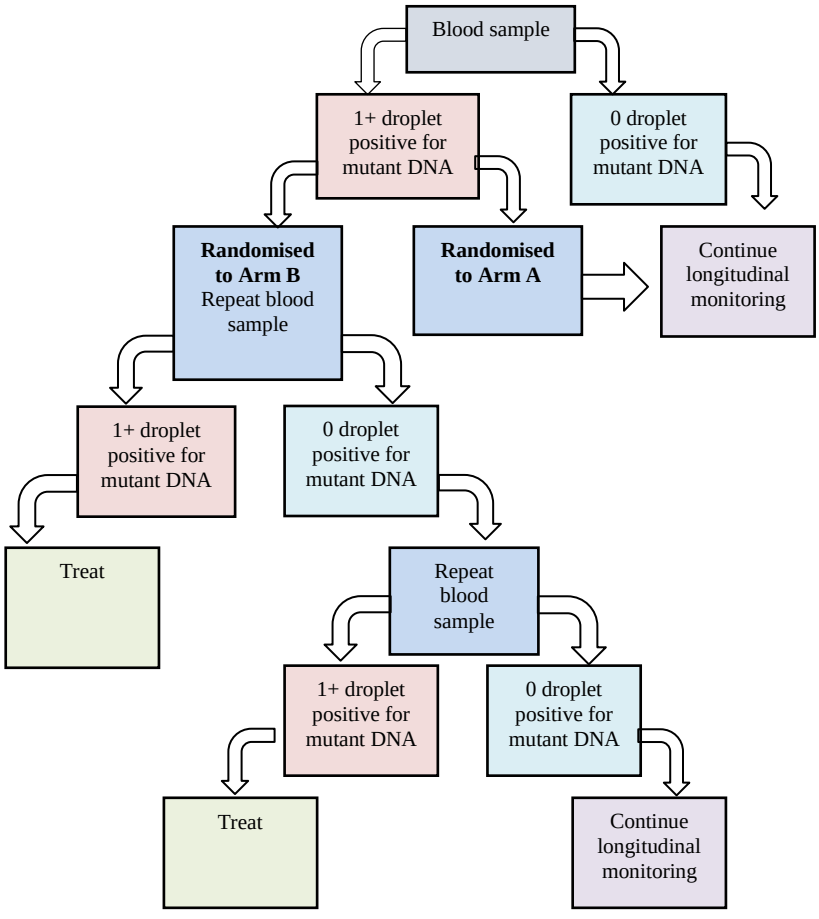

Fig 6.11. Decision tree to determine treatment course if ctDNA detected

following randomisation to confirm the result before treatment (Fig 6.11). If the second blood test is negative, a third test will be performed and treatment commenced if positive or the patient will continue further monitoring if negative (Fig 6.11). At the time of interim stop/go analysis we will decide whether repeat blood tests are required for the on-going study. For the purposes of secondary endpoints, the first positive blood result will define time to molecular relapse.

6.18 Process of result reporting

Bloods will be taken in Streck tubes (stabilises ctDNA for up to 14 days) at the patient's appointment with the clinical team with a pre-specified 96 hour window between the blood being taken and plasma extraction. The patient will be assigned a unique de-identified number to ensure the laboratory does not receive any patient identifiable information. Bloods will be posted to the Clinical & Experimental Pharmacology laboratory (CEP) using the Royal Mail Safebox system^{TM}, which has been reliably used for a number of clinical trials. The sample will be processed, quality assured and the result reported to the Liverpool clinical trials unit. If ctDNA is detected the patient will be randomised 1:1.

If the patient is randomised to Arm B, the result will be reported to the clinical team via a secure results portal and email to the principal investigator/research nurse who will telephone the patient to attend the next available clinic (within 1 week). The patient will have a repeat blood test and consent will be confirmed to commence treatment. Repeat tests will be fast-tracked. The results of the second blood test will be given to the patient the following week when they will commence treatment. Patients will be told in the patient information sheet how results will be reported and that they may need to attend for repeat testing for technical reasons; however positive test results will be discussed in clinic.

6.19 DETECTION Inclusion/Exclusion criteria

See Appendix 21 for inclusion/exclusion criteria

6.20 DETECTION Statistical considerations

Statistical calculations for this section were performed by Dr. Richard Jackson. I liased with him regarding the assumptions on which to make the calculations and the design.

6.20.1 Sample Size Calculation

The primary outcome for the study is OS measured as the time from randomisation until death by any cause with a clinically relevant difference considered to be given by a HR of 0.7. A two-sided alpha level of 0.05 will be used for the primary outcome. Power calculations are calculated adjusting for the interim analysis based on the surrogate of RFS. There is no adjustment of the power calculation for the initial stop/go criteria based on the pooled RFS rates as this assessment does not include any comparisons between treatment arms and power calculations should be considered conditional on the study progressing past this point.

At the planned RFS interim analysis, the study will continue if the point estimate of the HR is in the direction favouring early treatment with a magnitude defined by HR < 0.9. This analysis is planned to take place after 100 RFS events have been observed and for this assessment there is a 40% chance of erroneously continuing if there is no true difference between the two treatment groups (HR 0) and a 95% chance of continuing if true difference between the two groups is represented by HR 0.7.

The power calculations for the primary analysis needs to take account of this interim assessment and to do this, we assume a conservative correlation between the two endpoints of 0.3. Following adjustment a total of 264 events are required which gives a power for the final analysis of 82% and preserves the family-wise power for the full study at 80%.

To obtain the 264 events required for the study, recruitment is planned to take place over a period of 72 months with a minimum follow up of 36 months for every patient. In total 930 patients will be recruited and this is inflated to include a 5% patient attrition rate. Estimates of events from the patients recruited are made based on an estimated 10% of patients having ctDNA at presentation, which was based on the data from chapter 5 and this rate increasing to 30% over three years. Estimates of RFS and OS are measured from the points of ctDNA detection and estimate that the median RFS rate to be approximately 3 months and the median OS to be approximately 30 months. Hazard functions for each of these distributions are estimated using a piecewise exponential model for the purpose of estimating the accumulating numbers of events during the study. Figure 6.11 below shows estimated accumulation of ctDNA detections, RFS events and OS events and shows that 264 events are required for final analysis, which should accumulate at approximately 104 months.

6.20.2 Randomisation

Patients will be randomised 1:1 and stratified using randomly permuted blocks controlling for detected ctDNA at baseline blood draw vs. subsequent blood draws (2-levels) and stage of disease (IIB/C). Stage is a well known prognostic factor and the data in chapter 5 shows that ctDNA within 12 weeks of surgery is a poor prognostic factor. Therefore it will be important to stratify based on these factors and perform subgroup analyses to assess efficacy of the approach within these groups.

6.20.3 Interim analyses and early stopping rules

Stop/Go interim analysis. An initial stop/go assessment will be carried out once 50 patients have had 3 months follow-up following the detection of ctDNA. As this assessment does not include any comparisons between treatment arms, no adjustment to power calculations

are made on the outcome of this assessment. The purpose of this assessment is to demonstrate that ctDNA can be detected in a timely manner with the aim being to demonstrate that the median RFS rate following detection is at least 3 months. If the median RFS rate for this assessment is less than 3 months the study will be suspended.

Second interim analysis (RFS): A second interim analysis will be carried out based on the surrogate outcome of RFS. OS is not used for the interim analysis as by the time sufficient events have accumulated it is anticipated the study will have stopped recruiting. At this interim analysis, it is required that some benefit is demonstrated in terms of RFS. This will be evaluated by a point estimate being a HR ≤ 0.95 being observed favouring early treatment.

6.20.4 Patient Groups for Analysis

In order to follow the Intention to Treat (ITT) principle the patient group for final analysis will consist of all randomised patients with assessment of the primary outcome except for a) patients withdrawing consent between randomisation and starting ctDNA monitoring, b) patients withdrawn from the study after randomisation because of irregularities with the consent process, and c) patients whose information determining ineligibility existed before randomisation but was not read until after randomisation. Mis-randomised patients will be analysed as randomised.

6.20.5 Data Description

Continuous variables will be summarised by descriptive statistics (mean, standard deviation, minimum, median and maximum) and categorical data will be summarised in terms of frequency (n) and percentage, presented by treatment arm.

6.20.6 Levels of Significance

Analysis of the primary outcome will be assessed at the two-sided 0.05 level as is consistent with the Type I alpha level used in the study design with estimated of efficacy reported alongside a two-sided 80% CI. All analyses of secondary outcomes will use the nominal $p<0.05$ level.

6.20.7 Missing Data

The amount of missing data is expected to be small and final analyses will be carried out on a complete case basis. If substantial missing data (>10%) are observed in either a study outcome or key prognostic covariate then multiple imputation using chained equations will be applied.

6.20.8 Analysis of Primary Outcome

Estimates of OS will be obtained using the Kaplan Meier approach with comparisons across treatment arms carried out using a stratified log-rank test. Further multivariable analyses shall be carried out using Cox proportional hazards modelling techniques. Models shall be constructed with stratification factors and the treatment identifiers forced into the model with further clinical/demographic factors considered for inclusion using a stepwise procedure base on Akaikes Information Criterion (AIC).

6.21 Patient and Public involvement (PPI)

As part of the work-up involved in the trials I have been liaising with a patient representative to ensure that any patient-facing information is appropriately written. Furthermore, for DETECTION I was able to attend one patient support group (Cambridge support group) and one focus group of members of the public in order to obtain input into the

trial. I found this an extremely helpful process as it raised points that I had not previously considered.

6.21.1 Acceptability of the trial aims and blood testing

It was clear that both the patients and public were supportive of the aims of the trial and that additional blood testing was acceptable to them.

Member of the public 1: *"After cancer any diagnostic test is important."*

They liked the idea of a more precise approach in treating patients both in terms of reducing the burden of toxicity, but they also recognised that it potentially would save the NHS money, which they thought was important.

Member of the public 2: *"Potentially could be saving the patient and the NHS."*

6.21.2 Acceptability of the trial design

The main discussion around the acceptability of the trial design was around having a standard of care arm. The Cambridge support group felt that whilst patients would prefer to be randomised to Arm B rather than standard of care, they accepted that a comparison would need to be made. The members of the public also discussed that keeping Arm A blinded was not an issue.

Member of the public 3: *"If you didn't do the trial everyone would be getting the standard treatment anyway*."

They felt it was similar to a placebo-controlled trial and they understood the need to have a standard of care arm.

6.21.3 Acceptability of treatment based on a blood test result

We also discussed acceptability of treating early based on the blood test. Potential side effects were explained to them, however they felt they would want treatment.

Member of the public 2: *"I would rather have treatment, it's a ticking time bomb otherwise."*

6.21.4 Delivering the positive test result to the patient

In addition, the Cambridge support group identified that it would be important as to how the patient in Arm B would be informed of positive test results. It was felt that it would be important to discuss the results in person. The members of the public also thought that patients in Arm B with detectable ctDNA should be telephoned to come back to clinic by a healthcare professional rather than receiving a letter. Appointments following the call would need to be soon after and we discussed that within a week as per trial protocol would be acceptable.

6.22 Chapter Discussion

CtDNA is a powerful, minimally invasive tool to monitor tumour burden, MRD and early relapse. This chapter highlights two potential clinical uses, one in the metastatic setting to inform a therapy switch and the other in the post surgical setting to identify patients who potentially could benefit from early treatment. Whether these strategies will improve patient outcomes will be tested in the trials.

According to the database PubMed, the number of publications regarding ctDNA has been steadily increasing over time (71 in year 2000 vs. 709 in 2017, search terms "circulating tumour DNA" or "ctDNA"), however the majority of the published data are observational studies reporting characteristics of ctDNA, such as the ability to monitor tumour burden or analyse for specific mutations. In addition, the vast majority of clinical studies entered into

clinicaltrials.gov (accessed 12th July 2018) are monitoring ctDNA in a variety of situations with very few designed to use ctDNA as a tool to make a clinical decision. Exceptions to this are c-TRAK (NCT03145961), which is a randomised phase II trial in early stage, high-risk, triple negative breast cancer that examines whether patient outcomes will be improved through monitoring ctDNA following standard therapy and treating patients with anti-PD-1 agent pembrolizumab if increased ctDNA is detected. Another trial TARGET uses mutations identified in ctDNA to guide Phase I trial selection (435). Recently, the American Society of Clinical Oncology and College of American Pathologists have conducted a joint literature review on the clinical validity and utility of ctDNA (436). They concluded that at present there is insufficient evidence of clinical validity and utility for the majority of ctDNA assays in advanced cancer or early stage treatment monitoring/residual disease detection (436). CAcTUS and DETECTION are part of the next stage of translating ctDNA into the clinic. Through testing the assays properly within clinical trials we will provide evidence as to their ability to improve patient outcomes. In addition, DETECTION will provide a benchmark for further research into early detection of recurrence in early stage melanoma. In ensuring that the treatments surrounding the ctDNA based clinical decisions are active in melanoma and specifically in those clinical scenarios, I feel that the designs can really test whether ctDNA can aid clinical decision making rather than being confounded by ineffective therapy.

6.23 CtDNA assay development and considerations for both studies

6.23.1 GCP assay development and quality assurance

One of the first steps in translating my preclinical research to the clinic is to optimise and test the ddPCR assay to detect ctDNA to be in line according to the strict quality assurance criteria to GCP standards. As clinical decisions will be a taken based on the results of the tests then it is extremely important that it performs consistently. The assay has now passed the

quality assurance process (performed by the CEP laboratory) for CAcTUS and therefore it is highly likely that it will also be optimised for DETECTION. The standard operating procedures will be rolled out to other laboratories (Oxford and potentially Australia) as part of the remit for DETECTION, which I believe will be an important further step to bringing it into routine clinical testing.

6.23.2 Future-proofing the assays

The field of ctDNA and early detection of relapse is fast moving and therefore it will be important (especially for DETECTION due to its longevity) that the trials react to any external information that comes available that could improve the test. Some of the NGS methods currently utilised by other groups may improve sensitivity, however as discussed in chapter 5 (see section 5.6.4) there has not been a head-to-head comparison of techniques. Furthermore, any improvement to the test will also have to be cost-effective and have a comparable turn-around time. Calculating the budget for these trials has made me realise how important the cost aspect will be once it is multiplied by the number of tests over time (e.g. DETECTION is estimated to require 16190 tests). In translating biomarker research to the clinic it is therefore crucial that a number of competing factors are considered as part of a decision to use one technique over another. One of the key aspects of the trials are the additional research samples that will be taken. It will therefore enable any potential assay changes to be validated within the trial's own samples against the ddPCR benchmark.

6.24 Chapter Summary

CtDNA has a great potential for use as a clinical tool and this chapter describes some of the ways in which it might be used in melanoma. Whilst the assays can always be improved especially in terms of their sensitivity in detecting MRD/early relapse, there is now sufficient evidence to test them as part of clinical trials. These will provide much needed data in terms of their real-time performance and their efficacy in improving patient outcomes. Furthermore, the logistics of providing a quick and accurate turn around of results will be developed and tested, which is a critically important aspect of translating ctDNA assays into the clinic. These trials will provide a benchmark for future methods refining the technology and will inform as to the best clinical uses of ctDNA.

Chapter 7. Discussion and Summary

Precision medicine involves "tailoring of medical treatment to the characteristics of each patient to classify individuals into subpopulations that differ in their susceptibility to a particular disease or their response to a specific treatment" (437). In order to achieve optimal responses to therapy, it is important to consider not only the genetic and transcriptomic characteristics of the tumour, but also the interactions with its microenvironment, the evolution under therapy-induced selection pressure and the timing of treatments. In addition, to achieve the best outcomes for patients, the precision medicine approach should be anticipatory rather than reactionary. Through assessing baseline characteristics of a tumour and instigating early treatment or combining treatments to prevent resistance occurring, I would argue it is more likely that patients will achieve better responses. Furthermore, future strategies may be able to drive the tumour to a state vulnerable to the next line of treatment rather than the current status quo in which there are diminishing returns as a patient progresses through treatment lines.

7.1 Predicting response to therapy

The ability to predict the likelihood of response to therapy is integral to a precision medicine approach. It enables patients to be selected for a treatment that will benefit them, whilst those who are unlikely to respond are spared potential toxicity. For BRAFi/MEKi the most obvious predictor of response is a *BRAF* mutation, however duration of response may be affected by a number of mechanisms of resistance, and primary resistance is a challenge in a minority of patients. In addition, many groups have examined ways of stratifying responders vs. non-responders to immune therapy. In this thesis, I have explored some of the ways in which patients can be stratified.

7.1.1 Anticipating resistance to targeted therapy

The identification of a pan-RAF inhibitor in our laboratory in collaboration with Prof. Caroline Springer provided an opportunity to study potential mechanisms of resistance to the drug at an early stage in its development. In chapter 4, I show that resistance appears to be mediated by up-regulation of the MAPK pathway or activation of the PI3K/AKT pathway through a combination of genetic and transcriptional changes. Targeting PI3K/AKT signalling resulted in synergy with CCT3833 even in cells resistant to BRAFi/MEKi. Therefore, through identifying mechanisms of resistance at an early stage in drug development it is possible to guide combination therapy strategies.

7.1.2 Personalising strategies for patients based on mutation profile

My data revealed potential mutations that would result in resistance to CCT3833. Early knowledge of these potential mechanisms of resistance enables a more personalised approach towards drug development. For example, my data suggests that a *MAP2K1* or *PIK3R4* mutation is a biomarker of decreased efficacy for single agent CCT3833 and therefore patients with melanoma harbouring a *MAP2K1* or *PIK3R4* mutation could be screened out of trials. Such patients might benefit more from ERK inhibitors and therefore a more sophisticated approach would be to test CCT3833 within an umbrella trial in combination with other inhibitors using a genomically guided, biomarker driven approach. For example, they could be selected for different combination therapy arms such as CCT3833+ERK inhibitor if they had a *MAP2K1* mutation or CCT3833 + PI3K/AKT inhibitor if they had a mutation in the PI3K/AKT pathway. This would need further testing pre-clinically to optimise the combinations *in vivo* but would then enable a precision-based approach to patient selection for an optimal CCT3833 combination.

7.1.3 Tumour mutational burden and response to immune therapy

Tumour mutational burden (TMB) has become a biomarker of huge interest for the immuno-oncology (IO) field. It has been used as a surrogate for neoantigen burden although depending on the technique used it is not always possible to infer further useful information which can predict IO response such as clonality (206,316). The more neoantigens present, the greater the chance of T cell recognition and response, therefore TMB or neoantigen burden has the potential to be a biomarker of response to immune therapy. Furthermore, the cost of sequencing, especially targeted sequencing, has reduced significantly over the past 10 years (although bioinformatics analysis remains a bottleneck in the pipeline) enabling it be a realistic test for clinical use in high-income countries at least.

One of the first clinical studies to prospectively evaluate TMB as a biomarker of response to combination N+I in patients with lung cancer has been recently reported (438). It defined TMB as the number of somatic, coding base substitutions and short insertions and deletions (indels) per megabase of genome examined, determined by the FoundationOne CDx assay (438). In patients with a TMB of >10 mutations/megabase, PFS was 42.6% for those treated with N+I versus 13.2% for those treated with chemotherapy, and the median PFS was 7.2 months (95% CI, 5.5 to 13.2) versus 5.5 months respectively (95% CI, 4.4 to 5.8) (HR for disease progression or death, 0.58; 97.5% CI, 0.41 to 0.81; P<0.001) (438). There was no significant difference in PFS for patients with low TMB treated with N+I or chemotherapy (HR for disease progression or death, 1.07; 95% CI, 0.84 to 1.35). Median PFS was 3.2 months (95% CI, 2.7 to 4.3) with N+I and 5.5 months (95% CI, 4.3 to 5.6) with chemotherapy for low TMB patients (438). This trial is likely to set a precedent for further trials to at least stratify patients based on TMB, however there are important aspects to take into consideration. Firstly, the FoundationOne CDx assay is based on hybridised-based capture of 324 genes only representing approximately 800,000 base pairs of the 30 million base pairs in the human exome

and therefore may not be truly representative of the number of mutations across the whole exome (439,440). As the TMB of a sample decreases, the percent deviation from the actual TMB (measured using WES on a Illumina Next-Seq platform) decreases considerably from approximately 10% deviation (95% CI 0-18%) for samples with TMB of >100 mutations/megabase to 25% deviation (95% CI ~0-50%) if there are only 10 mutations/megabase present (439). Thus the assay may not be very accurate particularly with samples with lower TMB.

Although my data was limited to one patient, they achieved a complete response to immune therapy despite having a low number of mutations. This highlights the challenge in predicting response to immune therapy; there are a multitude of factors that could affect response including mutational status, neoantigens, secreted cytokines, tumour burden, LDH and the microbiome. For an individual, to predict response based on a single aspect such as TMB is extremely challenging. Furthermore, in the case of acral melanoma the mutational rate is known to be low, with a previous report of 5 patients with acral melanoma having a range of 1.02–3.68 SNVs per megabase (76). However, it is known to have a similar response to immune therapy as cutaneous melanoma (297,441). Therefore, TMB may not be especially important for this melanoma subtype whilst other factors may be contributing to immune response. An interesting follow up study would be to understand why acral melanomas respond to checkpoint blockade despite their low TMB. In terms of the clinic, my data cautions against excluding patients from immune therapies solely due to low mutation burden and neoantigen load. Furthermore, before commencing clinical trials based on TMB it may be important to validate different cut offs for numbers of mutations per megabase depending on the tumour type.

7.2 Optimising response to therapy

There are a number of potential ways in which treatment can be optimised in order to improve responses depending on stage of presentation and during the patient's disease course.

7.2.1 Combination strategies upfront in drug development programmes

Traditionally, drug development programmes often test single agent therapies up to Phase III before combining them with other agents, however one of the most effective and rapid drug development programmes took a strategy of performing combination and monotherapy trials in parallel. The phase III trial of D+T was commenced in the same year (2010) as the BREAK trial of dabrafenib monotherapy and METRIC study of trametinib monotherapy, with all three studies reporting in 2012 (8,313,339,442). This was quite risky in terms of drug development as toxicity could have impacted the whole programme. However, in this instance the inhibitors were well tolerated both as monotherapies and in combination.

These studies have really shown the need to combine targeted therapies in melanoma in order to achieve the most durable responses. For example the PFS of dabrafenib was 8.8 months, trametinib was 4.8 months, whilst combination D+T was around 11 months (8,120,313,339). Therefore, an approach of upfront combination therapy drug development from Phase Ib onwards would potentially be a good strategy for CCT3833. As melanoma progresses, it can accumulate genomic complexity, which might increase the chance of treatment failure due to an underlying mutation or pathway up-regulation conferring resistance. Therefore if CCT3833 were used in the second line setting, combining with a PI3K inhibitor upfront would reduce the potential impact of cross-resistance in BRAFi/MEKi resistant disease.

7.2.2 Synergising therapies to target tumour-microenvironment interactions

In chapter 3, I show that the tumour microenvironment could be associated with resistance to targeted and immune therapy. The brain in particular is a unique environment as it is surrounded in CSF, which contains many growth factors and other nutrients. Furthermore, the brain has a completely different composition of immune and stromal cells to anywhere else in the body. I show that in a patient who developed brain metastases whilst undergoing treatment with nivolumab, the tumour had a much higher number of M2 switched macrophages, which are known to be tumour promoting and may have contributed to the resistance to therapy (318). In addition, when tumour cells were cultured in CSF, dabrafenib was less effective due to the cells up-regulating the PI3K/AKT pathway. Targeting of the PI3K/AKT pathway resulted in decreased cell growth in the presence of CSF. Thus, in order to optimise precision medicine, it is important to consider the microenvironment in which the patient's metastases are located and adapt or combine treatments in order to target potential tumour interactions with its microenvironment.

The involvement of the PI3K/AKT pathway in resistance to dabrafenib in the presence of CSF suggested that this is an important target in treatment of brain metastases. Although my data was limited to a case study, it adds to a number of other studies with similar findings indicating that it has potential to be a common drug target in melanoma brain metastases. Unfortunately, PI3K inhibitors have been disappointing in the clinic. In general, low response rates have been seen in solid tumours at tolerable doses for a number of different agents in development. On target toxicity is also a challenge, particularly gastro-intestinal and skin AEs, hypertension and hyperglycaemia (443,444). However, one of the newest PI3K inhibitors to reach the clinic has recently reported phase III preliminary data showing a PFS benefit of 7.4 vs. 5.4 months (HR 0.7) in combination with fulvestrant in patients with localised unresectable or metastatic breast cancer that had progressed on an aromatase inhibitor (112). There were

more taselisib discontinuations (17% vs. 2%) and dose reductions (37% vs. 2%), compared to placebo due to AEs, however it was generally well tolerated.

One of the major issues for developing systemic therapy targeting melanoma brain metastases is the ability of the drugs to cross the BBB. The BBB comprises endothelial cells lining the brain microvessels as well as astrocytes and pericytes (445). The ability of cells and molecules to cross the BBB is tightly controlled through a combination of low passive permeability, presence of specific transport systems, enzymes and receptors (445). Some of the enzyme systems can degrade drugs as they cross the BBB, rendering them ineffective. Furthermore, ATP-binding cassette (ABC) membrane bound proteins can support drug efflux of the brain resulting in decreased drug penetration (446). However, a recent observation in the OPARATIC trial in glioblastoma provides evidence that drugs may still be able to penetrate brain tumours despite the BBB (447). Olaparib, a PARP inhibitor, is normally unable to penetrate an intact BBB, however due to disruption by the tumour, olaparib was detected in 71/75 tumour core specimens (27 patients); mean concentration 588nM (97-1374nM), and 27/28 tumour margin specimens (10 patients); mean concentration 500nM (97-1237nM) (447). Therefore, drugs need to be evaluated in the presence of tumours to provide a signal as to their ability to cross a disrupted BBB.

The only PI3K inhibitor that has progressed beyond Phase I that is known to be brain penetrant is buparlisib, a pan-PI3K inhibitor (111,448). Unfortunately, Novartis discontinued its development due to a low efficacy to AEs profile seen in the BELLE-3 study of fulvestrant in combination with buparlisib or placebo (111). Intriguingly, one of the AEs was suicidal ideation, which was reported in the buparlisib (2%) and placebo (1%) groups; and three suicide attempts were reported in the buparlisib group (111) suggesting that the drug's ability to cross the BBB might have resulted in brain specific toxicities. Further studies are therefore needed to

find alternative, potentially more selective PI3K inhibitors that are able to penetrate the BBB with better toxicity profiles.

One of the challenges for the clinic highlighted by my data is that heterogeneous tumour microenvironments may contribute to different responses and resistance to therapy. The brain microenvironment has unique characteristics and therefore in developing personalised medicine approaches for patients with brain metastases, a strategy incorporating the reciprocal signalling of the brain microenvironment with melanoma could be more beneficial. However, this becomes difficult if combination therapy is already standard of care, as in general, therapy with triple combinations tends to result in a large burden of toxicity. Thus, the addition of a brain penetrant PI3K inhibitor in addition to BRAFi may be a better combination for those patients with brain metastases compared to MEKi, as inhibition with a PI3K/BRAF/MEK triple combination is extremely likely to result in significant toxicity. Other factors would have to be considered such as the pace of extra-cranial to intra-cranial disease, as a BRAFi/MEKi combination is likely to be more effective extra-cranially. One alternative is to schedule alternate dosing of PI3K and MEK inhibitors with a BRAFi backbone. Such schedules would have to take into consideration the long half-life of MEKi, again highlighting the complexity of these approaches.

7.2.3 Modulating the tumour microenvironment to enhance response

In addition, it may be possible to modulate the tumour and its microenvironment with one therapy in order to make it more likely to respond to a second therapy. In chapter 6, I designed a trial, which hypothesises that in response to targeted therapy, the tumour becomes more sensitive to immune therapy. Research by other groups has shown that in response to targeted therapy, LDH reduces, melanoma antigens increase, immunosuppressive cytokines decrease and the tumours have improved T cell infiltration (410,412–414). Therefore, it may be

possible to modify the melanoma cells and their microenvironment with targeted therapy in order to enhance the effect of immune therapy.

As ctDNA is a dynamic marker of tumour burden, in the CAcTUS trial described in chapter 6, I have used it to define response to targeted therapy in order to guide a switch to immune therapy. The aim of this is to quickly switch from targeted to immune therapy before resistant clones become established with a more immune stimulating microenvironment to be present. Using ctDNA allows treatment to be tailored to the individual's response rather than specifying a short duration of targeted treatment, which may not be optimal timing for every patient.

7.2.3 Rational scheduling of therapies

7.2.3.1 CCT3833 in the current melanoma treatment landscape

BRAFi/MEKi have been shown to be an effective combination in stage IV *BRAF* mutant melanoma (118,339). Currently there is no standard targeted therapy option for patients with *NRAS* mutant melanoma and therefore CCT3833 would potentially represent a good first line targeted therapy option to be tested in clinical trials. In *BRAF* mutant melanoma the strategy becomes more difficult to define. Based on previous work with compounds in the series and my data, CCT3833 in a preclinical setting is better than first generation BRAFi (vemurafenib/dabrafenib) because of its ability to break the paradox due to inhibition of CRAF (335). However, further work would be needed to test whether it would be better in comparison to BRAFi/MEKi in targeted treatment naïve tumours.

An alternative strategy is to use CCT3833 as a second line treatment in *BRAF* mutant melanoma in order to extend the overall benefit of targeted therapy. Through scheduling BRAFi/MEKi followed by CCT3833/PI3K inhibitors, which could be effective in BRAFi/MEKi resistant disease, it may be possible to increase overall PFS. This is in

comparison to treating intensively upfront with a CCT3833/PI3K or CCT3833/MAPK inhibitor (e.g MEKi or ERK inhibitor) combination, but having no effective second line targeted therapy for CCT3833 resistant disease. This approach potentially would be augmented if it was possible to have a break from targeted therapy before giving the second line targeted treatment as it has been shown that further responses can be obtained following a targeted therapy break (449). The combination of CCT3833 with a PI3K inhibitor such as taselisib targets a number of mechanisms of resistance to BRAFi/MEKi. In combination with a PI3K inhibitor although only *in vitro*, my data suggests CCT3833 is effective in inhibiting growth of cells resistant to PLX4720 (vemurafenib analogue for *in vivo* studies)/dabrafenib or D+T. Therefore, sequential treatment with BRAFi/MEKi followed by CCT3833 plus PI3K inhibitors could be an effective strategy, which should be tested further.

7.2.3.2 CtDNA as a tool to guide timing of therapy

Timing of therapy is extremely important in the treatment of any cancer. In the clinical setting, decisions are constantly being made as to when to start or switch treatment. Conventional tools such as imaging and LDH are useful, however have limitations. LDH is not very specific and does not always recapitulate disease progression. Imaging exposes patients to radiation and therefore is limited in terms of the number of scans that can be performed over time. Chapter 5 and 6 show that ctDNA is a very sensitive tool, which can be used to dynamically monitor tumour burden. As such, it can be used to guide real-time clinical decision-making.

7.2.3.3 Adaptive treatment strategies

One of the other potential clinical uses for ctDNA is to aid adaptive targeted treatment strategies. The rationale for adaptive treatment is to maintain a sensitive population of cells to

exploit their competition with resistant cells (450). Resistant cells in general have a reduced fitness compared to sensitive cells which allows the sensitive cells to outgrow and trap resistant cells within the tumour (451,452). In melanoma, resistance to therapy is typically associated with a phenotypic switch from a MITF high proliferative phenotype to a MITF low invasive phenotype (163). Therefore, this may play a role in slowing the rate of tumour growth using an adaptive strategy. Finally as discussed in chapter 4, resistant melanoma cells can become drug addicted and when drug is removed lose their fitness through ERK hyperactivation (165–167). Taken together, these data suggest an adaptive approach to treatment with BRAFi/MEKi combinations may improve PFS.

In order to implement an adaptive treatment strategy, a dynamic marker of tumour activity is required. In prostate cancer, prostate specific antigen (PSA) has been used to guide adaptive abiraterone (CYP17A inhibitor) treatment in a pilot clinical trial (452). Patients were commenced on abiraterone and when their PSA levels decreased by 50%, it was stopped (452). Abiraterone was restarted when the patient's PSA levels increased to ≥their baseline level. In this way the treatment was adapted to the activity of the disease (452). At a median follow up of 10 months, 1/11 patients treated with adaptive therapy had progressed compared to 14/16 in a contemporaneous cohort (452).

BRAF mutant ctDNA as a dynamic tumour marker of burden and activity could provide a similar signal to give adaptive treatment in melanoma. Patients would be commenced on BRAFi/MEKi and monitored regularly with ctDNA. When the percentage ctDNA from baseline fell below 50%, the drugs would be withdrawn and only restarted when the ctDNA increased by ≥50%. Given the data from chapter 4, caution would be required with this approach to not select for cells associated with a more invasive, stem-cell-like phenotype. As previously discussed in chapter 4, this approach might benefit from alternate scheduling with inhibitors targeting stem cell activity. Additional key factors which would need to be considered is the target decrease in

ctDNA, whether this strategy would be suitable for patients with rapidly growing disease and whether pharmacodynamics of the drugs would affect the efficacy especially as MEKi are associated with an extremely long half life.

7.3 Driving tumour evolution to a more vulnerable state

One of the important observations I made in chapter 4 was that when cells became resistant to CCT3833 via a mechanism that up-regulated the MAPK pathway, they became addicted to the drug. When drug was withdrawn, ERK/JunB became hyperactivated resulting in decreased fitness of the cells, which is consistent with previous studies using BRAFi/MEKi (165,166). *In vitro* this can result in significant reductions in tumour growth and a survival benefit through withdrawal of drug alone, however when these drugs have been stopped in the clinic the effects seen in patients do not appear to be so pronounced. This could be due to a number of reasons including lack of the tumour microenvironment as well as the long half-life of agents resulting in more gradual drug withdrawal, thus providing the melanoma opportunity to adapt. Of note, I showed preliminary data suggesting that if resistance occurs via mechanisms such as PI3K/AKT activation rather than MAPK up-regulation, then cells are less likely to exhibit the drug addiction phenotype (Chapter 4). If this is validated, then it suggests that patients with a activating mutation in the MAPK pathway might be more likely to have a deeper response to drug withdrawal and PKC agonism, although activation of PKC still resulted in loss of fitness in non-drug addicted cells. Therefore trials using drug withdrawal as a strategy might benefit from patient selection based on mutational status to enrich for resistance mutations such as *MAP2K1* associated with MAPK up-regulation. Upfront inhibition of potential mechanisms of resistance (such as PI3K/AKT activation) that are less likely to result in loss of fitness upon drug withdrawal may also drive tumour evolution towards a more vulnerable state however, this needs to be tested further. Taken together, my data suggests that evolution of resistance under

the selection pressure of MAPK inhibitors can result in a vulnerability that can be exploited in the next line of treatment.

Culturing CCT3833 resistant cells with a PKC agonist augmented the drug addiction phenotype and resulted in decreased fitness even in cells that were resistant but not drug addicted or when CCT3833 was still present. This data suggests that ERK activity in melanoma cells is finely balanced, as PKC agonism results in disequilibrium of ERK activity towards a cell fate decision of growth arrest and death rather than pro-survival. Therefore, the lack of a strong phenotype seen upon withdrawal of drugs in the clinic could be pharmacologically enhanced with a PKC agonist.

This requires further pre-clinical testing *in vivo* before it could be tested within clinical trials. As CCT3833 is only in early phase development, it would be important to test PKC agonism in the context of BRAFi/MEKi withdrawal to potentially enhance current standard of care therapy. As the drug addiction phenomenon has previously been seen with BRAFi/MEKi withdrawal and when the mechanism would be the same, I would hypothesise that a PKC agonist would also enhance cell death/growth inhibition upon withdrawal of these drugs.

Finally, further work would be required to optimise a PKC agonist for this approach. I used PMA as a tool compound for my studies, however it has been rarely used in clinic. Bryostatin-1 also showed a similar effect on the cells, however the drug is difficult to make as is derived from large quantities of marine bryozoans, therefore manufacturing would be a challenge. Thus, if these data were validated *in vivo,* better PKC agonists would need to be developed in order to translate this research into the clinic.

Clearly, further work needs to be performed to optimise the use of PKC agonists as part of a targeted therapy scheduling strategy. *In vivo* experiments would increase preclinical understanding how PKC agonists given at the end of targeted treatment when tumours are growing on therapy compared to drug holiday schedules (i.e. 2 weeks 3833/taselisib followed

by 1 week of PKC agonist) target emerging resistant clones within the population. However, my data provides preliminary mechanistic insight into how drug holiday approaches can be optimised using PKC agonists.

7.4 Early treatment of disease

One of the ways in which melanoma outcomes may be improved is through treating micro-metastatic relapse at an early stage. However standard methods of predicting risk of relapse are not very precise, resulting in over-treatment of some patients. In chapter 5, I show that if ctDNA is detected following surgery, then >90% of patients relapse. Based on this data, I designed a trial in chapter 6, which is examining whether early treatment based on detection of ctDNA in stage IIB/C melanoma can improve outcomes. Although numbers are small, detection of ctDNA in the pre-operative setting also appears to predict for distant metastasis, with surgery having little impact on chance of relapse in these patients. Thus, these patients in particular may benefit from neoadjuvant systemic therapy, as failure of local treatment is high. Future clinical trials will be needed to test this as discussed below.

7.4.1 Potential clinical value of ctDNA in the neoadjuvant setting in melanoma

One of the future areas in melanoma that may benefit from using ctDNA is neoadjuvant immune therapy treatment. The rationale for using neoadjuvant therapy in melanoma is that the resectable tumour provides a source of antigens that elicit an immune response when checkpoint inhibitors are given. Two trials have reported preliminary findings showing that combination N+I resulted in greater pathological complete responses (pCR) than nivolumab alone. The Amaria *et al* study, which was closed early after enrolling 23 patients, reported a 25% pCR and radiological response rate of 25% for nivolumab vs. a pCR of 45% and radiological response rate of 73% for N+I (453). This was at the expense of considerable AEs

with 73% patients on N+I reporting grade 3/4 toxicity (453). The OpACIN trial of neoadjuvant N+I showed similar findings with tumour load decreasing in 8/10 patients evaluable, but 18/20 patients stopping treatment early due to grade 3/ 4 toxicity (454). Trials with decreased doses of combination N+I are on going and will hopefully result in a more favourable toxicity profile without decrease in efficacy.

The ctDNA data from the prospective pre-operative patient cohort in chapter 5, which validated the findings in the Melbourne cohort (Fig 5.5) shows that detectable pre-operative ctDNA is also associated with a high risk of predominantly distant relapse (455). Furthermore, 20/22 patients with detectable ctDNA in the pre-operative period relapsed in the post-operative period, suggesting that surgery had little effect on outcome (455). Therefore these are patients that could potentially benefit from early systemic therapy. One of my future trial ideas is to initiate neoadjuvant therapy in patients with pre-operative detectable ctDNA and compare outcomes to those treated with sentinel node biopsy (SLNB) or completion lymph node dissection (CLND) +/- adjuvant therapy. Alternatively ctDNA could be used to monitor response to neoadjuvant immune therapy and if ctDNA remains detectable following SLNB/CLND in *BRAF* mutant patients, to switch to targeted therapy as adjuvant treatment, as persistently detectable ctDNA would suggest an alternative treatment strategy is needed.

7.4.2 Potential clinical value of ctDNA in the adjuvant setting in melanoma

There are three main uses for ctDNA in the post-operative early stage setting which are further discussed below:

1. Stratification of high-risk patients
2. Monitoring for molecular relapse
3. Monitoring for treatment response to adjuvant therapy

7.4.2.1 Stratification of high-risk patients

My data shows that patients with detectable ctDNA post surgery have an inferior prognosis. This was independent of AJCC staging and therefore could be a further method of stratifying patients. An opinion paper has recently suggested that ctDNA should be added to the tumour, node, metastasis system that is widely used in oncology (456). In principle I would agree with this, as higher ctDNA levels at each stage of cancer progression (II/III/IV) have consistently been associated with poorer prognosis. There are, however a number of aspects which would need to be internationally agreed and tested prior to this becoming a new model. Firstly, as previously discussed, the technique(s) used would need to be standardised as the levels of ctDNA and the sensitivity of the test varies between platforms. Secondly, a decision would have to be made on which mutation(s) and the number of mutations you would focus on as this would vary between melanoma subtypes. *BRAF* and *NRAS* mutations would be obvious candidates, but *BRAF/NRAS/NF1* wild type disease would be more complex to define. Furthermore a decision would have to be made regarding whether the detection of ctDNA is a binary test i.e. patients with or without detectable ctDNA or whether different ctDNA VAF levels (associated with poorer outcomes) would be used. The binary output I would argue is most suited to early stage melanoma where you are working at the limits of detection of the test and therefore there is a higher degree of error in reporting the VAF level. However, when assessing stage IV disease, different levels of ctDNA would potentially provide a more precise measure of prognosis. A study examining detectable baseline *BRAF* VAF and response to BRAFi +/- MEKi across 4 trials showed that cfDNA mutation fraction was positively correlated with factors associated with poor prognosis such as baseline sum of longest diameters (as a surrogate of tumour burden) and LDH (Spearman correlation R=0.45–0.72) (376). Furthermore, cfDNA mutation fraction levels were higher in LDH high compared with LDH normal patients

(376). However, they did not perform an analysis of different levels of ctDNA VAF and prognosis.

The ability to predict progression to stage IV disease is extremely important in light of recent findings that immune checkpoint inhibition and combination BRAFi and MEKi improve OS in stage III melanoma (228,373,374,457). Detection of ctDNA allows identification of a subgroup of patients at high risk of early relapse and inferior survival, allowing stratification of patients to adjuvant regimens associated with higher toxicity but greater potential for efficacy [14]. In addition, when taken at a single time point following surgery, it can add to AJCC staging in informing individual prognosis and therefore a discussion with a patient regarding risks and benefits of adjuvant therapy. If ctDNA was detected, the patient would be more likely to require further treatment as they are at higher risk of relapse, however at present there are no data available as to whether ctDNA is a predictive biomarker for a particular therapy in this situation. Further research is required to assess baseline ctDNA detection and response to different adjuvant therapies.

7.4.2.2 Monitoring for molecular relapse

CtDNA is a very useful tool for monitoring early disease relapse/molecular progression. Longitudinal monitoring has been shown to detect micro-metastatic relapse in a variety of cancer types in the adjuvant setting. In breast cancer, a study demonstrated a lead time of ctDNA detection of between 0.07-8.87 months compared to clinical recurrence in patients following treatment with neoadjuvant chemotherapy and surgery (458). Another study showed that longitudinal monitoring of ctDNA was able to detect breast cancer relapse with a median of 7.9 months (range 0.3 to 13.6 months) lead-time over clinical relapse in 55 patients receiving neoadjuvant chemotherapy (383). This has led to the development of the c-TRAK TN study; "A Trial Using ctDNA Blood Tests to Detect Cancer Cells After Standard Treatment to Trigger

Additional Treatment in Early Stage Triple Negative Breast Cancer Patients" (NCT03145961) (459). Patients undergo 3 monthly ctDNA surveillance following standard of care surgery +/- adjuvant chemotherapy and then if ctDNA is detected they are randomised 2:1 to pembrolizumab or observation (459).

CtDNA identified recurrence of a median 167 days (interquartile range 81-279) prior to radiological recurrence following surgery for stage II colorectal cancer in 9 patients (384). This was significantly longer (P=0.04) than the time between serum carcinoembryonic antigen elevation (a serological marker of colorectal cancer) and radiological recurrence (median 61 days; interquartile range 81-279 days) (384). Furthermore, the $TRACER_X$ lung cancer study showed that in 13 patients the median interval between ctDNA detection and NSCLC relapse confirmed by CT imaging indicated by clinical and chest radiograph follow-up was 70 days (range, 10–346 days) (428). Although these are small cohorts of patients and require further validations in larger studies, these data provide proof-of-principle that longitudinal monitoring of ctDNA identifies early relapse of cancer.

7.4.2.3. Monitoring for treatment response to adjuvant therapy

The ability to perform longitudinal ctDNA surveillance also enables monitoring of treatment response to adjuvant therapy and early identification of treatment failure. A study in 52 patients with stage II colorectal cancer showed that detectable ctDNA (6/52 patients) immediately after adjuvant chemotherapy was associated with poorer RFS (HR 11; 95% CI, 1.8 to 68; P=0.001) (384). In addition, 5 patients had a change of ctDNA from positive to negative during the course of their adjuvant therapy with 3/5 not recurring and 2/5 relapsing in ctDNA followed by radiological recurrence a few months later (384).

Although there are very few publications regarding monitoring of response to adjuvant therapy, the ability to monitor for response to treatment in the stage IV setting has been widely

described including data from our group that ctDNA can be used to monitor patients undergoing treatment with targeted, immune and chemotherapy (136,270). Longitudinal ctDNA levels reflected responses seen on scan in 7 patients treated with immune and targeted therapy (136,270). One example was a patient who presented with rapidly progressing metastatic *BRAF* V600R mutant melanoma (136). Ipilimumab was ineffective, but the melanoma responded to D+T, with tumour shrinkage in multiple lesions, which was seen in the ctDNA whereas serum LDH failed to predict these responses (136). Another patient with mucosal melanoma had a heterogeneous response to therapy and using ctDNA we identified two subclones; one with a *KIT* mutation that responded to imatinib and a second *KIT*-wild-type subclone that did not respond to imatinib (270). However, both subclones responded to carboplatin/paclitaxel (270). This study revealed the power of ctDNA to understand causes of heterogeneous treatment responses without the need for multiple tumour biopsies, which has been reported in a number of similar studies (377,389,430,460).

Future research in melanoma should focus on ctDNA monitoring of response to both adjuvant targeted and immune therapy. This could be within the context of a clinical trial where a new treatment is initiated based on molecular relapse during/post adjuvant therapy.

7.5 Summary and conclusions

In this thesis, I have explored a number of approaches to precision medicine in melanoma. Resistance remains a challenge even with the next generation of MAPK pathway inhibitors such as CCT3833. However, combination treatment with a PI3K inhibitor can overcome some of the potential mechanisms of resistance in both *BRAF* and *NRAS* mutant melanoma. Furthermore, as tumours develop resistance to targeted therapy, they become increasingly vulnerable to ERK hyperactivation. This can be augmented using a PKC agonist resulting in decreased cell growth. The tumour microenvironment can affect response to therapy and therefore strategies are needed which target not only cell-intrinsic, but also cell-extrinsic mechanisms of resistance. Finally, I show how ctDNA can be used as a dynamic marker of tumour burden and activity, which can be used to inform treatment changes and to detect early progression. Therefore, it is a useful tool to guide precision medicine approaches in melanoma management.

In the future, I would envision that ctDNA becomes an integral part of the management of melanoma and other types of cancer. In patients diagnosed with early stage melanoma it may be used to detect early relapse, perhaps in combination with other multi-omics markers of progression. In stage IV melanoma, it may guide therapy switches and inform as to whether patients are unlikely to respond to the next line of treatment or point towards a better combination strategy for that individual.

Immune therapy will continue to be a huge area of focus in melanoma, although benefits may be more incremental than the paradigm shifts seen with checkpoint inhibitors. Oncolytic viruses, personalised vaccines and cell-based therapies are likely to be some of the key therapeutic areas over the next 10 years. Biomarker research defining different patient and tumour characteristics such as gene signatures in which certain immune therapy combinations may have greater efficacy will enable precision immune therapy to be given. Furthermore, we

will improve how different therapies are scheduled, with adaptive strategies combining both immune and MAPK targeting therapies with other therapies targeting different elements regulating the MAPK pathway such as PKC agonists or drugs that target cells when they have undergone a phenotypic switch. Future research will improve blood-based RNA biomarkers to show when phenotypic switching has occurred in order that it can be targeted at the right time or to better predict for response to immune therapy without having to perform biopsies.

Melanoma management has completely changed over the past 10 years resulting in huge improvements in survival and quality of life for patients. This thesis demonstrates possible approaches to improve treatments already in the clinic by correctly timing their use and combining them with other agents. We now have the tools to be able to guide precision medicine in melanoma and trials such as CAcTUS and DETECTION may help translate these preclinical findings into the clinic.

References

1. Thompson JF, Scolyer RA, Kefford RF. Cutaneous melanoma. Lancet. 2005;365(9460):687–701.
2. Siegel R, Ma J, Zou Z, Jemal A. Cancer statistics, 2014. CA Cancer J Clin. 64(1):9–29.
3. Cancer Research UK. Skin cancer statistics [Internet]. Cancer Research UK; 2015 [cited 2015 Jan 13]. Available from: http://www.cancerresearchuk.org/cancer-info/cancerstats/types/skin/
4. Gershenwald JE, Scolyer RA, Hess KR, Sondak VK, Long G V., Ross MI, et al. Melanoma staging: Evidence-based changes in the American Joint Committee on Cancer eighth edition cancer staging manual. CA Cancer J Clin. 2017;67(6):472–92.
5. Balch CM, Gershenwald JE, Soong S-J, Thompson JF, Atkins MB, Byrd DR, et al. Final version of 2009 AJCC melanoma staging and classification. J Clin Oncol. 2009;27(36):6199–206.
6. Lee RJ, Ul-Ain-Tariq N, Fusi A, Bowyer S, Lorigan P. The role of chemotherapy in the modern management of melanoma. Melanoma Manag. 2014;1(2):173–84.
7. Chapman PB, Hauschild A, Robert C, Haanen JB, Ascierto P, Larkin J, et al. Updated overall survival (OS) results for BRIM-3, a phase III randomized, open-label, multicenter trial comparing BRAF inhibitor vemurafenib (vem) with dacarbazine (DTIC) in previously untreated patients w. J Clin Oncol. 2012;30:8502.
8. Flaherty KT, Infante JR, Daud A, Gonzalez R, Kefford RF, Sosman J, et al. Combined BRAF and MEK inhibition in melanoma with BRAF V600 mutations. N Engl J Med. 2012;367(18):1694–703.
9. Long G V., Stroyakovskiy D, Gogas H, Levchenko E, de Braud F, Larkin J, et al.

Combined BRAF and MEK Inhibition versus BRAF Inhibition Alone in Melanoma. N Engl J Med. 2014;371(20):1877–88.

10. Schadendorf D, et al. Pooled analysis of long-term survival data from phase II and phase III trials of ipilimumab in metastatic or locally advanced, unresectable melanoma. ESMO Annu Meet. 2013;Abstract 24.
11. Hodi FS, O'Day SJ, McDermott DF, Weber RW, Sosman J a, Haanen JB, et al. Improved survival with ipilimumab in patients with metastatic melanoma. N Engl J Med. 2010;363(8):711–23.
12. Gray-Schopfer V, Wellbrock C, Marais R. Melanoma biology and new targeted therapy. Nature. 2007;445(7130):851–7.
13. Smoller BR. Histologic criteria for diagnosing primary cutaneous malignant melanoma. Mod Pathol. 2006;19 Suppl 2(S2):S34-40.
14. Garbe C, Leiter U. Melanoma epidemiology and trends. Clin Dermatol. 2009;27(1):3–9.
15. Bradford PT, Goldstein AM, McMaster ML, Tucker MA. Acral lentiginous melanoma: incidence and survival patterns in the United States, 1986-2005. Arch Dermatol. 2009;145(4):427–34.
16. Singh AD, Bergman L, Seregard S. Uveal melanoma: epidemiologic aspects. Ophthalmol Clin North Am. 2005;18(1):75–84, viii.
17. Satzger I, Schaefer T, Kuettler U, Broecker V, Voelker B, Ostertag H, et al. Analysis of c-KIT expression and KIT gene mutation in human mucosal melanomas. Br J Cancer. 2008;99(12):2065–9.
18. Zhang W, Liu HT. MAPK signal pathways in the regulation of cell proliferation in mammalian cells. Cell Res. 2002;12(1):9–18.
19. Marshall C. J. Specificity of receptor tyrosine kinase signaling: Transient versus sustained extracellular signal-regulated kinase activation. Cell. 1995;80(2):179–85.

20. Marshall CJ. MAP kinase kinase kinase, MAP kinase kinase and MAP kinase. Curr Opin Genet Dev. 1994;4(1):82–9.

21. Harvey JJ. An unidentified virus which causes the rapid production of tumours in mice. Nature. 1964;204:1104–5.

22. Kirsten WH, Mayer LA. Morphologic responses to a murine erythroblastosis virus. J Natl Cancer Inst. 1967;39(2):311–35.

23. McCormick F. How receptors turn Ras on. Nature. 1993;363(6424):15–6.

24. Warne PH, Vician PR, Downward J. Direct interaction of Ras and the amino-terminal region of Raf-1 in vitro. Nature. 1993;364(6435):352–5.

25. Zhang X-F, Settleman J, Kyriakis J, Takeuchi-Suzuki E, Elledge SJ, Marshall MS, et al. Normal and oncogenic p21ras proteins bind to the amino-terminal regulatory domain of c-Raf-1. Nature. 1993;364(6435):308–13.

26. Vojtek AB, Hollenberg SM, Cooper JA. Mammalian Ras interacts directly with the serine/threonine kinase Raf. Cell. 1993;74(1):205–14.

27. Kyriakis JM, App H, Zhang X, Banerjee P, Brautigan DL, Rapp UR, et al. Raf-1 activates MAP kinase-kinase. Nature. 1992;358(6385):417–21.

28. Anderson NG, Maller JL, Tonks NK, Sturgill TW. Requirement for integration of signals from two distinct phosphorylation pathways for activation of MAP kinase. Nature. 1990;343(6259):651–3.

29. Roskoski R. ERK1/2 MAP kinases: Structure, function, and regulation. Pharmacol Res. 2012;66(2):105–43.

30. Yoon S, Seger R. The extracellular signal-regulated kinase: Multiple substrates regulate diverse cellular functions. Growth Factors. 2006;24(1):21–44.

31. Boulton TG, Yancopoulos GD, Gregory JS, Slaughter C, Moomaw C, Hsu J, et al. An insulin-stimulated protein kinase similar to yeast kinases involved in cell cycle control.

Science. 1990;249(4964):64–7.

32. Eblen ST, Kumar NV, Shah K, Henderson MJ, Watts CKW, Shokat KM, et al. Identification of Novel ERK2 Substrates through Use of an Engineered Kinase and ATP Analogs. J Biol Chem. 2003;278(17):14926–35.

33. Lewis TS, Hunt JB, Aveline LD, Jonscher KR, Louie DF, Yeh JM, et al. Identification of novel MAP kinase pathway signaling targets by functional proteomics and mass spectrometry. Mol Cell. 2000;6(6):1343–54.

34. Baljuls A, Mueller T, Drexler HCA, Hekman M, Rapp UR. Unique N-region determines low basal activity and limited inducibility of A-RAF kinase: the role of N-region in the evolutionary divergence of RAF kinase function in vertebrates. J Biol Chem. 2007;282(36):26575–90.

35. Marais R, Light Y, Paterson HF, Marshall CJ. Ras recruits Raf-1 to the plasma membrane for activation by tyrosine phosphorylation. EMBO J. 1995;14(13):3136–45.

36. Hu J, Stites EC, Yu H, Germino EA, Meharena HS, Stork PJS, et al. Allosteric activation of functionally asymmetric RAF kinase dimers. Cell. 2013;154(5):1036–46.

37. Lo YY, Wong JM, Cruz TF. Reactive oxygen species mediate cytokine activation of c-Jun NH2-terminal kinases. J Biol Chem. 1996;271(26):15703–7.

38. Sluss HK, Barrett T, Dérijard B, Davis RJ. Signal transduction by tumor necrosis factor mediated by JNK protein kinases. Mol Cell Biol. 1994;14(12):8376–84.

39. Davis RJ. Signal transduction by the JNK group of MAP kinases. Cell. 2000;103(2):239–52.

40. Dérijard B, Raingeaud J, Barrett T, Wu IH, Han J, Ulevitch RJ, et al. Independent human MAP-kinase signal transduction pathways defined by MEK and MKK isoforms. Science. 1995;267(5198):682–5.

41. Lawler S, Cuenda A, Goedert M, Cohen P. SKK4, a novel activator of stress-activated

protein kinase-1 (SAPK1/JNK). FEBS Lett. 1997;414:153–8.

42. Xia Y, Wu Z, Su B, Murray B, Karin M. JNKK1 organizes a MAP kinase module through specific and sequential interactions with upstream and downstream components mediated by its amino-terminal extension. Genes Dev. 1998;12(21):3369–81.

43. Lu X, Nemoto S, Lin A. Identification of c-Jun NH2-terminal protein kinase (JNK)-activating kinase 2 as an activator of JNK but not p38. J Biol Chem. 1997;272(40):24751–4.

44. Ellinger-Ziegelbauer H, Brown K, Kelly K, Siebenlist U. Direct activation of the stress-activated protein kinase (SAPK) and extracellular signal-regulated protein kinase (ERK) pathways by an inducible mitogen-activated protein Kinase/ERK kinase kinase 3 (MEKK) derivative. J Biol Chem. 1997;272(5):2668–74.

45. Yan M, Dai T, Deak JC, Kyriakis JM, Zon LI, Woodgett JR, et al. Activation of stress-activated protein kinase by MEKK1 phosphorylation of its activator SEK1. Nature. 372(6508):798–800.

46. Minden A, Lin A, McMahon M, Lange-Carter C, Dérijard B, Davis RJ, et al. Differential activation of ERK and JNK mitogen-activated protein kinases by Raf-1 and MEKK. Science. 1994;266(5191):1719–23.

47. Lange-Carter CA, Pleiman CM, Gardner AM, Blumer KJ, Johnson GL. A divergence in the MAP kinase regulatory network defined by MEK kinase and Raf. Science (80-). 1993;260(5106):315 LP-319.

48. Ichijo H, Nishida E, Irie K, ten Dijke P, Saitoh M, Moriguchi T, et al. Induction of apoptosis by ASK1, a mammalian MAPKKK that activates SAPK/JNK and p38 signaling pathways. Science. 1997;275(5296):90–4.

49. Gupta S, Barrett T, Whitmarsh AJ, Cavanagh J, Sluss HK, Dérijard B, et al. Selective interaction of JNK protein kinase isoforms with transcription factors. EMBO J.

1996;15(11):2760–70.

50. Ip YT, Davis RJ. Signal transduction by the c-Jun N-terminal kinase (JNK) — from inflammation to development. Curr Opin Cell Biol. 1998;10(2):205–19.

51. Yang D, Tournier C, Wysk M, Lu HT, Xu J, Davis RJ, et al. Targeted disruption of the MKK4 gene causes embryonic death, inhibition of c-Jun NH2-terminal kinase activation, and defects in AP-1 transcriptional activity. Proc Natl Acad Sci U S A. 1997;94(7):3004–9.

52. Shaulian E, Karin M. AP-1 as a regulator of cell life and death. Nat Cell Biol. 2002;4(5):E131–6.

53. Kovary K, Bravo R. The jun and fos protein families are both required for cell cycle progression in fibroblasts. Mol Cell Biol. 1991;11(9):4466–72.

54. Brown JR, Nigh E, Lee RJ, Ye H, Thompson MA, Saudou F, et al. Fos family members induce cell cycle entry by activating cyclin D1. Mol Cell Biol. 1998;18(9):5609–19.

55. Bakiri L, Lallemand D, Bossy-Wetzel E, Yaniv M. Cell cycle-dependent variations in c-Jun and JunB phosphorylation: a role in the control of cyclin D1 expression. EMBO J. 2000;19(9):2056–68.

56. Shaulian E, Karin M. AP-1 in cell proliferation and survival. Oncogene. 2001;20(19):2390–400.

57. Lee JC, Laydon JT, McDonnell PC, Gallagher TF, Kumar S, Green D, et al. A protein kinase involved in the regulation of inflammatory cytokine biosynthesis. Nature. 1994;372(6508):739–46.

58. Zarubin T, Han J. Activation and signaling of the p38 MAP kinase pathway. Cell Res. 2005;15(1):11–8.

59. Jiang Y, Gram H, Zhao M, New L, Gu J, Feng L, et al. Characterization of the structure and function of the fourth member of p38 group mitogen-activated protein kinases,

p38delta. J Biol Chem. 1997;272(48):30122–8.

60. Jiang Y, Chen C, Li Z, Guo W, Gegner JA, Lin S, et al. Characterization of the structure and function of a new mitogen-activated protein kinase (p38beta). J Biol Chem. 1996;271(30):17920–6.

61. Kumar S, McDonnell PC, Gum RJ, Hand AT, Lee JC, Young PR. Novel Homologues of CSBP/p38 MAP Kinase: Activation, Substrate Specificity and Sensitivity to Inhibition by Pyridinyl Imidazoles. Biochem Biophys Res Commun. 1997;235(3):533–8.

62. Ge B, Gram H, Di Padova F, Huang B, New L, Ulevitch RJ, et al. MAPKK-Independent Activation of p38alpha Mediated by TAB1-Dependent Autophosphorylation of p38alpha. Science (80-). 2002;295(5558):1291–4.

63. Janknecht R, Hunter T. Convergence of MAP kinase pathways on the ternary complex factor Sap-1a. EMBO J. 1997;16(7):1620–7.

64. Whitmarsh AJ, Yang SH, Su MS, Sharrocks AD, Davis RJ. Role of p38 and JNK mitogen-activated protein kinases in the activation of ternary complex factors. Mol Cell Biol. 1997;17(5):2360–71.

65. Han J, Jiang Y, Li Z, Kravchenko V V., Ulevitch RJ. Activation of the transcription factor MEF2C by the MAP kinase p38 in inflammation. Nature. 1997;386(6622):296–9.

66. Huang C, Ma WY, Maxiner A, Sun Y, Dong Z. p38 kinase mediates UV-induced phosphorylation of p53 protein at serine 389. J Biol Chem. 1999;274(18):12229–35.

67. Guan Z, Buckman SY, Pentland AP, Templeton DJ, Morrison AR. Induction of cyclooxygenase-2 by the activated MEKK1; SEK1/MKK4; p38 mitogen-activated protein kinase pathway. J Biol Chem. 1998;273(21):12901–8.

68. Badger AM, Cook MN, Lark MW, Newman-Tarr TM, Swift BA, Nelson AH, et al. SB 203580 inhibits p38 mitogen-activated protein kinase, nitric oxide production, and inducible nitric oxide synthase in bovine cartilage-derived chondrocytes. J Immunol.

1998;161(1):467–73.

69. Pietersma A, Tilly BC, Gaestel M, de Jong N, Lee JC, Koster JF, et al. P38 Mitogen Activated Protein Kinase Regulates Endothelial VCAM-1 Expression at the Post-transcriptional Level. Biochem Biophys Res Commun. 1997;230(1):44–8.

70. Da Silva J, Pierrat B, Mary JL, Lesslauer W. Blockade of p38 mitogen-activated protein kinase pathway inhibits inducible nitric-oxide synthase expression in mouse astrocytes. J Biol Chem. 1997;272(45):28373–80.

71. Heidorn SJ, Milagre C, Whittaker S, Nourry A, Niculescu-Duvas I, Dhomen N, et al. Kinase-dead BRAF and oncogenic RAS cooperate to drive tumor progression through CRAF. Cell. 2010;140(2):209–21.

72. Siroy AE, Boland GM, Milton DR, Roszik J, Frankian S, Malke J, et al. Beyond BRAF(V600): Clinical Mutation Panel Testing by Next-Generation Sequencing in Advanced Melanoma. J Invest Dermatol. 2015;135(2):508–15.

73. Jakob JA, Bassett RL, Ng CS, Curry JL, Joseph RW, Alvarado GC, et al. NRAS mutation status is an independent prognostic factor in metastatic melanoma. Cancer. 2012;118(16):4014–23.

74. Hodis E, Watson IR, Kryukov G V, Arold ST, Imielinski M, Theurillat J-P, et al. A landscape of driver mutations in melanoma. Cell. 2012;150(2):251–63.

75. Curtin JA, Fridlyand J, Kageshita T, Patel HN, Busam KJ, Kutzner H, et al. Distinct Sets of Genetic Alterations in Melanoma. N Engl J Med. 2005;353(20):2135–47.

76. Furney SJ, Turajlic S, Stamp G, Thomas JM, Hayes A, Strauss D, et al. The mutational burden of acral melanoma revealed by whole-genome sequencing and comparative analysis. Pigment Cell Melanoma Res. 2014;27(5):835–8.

77. Turajlic S, Furney SJ, Lambros MB, Mitsopoulos C, Kozarewa I, Geyer FC, et al. Whole genome sequencing of matched primary and metastatic acral melanomas. Genome Res.

2012;22(2):196–207.

78. Van Raamsdonk CD, Griewank KG, Crosby MB, Garrido MC, Vemula S, Wiesner T, et al. Mutations in GNA11 in uveal melanoma. N Engl J Med. 2010;363(23):2191–9.

79. Van Raamsdonk CD, Bezrookove V, Green G, Bauer J, Gaugler L, O'Brien JM, et al. Frequent somatic mutations of GNAQ in uveal melanoma and blue naevi. Nature. 2009;457(7229):599–602.

80. Harbour JW, Onken MD, Roberson EDO, Duan S, Cao L, Worley LA, et al. Frequent mutation of BAP1 in metastasizing uveal melanomas. Science. 2010;330(6009):1410–3.

81. Furney SJ, Pedersen M, Gentien D, Dumont AG, Rapinat A, Desjardins L, et al. SF3B1 mutations are associated with alternative splicing in uveal melanoma. Cancer Discov. 2013;3(10):1122–9.

82. Lake D, Corrêa SAL, Müller J. Negative feedback regulation of the ERK1/2 MAPK pathway. Cell Mol Life Sci. 2016;73(23):4397–413.

83. Zakrzewska M, Haugsten EM, Nadratowska-Wesolowska B, Oppelt A, Hausott B, Jin Y, et al. ERK-Mediated Phosphorylation of Fibroblast Growth Factor Receptor 1 on Ser777 Inhibits Signaling. Sci Signal. 2013;6(262):ra11-ra11.

84. Mandl M, Slack DN, Keyse SM. Specific Inactivation and Nuclear Anchoring of Extracellular Signal-Regulated Kinase 2 by the Inducible Dual-Specificity Protein Phosphatase DUSP5. Mol Cell Biol. 2005;25(5):1830–45.

85. Karlsson M, Mathers J, Dickinson RJ, Mandl M, Keyse SM. Both Nuclear-Cytoplasmic Shuttling of the Dual Specificity Phosphatase MKP-3 and Its Ability to Anchor MAP Kinase in the Cytoplasm Are Mediated by a Conserved Nuclear Export Signal. J Biol Chem. 2004;279(40):41882–91.

86. Ozaki K, Kadomoto R, Asato K, Tanimura S, Itoh N, Kohno M. ERK Pathway Positively Regulates the Expression of Sprouty Genes. 2001;

87. Yusoff P, Lao D-H, Ong SH, Wong ESM, Lim J, Lo TL, et al. Sprouty2 Inhibits the Ras/MAP Kinase Pathway by Inhibiting the Activation of Raf. J Biol Chem. 2002;277(5):3195–201.

88. Hanafusa H, Torii S, Yasunaga T, Nishida E. Sprouty1 and Sprouty2 provide a control mechanism for the Ras/MAPK signalling pathway. Nat Cell Biol. 2002;4(11):850–8.

89. Sasaki A, Taketomi T, Kato R, Saeki K, Nonami A, Sasaki M, et al. Mammalian Sprouty4 suppresses Ras-independent ERK activation by binding to Raf1. Nat Cell Biol. 2003;5(5):427–32.

90. Rosse C, Linch M, Kermorgant S, Cameron AJM, Boeckeler K, Parker PJ. PKC and the control of localized signal dynamics. Nat Rev Mol Cell Biol. 2010;11(2):103–12.

91. Mellor H, Parker PJ. The extended protein kinase C superfamily. Biochem J. 1998;332 (Pt 2):281–92.

92. Horikoshi Y, Suzuki A, Yamanaka T, Sasaki K, Mizuno K, Sawada H, et al. Interaction between PAR-3 and the aPKC-PAR-6 complex is indispensable for apical domain development of epithelial cells. J Cell Sci. 2009;122(10):1595–606.

93. Marais R, Light Y, Mason C, Paterson H, Olson MF, Marshall CJ. Requirement of Ras-GTP-Raf complexes for activation of Raf-1 by protein kinase C. Science. 1998;280(5360):109–12.

94. Rosse C, Formstecher E, Boeckeler K, Zhao Y, Kremerskothen J, White MD, et al. An aPKC-Exocyst Complex Controls Paxillin Phosphorylation and Migration through Localised JNK1 Activation. Yamada KM, editor. PLoS Biol. 2009;7(11):e1000235.

95. Ng T, Shima D, Squire A, Bastiaens PIH, Gschmeissner S, Humphries MJ, et al. PKCα regulates β1 integrin-dependent cell motility through association and control of integrin traffic. EMBO J. 1999;18(14):3909–23.

96. Watts JL, Etemad-Moghadam B, Guo S, Boyd L, Draper BW, Mello CC, et al. par-6, a

gene involved in the establishment of asymmetry in early C. elegans embryos, mediates the asymmetric localization of PAR-3. Development. 1996;122(10):3133–40.

97. Kermorgant S, Parker PJ. Receptor trafficking controls weak signal delivery: a strategy used by c-Met for STAT3 nuclear accumulation. J Cell Biol. 2008;182(5):855–63.

98. Marsland BJ, Kopf M. T-cell fate and function: PKC-θ and beyond. Trends Immunol. 2008;29(4):179–85.

99. Davies MA. The role of the PI3K-AKT pathway in melanoma. Cancer J. 2012;18(2):142–7.

100. Auger KR, Serunian LA, Soltoff SP, Libby P, Cantley LC. PDGF-dependent tyrosine phosphorylation stimulates production of novel polyphosphoinositides in intact cells. Cell. 1989;57(1):167–75.

101. Whitman M, Downes CP, Keeler M, Keller T, Cantley L. Type I phosphatidylinositol kinase makes a novel inositol phospholipid, phosphatidylinositol-3-phosphate. Nature. 1988;332(6165):644–6.

102. Chang HW, Aoki M, Fruman D, Auger KR, Bellacosa A, Tsichlis PN, et al. Transformation of chicken cells by the gene encoding the catalytic subunit of PI 3-kinase. Science. 1997;276(5320):1848–50.

103. Fruman DA, Chiu H, Hopkins BD, Bagrodia S, Cantley LC, Abraham RT. Leading Edge The PI3K Pathway in Human Disease. Cell. 2017;170:605–35.

104. De Henau O, Rausch M, Winkler D, Campesato LF, Liu C, Cymerman DH, et al. Overcoming resistance to checkpoint blockade therapy by targeting PI3Kγ in myeloid cells. Nature. 2016;539(7629):1–16.

105. Kaneda MM, Messer KS, Ralainirina N, Li H, Leem C, Gorjestani S, et al. PI3Kγ is a molecular switch that controls immune suppression. Nature. 2016;539(7629):437–42.

106. Herter S, Palazzo A, Bacac M, Grosmaire L, Frey C, Pflanz S, et al. The PI3K Delta

Selective Inhibitor Idelalisib Minimally Interferes with Immune Effector Function and B Cell Depletion Mediated By Obinutuzumab (GA101) and Rituximab. Blood. 2014;124(21).

107. Samuels Y, Wang Z, Bardelli A, Silliman N, Ptak J, Szabo S, et al. High frequency of mutations of the PIK3CA gene in human cancers. Science. 2004;304(5670):554.

108. Li DM, Sun H. PTEN/MMAC1/TEP1 suppresses the tumorigenicity and induces G1 cell cycle arrest in human glioblastoma cells. Proc Natl Acad Sci U S A. 1998;95(26):15406–11.

109. Myers MP, Pass I, Batty IH, Van der Kaay J, Stolarov JP, Hemmings BA, et al. The lipid phosphatase activity of PTEN is critical for its tumor supressor function. Proc Natl Acad Sci U S A. 1998;95(23):13513–8.

110. Chin L, Garraway LA, Fisher DE. Malignant melanoma: genetics and therapeutics in the genomic era. Genes Dev. 2006;20(16):2149–82.

111. Di Leo A, Johnston S, Lee KS, Ciruelos E, Lønning PE, Janni W, et al. Buparlisib plus fulvestrant in postmenopausal women with hormone-receptor-positive, HER2-negative, advanced breast cancer progressing on or after mTOR inhibition (BELLE-3): a randomised, double-blind, placebo-controlled, phase 3 trial. Lancet Oncol. 2018;19(1):87–100.

112. Baselga J, Dent S., Cortés J, Im Y, Diéras V, Harbeck N, et al. Phase III study of taselisib (GDC-0032) + fulvestrant (FULV) v FULV in patients (pts) with estrogen receptor (ER)-positive, PIK3CA-mutant (MUT), locally advanced or metastatic breast cancer (MBC): Primary analysis from SANDPIPER. | 2018 ASCO Annual Meetin. In: ASCO Annual Meeting. Chicago; 2018.

113. Hopkins BD, Pauli C, Xing D, Wang DG, Li X, Wu D, et al. Suppression of insulin feedback enhances the efficacy of PI3K inhibitors. Nature. 2018;560(7719):499–503.

114. Chapman PB, Hauschild A, Robert C, Haanen JB, Ascierto P, Larkin J, et al. Improved survival with vemurafenib in melanoma with BRAF V600E mutation. N Engl J Med. 2011;364(26):2507–16.

115. Schadendorf D, Flaherty KT, Hersey P, Nathan PD, Garbe C, Milhem MM, et al. Overall survival (OS) update on METRIC (NCT01245062), a randomized phase 3 study to assess efficacy of trametinib (T) compared with chemotherapy (C) in patients (pts) with BRAFV600E/K mutation positive (+) advanced or metastatic melanoma (MM). Pigment Cell Melanoma Res. 2013;26(6):997.

116. Center for Drug Evaluation and Research. Approved Drugs - Hematology/Oncology (Cancer) Approvals & Safety Notifications [Internet]. Center for Drug Evaluation and Research; [cited 2015 Jan 18]. Available from: http://www.fda.gov/Drugs/InformationOnDrugs/ApprovedDrugs/ucm279174.htm

117. Hauschild A, Grob J-J, Demidov L V, Jouary T, Gutzmer R, Millward M, et al. Dabrafenib in BRAF-mutated metastatic melanoma: a multicentre, open-label, phase 3 randomised controlled trial. Lancet. 2012;380(9839):358–65.

118. Dummer R, Ascierto PA, Gogas HJ, Arance A, Mandala M, Liszkay G, et al. Encorafenib plus binimetinib versus vemurafenib or encorafenib in patients with BRAF -mutant melanoma (COLUMBUS): a multicentre, open-label, randomised phase 3 trial. Lancet Oncol. 2018;19(5):603–15.

119. Larkin J, Ascierto PA, Dréno B, Atkinson V, Liszkay G, Maio M, et al. Combined Vemurafenib and Cobimetinib in BRAF-Mutated Melanoma. N Engl J Med. 2014;371(20):1867–76.

120. Long G V, Stroyakovskiy D, Gogas H, Levchenko E, de Braud F, Larkin J, et al. Dabrafenib and trametinib versus dabrafenib and placebo for Val600 BRAF-mutant melanoma: a multicentre, double-blind, phase 3 randomised controlled trial. Lancet.

2015;

121. Ugurel S, Loquai C, Kähler K, Hassel J, Berking C, Zimmer L, et al. A multicenter DeCOG study on predictors of vemurafenib therapy outcome in melanoma: pretreatment impacts survival. Ann Oncol. 2015;26(3):573–82.

122. Long G V, Grob J-J, Nathan P, Ribas A, Robert C, Schadendorf D, et al. Factors predictive of response, disease progression, and overall survival after dabrafenib and trametinib combination treatment: a pooled analysis of individual patient data from randomised trials. Lancet Oncol. 2016;17(12):1743–54.

123. McArthur GA, Puzanov I, Amaravadi R, Ribas A, Chapman P, Kim KB, et al. Marked, Homogeneous, and Early [^{18} F]Fluorodeoxyglucose–Positron Emission Tomography Responses to Vemurafenib in *BRAF* -Mutant Advanced Melanoma. J Clin Oncol. 2012;30(14):1628–34.

124. McQuade JL, Daniel CR, Hess KR, Mak C, Wang DY, Rai RR, et al. Association of body-mass index and outcomes in patients with metastatic melanoma treated with targeted therapy, immunotherapy, or chemotherapy: a retrospective, multicohort analysis. Lancet Oncol. 2018;19(3):310–22.

125. Poulikakos PI, Persaud Y, Janakiraman M, Kong X, Ng C, Moriceau G, et al. RAF inhibitor resistance is mediated by dimerization of aberrantly spliced BRAF(V600E). Nature. 2011;480(7377):387–90.

126. Girotti MR, Marais R. Deja Vu: EGF receptors drive resistance to BRAF inhibitors. Cancer Discov. 2013;3(5):487–90.

127. Girotti MR, Pedersen M, Sanchez-Laorden B, Viros A, Turajlic S, Niculescu-Duvaz D, et al. Inhibiting EGF receptor or SRC family kinase signaling overcomes BRAF inhibitor resistance in melanoma. Cancer Discov. 2013;3(2):158–67.

128. Shi H, Hugo W, Kong X, Hong A, Koya RC, Moriceau G, et al. Acquired resistance and

clonal evolution in melanoma during BRAF inhibitor therapy. Cancer Discov. 2014;4(1):80–93.

129. Shi H, Hong A, Kong X, Koya RC, Song C, Moriceau G, et al. A novel AKT1 mutant amplifies an adaptive melanoma response to BRAF inhibition. Cancer Discov. 2014;4(1):69–79.

130. Lu H, Liu S, Zhang G, Bin Wu B, Zhu Y, Frederick DT, et al. PAK signalling drives acquired drug resistance to MAPK inhibitors in BRAF-mutant melanomas. Nature. 2017;550(7674):133.

131. Scholtens A, Geukes Foppen MH, Blank CU, van Thienen JV, van Tinteren H, Haanen JB. Vemurafenib for BRAF V600 mutated advanced melanoma: Results of treatment beyond progression. Eur J Cancer. 2015;51(5):642–52.

132. Chan MMK, Haydu LE, Menzies AM, Azer MWF, Klein O, Lyle M, et al. The nature and management of metastatic melanoma after progression on BRAF inhibitors: Effects of extended BRAF inhibition. Cancer. 2014;120(20):3142–53.

133. Tentler JJ, Tan AC, Weekes CD, Jimeno A, Leong S, Pitts TM, et al. Patient-derived tumour xenografts as models for oncology drug development. Nat Rev Clin Oncol. 2012;9(6):338–50.

134. Morton CL, Houghton PJ. Establishment of human tumor xenografts in immunodeficient mice. Nat Protoc. 2007;2(2):247–50.

135. Siolas D, Hannon GJ. Patient-derived tumor xenografts: transforming clinical samples into mouse models. Cancer Res. 2013;73(17):5315–9.

136. Girotti MR, Gremel G, Lee R, Galvani E, Rothwell D, Viros A, et al. Application of Sequencing, Liquid Biopsies, and Patient-Derived Xenografts for Personalized Medicine in Melanoma. Cancer Discov. 2016;6(3):286–99.

137. Hidalgo M, Bruckheimer E, Rajeshkumar N V, Garrido-Laguna I, De Oliveira E, Rubio-

Viqueira B, et al. A pilot clinical study of treatment guided by personalized tumorgrafts in patients with advanced cancer. Mol Cancer Ther. 2011;10(8):1311–6.

138. Fusi A, Metcalf R, Krebs M, Dive C, Blackhall F. Clinical utility of circulating tumour cell detection in non-small-cell lung cancer. Curr Treat Options Oncol. 2013;14(4):610–22.

139. Ashworth TR. A case of cancer in which cells similar to those in the tumors were seen in the blood after death. Aust Med J. 1869;14:146–9.

140. Aceto N, Bardia A, Miyamoto DT, Donaldson MC, Wittner BS, Spencer JA, et al. Circulating Tumor Cell Clusters Are Oligoclonal Precursors of Breast Cancer Metastasis. Cell. 2014;158(5):1110–22.

141. Fidler IJ. Metastasis: guantitative analysis of distribution and fate of tumor embolilabeled with 125 I-5-iodo-2'-deoxyuridine. J Natl Cancer Inst. 1970;45(4):773–82.

142. Reya T, Morrison SJ, Clarke MF, Weissman IL. Stem cells, cancer, and cancer stem cells. Nature. 2001;414(6859):105–11.

143. Tinhofer I, Saki M, Niehr F, Keilholz U, Budach V. Cancer stem cell characteristics of circulating tumor cells. Int J Radiat Biol. 2014;90(8):622–7.

144. Theodoropoulos PA, Polioudaki H, Agelaki S, Kallergi G, Saridaki Z, Mavroudis D, et al. Circulating tumor cells with a putative stem cell phenotype in peripheral blood of patients with breast cancer. Cancer Lett. 2010;288(1):99–106.

145. Chan KS, Espinosa I, Chao M, Wong D, Ailles L, Diehn M, et al. Identification, molecular characterization, clinical prognosis, and therapeutic targeting of human bladder tumor-initiating cells. Proc Natl Acad Sci U S A. 2009;106(33):14016–21.

146. Yu M, Ting DT, Stott SL, Wittner BS, Ozsolak F, Paul S, et al. RNA sequencing of pancreatic circulating tumour cells implicates WNT signalling in metastasis. Nature. 2012;487(7408):510–3.

147. Baccelli I, Schneeweiss A, Riethdorf S, Stenzinger A, Schillert A, Vogel V, et al. Identification of a population of blood circulating tumor cells from breast cancer patients that initiates metastasis in a xenograft assay. Nat Biotechnol. 2013;31(6):539–44.

148. Hodgkinson CL, Morrow CJ, Li Y, Metcalf RL, Rothwell DG, Trapani F, et al. Tumorigenicity and genetic profiling of circulating tumor cells in small-cell lung cancer. Nat Med. 2014;20(8):897–903.

149. Hoek KS, Eichhoff OM, Schlegel NC, Döbbeling U, Kobert N, Schaerer L, et al. In vivo switching of human melanoma cells between proliferative and invasive states. Cancer Res. 2008;68(3):650–6.

150. Hoek KS, Schlegel NC, Brafford P, Sucker A, Ugurel S, Kumar R, et al. Metastatic potential of melanomas defined by specific gene expression profiles with no BRAF signature. Pigment cell Res. 2006;19(4):290–302.

151. Garraway LA, Widlund HR, Rubin MA, Getz G, Berger AJ, Ramaswamy S, et al. Integrative genomic analyses identify MITF as a lineage survival oncogene amplified in malignant melanoma. Nature. 2005;436(7047):117–22.

152. Thomas AJ, Erickson CA. The making of a melanocyte: the specification of melanoblasts from the neural crest. Pigment Cell Melanoma Res. 2008;21(6):598–610.

153. Hoek KS, Goding CR. Cancer stem cells versus phenotype-switching in melanoma. Pigment Cell Melanoma Res. 2010;23(6):746–59.

154. Nishimura EK, Granter SR, Fisher DE. Mechanisms of Hair Graying: Incomplete Melanocyte Stem Cell Maintenance in the Niche. Science (80-). 2005;307(5710):720–4.

155. Nishimura EK, Suzuki M, Igras V, Du J, Lonning S, Miyachi Y, et al. Key Roles for Transforming Growth Factor β in Melanocyte Stem Cell Maintenance. Cell Stem Cell. 2010;6(2):130–40.

156. Osawa M, Egawa G, Mak S-S, Moriyama M, Freter R, Yonetani S, et al. Molecular

characterization of melanocyte stem cells in their niche. Development. 2005;132(24):5589–99.

157. Dorsky RI, Raible DW, Moon RT. Direct regulation of nacre, a zebrafish MITF homolog required for pigment cell formation, by the Wnt pathway. Genes Dev. 2000;14(2):158–62.

158. Mansky KC, Sankar U, Han J, Ostrowski MC. Microphthalmia Transcription Factor Is a Target of the p38 MAPK Pathway in Response to Receptor Activator of NF-κB Ligand Signaling. J Biol Chem. 2002;277(13):11077–83.

159. Takeda K, Yasumoto K, Takada R, Takada S, Watanabe K, Udono T, et al. Induction of melanocyte-specific microphthalmia-associated transcription factor by Wnt-3a. J Biol Chem. 2000;275(19):14013–6.

160. Rambow F, Rogiers A, Marin-Bejar O, Aibar S, Femel J, Dewaele M, et al. Toward Minimal Residual Disease-Directed Therapy in Melanoma. Cell. 2018;174(4):843–855.e19.

161. McGill GG, Horstmann M, Widlund HR, Du J, Motyckova G, Nishimura EK, et al. Bcl2 regulation by the melanocyte master regulator Mitf modulates lineage survival and melanoma cell viability. Cell. 2002;109(6):707–18.

162. Du J, Widlund HR, Horstmann MA, Ramaswamy S, Ross K, Huber WE, et al. Critical role of CDK2 for melanoma growth linked to its melanocyte-specific transcriptional regulation by MITF. Cancer Cell. 2004;6(6):565–76.

163. Müller J, Krijgsman O, Tsoi J, Robert L, Hugo W, Song C, et al. Low MITF/AXL ratio predicts early resistance to multiple targeted drugs in melanoma. Nat Commun. 2014;5:5712.

164. Lee RJ, Marais R. Cancer: Tumours addicted to drugs are vulnerable. Nature. 2017;550(7675):192–3.

165. Kong X, Kuilman T, Shahrabi A, Boshuizen J, Kemper K, Song J-Y, et al. Cancer drug addiction is relayed by an ERK2-dependent phenotype switch. Nature. 2017;550(7675):nature24037.

166. Hong A, Moriceau G, Sun L, Lomeli S, Piva M, Damoiseaux R, et al. Exploiting Drug Addiction Mechanisms to Select against MAPKi-Resistant Melanoma. Cancer Discov. 2018;8(1):74–93.

167. Das Thakur M, Salangsang F, Landman AS, Sellers WR, Pryer NK, Levesque MP, et al. Modelling vemurafenib resistance in melanoma reveals a strategy to forestall drug resistance. Nature. 2013;494(7436):251–5.

168. Moriceau G, Hugo W, Hong A, Shi H, Kong X, Yu CC, et al. Tunable-combinatorial mechanisms of acquired resistance limit the efficacy of BRAF/MEK cotargeting but result in melanoma drug addiction. Cancer Cell. 2015;27(2):240–56.

169. Wei SC, Duffy CR, Allison JP. Fundamental Mechanisms of Immune Checkpoint Blockade Therapy. Cancer Discov. 2018;8(9):1069–86.

170. Murata S, Sasaki K, Kishimoto T, Niwa S -i., Hayashi H, Takahama Y, et al. Regulation of CD8+ T Cell Development by Thymus-Specific Proteasomes. Science (80-). 2007;316(5829):1349–53.

171. Sakaguchi S, Sakaguchi N, Asano M, Itoh M, Toda M. Immunologic self-tolerance maintained by activated T cells expressing IL-2 receptor alpha-chains (CD25). Breakdown of a single mechanism of self-tolerance causes various autoimmune diseases. J Immunol. 1995;155(3):1151–64.

172. Kalekar LA, Schmiel SE, Nandiwada SL, Lam WY, Barsness LO, Zhang N, et al. CD4+ T cell anergy prevents autoimmunity and generates regulatory T cell precursors. Nat Immunol. 2016;17(3):304–14.

173. Carlow DA, Teh SJ, van Oers NS, Miller RG, Teh HS. Peripheral tolerance through

clonal deletion of mature CD4-CD8+ T cells. Int Immunol. 1992;4(5):599–610.

174. Pardoll DM. The blockade of immune checkpoints in cancer immunotherapy. Nat Rev Cancer. 2012;12(4):252–64.

175. Walunas TL, Lenschow DJ, Bakker CY, Linsley PS, Freeman GJ, Green JM, et al. CTLA-4 can function as a negative regulator of T cell activation. Immunity. 1994;1(5):405–13.

176. Leach DR, Krummel MF, Allison JP. Enhancement of antitumor immunity by CTLA-4 blockade. Science. 1996;271(5256):1734–6.

177. Corse E, Allison JP. Cutting Edge: CTLA-4 on Effector T Cells Inhibits In Trans. J Immunol. 2012;189(3):1123–7.

178. Brunner MC, Chambers CA, Chan FK, Hanke J, Winoto A, Allison JP. CTLA-4-Mediated inhibition of early events of T cell proliferation. J Immunol. 1999;162(10):5813–20.

179. van der Merwe PA, Bodian DL, Daenke S, Linsley P, Davis SJ. CD80 (B7-1) binds both CD28 and CTLA-4 with a low affinity and very fast kinetics. J Exp Med. 1997;185(3):393–403.

180. Linsley PS, Greene JL, Brady W, Bajorath J, Ledbetter JA, Peach R. Human B7-1 (CD80) and B7-2 (CD86) bind with similar avidities but distinct kinetics to CD28 and CTLA-4 receptors. Immunity. 1994;1(9):793–801.

181. Naidoo J, Page DB, Wolchok JD. Immune modulation for cancer therapy. Br J Cancer. 2014;111(12):2214–9.

182. Robert C, Thomas L, Bondarenko I, O'Day S, M D JW, Garbe C, et al. Ipilimumab plus dacarbazine for previously untreated metastatic melanoma. N Engl J Med. 2011;364(26):2517–26.

183. Hamid O, Robert C, Daud A, Hodi FS, Hwu W-J, Kefford R, et al. Safety and tumor

responses with lambrolizumab (anti-PD-1) in melanoma. N Engl J Med. 2013;369(2):134–44.

184. Brahmer JR, Tykodi SS, Chow LQM, Hwu W-J, Topalian SL, Hwu P, et al. Safety and activity of anti-PD-L1 antibody in patients with advanced cancer. N Engl J Med. 2012;366(26):2455–65.

185. Agata Y, Kawasaki A, Nishimura H, Ishida Y, Tsubata T, Yagita H, et al. Expression of the PD-1 antigen on the surface of stimulated mouse T and B lymphocytes. Int Immunol. 1996;8(5):765–72.

186. Freeman GJ, Long AJ, Iwai Y, Bourque K, Chernova T, Nishimura H, et al. Engagement of the PD-1 immunoinhibitory receptor by a novel B7 family member leads to negative regulation of lymphocyte activation. J Exp Med. 2000;192(7):1027–34.

187. Latchman Y, Wood CR, Chernova T, Chaudhary D, Borde M, Chernova I, et al. PD-L2 is a second ligand for PD-1 and inhibits T cell activation. Nat Immunol. 2001;2(3):261–8.

188. Yokosuka T, Takamatsu M, Kobayashi-Imanishi W, Hashimoto-Tane A, Azuma M, Saito T. Programmed cell death 1 forms negative costimulatory microclusters that directly inhibit T cell receptor signaling by recruiting phosphatase SHP2. J Exp Med. 2012;209(6):1201–17.

189. Rota G, Ne Niogret C, Dang AT, Birchmeier W, Vivier E, Correspondence GG, et al. Shp-2 Is Dispensable for Establishing T Cell Exhaustion and for PD-1 Signaling In Vivo In Brief Shp-2-/-CD8 + T cell control CD8 + T cell Shp-2 Is Dispensable for Establishing T Cell Exhaustion and for PD-1 Signaling In Vivo. CellReports. 2018;23:39–49.

190. Iwai Y, Ishida M, Tanaka Y, Okazaki T, Honjo T, Minato N. Involvement of PD-L1 on tumor cells in the escape from host immune system and tumor immunotherapy by PD-L1

blockade. Proc Natl Acad Sci U S A. 2002;99(19):12293–7.

191. Barber DL, Wherry EJ, Masopust D, Zhu B, Allison JP, Sharpe AH, et al. Restoring function in exhausted CD8 T cells during chronic viral infection. Nature. 2006;439(7077):682–7.

192. Herbst RS, Soria J-C, Kowanetz M, Fine GD, Hamid O, Gordon MS, et al. Predictive correlates of response to the anti-PD-L1 antibody MPDL3280A in cancer patients. Nature. 2014;515(7528):563–7.

193. Robert C, Long G V., Brady B, Dutriaux C, Maio M, Mortier L, et al. Nivolumab in Previously Untreated Melanoma without BRAF Mutation. N Engl J Med. 2014;141116004513004.

194. Robert C, Schachter J, Long G V., Arance A, Grob JJ, Mortier L, et al. Pembrolizumab versus Ipilimumab in Advanced Melanoma. N Engl J Med. 2015;372(26):2521–32.

195. Larkin J, Chiarion-Sileni V, Gonzalez R, Grob JJ, Cowey CL, Lao CD, et al. Combined Nivolumab and Ipilimumab or Monotherapy in Untreated Melanoma. N Engl J Med. 2015;373:23–34.

196. Weber JS, Minor DR, D'Angelo S. LBA3_PR - A phase 3 randomized, open-label study of nivolumab (anti-PD-1; BMS-936558; ONO-4538) versus investigator's choice chemotherapy (ICC) in patients with advanced melanoma after prior anti-CTLA-4 therapy. In: ESMO Annual Meeting. 2014.

197. Berman DM, Wolchok J, Weber J, Hamid O, O'Day S, Chasalow SD. Association of peripheral blood absolute lymphocyte count (ALC) and clinical activity in patients (pts) with advanced melanoma treated with ipilimumab. ASCO Meet Abstr. 2009;27(15S):3020.

198. Ku GY, Yuan J, Page DB, Schroeder SEA, Panageas KS, Carvajal RD, et al. Single-institution experience with ipilimumab in advanced melanoma patients in the

compassionate use setting. Cancer. 2010;116(7):1767–75.

199. Simeone E. Immunological and biological changes during ipilimumab (Ipi) treatment and their correlation with clinical response and survival. J Clin Oncol. 2012;30(15):suppl; abstr 8573.

200. Topalian SL, Hodi FS, Brahmer JR, Gettinger SN, Smith DC, McDermott DF, et al. Safety, Activity, and Immune Correlates of Anti–PD-1 Antibody in Cancer. Vol. 366, New England Journal of Medicine. 2012. p. 2443–54.

201. Ascierto PA, Kalos M, Schaer DA, Callahan MK, Wolchok JD. Biomarkers for immunostimulatory monoclonal antibodies in combination strategies for melanoma and other tumor types. Clin Cancer Res. 2013;19(5):1009–20.

202. Snyder A, Makarov V, Merghoub T, Yuan J, Zaretsky JM, Desrichard A, et al. Genetic Basis for Clinical Response to CTLA-4 Blockade in Melanoma. N Engl J Med. 2014;371(23):141119140020009.

203. van Rooij N, van Buuren MM, Philips D, Velds A, Toebes M, Heemskerk B, et al. Tumor exome analysis reveals neoantigen-specific T-cell reactivity in an ipilimumab-responsive melanoma. J Clin Oncol. 2013;31(32):e439-42.

204. Robbins PF, Lu Y-C, El-Gamil M, Li YF, Gross C, Gartner J, et al. Mining exomic sequencing data to identify mutated antigens recognized by adoptively transferred tumor-reactive T cells. Nat Med. 2013;19(6):747–52.

205. Rizvi NA, Hellmann MD, Snyder A, Kvistborg P, Makarov V, Havel JJ, et al. Mutational landscape determines sensitivity to PD-1 blockade in non-small cell lung cancer. Science (80-). 2015;348(6230):124–8.

206. McGranahan N, Furness AJS, Rosenthal R, Ramskov S, Lyngaa R, Saini SK, et al. Clonal neoantigens elicit T cell immunoreactivity and sensitivity to immune checkpoint blockade. Science. 2016;351(6280):1463–9.

207. Miao D, Margolis CA, Vokes NI, Liu D, Taylor-Weiner A, Wankowicz SM, et al. Genomic correlates of response to immune checkpoint blockade in microsatellite-stable solid tumors. Nat Genet. 2018;50(9):1271–81.

208. Carreno BM, Magrini V, Becker-Hapak M, Kaabinejadian S, Hundal J, Petti AA, et al. A dendritic cell vaccine increases the breadth and diversity of melanoma neoantigen-specific T cells. Science (80-). 2015;348(6236):803–8.

209. Sahin U, Derhovanessian E, Miller M, Kloke B-P, Simon P, Löwer M, et al. Personalized RNA mutanome vaccines mobilize poly-specific therapeutic immunity against cancer. Nature. 2017;547(7662):222–6.

210. Ott PA, Hu Z, Keskin DB, Shukla SA, Sun J, Bozym DJ, et al. An immunogenic personal neoantigen vaccine for patients with melanoma. Nature. 2017;547(7662):217–21.

211. Tumeh PC, Harview CL, Yearley JH, Shintaku IP, Taylor EJM, Robert L, et al. PD-1 blockade induces responses by inhibiting adaptive immune resistance. Nature. 2014;515(7528):568–71.

212. Huang RR, Jalil J, Economou JS, Chmielowski B, Koya RC, Mok S, et al. CTLA4 blockade induces frequent tumor infiltration by activated lymphocytes regardless of clinical responses in humans. Clin Cancer Res. 2011;17(12):4101–9.

213. Mariathasan S, Turley SJ, Nickles D, Castiglioni A, Yuen K, Wang Y, et al. TGFβ attenuates tumour response to PD-L1 blockade by contributing to exclusion of T cells. Nature. 2018;554(7693):544–8.

214. Spranger S, Bao R, Gajewski TF. Melanoma-intrinsic β-catenin signalling prevents anti-tumour immunity. Nature. 2015;523(7559):231–5.

215. Zaretsky JM, Garcia-Diaz A, Shin DS, Escuin-Ordinas H, Hugo W, Hu-Lieskovan S, et al. Mutations Associated with Acquired Resistance to PD-1 Blockade in Melanoma. N

Engl J Med. 2016;375(9).

216. Peng W, Chen JQ, Liu C, Malu S, Creasy C, Tetzlaff MT, et al. Loss of PTEN Promotes Resistance to T Cell-Mediated Immunotherapy. Cancer Discov. 2016;6(2):202–16.

217. Sharma P, Hu-Lieskovan S, Wargo JA, Ribas A. Primary, Adaptive, and Acquired Resistance to Cancer Immunotherapy. Cell. 2017;168(4):707–23.

218. Vo DD, Prins RM, Begley JL, Donahue TR, Morris LF, Bruhn KW, et al. Enhanced Antitumor Activity Induced by Adoptive T-Cell Transfer and Adjunctive Use of the Histone Deacetylase Inhibitor LAQ824. Cancer Res. 2009;69(22):8693–9.

219. Zelenay S, van der Veen AG, Böttcher JP, Snelgrove KJ, Rogers N, Acton SE, et al. Cyclooxygenase-Dependent Tumor Growth through Evasion of Immunity. Cell. 2015;162(6):1257–70.

220. Wang D, DuBois RN. The role of COX-2 in intestinal inflammation and colorectal cancer. Oncogene. 2010;29(6):781–8.

221. Tauriello DVF, Palomo-Ponce S, Stork D, Berenguer-Llergo A, Badia-Ramentol J, Iglesias M, et al. TGFβ drives immune evasion in genetically reconstituted colon cancer metastasis. Nature. 2018;554(7693):538–43.

222. Gebhardt C, Sevko A, Jiang H, Lichtenberger R, Reith M, Tarnanidis K, et al. Myeloid Cells and Related Chronic Inflammatory Factors as Novel Predictive Markers in Melanoma Treatment with Ipilimumab. Clin Cancer Res. 2015;21(24):5453–9.

223. Arce Vargas F, Furness AJS, Solomon I, Joshi K, Mekkaoui L, Lesko MH, et al. Fc-Optimized Anti-CD25 Depletes Tumor-Infiltrating Regulatory T Cells and Synergizes with PD-1 Blockade to Eradicate Established Tumors. Immunity. 2017;46(4):577–86.

224. Quezada SA, Peggs KS, Curran MA, Allison JP. CTLA4 blockade and GM-CSF combination immunotherapy alters the intratumor balance of effector and regulatory T cells. J Clin Invest. 2006;116(7):1935–45.

225. Hodi FS, Butler M, Oble DA, Seiden M V., Haluska FG, Kruse A, et al. Immunologic and clinical effects of antibody blockade of cytotoxic T lymphocyte-associated antigen 4 in previously vaccinated cancer patients. Proc Natl Acad Sci. 2008;105(8):3005–10.

226. Eggermont A, Chiarion-Sileni V, Grob J, Dummer R, Wolchok J. Ipilimumab versus placebo after complete resection of stage III melanoma: Initial efficacy and safety results from the EORTC 18071 phase III trial. | 2014 ASCO Annual Meeting | Abstracts | Meeting Library [Internet]. Journal of clinical oncology : official journal of the American Society of Clinical Oncology. 2014 [cited 2014 Sep 23]. p. 32; 5s. Available from: http://meetinglibrary.asco.org/content/130118-144

227. Weber J, Mandala M, Del Vecchio M, Gogas HJ, Arance AM, Cowey CL, et al. Adjuvant Nivolumab versus Ipilimumab in Resected Stage III or IV Melanoma. N Engl J Med. 2017;377(19):1824–35.

228. Long G V., Hauschild A, Santinami M, Atkinson V, Mandalà M, Chiarion-Sileni V, et al. Adjuvant Dabrafenib plus Trametinib in Stage III *BRAF* -Mutated Melanoma. N Engl J Med. 2017;377(19):1813–23.

229. Davies MA, Liu P, McIntyre S, Kim KB, Papadopoulos N, Hwu WJ, et al. Prognostic factors for survival in melanoma patients with brain metastases. Cancer. 2011;117(8):1687–96.

230. Seifert H, Hirata E, Gore M, Khabra K, Messiou C, Larkin J, et al. Extrinsic factors can mediate resistance to BRAF inhibition in central nervous system melanoma metastases. Pigment Cell Melanoma Res. 2016;29(1):92–100.

231. Chen G, Chakravarti N, Aardalen K, Lazar AJ, Tetzlaff MT, Wubbenhorst B, et al. Molecular profiling of patient-matched brain and extracranial melanoma metastases implicates the PI3K pathway as a therapeutic target. Clin Cancer Res. 2014;20(21):5537–46.

232. Niessner H, Schmitz J, Tabatabai G, Schmid AM, Calaminus C, Sinnberg T, et al. PI3K Pathway Inhibition Achieves Potent Antitumor Activity in Melanoma Brain Metastases In Vitro and In Vivo. Clin Cancer Res. 2016;22(23):5818–28.

233. Pyonteck SM, Akkari L, Schuhmacher AJ, Bowman RL, Sevenich L, Quail DF, et al. CSF-1R inhibition alters macrophage polarization and blocks glioma progression. Nat Med. 2013;19(10):1264–72.

234. Schulz C, Perdiguero EG, Chorro L, Szabo-Rogers H, Cagnard N, Kierdorf K, et al. A Lineage of Myeloid Cells Independent of Myb and Hematopoietic Stem Cells. Science (80-). 2012;336(6077):86–90.

235. Gomez Perdiguero E, Klapproth K, Schulz C, Busch K, Azzoni E, Crozet L, et al. Tissue-resident macrophages originate from yolk-sac-derived erythro-myeloid progenitors. Nature. 2015;518(7540):547–51.

236. Müller A, Brandenburg S, Turkowski K, Müller S, Vajkoczy P. Resident microglia, and not peripheral macrophages, are the main source of brain tumor mononuclear cells. Int J Cancer. 2015;137(2):278–88.

237. Izraely S, Ben-Menachem S, Sagi-Assif O, Telerman A, Zubrilov I, Ashkenazi O, et al. The Metastatic Microenvironment: Melanoma-Microglia Cross-Talk Promotes the Malignant Phenotype of Melanoma Cells. Int J Cancer. 2018;10.1002/ijc.31745.

238. Davies MA, Saiag P, Robert C, Grob J-J, Flaherty KT, Arance A, et al. Dabrafenib plus trametinib in patients with BRAF V600 -mutant melanoma brain metastases (COMBI-MB): a multicentre, multicohort, open-label, phase 2 trial. Lancet Oncol. 2017;18(7):863–73.

239. Long G V, Atkinson V, Lo S, Sandhu S, Guminski AD, Brown MP, et al. Combination nivolumab and ipilimumab or nivolumab alone in melanoma brain metastases: a multicentre randomised phase 2 study. Lancet Oncol. 2018;19(5):672–81.

240. Tawbi HA, Forsyth PA, Algazi A, Hamid O, Hodi FS, Moschos SJ, et al. Combined Nivolumab and Ipilimumab in Melanoma Metastatic to the Brain. N Engl J Med. 2018;379(8):722–30.

241. Gogas H, Eggermont AMM, Hauschild A, Hersey P, Mohr P, Schadendorf D, et al. Biomarkers in melanoma. Ann Oncol. 2009;20 Suppl 6(suppl_6):vi8-13.

242. Schwarzenbach H, Hoon DSB, Pantel K. Cell-free nucleic acids as biomarkers in cancer patients. Nat Rev Cancer. 2011;11(6):426–37.

243. Sorenson G, Pribish D, Valone F, Memoli V, Bzik D, Yao S. Soluble normal and mutated DNA sequences from single-copy genes in human blood. Cancer Epidemiol Biomarkers Prev. 1994;3(1):67–71.

244. Momtaz P, Gaskell A, Merghoub T, Viale A, Chapman P. Correlation of tumor-derived circulating cell free DNA (cfDNA) measured by digital PCR (DigPCR) with tumor burden measured radiographically in patients (pts) with BRAFV600E mutated melanoma (mel) treated with RAF inhibitor (RAFi) and/or ipilimumab (Ipi). [Internet]. Journal of Clinical Oncology. 2014 [cited 2015 Jan 2]. p. 32:5s. Available from: http://meetinglibrary.asco.org/content/133594-144

245. Diehl F, Schmidt K, Choti MA, Romans K, Goodman S, Li M, et al. Circulating mutant DNA to assess tumor dynamics. Nat Med. 2008;14(9):985–90.

246. Kim K, Shin DG, Park MK, Baik SH, Kim TH, Kim S, et al. Circulating cell-free DNA as a promising biomarker in patients with gastric cancer: diagnostic validity and significant reduction of cfDNA after surgical resection. Ann Surg Treat Res. 2014;86(3):136–42.

247. Choi J-J, Reich CF, Pisetsky DS. The role of macrophages in the in vitro generation of extracellular DNA from apoptotic and necrotic cells. Immunology. 2005;115(1):55–62.

248. Swystun LL, Mukherjee S, Liaw PC. Breast cancer chemotherapy induces the release of

cell-free DNA, a novel procoagulant stimulus. J Thromb Haemost. 2011;9(11):2313–21.

249. Forshew T, Murtaza M, Parkinson C, Gale D, Tsui DWY, Kaper F, et al. Noninvasive identification and monitoring of cancer mutations by targeted deep sequencing of plasma DNA. Sci Transl Med. 2012;4(136):136ra68.

250. Crowley E, Di Nicolantonio F, Loupakis F, Bardelli A. Liquid biopsy: monitoring cancer-genetics in the blood. Nat Rev Clin Oncol. 2013;10(8):472–84.

251. Diaz LA, Williams RT, Wu J, Kinde I, Hecht JR, Berlin J, et al. The molecular evolution of acquired resistance to targeted EGFR blockade in colorectal cancers. Nature. 2012;486(7404):537–40.

252. Leary RJ, Sausen M, Kinde I, Papadopoulos N, Carpten JD, Craig D, et al. Detection of chromosomal alterations in the circulation of cancer patients with whole-genome sequencing. Sci Transl Med. 2012;4(162):162ra154.

253. Chan KCA, Jiang P, Zheng YWL, Liao GJW, Sun H, Wong J, et al. Cancer genome scanning in plasma: detection of tumor-associated copy number aberrations, single-nucleotide variants, and tumoral heterogeneity by massively parallel sequencing. Clin Chem. 2013;59(1):211–24.

254. Newman AM, Bratman S V, To J, Wynne JF, Eclov NCW, Modlin LA, et al. An ultrasensitive method for quantitating circulating tumor DNA with broad patient coverage. Nat Med. 2014;20(5):548–54.

255. Dawson S-J, Tsui DWY, Murtaza M, Biggs H, Rueda OM, Chin S-F, et al. Analysis of circulating tumor DNA to monitor metastatic breast cancer. N Engl J Med. 2013;368(13):1199–209.

256. Spindler K-LG, Pallisgaard N, Vogelius I, Jakobsen A. Quantitative cell-free DNA, KRAS, and BRAF mutations in plasma from patients with metastatic colorectal cancer during treatment with cetuximab and irinotecan. Clin Cancer Res. 2012;18(4):1177–85.

257. Schadendorf D, Flaherty K, Hersey P, Nathan PD, Garbe C, Milhem M, et al. Tumor-specific circulating cell-free DNA (cfDNA) to predict clinical outcome in BRAF V600 mutation-positive melanoma patients (pts) treated with the MEK inhibitor trametinib (T) or chemotherapy (C). J Clin Oncol. 2013;(31 suppl).

258. Luo J, Shen L, Zheng D. Diagnostic value of circulating free DNA for the detection of EGFR mutation status in NSCLC: a systematic review and meta-analysis. Sci Rep. 2014;4:6269.

259. Yamada T, Nakamori S, Ohzato H, Oshima S, Aoki T, Higaki N, et al. Detection of K-ras gene mutations in plasma DNA of patients with pancreatic adenocarcinoma: correlation with clinicopathological features. Clin Cancer Res. 1998;4(6):1527–32.

260. Goto K, Ichinose Y, Ohe Y, Yamamoto N, Negoro S, Nishio K, et al. Epidermal growth factor receptor mutation status in circulating free DNA in serum: from IPASS, a phase III study of gefitinib or carboplatin/paclitaxel in non-small cell lung cancer. J Thorac Oncol. 2012;7(1):115–21.

261. Aung KL, Board RE, Ellison G, Donald E, Ward T, Clack G, et al. Current status and future potential of somatic mutation testing from circulating free DNA in patients with solid tumours. Hugo J. 2010;4(1–4):11–21.

262. Lebofsky R, Decraene C, Bernard V, Kamal M, Blin A, Leroy Q, et al. Circulating tumor DNA as a non-invasive substitute to metastasis biopsy for tumor genotyping and personalized medicine in a prospective trial across all tumor types. Mol Oncol. 2015;9(4):783–90.

263. Lipson EJ, Velculescu VE, Pritchard TS, Sausen M, Pardoll DM, Topalian SL, et al. Circulating tumor DNA analysis as a real-time method for monitoring tumor burden in melanoma patients undergoing treatment with immune checkpoint blockade. J Immunother cancer. 2014;2(1):42.

264. Shinozaki M, O'Day SJ, Kitago M, Amersi F, Kuo C, Kim J, et al. Utility of circulating B-RAF DNA mutation in serum for monitoring melanoma patients receiving biochemotherapy. Clin Cancer Res. 2007;13(7):2068–74.

265. Gonzalez-Cao M, Soriano V, Rodriguez D, Puertolas T, Munoz E, Soria A, et al. 1108P * BRAF mutation analysis In cell free tumoral DNA (cfDNA) of melanoma patients: preliminary results from the Spanish melanoma group prospective study GEM1304. Ann Onc. 2014;25(suppl_4):iv384-.

266. Daniotti M, Vallacchi V, Rivoltini L, Patuzzo R, Santinami M, Arienti F, et al. Detection of mutated BRAFV600E variant in circulating DNA of stage III-IV melanoma patients. Int J Cancer. 2007;120(11):2439–44.

267. Rubie H, Hartmann O, Michon J, Frappaz D, Coze C, Chastagner P, et al. N-Myc gene amplification is a major prognostic factor in localized neuroblastoma: results of the French NBL 90 study. Neuroblastoma Study Group of the Société Francaise d'Oncologie Pédiatrique. J Clin Oncol. 1997;15(3):1171–82.

268. Combaret V, Hogarty MD, London WB, McGrady P, Iacono I, Brejon S, et al. Influence of neuroblastoma stage on serum-based detection of MYCN amplification. Pediatr Blood Cancer. 2009;53(3):329–31.

269. Murtaza M, Dawson S-J, Tsui DWY, Gale D, Forshew T, Piskorz AM, et al. Non-invasive analysis of acquired resistance to cancer therapy by sequencing of plasma DNA. Nature. 2013;497(7447):108–12.

270. Gremel G, Lee RJ, Girotti MR, Mandal AK, Valpione S, Garner G, et al. Distinct subclonal tumour responses to therapy revealed by circulating cell-free DNA. Ann Oncol. 2016;27(10):1959–65.

271. Corrie PG, Marshall A, Dunn JA, Middleton MR, Nathan PD, Gore M, et al. Adjuvant bevacizumab in patients with melanoma at high risk of recurrence (AVAST-M):

preplanned interim results from a multicentre, open-label, randomised controlled phase 3 study. Lancet Oncol. 2014;15(6):620–30.

272. Mali P, Yang L, Esvelt KM, Aach J, Guell M, DiCarlo JE, et al. RNA-Guided Human Genome Engineering via Cas9. Science (80-). 2013;339(6121):823–6.

273. Shen B, Zhang J, Wu H, Wang J, Ma K, Li Z, et al. Generation of gene-modified mice via Cas9/RNA-mediated gene targeting. Cell Res. 2013;23(5):720–3.

274. Chou T-C, Talalay P. Quantitative analysis of dose-effect relationships: the combined effects of multiple drugs or enzyme inhibitors. Adv Enzyme Regul. 1984;22:27–55.

275. Chou T-C. Preclinical *versus* clinical drug combination studies. Leuk Lymphoma. 2008;49(11):2059–80.

276. Vichai V, Kirtikara K. Sulforhodamine B colorimetric assay for cytotoxicity screening. Nat Protoc. 2006;1(3):1112–6.

277. Creedon H, Gómez-Cuadrado L, Tarnauskaitė Ž, Balla J, Canel M, MacLeod KG, et al. Identification of novel pathways linking epithelial-to-mesenchymal transition with resistance to HER2-targeted therapy. Oncotarget. 2016;7(10):11539–52.

278. UniProt: the universal protein knowledgebase. Nucleic Acids Res. 2017;45(D1):D158–69.

279. Untergasser A, Nijveen H, Rao X, Bisseling T, Geurts R, Leunissen JAM. Primer3Plus, an enhanced web interface to Primer3. Nucleic Acids Res. 2007;35(Web Server):W71–4.

280. Ye J, Coulouris G, Zaretskaya I, Cutcutache I, Rozen S, Madden TL. Primer-BLAST: a tool to design target-specific primers for polymerase chain reaction. BMC Bioinformatics. 2012;13(1):134.

281. Labun K, Montague TG, Gagnon JA, Thyme SB, Valen E. CHOPCHOP v2: a web tool for the next generation of CRISPR genome engineering. Nucleic Acids Res. 2016;44(W1):W272–6.

282. Li H, Durbin R. Fast and accurate short read alignment with Burrows-Wheeler transform. Bioinformatics. 2009;25(14):1754–60.

283. McKenna A, Hanna M, Banks E, Sivachenko A, Cibulskis K, Kernytsky A, et al. The Genome Analysis Toolkit: A MapReduce framework for analyzing next-generation DNA sequencing data. Genome Res. 2010;20(9):1297–303.

284. Cibulskis K, Lawrence MS, Carter SL, Sivachenko A, Jaffe D, Sougnez C, et al. Sensitive detection of somatic point mutations in impure and heterogeneous cancer samples. Nat Biotechnol. 2013;31(3):213–9.

285. Nielsen M, Lundegaard C, Blicher T, Lamberth K, Harndahl M, Justesen S, et al. NetMHCpan, a method for quantitative predictions of peptide binding to any HLA-A and -B locus protein of known sequence. PLoS One. 2007;2(8):e796.

286. Wang K, Singh D, Zeng Z, Coleman SJ, Huang Y, Savich GL, et al. MapSplice: Accurate mapping of RNA-seq reads for splice junction discovery. Nucleic Acids Res. 2010;38(18):e178–e178.

287. Liao Y, Smyth GK, Shi W. featureCounts: an efficient general purpose program for assigning sequence reads to genomic features. Bioinformatics. 2014;30(7):923–30.

288. Reimand J, Arak T, Adler P, Kolberg L, Reisberg S, Peterson H, et al. g:Profiler—a web server for functional interpretation of gene lists (2016 update). Nucleic Acids Res. 2016;44(W1):W83–9.

289. Shannon P, Markiel A, Ozier O, Baliga NS, Wang JT, Ramage D, et al. Cytoscape: a software environment for integrated models of biomolecular interaction networks. Genome Res. 2003;13(11):2498–504.

290. Subramanian A, Tamayo P, Mootha VK, Mukherjee S, Ebert BL, Gillette MA, et al. Gene set enrichment analysis: a knowledge-based approach for interpreting genome-wide expression profiles. Proc Natl Acad Sci U S A. 2005;102(43):15545–50.

291. Mootha VK, Lindgren CM, Eriksson K-F, Subramanian A, Sihag S, Lehar J, et al. PGC-1α-responsive genes involved in oxidative phosphorylation are coordinately downregulated in human diabetes. Nat Genet. 2003;34(3):267–73.

292. Royston P, Sauerbrei W. A new measure of prognostic separation in survival data. Stat Med. 2004;23(5):723–48.

293. Nagelkerke NJD. A Note on a General Definition of the Coefficient of Determination. Biometrika. 1991;78(3):691–2.

294. Van Houwelingen JC, Le Cessie S. Predictive value of statistical models. Stat Med. 1990;9(11):1303–25.

295. Cohen J V., Tawbi H, Margolin KA, Amravadi R, Bosenberg M, Brastianos PK, et al. Melanoma central nervous system metastases: current approaches, challenges, and opportunities. Pigment Cell Melanoma Res. 2016;29(6):627–42.

296. Forschner A, Eichner F, Amaral T, Keim U, Garbe C, Eigentler TK. Improvement of overall survival in stage IV melanoma patients during 2011–2014: analysis of real-world data in 441 patients of the German Central Malignant Melanoma Registry (CMMR). J Cancer Res Clin Oncol. 2017;143(3):533–40.

297. Johnson DB, Peng C, Abramson RG, Ye F, Zhao S, Wolchok JD, et al. Clinical Activity of Ipilimumab in Acral Melanoma: A Retrospective Review. Oncologist. 2015;20(6):648–52.

298. Vinay DS, Ryan EP, Pawelec G, Talib WH, Stagg J, Elkord E, et al. Immune evasion in cancer: Mechanistic basis and therapeutic strategies. Semin Cancer Biol. 2015;35:S185–98.

299. Drake CG, Jaffee E, Pardoll DM. Mechanisms of Immune Evasion by Tumors. Vol. 90, Advances in Immunology. 2006. p. 51–81.

300. Sade-Feldman M, Jiao YJ, Chen JH, Rooney MS, Barzily-Rokni M, Eliane J-P, et al.

Resistance to checkpoint blockade therapy through inactivation of antigen presentation. Nat Commun. 2017;8(1):1136.

301. Schumacher TN, Schreiber RD. Neoantigens in cancer immunotherapy. Science (80-). 2015;348(6230):69–74.

302. Anagnostou V, Smith KN, Forde PM, Niknafs N, Bhattacharya R, White J, et al. Evolution of Neoantigen Landscape during Immune Checkpoint Blockade in Non–Small Cell Lung Cancer. Cancer Discov. 2017;7(3):264–76.

303. Verdegaal EME, de Miranda NFCC, Visser M, Harryvan T, van Buuren MM, Andersen RS, et al. Neoantigen landscape dynamics during human melanoma–T cell interactions. Nature. 2016;536(7614):91–5.

304. Liu C, Peng W, Xu C, Lou Y, Zhang M, Wargo JA, et al. BRAF inhibition increases tumor infiltration by T cells and enhances the antitumor activity of adoptive immunotherapy in mice. Clin Cancer Res. 2013;19(2):393–403.

305. Dong Y, Richards J-A, Gupta R, Aung PP, Emley A, Kluger Y, et al. PTEN functions as a melanoma tumor suppressor by promoting host immune response. Oncogene. 2014;33(38):4632–42.

306. Nagarsheth N, Wicha MS, Zou W. Chemokines in the cancer microenvironment and their relevance in cancer immunotherapy. Nat Rev Immunol. 2017;17(9):559–72.

307. Ott PA, Hodi FS, Buchbinder EI. Inhibition of Immune Checkpoints and Vascular Endothelial Growth Factor as Combination Therapy for Metastatic Melanoma: An Overview of Rationale, Preclinical Evidence, and Initial Clinical Data. Front Oncol. 2015;5:202.

308. Tjin EPM, Krebbers G, Meijlink KJ, Van De Kasteele W, Rosenberg EH, Sanders J, et al. Immune-Escape Markers in Relation to Clinical Outcome of Advanced Melanoma Patients Following Immunotherapy. Cancer Immunol Res. 2014;2(6):1–9.

309. Newman AM, Liu CL, Green MR, Gentles AJ, Feng W, Xu Y, et al. Robust enumeration of cell subsets from tissue expression profiles. Nat Methods. 2015;12(5):453–7.

310. Hugo W, Shi H, Sun L, Piva M, Song C, Kong X, et al. Non-genomic and Immune Evolution of Melanoma Acquiring MAPKi Resistance. Cell. 2015;162(6):1271–85.

311. Kingeter LM, Lin X. C-type lectin receptor-induced NF-κB activation in innate immune and inflammatory responses. Cell Mol Immunol. 2012;9(2):105–12.

312. Anderson AC, Joller N, Kuchroo VK. Lag-3, Tim-3, and TIGIT: Co-inhibitory Receptors with Specialized Functions in Immune Regulation. Immunity. 2016;44(5):989–1004.

313. Long G V, Trefzer U, Davies M a, Kefford RF, Ascierto P a, Chapman PB, et al. Dabrafenib in patients with Val600Glu or Val600Lys BRAF-mutant melanoma metastatic to the brain (BREAK-MB): a multicentre, open-label, phase 2 trial. Lancet Oncol. 2012;13(11):1087–95.

314. Martin MJ, Hayward R, Viros A, Marais R. Metformin Accelerates the Growth of BRAFV600E-Driven Melanoma by Upregulating VEGF-A. Cancer Discov. 2012;2(4):344–55.

315. Parakh S, Park JJ, Mendis S, Rai R, Xu W, Lo S, et al. Efficacy of anti-PD-1 therapy in patients with melanoma brain metastases. Br J Cancer. 2017;116(12):1558–63.

316. Riaz N, Havel JJ, Makarov V, Desrichard A, Urba WJ, Sims JS, et al. Tumor and Microenvironment Evolution during Immunotherapy with Nivolumab. Cell. 2017;171(4):934–949.e15.

317. Bentzen AK, Marquard AM, Lyngaa R, Saini SK, Ramskov S, Donia M, et al. Large-scale detection of antigen-specific T cells using peptide-MHC-I multimers labeled with DNA barcodes. Nat Biotechnol. 2016;34(10):1037–45.

318. Wu S-Y, Watabe K. The roles of microglia/macrophages in tumor progression of brain cancer and metastatic disease. Front Biosci (Landmark Ed. 2017;22:1805–29.

319. Aras S, Zaidi MR. TAMeless traitors: macrophages in cancer progression and metastasis. Br J Cancer. 2017;117(11):1583–91.

320. Owen JD, Strieter R, Burdick M, Haghnegahdar H, Nanney L, Shattuck-Brandt R, et al. Enhanced tumor-forming capacity for immortalized melanocytes expressing melanoma growth stimulatory activity/growth-regulated cytokine beta and gamma proteins. Int J cancer. 1997;73(1):94–103.

321. Dhawan P, Richmond A. Role of CXCL1 in tumorigenesis of melanoma. J Leukoc Biol. 2002;72(1):9–18.

322. Haqq C, Nosrati M, Sudilovsky D, Crothers J, Khodabakhsh D, Pulliam BL, et al. The gene expression signatures of melanoma progression. Proc Natl Acad Sci U S A. 2005;102(17):6092–7.

323. Fiorentino DF, Zlotnik A, Mosmann TR, Howard M, O'Garra A. IL-10 inhibits cytokine production by activated macrophages. J Immunol. 1991;147(11):3815–22.

324. Taga K, Mostowski H, Tosato G. Human interleukin-10 can directly inhibit T-cell growth. Blood. 1993;81(11):2964–71.

325. García-Hernández ML, Hernández-Pando R, Gariglio P, Berumen J. Interleukin-10 promotes B16-melanoma growth by inhibition of macrophage functions and induction of tumour and vascular cell proliferation. Immunology. 2002;105(2):231–43.

326. Itakura E, Huang R-R, Wen D-R, Paul E, Wünsch PH, Cochran AJ. IL-10 expression by primary tumor cells correlates with melanoma progression from radial to vertical growth phase and development of metastatic competence. Mod Pathol. 2011;24(6):801–9.

327. Harlin H, Meng Y, Peterson AC, Zha Y, Tretiakova M, Slingluff C, et al. Chemokine expression in melanoma metastases associated with CD8+ T-cell recruitment. Cancer Res. 2009;69(7):3077–85.

328. Alterman AL, Stackpole CW. B16 melanoma spontaneous brain metastasis: occurrence

and development within leptomeninges blood vessels. Clin Exp Metastasis. 7(1):15–23.

329. Taggart D, Andreou T, Scott KJ, Williams J, Rippaus N, Brownlie RJ, et al. Anti-PD-1/anti-CTLA-4 efficacy in melanoma brain metastases depends on extracranial disease and augmentation of CD8+ T cell trafficking. Proc Natl Acad Sci U S A. 2018;115(7):E1540–9.

330. Long G V, Eroglu Z, Infante J, Patel S, Daud A, Johnson DB, et al. Long-Term Outcomes in Patients With BRAF V600-Mutant Metastatic Melanoma Who Received Dabrafenib Combined With Trametinib. J Clin Oncol. 2018;36(7):667–73.

331. Long G V., Fung C, Menzies AM, Pupo GM, Carlino MS, Hyman J, et al. Increased MAPK reactivation in early resistance to dabrafenib/trametinib combination therapy of BRAF-mutant metastatic melanoma. Nat Commun. 2014;5(1):5694.

332. Emery CM, Vijayendran KG, Zipser MC, Sawyer AM, Niu L, Kim JJ, et al. MEK1 mutations confer resistance to MEK and B-RAF inhibition. Proc Natl Acad Sci U S A. 2009;106(48):20411–6.

333. Villanueva J, Vultur A, Lee JT, Somasundaram R, Fukunaga-Kalabis M, Cipolla AK, et al. Acquired resistance to BRAF inhibitors mediated by a RAF kinase switch in melanoma can be overcome by cotargeting MEK and IGF-1R/PI3K. Cancer Cell. 2010;18(6):683–95.

334. Nazarian R, Shi H, Wang Q, Kong X, Koya RC, Lee H, et al. Melanomas acquire resistance to B-RAF(V600E) inhibition by RTK or N-RAS upregulation. Nature. 2010;468(7326):973–7.

335. Girotti MR, Lopes F, Preece N, Niculescu-Duvaz D, Zambon A, Davies L, et al. Paradox-Breaking RAF Inhibitors that Also Target SRC Are Effective in Drug-Resistant BRAF Mutant Melanoma. Cancer Cell. 2014;27(1):85–96.

336. Lassen A, Atefi M, Robert L, Wong DJ, Cerniglia M, Comin-Anduix B, et al. Effects of

AKT inhibitor therapy in response and resistance to BRAF inhibition in melanoma. Mol Cancer. 2014;13(1):83.

337. Baljuls A, Mueller T, Drexler HCA, Hekman M, Rapp UR. Unique N-region Determines Low Basal Activity and Limited Inducibility of A-RAF Kinase. J Biol Chem. 2007;282(36):26575–90.

338. Bozic I, Reiter JG, Allen B, Antal T, Chatterjee K, Shah P, et al. Evolutionary dynamics of cancer in response to targeted combination therapy. Elife. 2013;2:e00747.

339. Robert C, Karaszewska B, Schachter J, Rutkowski P, Mackiewicz A, Stroiakovski D, et al. Improved Overall Survival in Melanoma with Combined Dabrafenib and Trametinib. N Engl J Med. 2015;372(1):30–9.

340. Long G V, Stroyakovskiy D, Gogas H, Levchenko E, De Braud FG. Overall survival in COMBI-d, a randomized, double-blinded, phase III study comparing the combination of dabrafenib and trametinib with dabrafenib and placebo as first-line therapy in patients (pts) with unresectable or metastatic BRAF V600E/K mutation-pos. In: ASCO Annual Meeting. 2015. p. J Clin Oncol 33, 2015 (suppl; abstr 102).

341. Kim KB, Kefford R, Pavlick AC, Infante JR, Ribas A, Sosman JA, et al. Phase II study of the MEK1/MEK2 inhibitor Trametinib in patients with metastatic BRAF-mutant cutaneous melanoma previously treated with or without a BRAF inhibitor. J Clin Oncol. 2013;31(4):482–9.

342. Furet P, Guagnano V, Fairhurst RA, Imbach-Weese P, Bruce I, Knapp M, et al. Discovery of NVP-BYL719 a potent and selective phosphatidylinositol-3 kinase alpha inhibitor selected for clinical evaluation. Bioorg Med Chem Lett. 2013;23(13):3741–8.

343. Ndubaku CO, Heffron TP, Staben ST, Baumgardner M, Blaquiere N, Bradley E, et al. Discovery of 2-{3-[2-(1-Isopropyl-3-methyl-1 *H* -1,2–4-triazol-5-yl)-5,6-dihydrobenzo[f]imidazo[1,2- *d*][1,4]oxazepin-9-yl]-1 *H* -pyrazol-1-yl}-2-

methylpropanamide (GDC-0032): A β-Sparing Phosphoinositide 3-Kinase Inhibitor with High Unbound Exposure and Robust in Vivo Antitumor Activity. J Med Chem. 2013;56(11):4597–610.

344. Yao Z, Yaeger R, Rodrik-Outmezguine VS, Tao A, Torres NM, Chang MT, et al. Tumours with class 3 BRAF mutants are sensitive to the inhibition of activated RAS. Nature. 2017;548(7666):234–8.

345. Johnson GL, Lapadat R. Mitogen-activated protein kinase pathways mediated by ERK, JNK, and p38 protein kinases. Science. 2002;298(5600):1911–2.

346. Shaul YD, Seger R. The MEK/ERK cascade: From signaling specificity to diverse functions. Biochim Biophys Acta - Mol Cell Res. 2007;1773(8):1213–26.

347. Lau E, Ronai ZA. ATF2 - at the crossroad of nuclear and cytosolic functions. J Cell Sci. 2012;125(Pt 12):2815–24.

348. Zarubin T, Han J. Activation and signaling of the p38 MAP kinase pathway. Vol. 15, Cell Research. 2005.

349. Schönwasser DC, Marais RM, Marshall CJ, Parker PJ. Activation of the mitogen-activated protein kinase/extracellular signal-regulated kinase pathway by conventional, novel, and atypical protein kinase C isotypes. Mol Cell Biol. 1998;18(2):790–8.

350. Mason JM, Morrison DJ, Albert Basson M, Licht JD. Sprouty proteins: multifaceted negative-feedback regulators of receptor tyrosine kinase signaling. Trends Cell Biol. 2006;16(1):45–54.

351. Sun M-K, Alkon DL. Bryostatin-1: Pharmacology and Therapeutic Potential as a CNS Drug. CNS Drug Rev. 2006;12(1):1–8.

352. Long G V, Fung C, Menzies AM, Pupo GM, Carlino MS, Hyman J, et al. Increased MAPK reactivation in early resistance to dabrafenib/trametinib combination therapy of BRAF-mutant metastatic melanoma. Nat Commun. 2014;5:5694.

353. Baljuls A, Schmitz W, Mueller T, Zahedi RP, Sickmann A, Hekman M, et al. Positive Regulation of A-RAF by Phosphorylation of Isoform-specific Hinge Segment and Identification of Novel Phosphorylation Sites. J Biol Chem. 2008;283(40):27239–54.

354. Yao Z, Torres NM, Tao A, Gao Y, Luo L, Li Q, et al. BRAF Mutants Evade ERK-Dependent Feedback by Different Mechanisms that Determine Their Sensitivity to Pharmacologic Inhibition. Cancer Cell. 2015;28(3):370–83.

355. Jaiswal BS, Janakiraman V, Kljavin NM, Eastham-Anderson J, Cupp JE, Liang Y, et al. Combined Targeting of BRAF and CRAF or BRAF and PI3K Effector Pathways Is Required for Efficacy in NRAS Mutant Tumors. Najbauer J, editor. PLoS One. 2009;4(5):e5717.

356. Whittaker SR, Cowley GS, Wagner S, Luo F, Root DE, Garraway LA. Combined Pan-RAF and MEK Inhibition Overcomes Multiple Resistance Mechanisms to Selective RAF Inhibitors. Mol Cancer Ther. 2015;14(12):2700–11.

357. Atefi M, Titz B, Avramis E, Ng C, Wong D, Lassen A, et al. Combination of pan-RAF and MEK inhibitors in NRAS mutant melanoma. Mol Cancer. 2015;14(1):27.

358. Atefi M, von Euw E, Attar N, Ng C, Chu C, Guo D, et al. Reversing Melanoma Cross-Resistance to BRAF and MEK Inhibitors by Co-Targeting the AKT/mTOR Pathway. Brandner JM, editor. PLoS One. 2011;6(12):e28973.

359. Posch C, Moslehi H, Feeney L, Green GA, Ebaee A, Feichtenschlager V, et al. Combined targeting of MEK and PI3K/mTOR effector pathways is necessary to effectively inhibit NRAS mutant melanoma in vitro and in vivo. Proc Natl Acad Sci U S A. 2013;110(10):4015–20.

360. Batlle E, Clevers H. Cancer stem cells revisited. Nat Med. 2017;23(10):1124–34.

361. Ozaki K, Kadomoto R, Asato K, Tanimura S, Itoh N, Kohno M. ERK Pathway Positively Regulates the Expression of Sprouty Genes. Biochem Biophys Res Commun.

2001;285(5):1084–8.

362. Casci T, Vinós J, Freeman M. Sprouty, an intracellular inhibitor of Ras signaling. Cell. 1999;96(5):655–65.

363. Akbulut S, Reddi AL, Aggarwal P, Ambardekar C, Canciani B, Kim MKH, et al. Sprouty proteins inhibit receptor-mediated activation of phosphatidylinositol-specific phospholipase C. Mol Biol Cell. 2010;21(19):3487–96.

364. SImpson CM, Bakal C. The dynamics of ERK signaling in melanoma, and the response to BRAF or MEK inhibition, are cell cycle dependent. bioarxiv. 2018;10.2139/ssrn.3188455.

365. Tan S-L, Parker PJ. Emerging and diverse roles of protein kinase C in immune cell signalling. Biochem J. 2003;376:545–52.

366. Early Breast Cancer Trialists' Collaborative Group (EBCTCG) EBCTCG, Peto R, Davies C, Godwin J, Gray R, Pan HC, et al. Comparisons between different polychemotherapy regimens for early breast cancer: meta-analyses of long-term outcome among 100,000 women in 123 randomised trials. Lancet (London, England). 2012;379(9814):432–44.

367. Figueredo A, Coombes ME, Mukherjee S. Adjuvant Therapy for completely resected Stage II Colon Cancer. Cochrane Database Syst Rev. 2008;(3):CD005390.

368. Arriagada R, Dunant A, Pignon J-P, Bergman B, Chabowski M, Grunenwald D, et al. Long-term results of the international adjuvant lung cancer trial evaluating adjuvant Cisplatin-based chemotherapy in resected lung cancer. J Clin Oncol. 2010;28(1):35–42.

369. Martin DS, Fugmann RA. Clinical Implications of the Interrelationship of Tumor Size and Chemotherapeutic Response. Ann Surg. 1960;151(1):97–100.

370. Moynihan KD, Opel CF, Szeto GL, Tzeng A, Zhu EF, Engreitz JM, et al. Eradication of large established tumors in mice by combination immunotherapy that engages innate and

adaptive immune responses. Nat Med. 2016;22(12):1402–10.

371. Huang AC, Postow MA, Orlowski RJ, Mick R, Bengsch B, Manne S, et al. T-cell invigoration to tumour burden ratio associated with anti-PD-1 response. Nature. 2017;545(7652):60–5.

372. Joseph RW, Elassaiss-Schaap J, Kefford RF, Hwu W-J, Wolchok JD, Joshua AM, et al. Baseline Tumor Size Is an Independent Prognostic Factor for Overall Survival in Patients With Melanoma Treated With Pembrolizumab. Clin Cancer Res. 2018;10.1158/1078-0432.CCR-17-2386.

373. Eggermont AMM, Blank CU, Mandala M, Long G V., Atkinson V, Dalle S, et al. Adjuvant Pembrolizumab versus Placebo in Resected Stage III Melanoma. N Engl J Med. 2018;378(19):1789–801.

374. Eggermont AMM, Chiarion-Sileni V, Grob J-J, Dummer R, Wolchok JD, Schmidt H, et al. Prolonged Survival in Stage III Melanoma with Ipilimumab Adjuvant Therapy. N Engl J Med. 2016;375(19):1845–55.

375. Eggermont AMM, Chiarion-Sileni V, Grob J-J, Dummer R, Wolchok JD, Schmidt H, et al. Adjuvant ipilimumab versus placebo after complete resection of high-risk stage III melanoma (EORTC 18071): a randomised, double-blind, phase 3 trial. Lancet Oncol. 2015;16(5):522–30.

376. Santiago-Walker A, Gagnon R, Mazumdar J, Casey M, Long G V., Schadendorf D, et al. Correlation of BRAF Mutation Status in Circulating-Free DNA and Tumor and Association with Clinical Outcome across Four BRAFi and MEKi Clinical Trials. Clin Cancer Res. 2016;22(3).

377. Gray ES, Rizos H, Reid AL, Boyd SC, Pereira MR, Lo J, et al. Circulating tumor DNA to monitor treatment response and detect acquired resistance in patients with metastatic melanoma. Oncotarget. 2015;6(39):42008–18.

378. Corrie PG, Marshall A, Nathan PD, Lorigan P, Gore M, Tahir S, et al. Adjuvant bevacizumab for melanoma patients at high risk of recurrence: survival analysis of the AVAST-M trial. Ann Oncol. 2018;29(8):1843–52.

379. Lee RJ, Gremel G, Marshall A, Myers KA, Fisher N, Dunn JA, et al. Circulating tumor DNA predicts survival in patients with resected high-risk stage II/III melanoma. Ann Oncol. 2018;29(2):490–6.

380. Corrie P., Marshall A, Nathan P, Lorigan P, Gore M, Tahir S, et al. Adjuvant bevacizumab as treatment for melanoma patients at high risk of recurrence: Final results for the AVAST-M trial. ASCO Gen Meet. 2017;In press.

381. Gerami P, Cook RW, Russell MC, Wilkinson J, Amaria RN, Gonzalez R, et al. Gene expression profiling for molecular staging of cutaneous melanoma in patients undergoing sentinel lymph node biopsy. J Am Acad Dermatol. 2015;72(5):780–5.e3.

382. John T, Black MA, Toro TT, Leader D, Gedye CA, Davis ID, et al. Predicting Clinical Outcome through Molecular Profiling in Stage III Melanoma. Clin Cancer Res. 2008;14(16).

383. Garcia-Murillas I, Schiavon G, Weigelt B, Ng C, Hrebien S, Cutts RJ, et al. Mutation tracking in circulating tumor DNA predicts relapse in early breast cancer. Sci Transl Med. 2015;7(302).

384. Tie J, Wang Y, Tomasetti C, Li L, Springer S, Kinde I, et al. Circulating tumor DNA analysis detects minimal residual disease and predicts recurrence in patients with stage II colon cancer. Sci Transl Med. 2016;8(346):346ra92-346ra92.

385. van Dongen JJM, van der Velden VHJ, Brüggemann M, Orfao A. Minimal residual disease diagnostics in acute lymphoblastic leukemia: need for sensitive, fast, and standardized technologies. Blood. 2015;125(26):3996–4009.

386. van Dongen JJ, Seriu T, Panzer-Grümayer ER, Biondi A, Pongers-Willemse MJ, Corral

L, et al. Prognostic value of minimal residual disease in acute lymphoblastic leukaemia in childhood. Lancet. 1998;352(9142):1731–8.

387. Cavé H, van der Werff ten Bosch J, Suciu S, Guidal C, Waterkeyn C, Otten J, et al. Clinical Significance of Minimal Residual Disease in Childhood Acute Lymphoblastic Leukemia. N Engl J Med. 1998;339(9):591–8.

388. Bradish JR, Richey JD, Post KM, Meehan K, Sen JD, Malek AJ, et al. Discordancy in BRAF mutations among primary and metastatic melanoma lesions: clinical implications for targeted therapy. Mod Pathol. 2015;28(4):480–6.

389. Haselmann V, Gebhardt C, Brechtel I, Duda A, Czerwinski C, Sucker A, et al. Liquid Profiling of Circulating Tumor DNA in Plasma of Melanoma Patients for Companion Diagnostics and Monitoring of BRAF Inhibitor Therapy. Clin Chem. 2018;64(5):830–42.

390. Santiago-Walker A, Gagnon R, Mazumdar J, Casey M, Long G V., Schadendorf D, et al. Correlation of BRAF mutation status in circulating-free DNA and tumor and association with clinical outcome across four BRAFi and MEKi clinical trials. Clin Cancer Res. 2015;1–9.

391. Wan JCM, Massie C, Garcia-Corbacho J, Mouliere F, Brenton JD, Caldas C, et al. Liquid biopsies come of age: towards implementation of circulating tumour DNA. Nat Rev Cancer. 2017;17(4):223–38.

392. Cohen JD, Li L, Wang Y, Thoburn C, Afsari B, Danilova L, et al. Detection and localization of surgically resectable cancers with a multi-analyte blood test. Science. 2018;eaar3247.

393. Wulfkuhle JD, Liotta LA, Petricoin EF. Early detection: Proteomic applications for the early detection of cancer. Nat Rev Cancer. 2003;3(4):267–75.

394. Mian S, Ugurel S, Parkinson EP, Parkinson E, Schlenzka I, Dryden I, et al. Serum Proteomic Fingerprinting Discriminates Between Clinical Stages and Predicts Disease

Progression in Melanoma Patients. J Clin Oncol. 2005;23(22):5088–93.

395. Fukumoto T, Nishiumi S, Fujiwara S, Yoshida M, Nishigori C. Novel serum metabolomics-based approach by gas chromatography/triple quadrupole mass spectrometry for detection of human skin cancers: Candidate biomarkers. J Dermatol. 2017;44(11):1268–75.

396. Leygo C, Williams M, Jin HC, Chan MWY, Chu WK, Grusch M, et al. DNA Methylation as a Noninvasive Epigenetic Biomarker for the Detection of Cancer. Dis Markers. 2017;2017:3726595.

397. Micevic G, Theodosakis N, Bosenberg M. Aberrant DNA methylation in melanoma: biomarker and therapeutic opportunities. Clin Epigenetics. 2017;9(1):34.

398. Brait M, Banerjee M, Maldonado L, Ooki A, Loyo M, Guida E, et al. Promoter methylation of MCAM, ERα and ERβ in serum of early stage prostate cancer patients. Oncotarget. 2017;8(9):15431–40.

399. Khoja L, Lorigan P, Zhou C, Lancashire M, Booth J, Cummings J, et al. Biomarker utility of circulating tumor cells in metastatic cutaneous melanoma. J Invest Dermatol. 2013;133(6):1582–90.

400. Hong X, Sullivan RJ, Kalinich M, Kwan TT, Giobbie-Hurder A, Pan S, et al. Molecular signatures of circulating melanoma cells for monitoring early response to immune checkpoint therapy. Proc Natl Acad Sci U S A. 2018;115(10):2467–72.

401. Ferreira MM, Ramani VC, Jeffrey SS. Circulating tumor cell technologies. Mol Oncol. 2016;10(3):374–94.

402. Stark MS, Klein K, Weide B, Haydu LE, Pflugfelder A, Tang YH, et al. The Prognostic and Predictive Value of Melanoma-related MicroRNAs Using Tissue and Serum: A MicroRNA Expression Analysis. EBioMedicine. 2015;2(7):671–80.

403. Cancer Research UK. Prognostic/Predictive Biomarker Roadmap [Internet]. [cited 2018

May 15]. Available from: http://www.cancerresearchuk.org/prod_consump/groups/cr_common/@fre/@fun/documents/generalcontent/cr_027486.pdf

404. Torga G, Pienta KJ. Patient-Paired Sample Congruence Between 2 Commercial Liquid Biopsy Tests. JAMA Oncol. 2017;

405. Cox AD, Fesik SW, Kimmelman AC, Luo J, Der CJ. Drugging the undruggable RAS: Mission possible? Nat Rev Drug Discov. 2014;13(11):828–51.

406. Bidard F-C, Fehm T, Ignatiadis M, Smerage JB, Alix-Panabières C, Janni W, et al. Clinical application of circulating tumor cells in breast cancer: overview of the current interventional trials. Cancer Metastasis Rev. 2013;32(1–2):179–88.

407. Carlino MS, Gowrishankar K, Saunders CAB, Pupo GM, Snoyman S, Zhang XD, et al. Antiproliferative effects of continued mitogen-activated protein kinase pathway inhibition following acquired resistance to BRAF and/or MEK inhibition in melanoma. Mol Cancer Ther. 2013;12(7):1332–42.

408. Atkins MB, Larkin J. Immunotherapy Combined or Sequenced With Targeted Therapy in the Treatment of Solid Tumors : Current Perspectives. 2016;108:1–9.

409. Merlino G, Herlyn M, Fisher DE, Bastian BC, Flaherty KT, Davies MA, et al. The state of melanoma: challenges and opportunities. Pigment Cell Melanoma Res. 2016;

410. Luke JJ, Flaherty KT, Ribas A, Long G V. Targeted agents and immunotherapies: optimizing outcomes in melanoma. Nat Rev Clin Oncol. 2017;advance on.

411. Song G, Gu L, Li J, Tang Z, Liu H, Chen B, et al. Serum microRNA expression profiling predict response to R-CHOP treatment in diffuse large B cell lymphoma patients. Ann Hematol. 2014;93(10):1735–43.

412. Hu-Lieskovan S, Mok S, Homet Moreno B, Tsoi J, Robert L, Goedert L, et al. Improved antitumor activity of immunotherapy with BRAF and MEK inhibitors in BRAFV600E

melanoma. Sci Transl Med. 2015;7(279):279ra41-279ra41.

413. Boni A, Cogdill AP, Dang P, Udayakumar D, Njauw CNJ, Sloss CM, et al. Selective BRAFV600E inhibition enhances T-cell recognition of melanoma without affecting lymphocyte function. Cancer Res. 2010;70(13):5213–9.

414. Khalili JS, Liu S, Rodr??guez-Cruz TG, Whittington M, Wardell S, Liu C, et al. Oncogenic BRAF(V600E) promotes stromal cell-mediated immunosuppression via induction of interleukin-1 in melanoma. Clin Cancer Res. 2012;18(19):5329–40.

415. Frederick DT, Piris A, Cogdill AP, Cooper ZA, Lezcano C, Ferrone CR, et al. BRAF inhibition is associated with enhanced melanoma antigen expression and a more favorable tumor microenvironment in patients with metastatic melanoma. Clin Cancer Res. 2013;19(5):1225–31.

416. Jiang X, Zhou J, Giobbie-Hurder A, Wargo J, Hodi FS. The activation of MAPK in melanoma cells resistant to BRAF inhibition promotes PD-L1 expression that is reversible by MEK and PI3K inhibition. Clin Cancer Res. 2013;19(3):598–609.

417. Ott PA, Henry T, Baranda SJ, Frleta D, Manches O, Bogunovic D, et al. Inhibition of both BRAF and MEK in BRAFV600E mutant melanoma restores compromised dendritic cell (DC) function while having differential direct effects on DC properties. Cancer Immunol Immunother. 2013;62(4):811–22.

418. Wang T, Xiao M, Ge Y, Krepler C, Belser E, Lopez-Coral A, et al. BRAF Inhibition Stimulates Melanoma-Associated Macrophages to Drive Tumor Growth. Clin Cancer Res. 2015;21(7).

419. Diem S, Kasenda B, Spain L, Martin-Liberal J, Marconcini R, Gore M, et al. Serum lactate dehydrogenase as an early marker for outcome in patients treated with anti-PD-1 therapy in metastatic melanoma. Br J Cancer. 2016;114(3):256–61.

420. Blank CU, Haanen JB, Ribas A, Schumacher TN. CANCER IMMUNOLOGY. The

"cancer immunogram". Science. 2016;352(6286):658–60.

421. Pilon-Thomas S, Kodumudi KN, El-Kenawi AE, Russell S, Weber AM, Luddy K, et al. Neutralization of Tumor Acidity Improves Antitumor Responses to Immunotherapy. Cancer Res. 2016;76(6):1381–90.

422. Brand A, Singer K, Koehl GE, Kolitzus M, Schoenhammer G, Thiel A, et al. LDHA-Associated Lactic Acid Production Blunts Tumor Immunosurveillance by T and NK Cells. Cell Metab. 2016;24(5):657–71.

423. Girotti MR, Gremel G, Lee R, Galvani E, Rothwell D, Viros A, et al. Application of sequencing, liquid biopsies, and patient-derived xenografts for personalized medicine in melanoma. Cancer Discov. 2016;

424. Luke JJ, Flaherty KT, Ribas A, Long G V. Targeted agents and immunotherapies: optimizing outcomes in melanoma. Nat Rev Clin Oncol. 2017;14(8):463–82.

425. Marsden JR, Newton-Bishop JA, Burrows L, Cook M, Corrie PG, Cox NH, et al. Revised U.K. guidelines for the management of cutaneous melanoma 2010. Br J Dermatol. 2010;163:238–56.

426. Larkin J, Acland K, Algurafi H, Lorigan P. Cutaneous Melanoma Follow-Up 2013 Position Paper: Follow-Up of High Risk Cutaneous Melanoma in the UK.

427. Bettegowda C, Sausen M, Leary RJ, Kinde I, Wang Y, Agrawal N, et al. Detection of circulating tumor DNA in early- and late-stage human malignancies. Sci Transl Med. 2014;6(224):224ra24.

428. Abbosh C, Birkbak NJ, Wilson GA, Jamal-Hanjani M, Constantin T, Salari R, et al. Phylogenetic ctDNA analysis depicts early-stage lung cancer evolution. Nature. 2017;545(7655):446–51.

429. Lee JH, Long G V., Boyd S, Lo S, Menzies AM, Tembe V, et al. Circulating tumour DNA predicts response to anti-PD1 antibodies in metastatic melanoma. Ann Oncol.

2017;28(5):1130–6.

430. Chang-Hao Tsao S, Weiss J, Hudson C, Christophi C, Cebon J, Behren A, et al. Monitoring response to therapy in melanoma by quantifying circulating tumour DNA with droplet digital PCR for BRAF and NRAS mutations. Sci Rep. 2015;5(1):11198.

431. Rustin GJS, van der Burg MEL, Griffin CL, Guthrie D, Lamont A, Jayson GC, et al. Early versus delayed treatment of relapsed ovarian cancer (MRC OV05/EORTC 55955): a randomised trial. Lancet (London, England). 2010;376(9747):1155–63.

432. Flaherty KT, Hennig M, Lee SJ, Ascierto PA, Dummer R, Eggermont AMM, et al. Surrogate endpoints for overall survival in metastatic melanoma: a meta-analysis of randomised controlled trials. Lancet Oncol. 2014;15(3):297–304.

433. McArthur GA, Chapman PB, Robert C, Larkin J, Haanen JB, Dummer R, et al. Safety and efficacy of vemurafenib in BRAF(V600E) and BRAF(V600K) mutation-positive melanoma (BRIM-3): extended follow-up of a phase 3, randomised, open-label study. Lancet Oncol. 2014;15(3):323–32.

434. Hindson BJ, Ness KD, Masquelier DA, Belgrader P, Heredia NJ, Makarewicz AJ, et al. High-Throughput Droplet Digital PCR System for Absolute Quantitation of DNA Copy Number. Anal Chem. 2011;83(22):8604–10.

435. Rothwell D, Ayub M, Gulati S, Brognard J, Wallace A, Miller C, et al. The TARGET trial: Molecular profiling of circulating tumour DNA to stratify patients to early phase clinical trials. Eur J Surg Oncol. 2016;42(11):S244–5.

436. Merker JD, Oxnard GR, Compton C, Diehn M, Hurley P, Lazar AJ, et al. Circulating Tumor DNA Analysis in Patients With Cancer: American Society of Clinical Oncology and College of American Pathologists Joint Review. J Clin Oncol. 2018;36(16):1631–41.

437. Yates LR, Seoane J, Le Tourneau C, Siu LL, Marais R, Michiels S, et al. The European Society for Medical Oncology (ESMO) Precision Medicine Glossary. Ann Oncol.

2018;29(1):30–5.

438. Hellmann MD, Ciuleanu T-E, Pluzanski A, Lee JS, Otterson GA, Audigier-Valette C, et al. Nivolumab plus Ipilimumab in Lung Cancer with a High Tumor Mutational Burden. N Engl J Med. 2018;378(22):2093–104.

439. Chalmers ZR, Connelly CF, Fabrizio D, Gay L, Ali SM, Ennis R, et al. Analysis of 100,000 human cancer genomes reveals the landscape of tumor mutational burden.

440. Ng SB, Turner EH, Robertson PD, Flygare SD, Bigham AW, Lee C, et al. Targeted capture and massively parallel sequencing of 12 human exomes. Nature. 2009;461(7261):272–6.

441. Shoushtari AN, Munhoz RR, Kuk D, Ott PA, Johnson DB, Tsai KK, et al. The efficacy of anti-PD-1 agents in acral and mucosal melanoma. Cancer. 2016;122(21):3354–62.

442. Flaherty KT, Robert C, Hersey P, Nathan P, Garbe C, Milhem M, et al. Improved Survival with MEK Inhibition in BRAF-Mutated Melanoma. N Engl J Med. 2012;367(2):107–14.

443. Greenwell IB, Ip A, Cohen JB. PI3K Inhibitors: Understanding Toxicity Mechanisms and Management. Oncology (Williston Park). 2017;31(11):821–8.

444. Fruman DA, Rommel C. PI3K and cancer: lessons, challenges and opportunities. Nat Rev Drug Discov. 2014;13(2):140–56.

445. Abbott NJ. Blood–brain barrier structure and function and the challenges for CNS drug delivery. J Inherit Metab Dis. 2013;36(3):437–49.

446. Wijaya J, Fukuda Y, Schuetz JD. Obstacles to Brain Tumor Therapy: Key ABC Transporters. Int J Mol Sci. 2017;18(12).

447. Chalmers AJ, Short S, Watts C, Herbert C, Morris A, Stobo J, et al. Phase I clinical trials evaluating olaparib in combination with radiotherapy (RT) and/or temozolomide (TMZ) in glioblastoma patients: Results of OPARATIC and PARADIGM phase I and early

results of PARADIGM-2. J Clin Oncol. 2018;36(15_suppl):2018.

448. Criscitiello C, Viale G, Curigliano G, Goldhirsch A. Profile of buparlisib and its potential in the treatment of breast cancer: evidence to date. Breast cancer (Dove Med Press. 2018;10:23–9.

449. Valpione S, Carlino MS, Mangana J, Mooradian MJ, McArthur G, Schadendorf D, et al. Rechallenge with BRAF-directed treatment in metastatic melanoma: A multi-institutional retrospective study. Eur J Cancer. 2018;91:116–24.

450. Bacevic K, Noble R, Soffar A, Wael Ammar O, Boszonyik B, Prieto S, et al. Spatial competition constrains resistance to targeted cancer therapy. Nat Commun. 2017;8(1):1995.

451. Gallaher JA, Enriquez-Navas PM, Luddy KA, Gatenby RA, Anderson ARA. Spatial Heterogeneity and Evolutionary Dynamics Modulate Time to Recurrence in Continuous and Adaptive Cancer Therapies. Cancer Res. 2018;78(8):2127–39.

452. Zhang J, Cunningham JJ, Brown JS, Gatenby RA. Integrating evolutionary dynamics into treatment of metastatic castrate-resistant prostate cancer. Nat Commun. 2017;8(1):1816.

453. Amaria RN, Reddy SM, Tawbi HA-H, Davies MA, Ross MI, Glitza IC, et al. Neoadjuvant (neo) immune checkpoint blockade (ICB) in patients (Pts) with high-risk resectable metastatic melanoma (MM). J Clin Oncol. 2018;36(15_suppl):9510.

454. Rozeman EA, Blank CU, Van Akkooi ACJ, Kvistborg P, Fanchi L, Van Thienen J V, et al. Neoadjuvant ipilimumab + nivolumab (IPI+NIVO) in palpable stage III melanoma: Updated data from the OpACIN trial and first immunological analyses. J Clin Oncol. 2017;35(15_suppl):9586.

455. Tan L, Sandhu S, Lee RJ, Li J. Prediction and monitoring of relapse in stage II and III melanoma using circulating tumor DNA. Submitt J Clin Oncol. 2018;

456. Yang M, Forbes ME, Bitting RL, O'Neill SS, Chou P-C, Topaloglu U, et al. Incorporating blood-based liquid biopsy information into cancer staging: time for a TNMB system? Ann Oncol. 2018;29(2):311–23.

457. Weber J, Mandala M, Del Vecchio M, Gogas HJ, Arance AM, Cowey CL, et al. Adjuvant Nivolumab versus Ipilimumab in Resected Stage III or IV Melanoma. N Engl J Med. 2017;NEJMoa1709030.

458. Chen Y-H, Hancock BA, Solzak JP, Brinza D, Scafe C, Miller KD, et al. Next-generation sequencing of circulating tumor DNA to predict recurrence in triple-negative breast cancer patients with residual disease after neoadjuvant chemotherapy. npj Breast Cancer. 2017;3(1):24.

459. ClinicalTrials.gov. A Trial Using ctDNA Blood Tests to Detect Cancer Cells After Standard Treatment to Trigger Additional Treatment in Early Stage Triple Negative Breast Cancer Patients (c-TRAK TN) [Internet]. [cited 2018 May 18]. Available from: https://clinicaltrials.gov/ct2/show/NCT03145961

460. Wan J, Murphy S, Gale D, Morris J, Mouliere FC, Marass F, et al. Individualised monitoring of patients with metastatic melanoma using plasma DNA. Lancet. 2017;389:S99.

Appendices

Appendix 1. WES of tumours

Sample	Gene	Genomic coordinate	Amino acid change	Protein position	Codon	Ensemble gene	Variant allele frequency	Consequence
Subcutaneous								
	C1orf112	1:169811574	A/D	581	gCt/gAt	ENSG00000000460	49.4	missense variant
	CNTNAP5	2:125285000	D/G	538	gAt/gGt	ENSG00000155052	42.7	missense variant
	RFC1	4:39310321	C/Y	607	tGt/tAt	ENSG00000035928	49.7	missense variant
	PHOX2B	4:41747862	G/S	303	Ggt/Agt	ENSG00000109132	46.4	missense variant
	UGT8	4:115544259	G/W	75	Ggg/Tgg	ENSG00000174607	44.7	missense variant
	PPP2CA	5:133536183	P/L	194	cCa/cTa	ENSG00000113575	8	missense variant
	ZNF451	6:57012243	K/E	454	Aaa/Gaa	ENSG00000112200	43.8	missense variant
	BRAF	7:140453136	V/E	600	gTg/gAg	ENSG00000157764	53.8	missense variant
	ZNF395	8:28210761	Q/K	250	Caa/Aaa	ENSG00000186918	96.9	missense variant
	SNTG1	8:51314887	E/K	49	Gag/Aag	ENSG00000147481	61.7	missense variant
	BIRC3	11:102196044	S/R	268	agT/agA	ENSG00000023445	31.2	missense variant
	KIRREL3	11:126310409	A/T	430	Gcc/Acc	ENSG00000149571	64.8	missense variant
	CD27	12:6559782	S/C	175	tCt/tGt	ENSG00000139193	43.1	missense variant
	SIRT4	12:120750489	V/A	243	gTt/gCt	ENSG00000089163	94	missense variant
	SACS	13:23910703	E/Q	2438	Gaa/Caa	ENSG00000151835	88.5	missense variant
	SACS	13:23910717	W/*	1683	tGg/tAg	ENSG00000151835	88.5	stop gained
	SACS	13:23910941	K/N	2358	aaG/aaC	ENSG00000151835	84.5	missense variant
	SACS	13:23910961	A/T	1602	Gca/Aca	ENSG00000151835	79.3	missense variant
	SYT16	14:62541922	A/D	269	gCt/gAt	ENSG00000139973	41.2	missense variant
	SLC16A13	17:6943182	F/L	394	ttC/ttA	ENSG00000174327	46	missense variant
	SLC16A11	17:6945074	G/E	415	gGg/gAg	ENSG00000174326	51.7	missense variant

CLEC10A	17:6980096	S/F	103	tCt/tTt	ENSG00000132514	31.4	missense variant
CLEC10A	17:6980099	A/E	102	gCa/gAa	ENSG00000132514	32.2	missense variant
CLEC10A	17:6981319	Q/E	61	Caa/Gaa	ENSG00000132514	47.7	missense variant
CLEC10A	17:6981383	C/*	39	tgC/tgA	ENSG00000132514	47.7	stop gained

Sample	Gene	Genomic coordinate	Amino acid change	Protein position	Codon	Ensemble gene	Variant allele frequency	Consequence
Lymph node								
	C1orf112	1:169811574	A/D	581	gCt/gAt	ENSG00000000460	31.7	missense variant
	CNTNAP5	2:125285000	D/G	538	gAt/gGt	ENSG00000155052	16.3	missense variant
	RIF1	2:152301858	E/*	665	Gaa/Taa	ENSG00000080345	5	stop gained
	ITPR1	3:4836803	S/L	2225	tCg/tTg	ENSG00000150995	13.7	missense variant
	ITPR1	3:4878462	R/K	2663	aGa/aAa	ENSG00000150995	15.9	missense variant
	RFC1	4:39310321	C/Y	607	tGt/tAt	ENSG00000035928	35	missense variant
	PHOX2B	4:41747862	G/S	303	Ggt/Agt	ENSG00000109132	35	missense variant
	UGT8	4:115544259	G/W	75	Ggg/Tgg	ENSG00000174607	28.4	missense variant
	ADAMTS2	5:178540896	R/Q	1203	cGg/cAg	ENSG00000087116	10.6	missense variant
	ZNF451	6:57012243	K/E	454	Aaa/Gaa	ENSG00000112200	28	missense variant
	BRAF	7:140453136	V/E	600	gTg/gAg	ENSG00000157764	33.6	missense variant
	ZNF395	8:28210761	Q/K	250	Caa/Aaa	ENSG00000186918	53.7	missense variant
	SNTG1	8:51314887	E/K	49	Gag/Aag	ENSG00000147481	42.4	missense variant
	BIRC3	11:102196044	S/R	268	agT/agA	ENSG00000023445	15.1	missense variant
	KIRREL3	11:126310409	A/T	430	Gcc/Acc	ENSG00000149571	35.4	missense variant
	CD27	12:6559782	S/C	175	tCt/tGt	ENSG00000139193	27.5	missense variant
	SIRT4	12:120750489	V/A	243	gTt/gCt	ENSG00000089163	36.4	missense variant
	SACS	13:23910703	E/Q	1688	Gaa/Caa	ENSG00000151835	39.4	missense variant
	SACS	13:23910717	W/*	1683	tGg/tAg	ENSG00000151835	37.9	stop gained
	SACS	13:23910941	K/N	1608	aaG/aaC	ENSG00000151835	32.7	missense variant
	SACS	13:23910961	A/T	2352	Gca/Aca	ENSG00000151835	26.2	missense variant
	POSTN	13:38160342	E/K	277	Gag/Aag	ENSG00000133110	31	missense variant

SYT16	14:62541922	A/D	269	gCt/gAt	ENSG00000139973	26.4	missense variant
SLC16A13	17:6943182	F/L	394	ttC/ttA	ENSG00000174327	31.3	missense variant
SLC16A11	17:6945074	G/E	447	gGg/gAg	ENSG00000174326	27.6	missense variant
CLEC10A	17:6981319	Q/E	61	Caa/Gaa	ENSG00000132514	28.2	missense variant
CLEC10A	17:6981383	C/*	39	tgC/tgA	ENSG00000132514	30.3	stop gained
CLEC10A	17:6980096	S/F	103	tCt/tTt	ENSG00000132514	26.9	missense variant
CLEC10A	17:6980099	A/E	102	gCa/gAa	ENSG00000132514	27.8	missense variant
MKL1	22:40814719	V/L	575	Gtg/Ctg	ENSG00000196588	13	missense variant

Sample	Gene	Genomic coordinate	Amino acid change	Protein position	Codon	Ensemble gene	Variant allele frequency	Consequence
Brain								
	C1orf112	1:169811574	A/D	581	gCt/gAt	ENSG00000000460	38.3	missense variant
	CNTNAP5	2:125285000	D/G	538	gAt/gGt	ENSG00000155052	20.9	missense variant
	ITPR1	3:4878462	R/K	2663	aGa/aAa	ENSG00000150995	21.9	missense variant
	CRMP1	4:5868444	D/N	141	Gat/Aat	ENSG00000072832	23.1	missense variant
	RFC1	4:39310321	C/Y	607	tGt/tAt	ENSG00000035928	21.6	missense variant
	PHOX2B	4:41747862	G/S	303	Ggt/Agt	ENSG00000109132	23.8	missense variant
	UGT8	4:115544259	G/W	75	Ggg/Tgg	ENSG00000174607	21.5	missense variant
	ZNF451	6:57012243	K/E	454	Aaa/Gaa	ENSG00000112200	35.2	missense variant
	BRAF	7:140453136	V/E	600	gTg/gAg	ENSG00000157764	30.5	missense variant
	ZNF395	8:28210761	Q/K	250	Caa/Aaa	ENSG00000186918	68.5	missense variant
	SNTG1	8:51314887	E/K	49	Gag/Aag	ENSG00000147481	50.8	missense variant
	BIRC3	11:102196044	S/R	268	agT/agA	ENSG00000023445	38.4	missense variant
	KIRREL3	11:126310409	A/T	430	Gcc/Acc	ENSG00000149571	36.9	missense variant
	CD27	12:6559782	S/C	175	tCt/tGt	ENSG00000139193	39.8	missense variant
	NUAK1	12:106532376	A/G	19	gCg/gGg	ENSG00000074590	35.7	missense variant
	SIRT4	12:120750489	V/A	243	gTt/gCt	ENSG00000089163	62.5	missense variant
	SACS	13:23910703	E/Q	2438	Gaa/Caa	ENSG00000151835	50.5	missense variant
	SACS	13:23910717	W/*	2433	tGg/tAg	ENSG00000151835	54.2	stop gained
	SACS	13:23910941	K/N	2358	aaG/aaC	ENSG00000151835	45.3	missense variant
	SACS	13:23910961	A/T	2352	Gca/Aca	ENSG00000151835	34.7	missense variant
	SYT16	14:62541922	A/D	269	gCt/gAt	ENSG00000139973	38.1	missense variant
	SLC16A13	17:6943182	F/L	394	ttC/ttA	ENSG00000174327	38.2	missense variant
	SLC16A11	17:6945074	G/E	415	gGg/gAg	ENSG00000174326	36.9	missense variant
	CLEC10A	17:6980096	S/F	103	tCt/tTt	ENSG00000132514	25.7	missense variant
	CLEC10A	17:6980099	A/E	102	gCa/gAa	ENSG00000132514	26.5	missense variant
	CLEC10A	17:6981319	Q/E	61	Caa/Gaa	ENSG00000132514	42.1	missense variant
	CLEC10A	17:6981383	C/*	39	tgC/tgA	ENSG00000132514	43.6	stop gained

Appendix 2. Neoantigens present in baseline and anti PD-1 resistant lesions

Tumour	Gene	Chr	Position	Ref	Alt	VAF	AA change	HLA type	Wt net CTL score	Rank WT	Mt net CTL score	Rank Mut	Wt peptide	Mt peptide	Gene expression RPKM
Subcutaneous (baseline)	SACS	13	23910941	C	G	84.5	K/N	HLA-A*01:01	0.53519	0.8	0.628	0.4	YVDSEKVSF	YVDSE**N**VSF	1.581232263
	SACS	13	23910961	C	T	79.3	A/T	HLA-A*02:01	0.99609	0.3	0.99942	0.3	FILVENAYV	FILVEN**T**YV	1.581232263
	SACS	13	23910703	C	G	88.5	E/Q	HLA-B*08:01	0.7912	0.2	0.7948	0.2	LIREKKQEF	LIR**Q**KKQEF	1.581232263
	PHOX2B	4	41747862	C	T	46.4	G/S	HLA-C*07:01	0.54857	1	0.57353	0.8	RPNGAKAAL	RPN**S**AKAAL	0
	UGT8	4	115544259	G	T	44.7	G/W	HLA-B*08:01	0.56496	1.5	0.6579	0.8	SLQRYPGIF	SLQRYP**W**IF	4.33925292
	SLC16A13	17	6943182	C	A	46	F/L	HLA-C*07:01	0.6764	0.15	0.60699	0.4	LTLPHFFCF	LTLPH**L**FCF	1.116974898
	CLEC10A	17	6980096	G	A	31.4	S/F	HLA-A*02:01	0.83132	1	0.87851	0.8	SLEETIASL	SLEETI**EF**L	0.23895441
		17	6980099	G	T	32.2	A/E								
Lymph node (resistant)	SACS	13	23910941	C	G	32.7	K/N	HLA-A*01:01	0.53519	0.8	0.628	0.4	YVDSEKVSF	YVDSE**N**VSF	1.72987289
	SACS	13	23910961	C	T	26.2	A/T	HLA-A*02:01	0.99609	0.3	0.99942	0.3	FILVENAYV	FILVEN**T**YV	1.72987289
	SACS	13	23910703	C	G	39.4	E/Q	HLA-B*08:01	0.7912	0.2	0.7948	0.2	LIREKKQEF	LIR**Q**KKQEF	1.72987289
	PHOX2B	4	41747862	C	T	35	G/S	HLA-C*07:01	0.54857	1	0.57353	0.8	RPNGAKAAL	RPN**S**AKAAL	0
	UGT8	4	115544259	G	T	28.4	G/W	HLA-B*08:01	0.56496	1.5	0.6579	0.8	SLQRYPGIF	SLQRYP**W**IF	0.851603759
	SLC16A13	17	6943182	C	A	31.3	F/L	HLA-C*07:01	0.6764	0.15	0.60699	0.4	LTLPHFFCF	LTLPH**L**FCF	1.297087606
	ITPR1	3	4836803	C	T	13.7	S/L	HLA-A*01:01	0.44893	1.5	0.53327	0.8	MSFWSSISF	MSFWSSI**L**F	1.7971032
	ITPR1	3	4836803	C	T	13.7	S/L	HLA-C*07:01	0.84393	0.01	0.78527	0.05			
	CLEC10A	17	6980096	G	A	26.9	S/F	HLA-A*02:01	0.83132	1	0.87851	0.8	SLEETIASL	SLEETI**EF**L	2.15467183
		17	6980099	G	T	27.8	A/E								
Brain (immune escape)	SACS	13	23910941	C	G	45.3	K/N	HLA-A*01:01	0.53519	0.8	0.628	0.4	YVDSEKVSF	YVDSE**N**VSF	1.72987289
	SACS	13	23910961	C	T	34.7	A/T	HLA-A*02:01	0.99609	0.3	0.99942	0.3	FILVENAYV	FILVEN**T**YV	1.72987289
	SACS	13	23910703	C	G	50.5	E/Q	HLA-B*08:01	0.7912	0.2	0.7948	0.2	LIREKKQEF	LIR**Q**KKQEF	1.72987289
	PHOX2B	4	41747862	C	T	23.8	G/S	HLA-C*07:01	0.54857	1	0.57353	0.8	RPNGAKAAL	RPN**S**AKAAL	0
	UGT8	4	115544259	G	T	21.5	G/W	HLA-B*08:01	0.56496	1.5	0.6579	0.8	SLQRYPGIF	SLQRYP**W**IF	0.851603759
	SLC16A13	17	6943182	C	A	38.2	F/L	HLA-C*07:01	0.6764	0.15	0.60699	0.4	LTLPHFFCF	LTLPH**L**FCF	1.297087606
	CLEC10A	17	6980096	G	A	25.7	S/F	HLA-A*02:01	0.83132	1	0.87851	0.8	SLEETIASL	SLEETI**EF**L	2.15467183

Appendix 3. Biological processes of pathways up-regulated in resistant compared to baseline lesion

Name	Term identifier	FDR	Gene intersection
leukocyte activation	GO:0045321	7.12E-14	FGR,CD38,ITGAL,CD4,BTK,SLC11A1,CD74,NR1H3,SLAMF7,STAP1,PRKCQ,CD84,STXBP2,EDN1,LAT2,SIRPG,CD209,UNC13D,IL12RB1,MFNG,GRAP2,SLA2,CD40LG,CORO1A,IL21R,RASAL3,EBI3,CD79A,MAP3K8,CCL2,SELPLG,PTPN6,VNN1,ITK,CD86,ZAP70,CD2,SLAMF1,VAMP8,CLU,CCR2,LAX1,NCKAP1L,BATF3,IRF1,IL1B,CD93,CCR7,RIPK3,LILRB2,PTPN22,RSAD2,DOCK2,ANXA1,TESPA1,LCP1,IL6,IL10,SIT1,CD27,VAV1,CD8A,SAMSN1,BATF,PRKCB,CD3D,NLRC3,LST1,IGHV3-23,HLA-DPB1,HLA-DPA1,HLA-DQB2,NFAM1,HLA-DMB,IGLL5,CCL5
leukocyte migration	GO:0050900	7.80E-11	ITGAL,CCL26,SELE,CD74,STAP1,CD84,TBX21,CXCL2,SIRPG,HMOX1,PROCR,HCK,MAG,RARRES2,CXCL12,CCL2,CCL8,PF4V1,SELPLG,PTPN6,CCL20,ZAP70,CD2,CD48,PADI2,TEK,CCR2,NCKAP1L,CXCL6,CCR7,RIPK3,ANXA1,IL6,MYO1G,IL10,NOV,ITGAX,XCL2,S100A8,PLA2G7,DOK2,PTPRO,MERTK,JAM2,SLC7A7,CXCL13,PF4,CXCL10,TNFRSF18,TNF,CCL5
adaptive immune response	GO:0002250	9.43E-08	BTK,WAS,SLC11A1,CD74,PRKCQ,IL12RB1,SLA2,CD40LG,EBI3,ITK,BCL6,ZAP70,CCR2,IRF1,IL1B,RIPK3,IGJ,RSAD2,ANXA1,CTSL,IL6,MYO1G,IL10,IL18BP,CD27,CD8A,SAMSN1,BATF,CXCL13,IGHV3-23,IGKV3-11,IGKV1-5,IGLL5
response to molecule of bacterial origin	GO:0002237	9.83E-08	SELE,LTF,SLC11A1,NR1H3,TNFRSF1B,STAP1,NGFR,CXCL2,HCK,CCL2,PF4V1,LY86,SLPI,CXCL6,IL1B,IRF5,LILRB2,CD180,PTPN22,CD36,IL6,IL10,TLR2,CD27,CXCL13,PF4,CXCL10,CD14,TNFRSF18,TNFRSF25,TNF,CCL5
cytokine production	GO:0001816	1.99E-07	FGR,CD4,BTK,LTF,SLC11A1,CD74,BIRC3,FLT4,PRKCQ,CD84,PTGS2,FCN1,NLRC4,NLRP1,IL12RB1,PCSK5,HMOX1,CD40LG,EBI3,DDX58,DHX58,CRTAM,ITK,CD86,CD2,SLAMF1,GBP1,CLU,CCR2,SRGN,NCKAP1L,ZBP1,IRF1,IL1B,C3,CCR7,IRF5,RIPK3,LILRB2,CHI3L1,PTPN22,RSAD2,ANXA1,HAVCR2,CD36,IL6,GATA4,IL10,TLR2,CYP1B1,S100A8,GBP5,BATF,PF4,NLRC3,CD14,ISG15,HLA-DPB1,LTB,HLA-DPA1,TNF,HLA-B,NFAM1
activation of immune response	GO:0002253	9.61E-07	FGR,CD38,CD4,BTK,LTF,WAS,MARCO,BIRC3,NR1H3,STAP1,PRKCQ,FYB,FCN1,LAT2,PSMC5,CD209,NLRC4,GRAP2,SLA2,HCK,CD79A,DDX58,MAP3K8,ICAM2,DHX58,MAPK10,CLEC4A,C7,ITK,ZAP70,GBP1,CLU,NCKAP1L,IRF1,IL1B,C3,CFP,RIPK3,PTPN22,RSAD2,CTSL,CD36,TESPA1,MYO1G,BLK,TLR2,SKAP1,VAV1,FCN3,SERPING1,FCGR1A,PRKCB,CD3D,CD14,IGHV3-23,HLA-DPB1,HLA-DPA1,HLA-DQB2,NFAM1,PSMB9,IGKV3-11,IGKV1-5,IGLL5
chemokine-mediated signaling pathway	GO:0070098	2.58E-06	CCL26,EDN1,CXCL2,TREM2,CXCL12,CCL2,CCL8,PF4V1,CCL20,PADI2,CCR2,CXCL6,CCR7,XCL2,CXCL13,PF4,CXCL10,CCL5
response to interferon-gamma	GO:0034341	8.59E-05	CCL26,SLC11A1,NR1H3,IL12RB1,HCK,CCL2,CCL8,PTPN6,CCL20,KYNU,GBP1,IRF1,IRF5,TRIM22,OASL,IRF8,IFITM3,XCL2,FCGR1A,HLA-DPB1,HLA-DPA1,HLA-DQB2,HLA-B,CCL5
regulation of phagocytosis	GO:0050764	0.00044	FGR,SLC11A1,STAP1,HCK,CCL2,NCKAP1L,IL1B,C3,DOCK2,BLK,MERTK,TNF
positive regulation of ERK1 and ERK2 cascade	GO:0070374	0.000557	CCL26,CD74,FLT4,FGFR2,MT3,TREM2,CCL2,CCL8,FGF1,CCL20,SLAMF1,TEK,CCR7,PLA2G5,CHI3L1,PTPN22,PDGFRA,CD36,XCL2,SCIMP,TNF,CCL5
type I interferon signaling pathway	GO:0060337	0.000906	IFI35,SAMHD1,PTPN6,IFIT3,IFIT2,EGR1,IRF1,IFI6,IRF5,XAF1,RSAD2,OASL,IRF8,IFITM3,ISG15,HLA-B
type 2 immune response	GO:0042092	0.00343	BCL6,CD86,CCR2,RSAD2,ANXA1,IL10,BATF
leukocyte apoptotic process	GO:0071887	0.00955	BTK,PRKCQ,CXCL12,BCL6,CCR7,RIPK3,IDO1,CTSL,IL6,IL10,MERTK,CCL5
regulation of antigen processing and presentation	GO:0002577	0.0098	WAS,SLC11A1,ABCB1,TREM2,CCR7,LILRB2,HLA-DOB
negative regulation of viral genome replication	GO:0045071	0.0171	LTF,APOBEC3H,SLPI,APOBEC3A,RSAD2,OASL,IFITM3,ISG15,TNF,CCL5
positive regulation of nitric oxide biosynthetic process	GO:0045429	0.0177	PTGS2,EDN1,CLU,IL1B,ASS1,TNF,HBB
cellular response to diacyl bacterial lipopeptide	GO:0071726	0.0306	CD36,TLR2,CD14
positive regulation of phospholipase activity	GO:0010518	0.0355	SELE,GNA15,FGFR2,ITK,PDE1A,S1PR4,PLA2G5,ADCY4,NGF,PDGFRA,ADCY5,APOC2,CCL5
regulation of membrane protein ectodomain proteolysis	GO:0051043	0.0496	TNFRSF1B,TIMP1,IL1B,IL10,TIMP4,TNF

Appendix 4. Gene signature associated with loss of PTEN

Taken from Peng *et al* 2016 and Dong *et al* 2014.

Gene	Subcutaneous	Brain	log2FC (Brain/Subcutaneous)
CCL2	5.30	106.61	4.33
VEGFA	13.92	4.29	-1.70
IL6	0.12	3.12	4.74
IL10	0.06	2.70	5.54
CCL21	0.26	0.24	-0.17
CXCL1	0.21	73.00	8.43
STAT3	17.27	13.37	-0.37
CXCL10	1.86	26.17	3.81
PTEN	22.90	17.92	-0.35

Appendix 5. Gene signature associated with WNT/β-catenin activation

Taken from Spranger *et al* 2015.

Gene	Subcutaneous	Brain	log2FC (Brain/Subcutaneous)
EFNB3	3.49	1.32	-1.40
VEGFA	13.92	4.29	-1.70
APC2	0.77	0.48	-0.68
HNF1A	0.00	0.00	0.00
MYC	151.31	45.32	-1.74
TCF12	26.70	6.22	-2.10

Appendix 6. Chemokines that are decreased in association with WNT/β-catenin activation

Taken from Spranger *et al* 2015.

Gene	Subcutaneous	Brain	log2FC (Brain/Subcutaneous)
CCL3	1.78	33.10	4.22
CXCL2	0.24	15.81	6.04
CCL4	0.36	16.05	5.47
CXCL1	0.21	73.00	8.43
CCL11	0.20	0.00	-17.61

Appendix 7. WES of cell line derived from brain lesion resected on progression on dabrafenib

Gene	Genomic coordinate	Amino acid change	Protein position	Codon	Ensemble gene	Variant allele frequency	Consequence
PER3	1:7895945-7895945	I/T	1104	aTc/aCc	ENSG00000049246	13.3	missense_variant
PER3	1:7895951-7895951	R/I	1106	aGa/aTa	ENSG00000049246	15.1	missense_variant
C1orf112	1:169811574-169811574	A/D	581	gCt/gAt	ENSG00000000460	44.6	missense_variant
ALK	2:29474041-29474041	V/M	712	Gtg/Atg	ENSG00000171094	6.3	missense_variant
CNTNAP5	2:125285000-125285000	D/G	538	gAt/gGt	ENSG00000155052	36.2	missense_variant
XIRP2	2:168102774-168102774	L/F	1624	ttG/ttT	ENSG00000163092	36.3	missense_variant
XIRP2	2:168106187-168106187	H/R	2762	cAt/cGt	ENSG00000163092	6.3	missense_variant
PIK3CA	3:178916687-178916687	L/S	25	tTa/tCa	ENSG00000121879	6.4	missense_variant
CRMP1	4:5868444-5868444	D/N	141	Gat/Aat	ENSG00000072832	70.6	missense_variant
RFC1	4:39310321-39310321	C/Y	607	tGt/tAt	ENSG00000035928	29.2	missense_variant
PHOX2B	4:41747862-41747862	G/S	303	Ggt/Agt	ENSG00000109132	29.6	missense_variant
PDGFRA	4:55139771-55139771	S/P	478	Tcc/Ccc	ENSG00000134853	20.9	missense_variant
UGT8	4:115544259-115544259	G/W	75	Ggg/Tgg	ENSG00000174607	8	missense_variant
ZFP42	4:188923984-188923984	R/Q	8	cGg/cAg	ENSG00000179059	24.6	missense_variant
APC	5:112176756-112176756	V/D	1822	gTc/gAc	ENSG00000134982	78.3	missense_variant
ZNF451	6:57012243-57012243	K/E	454	Aaa/Gaa	ENSG00000112200	48.2	missense_variant
ROS1	6:117683821-117683821	S/L	1109	tCa/tTa	ENSG00000047936	28.8	missense_variant
ROS1	6:117725448-117725448	T/P	145	Act/Cct	ENSG00000047936	42.3	missense_variant
BRAF	7:140453136-140453136	V/E	600	gTg/gAg	ENSG00000157764	37.5	missense_variant
ZNF395	8:28210761-28210761	Q/K	250	Caa/Aaa	ENSG00000186918	99.6	missense_variant
SNTG1	8:51314887-51314887	E/K	49	Gag/Aag	ENSG00000147481	66.8	missense_variant
KCNQ3	8:133153516-133153516	G/E	442	gGa/gAa	ENSG00000184156	2.6	missense_variant
CLP1	11:57427019-57427019	R/H	24	cGc/cAc	ENSG00000172409	3.3	missense_variant
BIRC3	11:102196044-102196044	S/R	268	agT/agA	ENSG00000023445	51.7	missense_variant
KIRREL3	11:126310409-126310409	A/T	430	Gcc/Acc	ENSG00000149571	49.8	missense_variant
CD27	12:6559782-6559782	S/C	175	tCt/tGt	ENSG00000139193	51.3	missense_variant
SIRT4	12:120750489-120750489	V/A	243	gTt/gCt	ENSG00000089163	100	missense_variant

SACS	13:23910703-23910703	E/Q	2438	Gaa/Caa	ENSG00000151835	100	missense_variant
SACS	13:23910717-23910717	W/*	2433	tGg/tAg	ENSG00000151835	100	stop_gained
SACS	13:23910727-23910727	E/K	2430	Gaa/Aaa	ENSG00000151835	100	missense_variant
SACS	13:23910941-23910941	K/N	2358	aaG/aaC	ENSG00000151835	100	missense_variant
SACS	13:23910961-23910961	A/T	2352	Gca/Aca	ENSG00000151835	100	missense_variant
SYT16	14:62541922-62541922	A/D	269	gCt/gAt	ENSG00000139973	46.3	missense_variant
VWA9	15:65890778-65890778	T/M	153	aCg/aTg	ENSG00000138614	66.7	missense_variant
SSTR5	16:1129544-1129544	V/L	226	Gtg/Ctg	ENSG00000162009	5.6	missense_variant
SLC16A13	17:6943182-6943182	F/L	394	ttC/ttA	ENSG00000174327	49.4	missense_variant
SLC16A11	17:6945074-6945074	G/E	447	gGg/gAg	ENSG00000174326	51.1	missense_variant
CLEC10A	17:6980096-6980096	S/F	103	tCt/tTt	ENSG00000132514	34.8	missense_variant
CLEC10A	17:6980099-6980099	A/E	102	gCa/gAa	ENSG00000132514	37.3	missense_variant
CLEC10A	17:6981319-6981319	Q/E	61	Caa/Gaa	ENSG00000132514	48.6	missense_variant
CLEC10A	17:6981383-6981383	C/*	39	tgC/tgA	ENSG00000132514	46.9	stop_gained
TP53	17:7572973-7572973	R/H	379	cGc/cAc	ENSG00000141510	2.8	missense_variant
TP53	17:7579472-7579472	P/R	72	cCc/cGc	ENSG00000141510	41.6	missense_variant
SUGP2	19:19121059-19121059	D/G	648	gAc/gGc	ENSG00000064607	4	missense_variant
DUSP9	X:152914776-152914776	G/S	155	Ggt/Agt	ENSG00000130829	60.3	missense_variant

Appendix 8. Analysis of *PI3KCA* L25S mutation by droplet digital PCR

Target	Concentration	CopiesPer20uLWell	Sample
pi3k mt	0	0	Neg control
pi3k wt	72.1	1442	
pi3k mt	0	0	Neg control
pi3k wt	68.3	1366	
pi3k mt	0	0	Subcutaneous cell line
pi3k wt	42.1	842	
pi3k mt	0	0	Subcutaneous cell line
pi3k wt	44.9	898	
pi3k mt	0	0	Subcutaneous cell line
pi3k wt	42.5	850	
pi3k mt	0	0	Dabrafenib resistant brain cell line
pi3k wt	53.6	1072	
pi3k mt	0	0	Dabrafenib resistant brain cell line
pi3k wt	52.8	1056	
pi3k mt	0	0	Dabrafenib resistant brain cell line
pi3k wt	42	840	

Appendix 9. RPPA analysis of brain derived cell line treated with DMSO or Dabrafenib (1μM) in RPMI or 50% CSF

Protein name	Normalised relative fluorescence intensity (average value of triplicate)			
	DMSO	Dabrafenib	DMSO + CSF	Dabrafenib + CSF
MEK 1/2	1898.426871	2515.523664	2185.882269	2812.987848
MEK1/2 P Ser217/221	1906.400329	272.1121359	1865.853604	300.3636393
PI3 Kinase p110-alpha	680.7935551	684.5502679	638.5095091	830.3803952
IGF-1R beta P Tyr1162,Tyr1163	2792.454264	3209.092209	2552.795115	3140.662677
ErbB-1/EGFR	112.4107869	125.4879973	119.2474221	112.1634508
EGFR P Tyr1173	2057.646659	2183.309445	2142.631491	2258.57687
Akt P Thr308	1296.255981	1344.026181	5006.123938	6707.299774
S6 Ribosomal protein P Ser235,Ser236	2690.414778	591.7004921	3243.750491	1274.066475
p44/42 MAPK (ERK1/2)	8218.64058	8906.724774	7693.954315	8413.358699
p44/42 MAPK (ERK1/2) PThr202/Thr185,Tyr204/Tyr187	17405.81747	643.003303	12805.82781	636.6986512
AKT	7171.96852	7610.630166	6344.953432	6340.596981
Akt P Ser473	1106.371708	1200.026315	5076.214748	7404.190434
PTEN	93.65532333	106.9297504	110.9061712	112.3985103
Tsc-2 (Tuberin) P Thr1462	190.2261377	224.9543389	171.6849506	203.0893503
Tsc-2 (Tuberin)	920.0616818	1046.059268	982.5832583	1039.644738
p70 S6 Kinase P Thr389	933.1147254	758.6820984	1115.282953	1005.515075
p70 S6 Kinase P Thr421,Ser424	1272.467773	886.3753906	1432.481434	1320.781799
mTOR P Ser2448	458.292043	373.0352463	496.2462341	512.0083114
mTOR	660.7155123	691.8087506	629.0729916	670.2319082
Raf P Ser259	246.334558	251.8413049	237.1588625	241.5851748
S6 Ribosomal protein p Ser240,Ser244	4363.541908	829.3155627	5156.392657	1989.353002
S6 Ribosomal Protein	4408.157179	3835.735189	4260.131906	3788.385983
Raf P Ser338	821.71695	854.2467156	801.9399785	904.6645577
EGFR P Tyr1086	3651.541896	4215.976341	3502.766569	4095.611146
IGF-1R beta	338.0423687	367.0837729	270.8039697	313.4813658
ErbB-2/Her2/EGFR	1697.372534	1907.338319	1676.264665	2069.40315
p90 S6 kinase (Rsk1-3)	2998.881119	3655.235899	3263.714234	3688.840469
mTOR P Ser2481	1220.535979	1340.267869	1292.445766	1312.053967
Fox01 P	150.1272403	170.2133974	175.2989188	195.2613306
FAK1	369.1690445	339.7185191	407.3738099	346.2693667
FAK1 P Y397	1205.759332	1338.098269	1128.843005	1246.061495
FLT3 P Tyr591 P Tyr591	547.5495744	661.6131979	514.2516314	595.452659
IkB-alpha	276.5429402	321.4744914	308.2127216	363.1716815
IKK alpha/beta P Ser176/Ser177	785.3167062	762.2339425	675.9145462	705.1545112
JAK1	249.9900142	220.5261601	232.0289822	225.3229292
Met P Tyr1234	1100.930218	1189.166656	1110.263143	1087.354629
PKC (pan) P Ser660 (beta-2)	3255.090728	2290.345002	2429.839241	1675.697341
PKC substrate P (R/K)X(S*)(Hyd)(R/k)	3450.471597	3429.666384	3331.908838	3100.825346
PKC-zeta	225.4865166	227.3357431	232.9430751	223.4248639

PKC-zeta/lambda P Thr410/403	934.6907641	914.0999166	944.5897857	943.9806757
Met P Tyr1349	1863.150184	2061.901493	2059.233722	2614.193494
ErbB-2/Her2/EGFR P Tyr1248/Tyr1173	400.2880792	350.0765688	317.5461941	277.1547891
ErbB-3/Her3/EGFR	1339.459149	1253.77497	1305.642135	1196.674497
ErbB-3/Her3/EGFR P Tyr1289	245.6528891	261.3345505	233.4036378	257.4447013
STAT5	1901.374651	1837.062431	1690.745607	1644.983899
Stat5 P Tyr694	506.8943735	514.6399767	557.4268061	564.7473445
Met	276.3511631	240.6349457	228.1722156	200.0022836
IkB-alpha P Ser32	673.8237901	665.7234783	605.7228882	621.4248055
NFkB p65 Ser536	1415.073194	1296.7033	1231.939492	1154.0571
M-CSF P Tyr723	744.0322283	664.0460157	678.1271852	604.2990677
EGFR P Tyr1086	3651.541896	4215.976341	3502.766569	4095.611146
IGF-1R beta	338.0423687	367.0837729	270.8039697	313.4813658
ErbB-2/Her2/EGFR	1697.372534	1907.338319	1676.264665	2069.40315
p90 S6 kinase (Rsk1-3)	2998.881119	3655.235899	3263.714234	3688.840469
mTOR P Ser2481	1220.535979	1340.267869	1292.445766	1312.053967
FOX01 P	150.1272403	170.2133974	175.2989188	195.2613306
SAPK/JNK P Thr183,Tyr185	573.5935936	505.5915106	552.9466167	475.2439232
MAPKAPK-2 P Thr334	339.5892933	320.1601236	330.3721772	317.6206487
Stat6	428.5359183	434.8131863	350.9548922	343.6868921
Stat1 P Tyr701	229.8858481	279.1078906	244.4509983	310.2007792
Smad2/3 P Ser465/Ser423,Ser467/Ser425	1056.530741	1075.279935	1033.236307	991.6769813
Smad1/5 P Ser463/Ser465	272.6489919	274.8513649	298.6359242	337.6973628
IRS-1	196.8436357	168.7379048	191.2821243	171.7436537
IRS-1 P S636/639	2194.151231	2367.558881	2135.958426	2221.745643
Puma	340.5660642	336.4152337	303.2597949	303.4613378
SHP2 P Tyr542	540.9914025	589.5597378	562.3953641	510.8309445
Smad2 P Ser465,Ser467	589.6171015	654.2232718	611.1884886	668.7398966
VEGFR P Tyr951	961.7979716	907.7593861	1049.919132	979.0488154
Smad3 P Ser423,Ser425	1815.046779	1723.636182	1822.499983	1658.527922
MAPKAPK-2	8015.463649	7520.32011	7879.132502	7222.793406
Stat3	4743.458947	4452.299658	4712.21113	4153.278699
VEGFR P Tyr1059	380.9656152	358.6666469	426.1440477	364.7180705
NFkB p105/p50	755.314292	751.5913704	804.6958503	735.2080822
PDGFR P Tyr1021	719.8830082	643.245105	690.6926359	670.4202744
PDGFR P Tyr751	268.175223	308.2641847	370.1137557	391.9456134

Appendix 10. Clinical characteristics of patients from which cell lines obtai

Patient number	Age at diagnosis of stage IV disease	Sex	M stage at diagnosis stage IV disease	LDH at diagnosis of stage IV disease	Number of disease sites at diagnosis of stage IV disease	Mutation status at time of sampling	Survival (days) from diagnosis of stage IV disease	Location of sample cell line derived from	Treatments prior to sampling	Treatments following sampling
RM11 PDX	60s	M	M1c	614	3 (brain, small bowel, lymph node)	BRAF V600E	228	Right axillary dissection	None	Dabrafenib+ Trametinib, Ipilimumab, Vemurafenib
RM209	60s	M	M1c	552	2 (Liver, lung)	BRAF V600E	267	Left axillary dissection	None	Dabrafenib + Trametinib
RM156 CDX	50s	M	M1c	11,918	3 (Liver, nodal, lung)	BRAF V600E	76	Left inguinal dissection	None	Dabrafenib
RM57 CDX	40s	M	M1c	1243	3 (axilla, liver, spleen)	BRAF V600E	106	Right axillary dissection	None	Vemurafenib,Dabrafenib
RM44	50s	M	M1c	489	2 (Liver, nodal)	BRAF V600K	513	Left axillary dissection	None	Nivolumab, Vemurafenib. Pembrolizumab
RM33	30s	F	M1d	NA	5 (Brain, lungs, spleen, subcutaneous, axilla)	BRAF K601E	473	Subcutaneous - back	Dacarbazine, Ipilimumab	Carboplatin + Paclitaxel
RM2	30s	F	M1d	671	4 (Liver, lung, brain, subcutaneous)	BRAF V600E and NRAS	214	Subcutaneous - chest wall	Vemurafenib, Ipilimumab	None
RM62	NA	F	NA	NA	NA	BRAF V600E and NRAS G13R	224	Subcutaneous right leg	Vemurafenib	None
RM103	50s	F	M1b	421	2 (lung, subcutaneous)	BRAF V600E and NRAS Q61K	597	Subcutaneous left thigh	Checkmate 067, Vemurafenib, Dabrafenib	Millenium study, Pembrolizumab
RM72	80s	F	M1c	469	3 (adrenal, lung, mesenteric)	NRAS Q61K	318	Left axillary dissection	None	Ipilimumab
RM49 PDX	NA	M	NA	NA	2 (Pelvic)	NRAS Q61L	742	Right inguinal dissection	None	Pembrolizumab, Ipilimumab
RM81	80s	M	M1d	478	1 (Brain)	NRAS Q61L	80	Right axillary dissection	None	None
RM59	50s	M	M1b	400	2 (Lung, axilla)	NRAS Q61R	212	Right axillary dissection	None	Dacarbazine, Ipilimumab

NA= data not available, M= male, F= female

Appendix 11. WES of acquired mutations in A375 cell line following culture in CCT3833

Gene	Genomic coordinate	Amino acid change	Protein position	Codon	Ensemble gene	Variant allele frequency	Consequence
UBR4	1:19536690	G/T	p.T18N	c.C53A	ENSG00000127481	27.8	missense variant
EIF4G3	1:21205892	T/A	p.D283V	c.A848T	ENSG00000075151	24.9	missense variant
EIF4G3	1:21205893	C/A	p.D283Y	c.G847T	ENSG00000075151	24.9	missense variant
KIAA1522	1:33236516	C/T	p.S520L	c.C1559T	ENSG00000162522	34.3	missense variant
WDR78	1:67358963	T/C	p.Y160C	c.A479G	ENSG00000152763	27	missense variant
ZNF648	1:182026116	A/C	p.F344V	c.T1030G	ENSG00000179930	22.7	missense variant
CDC42BPA	1:227216501	T/C	p.Q1367R	c.A4100G	ENSG00000143776	27.1	missense variant
CNGA3	2:98986452	A/G	p.N5S	c.A14G	ENSG00000144191	31.1	missense variant
KIAA1211L	2:99439999	C/T	p.R246H	c.G737A	ENSG00000196872	35.5	missense variant
MERTK	2:112754963	T/C	p.I329T	c.T986C	ENSG00000153208	31.7	missense variant
AMER3	2:131522146	G/T	p.C834F	c.G2501T	ENSG00000178171	37.9	missense variant
EVX2	2:176948468	C/A	p.E13X	c.G37T	ENSG00000174279	5.1	stopgain
GTF3C3	2:197643638	C/T	p.V143I	c.G427A	ENSG00000119041	29	missense variant
FAM124B	2:225265960	G/A	p.L176F	c.C526T	ENSG00000124019	61.6	missense variant
SP140	2:231106137	C/T	p.P142L	c.C425T	ENSG00000079263	35.8	missense variant
HTR2B	2:231978565	A/G	p.M144T	c.T431C	ENSG00000135914	48.1	missense variant
UGT1A5	2:234621929	C/G	p.Q98E	c.C292G	ENSG00000240224	47.3	missense variant
LRRFIP1	2:238601108	C/A	p.P4T	c.C10A	ENSG00000124831	52.6	missense variant
KIF15	3:44867581	A/G	p.Y502C	c.A1505G	ENSG00000163808	26.2	missense variant
PROS1	3:93692556	G/C	p.A13G	c.C38G	ENSG00000184500	35.4	missense variant
STXBP5L	3:121097617	A/T	p.K744I	c.A2231T	ENSG00000145087	39.3	missense variant
ILDR1	3:121712452	C/A	p.D293Y	c.G877T	ENSG00000145103	26.1	missense variant
ACAD11	3:132361565	T/C	p.T111A	c.A331G	ENSG00000240303	30.8	missense variant
FAM184B	4:17706768	C/T	p.R411H	c.G1232A	ENSG00000047662	5.5	missense variant
HPGDS	4:95229814	G/A	p.P103S	c.C307T	ENSG00000163106	44.8	missense variant
MTTP	4:100485255	G/A	p.M1I	c.G3A	ENSG00000138823	44.2	missense variant
MTTP	4:100504664	T/C	p.I128T	c.T383C	ENSG00000138823	54.8	missense variant
BANK1	4:102751072	T/C	p.Y60H	c.T178C	ENSG00000153064	47.9	missense variant
BDH2	4:104013796	T/C	p.N70S	c.A209G	ENSG00000164039	32.5	missense variant

CENPE	4:104061993	C/G	p.S1886T	c.G5657C	ENSG00000138778	45.1	missense variant
TBCK	4:107156462	C/T	p.M1I	c.G3A	ENSG00000145348	61.9	missense variant
CCDC109B	4:110581363	T/A	p.I63N	c.T188A	ENSG00000005059	46.9	missense variant
KIAA1109	4:123277795	A/T	p.K1509N	c.A4527T	ENSG00000138688	44.7	missense variant
C4orf33	4:130030652	A/G	p.M107V	c.A319G	ENSG00000151470	50.6	missense variant
MAB21L2	4:151504461	C/A	p.L94M	c.C280A	ENSG00000181541	50	missense variant
MAB21L2	4:151504462	T/A	p.L94Q	c.T281A	ENSG00000181541	51.1	missense variant
PRSS48	4:152201053	G/A	p.C53Y	c.G158A	ENSG00000189099	58.2	missense variant
FGB	4:155489608	C/T	p.P46L	c.C137T	ENSG00000171564	42	missense variant
MAP9	4:156274377	T/C	p.K499R	c.A1496G	ENSG00000164114	44.7	missense variant
DDX60L	4:169369920	C/T	p.C64Y	c.G191A	ENSG00000181381	38.7	missense variant
TRAPPC11	4:184612553	G/C	p.V266L	c.G796C	ENSG00000168538	51.1	missense variant
FAM149A	4:187078866	C/T	p.P241L	c.C722T	ENSG00000109794	40	missense variant
SLC6A18	5:1225618	C/T	p.P9L	c.C26T	ENSG00000164363	33.9	missense variant
SLC6A3	5:1443310	C/T	p.M1I	c.G3A	ENSG00000142319	60.7	missense variant
AP3B1	5:77334914	T/C	p.E921G	c.A2762G	ENSG00000132842	55.6	missense variant
PROB1	5:138730304	C/T	p.R156H	c.G467A	ENSG00000228672	23.5	missense variant
GRIA1	5:153174182	A/T	p.N678Y	c.A2032T	ENSG00000155511	35.7	missense variant
DNAH8	6:38723776	T/C	p.L262S	c.T785C	ENSG00000124721	29.7	missense variant
RCAN2	6:46424492	G/C	p.S74R	c.C222G	ENSG00000172348	32.4	missense variant
MDN1	6:90411380	T/G	p.Q2775P	c.A8324C	ENSG00000112159	47.3	missense variant
TRDN	6:123545267	T/G	p.E654A	c.A1961C	ENSG00000186439	59.2	missense variant
TRDN	6:123545268	C/A	p.E654X	c.G1960T	ENSG00000186439	58.8	missense variant
VWDE	7:12376679	C/T	p.G1498E	c.G4493A	ENSG00000146530	22.7	missense variant
POLD2	7:44157644	C/A	p.K80N	c.G240T	ENSG00000106628	22.1	missense variant
KCTD7	7:66103886	C/T	p.P123S	c.C367T	ENSG00000243335	41.8	missense variant
KCTD7	7:66103887	C/T	p.Q180X	c.C538T	ENSG00000243335	40.6	stopgain
PCLO	7:82476470	T/C	p.E4583G	c.A13748G	ENSG00000186472	54.7	missense variant
TRRAP	7:98606133	C/G	p.Y3604X	c.C10812G	ENSG00000196367	52.2	stopgain
ST18	8:53077713	T/G	p.N426T	c.A1277C	ENSG00000147488	31.2	missense variant
CALB1	8:91075674	A/T	p.S99T	c.T295A	ENSG00000104327	49.3	missense variant
LRRC6	8:133637534	T/A	p.K34X	c.A100T	ENSG00000129295	12.2	stopgain
FRMPD1	9:37745561	C/T	p.P1178S	c.C3532T	ENSG00000070601	44.6	missense variant
UBQLN1	9:86293441	A/T	p.L59Q	c.T176A	ENSG00000135018	43.4	missense variant

NUP214	9:134020117	C/T	p.A582V	c.C1745T	ENSG00000126883	51.3	missense variant
PRPF18	10:13639480	G/C	p.R30P	c.G89C	ENSG00000165630	50	missense variant
ANKRD26	10:27342311	C/T	p.D525N	c.G1573A	ENSG00000107890	34.2	missense variant
ZNF503	10:77159162	T/C	p.D429G	c.A1286G	ENSG00000165655	20.7	missense variant
WAPL	10:88220247	T/A	p.E97V	c.A290T	ENSG00000062650	33.6	missense variant
PDE6C	10:95395277	G/T	p.W431C	c.G1293T	ENSG00000095464	6.6	missense variant
INPP5A	10:134351607	G/C	p.G3R	c.G7C	ENSG00000068383	20	missense variant
TSSC4	11:2423909	G/A	p.E16K	c.G46A	ENSG00000184281	37	missense variant
NUP98	11:3784142	G/C	p.A359G	c.C1076G	ENSG00000110713	54.5	missense variant
DSCAML1	11:117375736	T/A	p.Q485H	c.A1455T	ENSG00000177103	60.2	missense variant
SIAE	11:124517985	A/G	p.L270P	c.T809C	ENSG00000110013	53.4	missense variant
TULP3	12:3043675	G/T	p.R18L	c.G53T	ENSG00000078246	30.3	missense variant
GXYLT1	12:42503436	G/T	p.P151T	c.C451A	ENSG00000151233	24.3	missense variant
NR4A1	12:52448129	C/G	p.A6G	c.C17G	ENSG00000123358	30.4	missense variant
PPFIA2	12:81671147	C/T	p.D623N	c.G1867A	ENSG00000139220	33.3	missense variant
HECTD4	12:112757248	C/G	p.R15T	c.G44C	ENSG00000173064	23.1	missense variant
CHAMP1	13:115089558	A/G	p.I81V	c.A241G	ENSG00000198824	27.7	missense variant
RPGRIP1	14:21775955	C/T	p.S289L	c.C866T	ENSG00000092200	50.6	missense variant
METTL3	14:21979365	T/C	p.M1V	c.A1G	ENSG00000165819	50	missense variant
PCNX	14:71522225	A/G	p.K1417E	c.A4249G	ENSG00000100731	62.5	missense variant
BCL11B	14:99642102	G/T	p.D163E	c.C489A	ENSG00000127152	42.5	missense variant
BUB1B	15:40492464	C/A	p.T474K	c.C1421A	ENSG00000156970	24.2	missense variant
SLC12A1	15:48539124	G/T	p.G491W	c.G1471T	ENSG00000074803	24.6	missense variant
VPS13C	15:62259574	T/C	p.Y952C	c.A2855G	ENSG00000129003	26.2	missense variant
MAP2K1	15:66727453	A/G	p.K57E	c.A169G	ENSG00000169032	23.9	missense variant
ACAN	15:89395094	A/G	p.E699G	c.A2096G	ENSG00000157766	24.6	missense variant
MAPK8IP3	16:1811285	C/A	p.S499R	c.C1497A	ENSG00000138834	27.7	missense variant
DNAH3	16:20975682	C/T	p.R3175H	c.G9524A	ENSG00000158486	52.3	missense variant
CES4A	16:67029659	A/C	p.I26L	c.A76C	ENSG00000172824	32	missense variant
ARID3A	19:971949	G/A	p.G556S	c.G1666A	ENSG00000116017	39.3	missense variant
WDR18	19:990281	G/A	p.A172T	c.G514A	ENSG00000065268	35.5	missense variant
CBARP	19:1231142	T/C	p.H365R	c.A1094G	ENSG00000099625	30.7	missense variant
ADAMTSL5	19:1510880	C/A	p.W21C	c.G63T	ENSG00000185761	31.5	missense variant
ABHD17A	19:1880950	T/C	p.K144E	c.A430G	ENSG00000129968	34.7	missense variant

SCAMP4	19:1924170	G/A	p.G159S	c.G475A	ENSG00000227500	29	missense variant
JSRP1	19:2255311	C/G	p.M1I	c.G3C	ENSG00000167476	26.8	missense variant
C19orf35	19:2278755	C/T	p.R147H	c.G440A	ENSG00000188305	29.4	missense variant
C19orf35	19:2280885	G/A	p.P16S	c.C46T	ENSG00000188305	35.3	missense variant
C19orf71	19:3543397	C/T	p.P83L	c.C248T	ENSG00000183397	34.5	missense variant
SWSAP1	19:11486620	G/T	p.M206I	c.G618T	ENSG00000173928	27.1	missense variant
RASAL3	19:15566952	A/G	p.C562R	c.T1684C	ENSG00000105122	21.6	missense variant
ZNF225	19:44636637	T/C	p.Y624H	c.T1870C	ENSG00000256294	31.5	missense variant
PRR12	19:50103019	A/G	p.K1390R	c.A4169G	ENSG00000126464	32.2	missense variant
SHANK1	19:51171024	T/A	p.H785L	c.A2354T	ENSG00000161681	41.2	missense variant
RPL28	19:55903051	G/T	p.G152W	c.G454T	ENSG00000108107	30.7	missense variant
GGT7	20:33440256	C/T	p.G469R	c.G1405A	ENSG00000131067	29.4	missense variant
KCNS1	20:43727189	C/G	p.R75P	c.G224C	ENSG00000124134	24.3	missense variant
CLDN5	22:19512005	C/T	p.G10E	c.G29A	ENSG00000184113	40.5	missense variant
NCF4	22:37272010	C/T	p.P315S	c.C943T	ENSG00000100365	47.2	missense variant
NPTXR	22:39222680	C/T	p.R308H	c.G923A	ENSG00000221890	31	missense variant
HCCS	ChrX:11136740	C/T	p.A174V	c.C521T	ENSG00000004961	54.9	missense variant
FRMPD4	ChrX:12736756	C/T	p.H1271Y	c.C3811T	ENSG00000169933	48.6	missense variant
OTC	ChrX:38260547	G/T	p.D136Y	c.G406T	ENSG00000036473	43.5	missense variant
FAAH2	ChrX:57473442	G/C	p.G400R	c.G1198C	ENSG00000165591	42.3	missense variant
FMR1	ChrX:147019025	G/T	p.R12M	c.G35T	ENSG00000102081	45.3	missense variant

Appendix 12. WES of acquired mutations in COLO829 cell line following culture in CCT3833

Gene	Genomic coordinate	Amino acid change	Codon	Protein position	Ensemble gene	Variant allele frequency	Consequence
FHAD1	1:15616136	C/T	c.C542T	p.A181V	ENSG00000142621	3.8	missense variant
RNF19B	1:33402750	G/C	c.C1853G	p.A618G	ENSG00000116514	4.4	missense variant
PRKD3	2:37543429	A/C	c.T239G	p.L80R	ENSG00000115825	4.6	missense variant
RUFY4	2:218954742	C/G	c.C1681G	p.P561A	ENSG00000188282	16.3	missense variant
SPHKAP	2:228881638	G/C	c.C3932G	p.A1311G	ENSG00000153820	4.2	missense variant
ARHGEF38	4:106473992	T/A	c.T70A	p.S24T	ENSG00000236699	22.8	missense variant
ZNF346	5:176477786	C/G	c.C258G	p.D86E	ENSG00000113761	29.7	missense variant
HIST1H3B	6:26031973	C/G	c.G316C	p.E106Q	ENSG00000124693	27.4	missense variant
ZNF165	6:28056428	C/T	c.C638T	p.S213L	ENSG00000197279	16.7	missense variant
ADGRB3	6:70071135	G/A	c.G862A	p.E288K	ENSG00000135298	25	missense variant
DYNLT1	6:159065719	C/G	c.G22C	p.E8Q	ENSG00000146425	41.1	missense variant
HECW1	7:43483954	C/A	c.C1183A	p.Q395K	ENSG00000002746	11.5	missense variant
PPP1R3B	8:8998595	C/A	c.G567T	p.R189S	ENSG00000173281	29.2	missense variant
FAM110B	8:59059828	A/G	c.A1039G	p.R347G	ENSG00000169122	3.5	missense variant
ZNF517	8:146033714	G/C	c.G1413C	p.Q471H	ENSG00000197363	31.9	missense variant
GKAP1	9:86414137	T/C	c.A323G	p.E108G	ENSG00000165113	16.8	missense variant
ZNF25	10:38241233	T/C	c.A1193G	p.Y398C	ENSG00000175395	31.5	missense variant
IFIT1	10:91162316	T/C	c.T284C	p.L95P	ENSG00000185745	41.3	missense variant
ZCRB1	12:42707566	C/A	c.G325T	p.E109X	ENSG00000139168	20.2	stopgain
NR1H4	12:100934549	T/A	c.T1049A	p.L350H	ENSG00000012504	3.5	missense variant
PGPEP1L	15:99511788	C/T	c.G510A	p.M170I	ENSG00000183571	19.7	missense variant
XPO6	16:28115914	C/G	c.G2899C	p.A967P	ENSG00000169180	16.7	missense variant
TNRC6C	17:76046671	G/A	c.G1528A	p.V510I	ENSG00000078687	3.9	missense variant
CCDC57	17:80085618	T/A	c.A77T	p.D26V	ENSG00000176155	5.9	missense variant
PPP1R37	19:45649073	C/T	c.C1759T	p.P587S	ENSG00000104866	23.5	missense variant
ARAF	X:47428945	C/G	c.C1308G	p.F436L	ENSG00000078061	48.4	missense variant
OCRL	X:128703296	G/C	c.G1522C	p.V508L	ENSG00000122126	6.2	missense variant
FAM122B	X:133922844	G/C	c.C294G	p.D98E	ENSG00000156504	6.9	missense variant
FLNA	X:153581987	T/C	c.A5675G	p.Y1892C	ENSG00000196924	4.7	missense variant

Appendix 13. WES of acquired mutations in D04 cell line following culture in CCT3833

Gene	Genomic coordinate	Amino acid change	Codon	Protein position	Ensemble gene	Variant allele frequency	Consequence
REV1	2:100022379	G/A	c.C2801T	p.P934L	ENSG00000135945	33	missense variant
SETMAR	3:4355106	G/C	c.G681C	p.E227D	ENSG00000170364	31	missense variant
TFEB	6:41658601	G/A	c.C310T	p.Q104X	ENSG00000112561	47.1	stopgain
AZIN1	8:103840865	A/G	c.T1277C	p.M426T	ENSG00000155096	22.2	missense variant
DAPK1	9:90321894	C/G	c.C3908G	p.S1303X	ENSG00000196730	34.3	stopgain

Appendix 14. WES of acquired mutations in RM59 cell line following culture in CCT3833

Gene	Genomic coordinate	Amino acid change	Codon	Protein position	Ensemble gene	Variant allele frequency	Consequence
ADGRL4	1:79392575	C/T	c.G1079A	p.R360Q	ENSG00000162618	9.4	missense variant
OR6K3	1:158687128	G/C	c.C778G	p.R260G	ENSG00000203757	15.1	missense variant
DPP6	7:153750096	G/A	c.G191A	p.G64D	ENSG00000130226	16.3	missense variant
SORCS1	10:108371731	T/G	c.A2971C	p.N991H	ENSG00000108018	55.4	missense variant
EPS8L2	11:726471	G/T	c.G1921T	p.A641S	ENSG00000177106	10.5	missense variant
OVCH1	12:29639269	C/G	c.G905C	p.G302A	ENSG00000187950	39.1	missense variant
CBX2	17:77758375	C/T	c.C1133T	p.T378I	ENSG00000173894	35.8	missense variant
PIEZO2	18:10761087	A/G	c.T3197C	p.I1066T	ENSG00000154864	54.4	missense variant
NCAN	19:19360650	G/C	c.G3896C	p.R1299P	ENSG00000130287	21.9	missense variant
SIGLEC8	19:51961431	C/A	c.G211T	p.D71Y	ENSG00000105366	31	missense variant

Appendix 15. Top 20 differentially expressed genes in 3833 resistant vs. parental cell lines

A375 cell line vs. A375/R (3833) cell line

Symbol	A375	A375/R (3833)	FC	log2 FC
KIT	1.00E-06	3.151398094	3151398.094	21.58756058
ST8SIA2	1.00E-06	1.863457285	1863457.285	20.82955032
ANKRD2	1.00E-06	1.776837132	1776837.132	20.76088002
SULT4A1	1.00E-06	1.680340498	1680340.498	20.68032217
WIF1	1.00E-06	1.28470651	1284706.51	20.29300738
NME5	1.00E-06	1.274480534	1274480.534	20.28147791
TMEM40	1.00E-06	0.887843492	887843.4915	19.75994586
APCDD1	1.00E-06	0.874371093	874371.0928	19.73788618
NPR3	1.00E-06	0.833650101	833650.1013	19.66908246
ALOX5AP	1.00E-06	0.805663777	805663.7772	19.61981837
NGF	1.00E-06	0.787965359	787965.359	19.58777268
LRRN4	1.00E-06	0.734235527	734235.527	19.4858834
LRMP	1.00E-06	0.662979686	662979.6865	19.33860514
CCDC85A	1.00E-06	0.656077301	656077.3014	19.32350628
HSPB3	1.00E-06	0.630733939	630733.9387	19.26667204
NPPB	1.00E-06	0.619146266	619146.2659	19.23992074
CTTNBP2	1.00E-06	0.535048121	535048.1208	19.02930912
CHST4	1.00E-06	0.437139031	437139.031	18.73773267
VPREB3	1.00E-06	0.366291399	366291.3993	18.4826323
RTP3	1.00E-06	0.33828585	338285.8502	18.36788331

COLO829 cell line vs. COLO829/R (3833) cell line

Symbol	COLO829	COLO829/R (3833)	FC	log2 FC
CDH12	1.00E-06	21.16567802	21165678.02	24.33522337
RXFP1	1.00E-06	6.658178827	6658178.827	22.66669619
AFP	1.00E-06	4.39103663	4391036.63	22.06613014
BMP5	1.00E-06	3.856653646	3856653.646	21.87891816
TMEM40	1.00E-06	3.699813758	3699813.758	21.81902122
C7orf69	1.00E-06	3.687550065	3687550.065	21.81423121
ZNF711	1.00E-06	3.256778438	3256778.438	21.63501414
IL34	1.00E-06	2.412043497	2412043.497	21.20182449
CCDC85A	1.00E-06	2.38865176	2388651.76	21.18776511
RPS6KA6	1.00E-06	1.645607804	1645607.804	20.65018911
GUCY1A2	1.00E-06	1.636835597	1636835.597	20.64247799
TMEFF2	1.00E-06	1.367241851	1367241.851	20.38283703
ATP6V1G3	1.00E-06	1.357700146	1357700.146	20.37273346
KRT32	1.00E-06	1.276946562	1276946.562	20.28426672
SFRP4	1.00E-06	0.876130042	876130.0416	19.7407855
PADI1	1.00E-06	0.735907848	735907.8476	19.48916559
DNAJC5B	1.00E-06	0.685159653	685159.6526	19.38608067
BMP3	1.00E-06	0.677014667	677014.6665	19.36882756
RASSF6	1.00E-06	0.665261951	665261.9511	19.343563
CSTA	1.00E-06	0.511225167	511225.1673	18.96359934

D04 cell line vs. D04/R (3833) cell line

Symbol	DO4	DO4/R (3833)	FC	log2 FC
snoU13	1.00E-06	122.4602647	122460264.7	26.86773847
UCA1	1.00E-06	48.7455823	48745582.3	25.53876814
SPANXD	1.00E-06	16.73703267	16737032.67	23.99654044
SAA1	1.00E-06	12.21001447	12210014.47	23.54156157
MIR663B	1.00E-06	12.02316215	12023162.15	23.51931305
RP11-269F21.3	1.00E-06	11.4102032	11410203.2	23.44382115
RP11-297P16.4	1.00E-06	7.774012825	7774012.825	22.89022806
RP11-48O20.4	1.00E-06	6.613583805	6613583.805	22.65700083
COLEC10	1.00E-06	6.60514016	6605140.16	22.65515774
SFTA1P	1.00E-06	6.038949701	6038949.701	22.52586623
AC136932.1	1.00E-06	5.477218855	5477218.855	22.3850121
SUN3	1.00E-06	5.278774561	5278774.561	22.33177162
LINC00922	1.00E-06	5.096463036	5096463.036	22.28106493
CTC-436P18.3	1.00E-06	5.071546773	5071546.773	22.27399439
RP11-54A9.1	1.00E-06	4.643417246	4643417.246	22.14675549
RP11-1002K11.1	1.00E-06	4.629809859	4629809.859	22.14252151
AC016717.1	1.00E-06	4.512189681	4512189.681	22.10539629
RP11-301G19.1	1.00E-06	4.498802384	4498802.384	22.10110957
CSF2	1.00E-06	4.022223563	4022223.563	21.93956184
XXyac-YM21GA2.4	1.00E-06	3.908710591	3908710.591	21.89826134

RM59 cell line vs. RM59/R (3833) cell line

Symbol	RM59	RM59/R (3833)	FC	log2 FC
KISS1	1.00E-06	47.00699402	47006994.02	25.48637209
RBP4	1.00E-06	33.94700717	33947007.17	25.01678105
CRABP1	1.00E-06	29.16169857	29161698.57	24.79757142
PRAC	1.00E-06	24.52965385	24529653.85	24.54802354
DCDC2	1.00E-06	17.79906139	17799061.39	24.08529783
B4GALNT2	1.00E-06	14.16076548	14160765.48	23.75539592
HNF1B	1.00E-06	12.16907847	12169078.47	23.53671659
UPK1B	1.00E-06	11.6180112	11618011.2	23.46985979
SH3GL3	1.00E-06	11.21415969	11214159.69	23.41881818
GNGT2	1.00E-06	10.6758949	10675894.9	23.34785367
NPY	1.00E-06	10.24913551	10249135.51	23.28899889
CA3	1.00E-06	9.479030277	9479030.277	23.17630805
MKX	1.00E-06	9.105256607	9105256.607	23.11826825
NPPB	1.00E-06	7.81819588	7818195.88	22.8984043
HES2	1.00E-06	6.570746239	6570746.239	22.6476258
PIK3AP1	1.00E-06	5.657740722	5657740.722	22.43179463
MASP1	1.00E-06	5.290889428	5290889.428	22.33507884
LGR5	1.00E-06	5.240075941	5240075.941	22.32115629
ESX1	1.00E-06	4.832459958	4832459.958	22.20432635
MOV10L1	1.00E-06	4.819535943	4819535.943	22.20046281

Appendix 16. Sensitivity of patient-derived cell lines to alpelisib and taselisib

A.

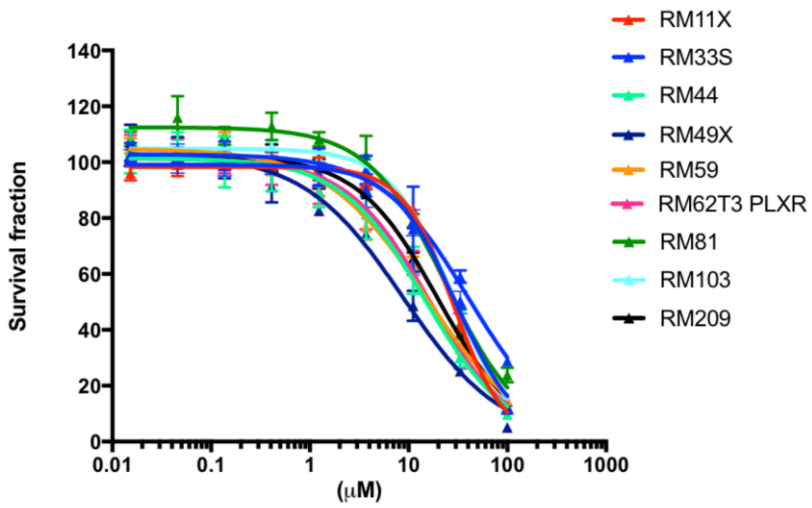

	RM2 PLXR	RM11X	RM33S	RM44	RM49X	RM59	RM62T3 PLXR	RM81	RM103
Sigmoidal dose-response (variable slope)									
Best-fit values									
Bottom	= 0	= 0	= 0	= 0	= 0	= 0	= 0	= 0	= 0
Top	99.15	98.31	102.8	101.5	103.1	104.8	101.3	112.5	104.9
LogEC50	1.48	1.452	1.606	1.166	0.9447	1.161	1.208	1.38	1.443
HillSlope	-1.359	-1.677	-0.9761	-1.018	-0.863	-0.8627	-1.04	-1.101	-1.377
EC50	30.17	28.32	40.36	14.66	8.805	14.48	16.15	24.01	27.72

B.

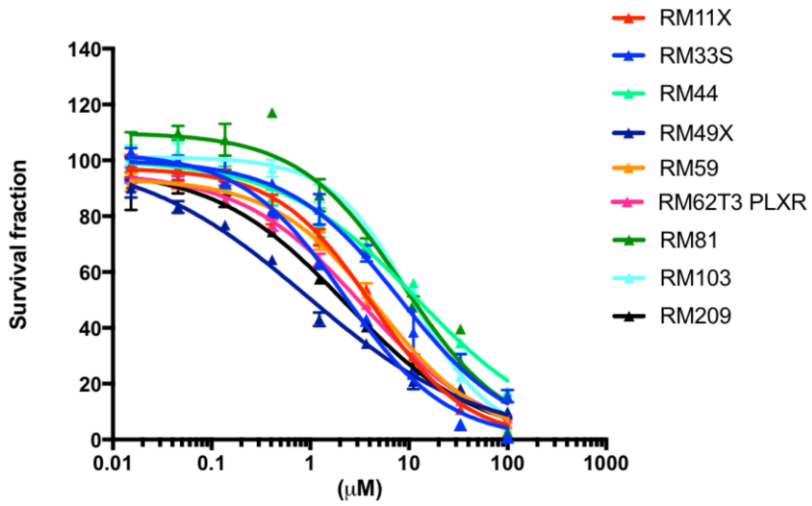

	RM2 PLXR	RM11X	RM33S	RM44	RM49X	RM59	RM62T3 PLXR	RM81	RM103
Sigmoidal dose-response (variable slope)									
Best-fit values									
Bottom	= 0	= 0	= 0	= 0	= 0	= 0	= 0	= 0	= 0
Top	102.8	97.29	100.3	100.5	102.6	93.54	95.8	110	101.2
LogEC50	0.3474	0.6216	0.913	1.084	-0.03075	0.6924	0.5407	0.9469	1.029
HillSlope	-0.8341	-0.907	-0.7621	-0.6294	-0.5029	-0.8134	-0.701	-0.8194	-1.064
EC50	2.225	4.184	8.185	12.15	0.9316	4.925	3.473	8.849	10.7

Figure A1. Growth inhibition of alpelisib and taselisib in patient-derived cell lines. Growth inhibition assays were performed on patient-derived cell lines with a variety of different *BRAF/NRAS* mutations, cultured in the presence of A. alpelisib (15nM-100μM) or B. taselisib (15nM-100μM) for 72 hours. Cell viability was measured using Cell-Titre Glo.

Appendix 17. GSEA of pathways up-regulated in A375/R (3833) following 5 days drug withdrawal compared to in the presence of drug

Name	Term identifier	Domain	P value	Gene intersection
Interferon Signaling	REAC:R-HSA-913531	rea	5.13E-14	CD44,SP100,IFI35,IP6K2,OAS1,ICAM1,MAPK3,DDX58,OAS2,STAT1,TRIM62,IFIT3,IFIT2,EGR1,MT2A,IRF1,IRF3,IFI6,BST2,TRIM21,TRIM22,XAF1,RSAD2,OASL,IFITM3,UBE2L6,EIF4A2,IFNGR2,GBP2,TRIM46,PRKCD,B2M,IRF2,UBB,STAT2,TRIM8,ISG20,HLA-DQB1,CIITA,UBA7,IFITM2,IRF7,IFIT1,IFITM1,ISG15,HLA-DRB1,HLA-DQA1,KPNA5,HLA-DRB5,PSMB8,HLA-DRA,HLA-C,HLA-E,HLA-G,HLA-F,HLA-A,IRF9,HLA-DPB1,HLA-DPA1,HLA-DQB2,HLA-B,HLA-DQA2
Interferon-gamma-mediated signaling pathway	GO:0060333	BP	1.66E-13	CD44,SP100,OAS1,ICAM1,OAS2,STAT1,TRIM62,MT2A,IRF1,IRF3,NR1H2,TRIM21,TRIM22,OASL,PARP9,IFNGR2,GBP2,PRKCD,B2M,IRF2,TRIM8,PARP14,CIITA,IRF7,HLA-DRB1,HLA-DQA1,HLA-DRB5,HLA-DRA,HLA-C,HLA-G,HLA-F,HLA-A,IRF9,HLA-DPB1,HLA-DPA1,HLA-DQB2,HLA-B,HLA-DQA2
Type I interferon signaling pathway	GO:0060337	BP	2.29E-11	SP100,IFI35,IP6K2,OAS1,OAS2,WNT5A,STAT1,IFIT3,IFIT2,EGR1,IRF1,IRF3,IFI6,BST2,XAF1,RSAD2,OASL,IFITM3,GBP2,IRF2,STAT2,ISG20,MYD88,IFITM2,IRF7,IFIT1,IFITM1,ISG15,PSMB8,HLA-C,HLA-G,HLA-F,HLA-A,IRF9,HLA-B
Type I diabetes mellitus	KEGG:04940	keg	1.49E-09	ICA1,PTPRN,CPE,IL1A,IL1B,HLA-DQB1,HLA-DRB1,HLA-DQA1,HLA-DRB5,HLA-DOA,HLA-DMA,HLA-DRA,HLA-C,HLA-E,HLA-G,HLA-F,HLA-A,HLA-DPB1,HLA-DPA1,HLA-B,HLA-DQA2,HLA-DMB
Antigen processing and presentation	KEGG:04612	keg	5.43E-09	CD74,PSME1,PSME2,CTSL,CTSS,CTSB,B2M,HLA-DQB1,CIITA,HLA-DRB1,HLA-DQA1,HLA-DRB5,HLA-DOA,HLA-DMA,HLA-DRA,HSPA1B,HSPA1A,HSPA1L,HLA-C,HLA-E,HLA-G,HLA-F,HLA-A,HLA-DPB1,HLA-DPA1,HLA-B,HLA-DQA2,HLA-DMB
Graft-versus-host disease	KEGG:05332	keg	3.97E-08	IL1A,IL1B,HLA-DQB1,HLA-DRB1,HLA-DQA1,HLA-DRB5,HLA-DOA,HLA-DMA,HLA-DRA,HLA-C,HLA-E,HLA-G,HLA-F,HLA-A,HLA-DPB1,HLA-DPA1,HLA-B,HLA-DQA2,HLA-DMB
Lysosome	KEGG:04142	keg	5.69E-08	CTSA,GNPTG,ARSA,CTSZ,ACP5,ASAH1,MAN2B1,NAGLU,CTSC,CTSD,NPC2,SLC17A5,IDUA,CD68,ACP2,CTSL,CD63,SCARB2,GALNS,ARSG,NPC1,CTSK,ATP6V0D2,ABCB9,LAPTM5,CTSS,CTSB,HGSNAT,SMPD1,TPP1,CTSF,GBA,PSAP,NEU1,AP1G2,PPT2,CTSO
Allograft rejection	KEGG:05330	keg	5.09E-07	HLA-DQB1,HLA-DRB1,HLA-DQA1,HLA-DRB5,HLA-DOA,HLA-DMA,HLA-DRA,HLA-C,HLA-E,HLA-G,HLA-F,HLA-A,HLA-DPB1,HLA-DPA1,HLA-B,HLA-DQA2,HLA-DMB
Leishmaniasis	KEGG:05140	keg	5.09E-07	CYBA,PTGS2,NFKBIA,MAPK3,TGFB1,IL1A,STAT1,IL1B,C3,FCGR2A,IFNGR2,FOS,MYD88,MARCKSL1,HLA-DQB1,HLA-DRB1,HLA-DQA1,HLA-DRB5,HLA-DOA,HLA-DMA,HLA-DRA,HLA-DPB1,HLA-DPA1,HLA-DQA2,HLA-DMB
Granulocyte activation	GO:0036230	BP	1.72E-06	ALDH3B1,PLAUR,MVP,ACPP,SERPINB1,CD44,GRN,TIMP2,CYBA,SLC2A3,CTSA,PLD1,STXBP2,CEACAM1,CD59,FTL,LYZ,TOM1,ARSA,SYNGR1,PYGB,CTSZ,CST3,ATP8B4,ASAH1,MAN2B1,RAB3D,TSPAN14,VAT1,CTSC,RAB5B,STXBP3,CD58,CTSD,VAMP8,NPC2,YPEL5,CYSTM1,PLAU,TNFAIP6,ATP8A1,SERPINB6,C3,CD68,BST2,LGALS3,AMPD3,TCN1,CD63,SDCBP,RHOF,ITGAX,GALNS,TMC6,FCGR2A,ARL8A,GSN,COMMD3,ADAM8,FCER1G,CSTB,NCSTN,CTSS,S100A11,PRKCD,F2RL1,CTSB,HGSNAT,B2M,RAB4B,GHDC,FTH1,RAB31,RAB24,IL8,C3AR1,JUP,DPP7,METTL7A,TMEM179B,SERPINA3,CD55,C5AR1,PSAP,CFD,NEU1,HSPA1B,HSPA1A,HLA-C,HLA-B,PLEKHO2,CCL3
Viral myocarditis	KEGG:05416	keg	2.11E-06	FYN,ICAM1,CASP9,HLA-DQB1,HLA-DRB1,CD55,HLA-DQA1,HLA-DRB5,HLA-DOA,HLA-DMA,HLA-DRA,HLA-C,HLA-E,HLA-G,HLA-F,HLA-A,HLA-DPB1,HLA-DPA1,HLA-B,HLA-DQA2,HLA-DMB
Phagosome	KEGG:04145	keg	2.11E-06	MRC2,CYBA,ITGB5,TUBB4A,RAB5B,C3,ATP6V1F,CTSL,FCGR2A,RAB5A,ATP6V0D2,PLA2R1,C1R,ITGA5,CTSS,ITGA2,TUBA1A,RILP,THBS3,HLA-DQB1,THBS2,HLA-DRB1,HLA-DQA1,HLA-DRB5,HLA-DOA,HLA-DMA,HLA-DRA,HLA-C,HLA-E,HLA-G,HLA-F,HLA-A,HLA-DPB1,HLA-DPA1,HLA-B,HLA-DQA2,HLA-DMB,ITGB3
Staphylococcus aureus infection	KEGG:05150	keg	2.33E-06	ICAM1,C3,FCGR2A,C1R,C3AR1,HLA-DQB1,C1S,HLA-DRB1,HLA-DQA1,C5AR1,CFD,HLA-DRB5,HLA-DOA,HLA-DMA,HLA-DRA,CFI,HLA-DPB1,HLA-DPA1,HLA-DQA2,HLA-DMB
Tuberculosis	KEGG:05152	keg	2.71E-06	BAD,MRC2,CD74,TNFRSF1A,TRADD,MAPK3,TGFB1,VDR,RAB5B,IL1A,STAT1,CTSD,IL1B,C3,CASP9,IRAK2,ITGAX,FCGR2A,RAB5A,ATP6V0D2,PLA2R1,FCER1G,IFNGR2,CTSS,CEBPB,MYD88,PLK3,TLR1,HLA-DQB1,CIITA,HLA-DRB1,HLA-DQA1,SRC,HLA-DRB5,HLA-DOA,HLA-DMA,HLA-DRA,HLA-DPB1,HLA-DPA1,HLA-DQA2,HLA-DMB,IL10RB
Hematopoietic cell lineage	KEGG:04640	keg	3.12E-06	CD9,CD44,IL4R,CD59,FLT3LG,IL11,IL1A,IL1R1,IL1B,CD1D,ITGA5,ITGA2,HLA-DQB1,CSF1R,EPOR,HLA-DRB1,CD55,HLA-DQA1,HLA-DRB5,HLA-DOA,HLA-DMA,HLA-DRA,ITGA1,HLA-DPB1,HLA-DPA1,HLA-DQA2,HLA-DMB,ITGB3
Negative regulation of	GO:0045071	BP	3.36E-06	OAS1,APOBEC3H,PROX1,APOBEC3F,BST2,C19ORF66,INPP5K,RSAD2,OASL,IFITM3,HMGA2,IFIT5,IFI16,ISG20,PARP10,IFITM2,IFIT1,IFITM1,ISG1

viral genome replication				5,PLSCR1,APOBEC3D
Rheumatoid arthritis	KEGG:05323	keg	5.87E-06	ICAM1,IL11,ACP5,TGFB1,VEGFA,IL1A,IL1B,ATP6V1F,CTSL,CTSK,ATP6V0D2,IL8,FOS,HLA-DQB1,HLA-DRB1,MMP1,HLA-DQA1,HLA-DRB5,HLA-DOA,HLA-DMA,HLA-DRA,HLA-DPB1,HLA-DPA1,HLA-DQA2,HLA-DMB,CCL3
Neutrophil degranulation	REAC:R-HSA-6798695	rea	6.12E-06	ALDH3B1,PLAUR,MVP,ACPP,SERPINB1,CD44,GRN,TIMP2,CYBA,SLC2A3,CTSA,PLD1,CEACAM1,CD59,FTL,LYZ,TOM1,ARSA,SYNGR1,PYGB,CTSZ,CST3,ATP8B4,ASAH1,MAN2B1,RAB3D,TSPAN14,VAT1,CTSC,RAB5B,CD58,CTSD,VAMP8,NPC2,YPEL5,CYSTM1,PLAU,TNFAIP6,ATP8A1,SERPINB6,C3,CD68,BST2,LGALS3,AMPD3,TCN1,CD63,SDCBP,RHOF,ITGAX,GALNS,TMC6,FCGR2A,ARL8A,GSN,COMMD3,ADAM8,FCER1G,CSTB,NCSTN,CTSS,S100A11,PRKCD,CTSB,HGSNAT,B2M,RAB4B,GHDC,FTH1,RAB31,RAB24,C3AR1,JUP,DPP7,METTL7A,TMEM179B,SERPINA3,CD55,C5AR1,PSAP,CFD,NEU1,HSPA1B,HSPA1A,HLA-C,HLA-B,PLEKHO2
Toxoplasmosis	KEGG:05145	keg	1.00E-05	BAD,LAMA3,TNFRSF1A,NFKBIA,MAPK3,TGFB1,LAMA4,STAT1,LAMA5,CASP9,LY96,IFNGR2,MYD88,HLA-DQB1,CIITA,HLA-DRB1,HLA-DQA1,LAMB3,HLA-DRB5,HLA-DOA,HLA-DMA,HLA-DRA,HSPA1B,HSPA1A,HSPA1L,HLA-DPB1,HLA-DPA1,HLA-DQA2,HLA-DMB,IL10RB
Endosomal/Vacuolar pathway	REAC:R-HSA-1236977	rea	1.40E-05	CTSL,CTSS,B2M,HLA-C,HLA-E,HLA-G,HLA-F,HLA-A,HLA-B
Human papillomavirus infection	KEGG:05165	keg	1.81E-05	BAD,DVL2,LAMA3,TNFRSF1A,LLGL2,PTGS2,NOTCH3,DLG3,ITGB5,COL9A3,HDAC10,TRADD,MAPK3,PARD6A,ITGB8,VEGFA,LAMA4,WNT5A,HES1,APC2,STAT1,SPP1,PARD6B,CDKN1A,IRF1,IRF3,LAMA5,ITGB4,WNT2B,OASL,ITGA7,COL6A1,COL6A2,ITGA10,CREB3L4,WNT9A,FZD1,ITGA5,HDAC11,ITGA2,HEY1,THBS3,STAT2,FZD8,HES7,MAML2,THBS2,ISG15,FZD9,MAML3,LAMB3,NOTCH4,HLA-C,HLA-E,HLA-G,HLA-F,HLA-A,IRF9,ITGA1,HLA-B,ITGB3
Defense response to virus	GO:0051607	BP	3.07E-05	EXOSC5,APOBEC3H,DDX58,DHX58,IFIH1,STAT1,IFIT3,IFIT2,IRF1,IRF3,APOBEC3F,BST2,C19ORF66,SERINC3,RSAD2,OASL,RTP4,DDX60,IFI44L,PARP9,IFITM3,IFIT5,IFI16,AIM2,DTX3L,F2RL1,DDIT4,IRF2,STAT2,ISG20,IRF7,IFIT1,ISG15,PLSCR1,APOBEC3D
Th1 and Th2 cell differentiation	KEGG:04658	keg	4.62E-05	NOTCH3,IL4R,NFKBIA,MAPK3,STAT1,STAT5A,DLL4,IFNGR2,STAT6,FOS,MAF,HLA-DQB1,MAML2,HLA-DRB1,HLA-DQA1,MAML3,HLA-DRB5,DLL1,HLA-DOA,HLA-DMA,HLA-DRA,HLA-DPB1,HLA-DPA1,HLA-DQA2,HLA-DMB
Influenza A	KEGG:05164	keg	5.39E-05	TNFRSF1A,OAS1,ICAM1,NFKBIA,MAPK3,DDX58,OAS2,IL1A,IFIH1,STAT1,IL1B,IRF3,CASP9,RSAD2,IL33,CASP1,IFNGR2,IL8,STAT2,MYD88,TNFRSF10C,HLA-DQB1,CIITA,IRF7,HLA-DRB1,HLA-DQA1,HLA-DRB5,HLA-DOA,HLA-DMA,HLA-DRA,HSPA1B,HSPA1A,HSPA1L,IRF9,HLA-DPB1,HLA-DPA1,HLA-DQA2,HLA-DMB
Autoimmune thyroid disease	KEGG:05320	keg	8.81E-05	HLA-DQB1,HLA-DRB1,HLA-DQA1,HLA-DRB5,HLA-DOA,HLA-DMA,HLA-DRA,HLA-C,HLA-E,HLA-G,HLA-F,HLA-A,HLA-DPB1,HLA-DPA1,HLA-B,HLA-DQA2,HLA-DMB
Asthma	KEGG:05310	keg	0.000137	FCER1G,HLA-DQB1,HLA-DRB1,HLA-DQA1,HLA-DRB5,HLA-DOA,HLA-DMA,HLA-DRA,HLA-DPB1,HLA-DPA1,HLA-DQA2,HLA-DMB
Inflammatory bowel disease (IBD)	KEGG:05321	keg	0.000164	IL4R,TGFB1,IL1A,STAT1,IL1B,IFNGR2,STAT6,MAF,HLA-DQB1,HLA-DRB1,HLA-DQA1,HLA-DRB5,HLA-DOA,HLA-DMA,HLA-DRA,HLA-DPB1,HLA-DPA1,HLA-DQA2,HLA-DMB
Notch signaling pathway	KEGG:04330	keg	0.00019	DVL2,NOTCH3,NUMBL,HES1,DLL4,NUMB,CIR1,APH1B,NCSTN,DTX3L,DTX3,MAML2,MAML3,DLL1,NOTCH4,PSENEN
Translocation of ZAP-70 to Immunological synapse	REAC:R-HSA-202430	rea	0.000221	PTPN22,HLA-DQB1,HLA-DRB1,HLA-DQA1,HLA-DRB5,HLA-DRA,HLA-DPB1,HLA-DPA1,HLA-DQB2,HLA-DQA2
Extracellular matrix organization	REAC:R-HSA-1474244	rea	0.000221	CD44,TIMP2,LTBP1,LAMA3,CEACAM1,COL5A3,COL19A1,ITGB5,MMP2,ICAM1,COL9A3,MMP11,TIMP1,TGFB1,ICAM5,ITGB8,LAMA4,SPARC,MFAP2,CTSD,SPP1,MMP19,BMP2,LAMA5,ITGB4,CTSL,ITGA7,ITGAX,COL6A1,COL6A2,ITGA10,CTSK,SCUBE3,CAPN5,P4HA3,ADAM8,ADAMTS5,MMP14,ITGA5,NCSTN,CTSS,ADAMTS9,ITGA2,CTSB,HTRA1,MMP10,LTBP3,COL24A1,EFEMP2,CD151,COL18A1,MMP1,LAMB3,COL11A2,DDR1,ITGA1,ITGB3

Appendix 18. GSEA of pathways down-regulated in A375/R (3833) following 5 days drug withdrawal compared to in the presence of drug

Name	Term identifier	Domain	P value	Gene intersection
DNA replication	GO:0006260	BP	1.74E-27	DBF4,REV3L,BRCA1,RFC1,KITLG,RFC2,RAD51,POLQ,POLD1,MCM10,NUCKS1,SMC1A,MCM2,GLI2,TIPIN,MCM6,POLD3,ORC1,ORC6,CLSPN,CDC45,CDC6,CDC7,MCM5,PDGFB,POLE2,GINS1,RBBP8,POLA1,MCM4,LIG1,FBXW7,RFC5,TIMELESS,MCM3,GMNN,CCDC88A,MCM8,CHTF18,E2F8,GINS2,RPA1,PCNA,RFC3,USP37,BRIP1,DSCC1,DNA2,BARD1,EGF,BRCA2,PIF1,TICRR,PARP1,PDGFC,PRIM2,MMS22L,GINS4,POLE3,EME1,TONSL,DBF4B,TOPBP1,RFC4,CDC25A,CDT1,RFWD3,FEN1,CDK1,ESCO2,RNASEH1,EXO1,ATR,POLE,TOP3A,RMI1,GINS3,NF2,FANCM,BLM,PRIM1,NT5M,RBM14,RTEL1
DNA strand elongation	REAC:R-HSA-69190	rea	2.53E-19	RFC1,RFC2,POLD1,MCM2,MCM6,POLD3,CDC45,MCM5,GINS1,POLA1,MCM4,LIG1,RFC5,MCM3,MCM8,GINS2,RPA1,PCNA,RFC3,DNA2,PRIM2,GINS4,RFC4,FEN1,GINS3,PRIM1
Cell Cycle Checkpoints	REAC:R-HSA-69620	rea	7.23E-17	DBF4,BRCA1,SPDL1,RFC2,MCM10,MCM2,GTSE1,MCM6,NDC80,XPO1,SEH1L,ORC1,BIRC5,ORC6,CLSPN,CDC45,CDC6,CDC7,CENPM,MCM5,RBBP8,CENPI,MCM4,RFC5,MCM3,CENPA,CDC20,CENPF,CENPL,KIF18A,ZWINT,CENPK,HIST1H2BJ,MCM8,PKMYT1,SGOL1,RPA1,RFC3,CCNB1,CDCA8,BRIP1,MDC1,CENPO,DNA2,BARD1,CENPE,KIF2C,NUF2,CCNA2,INCENP,MLF1IP,SPC25,ANAPC1,SKA1,BUB1B,CCNB2,SPC24,TOPBP1,RFC4,CDC25A,MAD2L1,CENPN,PLK1,BUB1,CDK1,EXO1,ATR,CCNE2,SFN,TOP3A,RMI1,AURKB,KNTC1,BRCC3,ERCC6L,CENPP,BLM,HIST1H2BK
DNA replication	KEGG:03030	keg	1.77E-15	RFC1,RFC2,POLD1,MCM2,MCM6,POLD3,MCM5,POLE2,POLA1,MCM4,LIG1,RFC5,MCM3,RPA1,PCNA,RFC3,DNA2,PRIM2,POLE3,RFC4,FEN1,RNASEH1,POLE,PRIM1
Mitotic Prometaphase	REAC:R-HSA-68877	rea	2.07E-15	NCAPD2,SPDL1,SMC1A,NDC80,XPO1,PDS5B,SEH1L,BIRC5,CENPM,CEP192,CENPI,CCP110,CEP152,NCAPG,CEP72,SMC4,CENPA,CDC20,NEK2,CENPF,CENPL,NCAPH,KIF18A,ZWINT,CENPK,SGOL1,CCNB1,CDCA8,SMC2,HAUS2,TUBGCP4,CENPO,CENPE,PLK4,KIF2C,NUF2,CDCA5,CEP78,INCENP,MLF1IP,CENPJ,SPC25,SKA1,BUB1B,CCNB2,PCNT,SPC24,MAD2L1,CENPN,PLK1,BUB1,CDK1,AURKB,KNTC1,ERCC6L,CENPP,HAUS7
HDR through Homologous Recombination (HRR)	REAC:R-HSA-5685942	rea	3.11E-15	BRCA1,RFC1,RFC2,RAD51,POLD1,POLD3,POLE2,RBBP8,RAD51C,RAD51AP1,RFC5,XRCC3,RPA1,PCNA,RFC3,BRIP1,DNA2,BARD1,BRCA2,POLE3,EME1,TOPBP1,RFC4,POLH,EXO1,ATR,POLE,TOP3A,GEN1,RMI1,XRCC2,BLM,RTEL1
Cell cycle	KEGG:04110	keg	6.72E-13	DBF4,E2F2,SMC1A,MCM2,MCM6,RBL1,ORC1,ORC6,CDC45,CDC6,CDC7,GADD45B,MCM5,E2F1,MCM4,CDK6,MCM3,TTK,GADD45A,CDC20,CDKN2C,PKMYT1,PCNA,CCNB1,ESPL1,MYC,CCNA2,SKP2,ANAPC1,BUB1B,CCNB2,CDC25A,MAD2L1,PLK1,BUB1,CDK1,ATR,CCNE2,SFN,TFDP1,PRKDC
Telomere C-strand (Lagging Strand) Synthesis	REAC:R-HSA-174417	rea	1.42E-12	RFC1,RFC2,POLD1,POLD3,POLE2,POLA1,LIG1,RFC5,RPA1,PCNA,RFC3,DNA2,PRIM2,POLE3,RFC4,FEN1,POLE,PRIM1
RHO GTPases Activate Formins	REAC:R-HSA-5663220	rea	1.39E-09	SPDL1,NDC80,XPO1,SEH1L,BIRC5,CENPM,CENPI,CENPA,CDC20,CENPF,CENPL,KIF18A,ZWINT,CENPK,SGOL1,CDCA8,CENPO,CENPE,DIAPH3,KIF2C,NUF2,INCENP,MLF1IP,SPC25,SKA1,BUB1B,SPC24,MAD2L1,CENPN,PLK1,BUB1,AURKB,KNTC1,ERCC6L,CENPP,EVL
Fanconi anemia pathway	KEGG:03460	keg	6.90E-09	REV3L,BRCA1,RAD51,UBE2T,RAD51C,FANCE,RPA1,BRIP1,BRCA2,FANCI,FANCD2,EME1,FANCC,USP1,POLH,ATR,TOP3A,RMI1,FANCB,FANCA,FANCM,BLM
Homologous recombination	KEGG:03440	keg	1.74E-08	BRCA1,RAD51,POLD1,POLD3,RAD54L,RBBP8,RAD51C,XRCC3,RPA1,BRIP1,BARD1,BRCA2,EME1,TOPBP1,TOP3A,BRCC3,XRCC2,RAD54B,BLM
Mismatch repair	KEGG:03430	keg	3.21E-07	RFC1,RFC2,POLD1,POLD3,MSH2,LIG1,RFC5,MSH6,RPA1,PCNA,RFC3,RFC4,EXO1
Gap-filling DNA repair synthesis and ligation in GG-NER	REAC:R-HSA-5696397	rea	1.14E-06	RFC1,RFC2,POLD1,POLD3,POLE2,LIG1,RFC5,RPA1,PCNA,RFC3,POLE3,RFC4,POLE

Regulation of TP53 Activity through Phosphorylation	REAC:R-HSA-6804756	rea	1.74E-06	BRCA1,RFC2,NUAK1,AURKA,TPX2,RBBP8,PRKAG2,RFC5,MAPK14,DYRK2,PRKAB2,RPA1,RFC3,BRIP1,DNA2,BARD1,CCNA2,SSRP1,TOPBP1,RFC4,EXO1,ATR,TOP3A,RMI1,AURKB,BLM
Kinesins	REAC:R-HSA-983189	rea	5.51E-06	KIF1B,KIF4A,KIF20A,KIF18A,KIF23,KIF11,KIF20B,CENPE,KIF21A,KIF2C,RACGAP1,KIF26B,KIF15,KIF18B,KIF4B,KIFC1
Purine metabolism	KEGG:00230	keg	4.16E-05	POLR3B,POLD1,POLR1A,POLD3,POLE2,POLA1,PRPS2,TWISTNB,PDE10A,POLR3G,GDA,PAICS,POLR1E,ADCY3,PDE5A,POLR2D,PRIM2,PRPS1,POLE3,PDE3B,AK5,PDE1C,XDH,ADCY9,AK4,ADCY1,RRM1,PGM2,RRM2,POLE,PFAS,PRIM1,PAPSS2,NT5M,PRPS1L1
response to ionizing radiation	GO:0010212	BP	4.32E-05	BRCA1,RAD51,NUCKS1,TP73,MSH2,RAD51C,RAD51AP1,MAPK14,ECT2,GADD45A,XRCC3,FIGNL1,MYC,TICRR,FANCD2,PAXIP1,TOPBP1,IKBIP,RFWD3,ATR,BRCC3,KDM4D,XRCC2,BLM
Polo-like kinase mediated events	REAC:R-HSA-156711	rea	4.41E-05	MYBL2,FOXM1,CENPF,PKMYT1,CCNB1,CCNB2,CDC25A,PLK1,LIN9
SUMOylation of DNA replication proteins	REAC:R-HSA-4615885	rea	6.07E-05	NDC1,SEH1L,AURKA,BIRC5,NUP188,NUP155,NUP153,TOP2A,NUP210,PCNA,CDCA8,INCENP,NUP205,AURKB,POM121
Pyrimidine metabolism	KEGG:00240	keg	7.90E-05	POLR3B,POLD1,POLR1A,POLD3,CAD,POLE2,POLA1,DHODH,TWISTNB,POLR3G,POLR1E,POLR2D,PRIM2,POLE3,RRM1,TK1,DTYMK,CTPS1,RRM2,TYMS,POLE,DCTPP1,PRIM1,NT5M
p53 signaling pathway	KEGG:04115	keg	7.90E-05	FAS,GTSE1,TP73,SESN1,GADD45B,CDK6,CCNG1,GADD45A,APAF1,CCNB1,THBS1,PMAIP1,CCNB2,CDK1,RRM2,ZMAT3,ATR,CCNE2,SFN
Nucleotide excision repair	KEGG:03420	keg	0.000101	RFC1,RFC2,POLD1,POLD3,POLE2,ERCC2,LIG1,GTF2H3,RFC5,RPA1,PCNA,RFC3,POLE3,RFC4,POLE
cell-cell junction organization	GO:0045216	BP	0.000128	CDH10,EPHA3,DSG2,PKP2,WDR1,MPP5,PVR,FERMT2,DLG1,DSP,CAV1,CORO1C,CDH6,ECT2,KIAA0754,ROCK2,THBS1,PKP4,PHLDB2,SDK1,PTPRJ,MPP7,GJA1,PRKCA,RUNX1,CLDN1,DLC1,PLEKHA7,CDH2,TLN2,PARD6G,CDH4,GJC1,CADM1,ZNF703,EFNA5
mitotic nuclear envelope disassembly	GO:0007077	BP	0.000287	NDC1,SEH1L,NUP188,NUP155,NEK6,NUP153,NUP210,CCNB1,PRKCA,NUP205,CCNB2,PLK1,CDK1,POM121
Phosphorylation of Emi1	REAC:R-HSA-176417	rea	0.000502	FBXO5,CDC20,CCNB1,PLK1,CDK1
DNA damage response, detection of DNA damage	GO:0042769	BP	0.000859	RFC1,RFC2,POLD1,RAD18,POLD3,RFC5,RPA1,PCNA,RFC3,DTL,USP1,RFC4
pteridine-containing compound metabolic process	GO:0042558	BP	0.000977	MTHFD2,SLC46A1,MTHFD1L,MTRR,GCH1,ALDH1L2,SLC19A1,TYMS,SHMT2,DHFR
Base excision repair	KEGG:03410	keg	0.00153	POLD1,UNG,POLD3,POLE2,LIG1,NEIL3,PCNA,PARP1,POLE3,FEN1,POLE
Gap-filling DNA repair synthesis and ligation in TC-NER	REAC:R-HSA-6782210	rea	0.00167	RFC1,RFC2,POLD1,POLD3,POLE2,ERCC2,LIG1,GTF2H3,RFC5,RPA1,PCNA,RFC3,POLR2D,POLE3,RFC4,POLE
Transcriptional Regulation by E2F6	REAC:R-HSA-8953750	rea	0.00167	BRCA1,RAD51,CBX5,CDC7,E2F1,RBBP8,EZH2,APAF1,RRM2,MGA,TFDP1

Appendix 19. Clinical characteristics and ctDNA status of patients in Manchester validation cohort (n=29)

Patient ID	Age	Gender	Stage	Mutations identified in tumour tissue	Mutations identified in tumour tissue used for plasma analysis	Time to relapse or last follow-up from surgery (months)	Clinical relapse	Site of relapse	Baseline ctDNA status	Post-op ctDNA status	Serial ctDNA status up to time of relapse or last follow-up
C004350	28	Female	IIIA (T1b, N1a)	*BRAF* p.V600E	*BRAF* p.V600E	16.3	No	-	Not detected	Not detected	-
C003898	68	Male	IIIB (T3a, N1a)	*NRAS* p.Q61L	*NRAS* p.Q61L	2.4	Yes	Left cervical node	Detected	Detected	-
C004220	75	Male	IIIB (T2b, N2b)	*NRAS* p.Q61K	*NRAS* p.Q61K	16.1	Yes	Brain	Detected	Detected	Detected
C004221	80	Female	IIIB (T2a, N1b)	*NRAS* p.Q61R	*NRAS* p.Q61R	19	No	-	Not detected	Detected	Detected
C004340	47	Male	IIIB (T1b, N2b)	*BRAF* p.V600E	*BRAF* p.V600E	17.8	No	-	Detected	Not detected	Detected
C004620	78	Female	IIIB (T3a, N1b)	*NRAS* p.Q61R	*NRAS* p.Q61R	0.5	Yes	Brain	Detected	-	-
C004690	75	Female	IIIB (T3a, N1a)	*BRAF* p.V600E	*BRAF* p.V600E	14.2	No	-	Not detected	Not detected	-
C004763	43	Male	IIIB (Tx, N1b)	*NRAS* p.Q61K	*NRAS* p.Q61K	7.7	Yes	Lung	Not detected	Detected	-
C005017	58	Female	IIIB (T2a, N1a)	*BRAF* p.V600E	*BRAF* p.V600E	10.8	No	-	Not detected	Not detected	Not detected
C005018	60	Male	IIIB (T3a, N1a)	*BRAF* p.V600E	*BRAF* p.V600E	8.1	No	-	Not detected	-	-
C004286	53	Male	IIIC (T4b, N2b)	*BRAF* p.V600E	*BRAF* p.V600E	16.3	No	-	Not detected	Not detected	Not detected
C004287	73	Male	IIIC (T3b, N3b)	*BRAF* p.V600K	*BRAF* p.V600K	19.3	Yes	Subcutaneous, brain, bone	Not detected	Not detected	Detected
C004457	64	Female	IIIC (T3b, N1a)	*BRAF* p.V600E	*BRAF* p.V600E	14.5	No	-	Not detected	Not detected	Not detected
C004588	35	Male	IIIC (T1a, N3b)	*BRAF* p.V600E	*BRAF* p.V600E	4.7	Yes	Brain	Detected	-	-
C004862	61	Male	IIIC (T2a, N2c)	*NRAS* p.Q61K	*NRAS* p.Q61K	12.1	No	-	Not detected	-	-
C005151	43	Male	IIIC (T3b, N3a)	*BRAF* p.V600E	*BRAF* p.V600E	7	Yes	Subcutaneous	Not detected	Not detected	Not detected
C005197	67	Female	IIIC (T2a, N3a)	*BRAF* p.V600E	*BRAF* p.V600E	7.7	No	-	Detected	-	-
C004434	79	Male	IIID (T4b, N3c)	*NRAS* p.Q61R	*NRAS* p.Q61R	14.1	Yes	Lung	Detected	Detected	Detected

C002380	76	Male	IIID (T4b, N3b)	*BRAF* p.V600E	*BRAF* p.V600E	4.8	Yes	Liver	Detected	Detected	Detected
C004542	47	Female	IIIB (T3a, N1a)	*NRAS* p.G12N	*NRAS* p.G12N	15.4	No	-	Not detected	Not detected	Not detected
C005552	80	Male	IIIC (T4x, N1b)	*TERT* c.- 124 C>T	*TERT* c.- 124 C>T	4.1	No	-	Not detected	Not detected	-
C001044	47	Female	IIID (Tx,N3c)	WT	-	12.4	Yes	In transit	-	-	-
C003630	66	Male	IIIC (T4a, N1b)	WT	-	16.1	Yes	Brain	-	-	-
C004337	61	Female	IIIA (T2a, N1a)	WT	-	17	No	-	-	-	-
C004339	53	Male	IIIA (T1a, N1a)	WT	-	18.4	No	-	-	-	-
C005026	48	Female	IIIA (T2a, N1a)	WT	-	9.4	No	-	-	-	-
C004381	75	Male	IIID (T4x, N3b)	WT	-	-	-	-	-	-	-
C004799*	37	Female	IIIX (T2x, N1a)	*BRAF/TERT* WT	-	12.3	-	-	-	-	-
C005011*	70	Female	IIIC (T3a, N2a)	*BRAF/TERT* WT	-	9.4	-	-	-	-	-

*No further tissue available for *NRAS* testing

Appendix 20. CAcTUS Key Inclusion/Exclusion criteria

Subjects with histologically confirmed cutaneous melanoma that is either un-resectable or metastatic (Stages III or IV) will be screened for eligibility. Eligible subjects must be *BRAF* V600E/K/R mutation positive (determined by a CPP accredited laboratory) and the exact point mutation must be identified in order to perform the correct ddPCR analysis. Subjects who have had prior systemic MAPK targeted therapy or immune therapy will not be eligible.

2.1 Key Inclusion criteria

1. Histological confirmation of cutaneous melanoma
2. $\geq$ 16 years
3. Stage III un-resectable/ IV disease
4. *BRAF* p.V600E/K/R mutation confirmed (exact point mutation must be provided to the investigators)
5. At least one target lesion measurable by CT or MRI as per RECIST 1.1
6. Baseline ctDNA (as defined by the mutant *BRAF* VAF in plasma) ≥5%
7. Adequate organ function (see table)
8. ECOG performance status 0/1
9. Prior radiotherapy or radiosurgery must have been completed at least 2 weeks prior to the first dose of study drug
10. Women of childbearing potential participating in the study must have a negative serum or urine pregnancy test (minimum sensitivity 25 IU/L or equivalent units of HCG) within 24 hours prior to the start of study drug.

System	Laboratory Values
Haematologic	
Haemoglobin	≥ 9 g/dL
White blood count	≥ 2 x10^9/L
ANC	≥ 1.2 x10^9/L
Platelet count	≥ 75x10^9/L
PT/INR[a] and PTT	≤ 1.5 x ULN
Hepatic	
Albumin	≥ 2.5 g/dL
Total bilirubin	≤ 1.5 x ULN
AST and ALT	≤ 2.5 x ULN
Renal	
Calculated creatinine clearance[b]	≥ 50ml/min
Cardiac	
Left Ventricular Ejection fraction (LVEF)	≥ LLN by ECHO

Inclusion laboratory values criteria.

Abbreviations: ALT = alanine transaminase; ANC = absolute neutrophil count; AST = aspartate aminotransferase; INR = international normalised ratio; LLN = lower limit of normal; PT = prothrombin time; PTT = partial thromboplastin time; ULN = upper limit of normal.
a. Subjects receiving anticoagulation treatment may be allowed to participate with INR established within the therapeutic range prior to randomisation.
b. Calculate creatinine clearance using standard Cockcroft-Gault formula or Wright formula. Creatinine clearance must be ≥50 mL/min to be eligible.

2.2 Exclusion criteria

1. Prior systemic anti-cancer treatment (immune therapy, targeted therapy, vaccine therapy, or investigational treatment) for Stage III or Stage IV (metastatic) melanoma.
2. History of another malignancy. **Exception:** Subjects who have been disease-free for 3 years, (i.e. subjects with second malignancies that are indolent or definitively treated at least 3 years ago) or subjects with a history of completely resected non-melanoma skin cancer. No additional therapy should be required whilst the patient is on study.
3. Any serious or unstable pre-existing medical conditions (aside from malignancy exceptions specified above), psychiatric disorders, or other conditions that could interfere with the subject's safety, obtaining informed consent, or compliance with study

procedures.

4. Subjects with a condition requiring systemic treatment with either corticosteroids (>10 mg daily prednisone equivalent) or other immunosuppressive medications within 14 days of study drug administration. Inhaled or topical steroids and adrenal replacement steroid doses > 10 mg daily prednisone equivalent are permitted in the absence of active autoimmune disease.

5. Brain metastases and leptomeningeal metastases are excluded unless:
    - Asymptomatic and untreated at presentation, OR
    - Symptomatic lesions have been definitively treated with surgery or stereotactic surgery (whole-brain radiation may be given as adjuvant treatment), and do not require steroids for control of symptoms
    - Symptomatic metastases, treated or untreated, or metastases requiring steroids to control symptoms, are excluded

6. No contraindications to the drug treatments dabrafenib, trametinib, ipilimumab or nivolumab.

Appendix 21. DETECTION Key Inclusion/Exclusion criteria

3.1 Key Inclusion Criteria

1. Histological confirmation of cutaneous melanoma ≥ 16 years

2. Stage IIB or IIC melanoma (sentinel lymph node staged)

3. Complete resection must be performed within 12 weeks prior to randomisation

4. Disease free status documented both clinically and radiologically within 4 weeks prior to randomisation

5. *BRAF* mutation confirmed with exact point mutation known

6. No prior immunotherapy, chemotherapy, vaccine therapy or BRAFi/MEKi targeted therapy

7. ECOG performance status 0/1

3.2 Key Exclusion Criteria

1. Known severe medical or physiological co-morbidities conditions that would compromise or impede participation

2. Known contraindications to the study drugs

3. Pregnant or nursing females